Application Driven Advances in Laser Micro-Machining Technology

by

Hoang Le

A thesis submitted to the University of Birmingham for the degree of

DOCTOR OF PHILOSOPHY

December 2022

Department of Mechanical Engineering

School of Engineering

University of Birmingham

Abstract

The use of a laser as a machining tool in micro manufacturing has several distinct advantages, including high speed non-contact processing, high accuracy, repeatability, and reproducibility, excellent control flexibility, and no restrictions on the types of materials that can be machined. Possibilities for further improvement of laser material processing are still in progress and facing challenges. There are limitations that prevent laser micro-machining from improving performance and expanding the range of manufacturing applications for this technology, such as the poor removal rate of ultrashort pulse processing and the tapering effect at side walls of microstructures. Therefore, the primary goal of the thesis is to address these important issues, thus, to advance this technology, i.e. achieving quality and process efficiency improvements in machining of various materials.

The research focuses on implementation and investigation of generic solutions to improve quality of fabricated products and process efficiency, as well as demonstration of the laser micro-machining capabilities in various industrial applications. Firstly, a refractive beam shaper was deployed to attain top-hat intensity profile at the focus position of a nanosecond pulsed laser source for micro-machining of blind structure. The top-hat processing was able to reduce taper in range from 4% to 15% and surface roughness in range from 15% to 21% for different scanning strategies. Advantages of top-hat profile over Gaussian profile also presented at various machining conditions. Secondly, MHz burst mode of ultrashort laser pulses was proven to scale-up material removal rate in laser micro-machining of stainless steel and copper. Specifically, material removal rate was increased by 2 to 6.5 times when machining copper and by

5.7 to 16.3 times when machining stainless steel. This technique allows the laser power to be fully utilised while laser fluence is kept closely to optimum level. The advantages of MHz burst mode in removal rate consequently led to the improvement of surface quality in some cases due to less required number of scanning layer in comparison to single mode. Thirdly, a novel fabrication process, called precession laser machining, was investigated and employed to produced THz devices. The use of this technology was able to reduce taper angle at the sidewall by 3 times (from 4.1° to 1.6°) and 6 times (from 11.5° to 1.9°) in producing through structure on 300 µm and 600 µm thickness, respectively, when compared with conventional laser machining process. The performance of fabricated THz devices satisfied all requirements with 1% error. Fourthly, the precession laser machining was investigated systematically to study its capabilities and limitations. The results showed that it was possible to drill hole with zero or even negative taper angle on 0.6 mm and 1 mm Nickel alloy substrate for hole diameter from 100 µm to 500 µm. It was not possible to achieve zero tapering when drilling on 2 mm substrate thickness. However, there still is a significant reduction in hole's taper angle when machining on 2 mm substrate, where aspect ratios were up to 20:1. The precession beam is clipped at the hole entrance when beam is refocused downward that indirectly limits the machining capability of this technique on thick substrate.

In summary, the obtained results clearly demonstrated the capability of employed technologies in enhancing the material removal rate and quality of microstructures. In addition, the limitations of these technologies were also discussed and clarified. The research advances the knowledge in laser-based manufacturing technology and contributes to broaden the use of this technology in industrial applications.

Acknowledgement

I would like to acknowledge and give my warmest thanks to my supervisor, Professor Stefan Dimov, who made this thesis possible. Without his invaluable advice, continuous support, and patience, my PhD would not make it this far. His immense knowledge and plentiful experience have encouraged me in all the time of my academic research and daily life.

My thanks and appreciations also go to my colleagues – my friends, Dr Vahid Nasrollahi, Dr Pavel Penchev, Dr Anvesh Gaddam, and fellow PhD candidates, Aleksandra Michalek and Themistoklis Karkantonis, who have willingly helped me out with their abilities. It is their kind help and support that have made my study and life in the UK a wonderful time.

I would like to give special thanks to my friend, Ta Quynh Chi, for inspiring and motivating me in my decision to pursue this PhD path. Also, I would like to sincerely thank my friend, Nguyen Hong Ngoc, for being with me in the difficult times of this journey.

Finally, I would like to express my deepest gratitude to my loving family, especially my parents. Without their love, tremendous understanding, continuous support, and encouragement during my studies in the UK, it would be impossible for me to complete my study.

Table of contents

List of Figures

Chapter 2

Chapter 3

Chapter 4

Chapter 5

Chapter 6

List of Tables

Chapter 2

Chapter 3

Chapter 4

Chapter 5

Chapter 6

Abbreviations

2D	Two Dimensional
3D	Three Dimensional
EDM	Electron Discharge Machining
ECM	Electron Chemical Machining
HAZ	Heat Affect Zone
TEM	Transverse Electro-Magnetic
HA	Heat Accumulation
SLM	Spatial Light Modulator
MPLC	Multiplane Light Conversion
LCoS-SLM	Liquid Crystal on Silicon for Spatial Light Modulation
AOS	Acousto-Optics Shaping
ROE	Refractive Optic Element
DOE	Diffractive Optic Element
MOPA	Master Oscillator Power Amplifier
SEM	Scanning Electron Microscope
DOF	Depth of Focus
SRR	Specific Removal Rate
SP	Single Pulse
BM	Burst Mode
XPS	X-Ray Photoelectron Spectroscopy
FIB	Focus of Individual Beam
FRB, FPB	Focus of Rotary Beam, Focus of Precession Beam

Nomenclatures

Symbol	Unit	Parameter definition
E_1	eV	Ground state energy level
E_2	eV	Metastable state energy level
M^2	-	Beam quality factor
P_d	µm	Pulse distance
v	mm/s	Scanning speed
f, f_p	Hz	Frequency
S_a	µm	Area surface roughness
E,E_P	µJ	Pulse energy
F	J/cm^2	Fluence
F_{Peak}	J/cm^2	Peak fluence
δ	nm	Optical penetration depth
F_{th}	J/cm^2	Ablation threshold fluence
f_{IB}	Hz	Intraburst frequency
$\%Overlap$	%	Percentage of overlap
A	cm^2	Beam spot area
V_a	µm^3	Ablated volume
N_{Total}^{p}	-	The total delivered pulses
N_{Line}^{p}	-	The number pulses per line
N_{Line}	-	The number of lines
N_{Layer}	-	The number of layers
SRR_{Total}^{BM}	µm^3/µJ	Specific removal rate of burst mode processing
SRR^{BM}	µm^3/µJ	Specific removal rate of a single burst
SRR_{HA}^{BM}	µm^3/µJ	Specific removal rate of burst mode processing due to heat accumulation
SRR_{Total}^{sp}	µm^3/µJ	Specific removal rate of single pulse processing
SRR^{sp}	µm^3/µJ	Specific removal rate of a single pulse
SRR_{HA}^{sp}	µm^3/µJ	Specific removal rate of single pulse processing due to heat accumulation
σ_{eff}	S/m	Efficient electric conductivity
σ_0	S/m	Theoretical electric conductivity
K_{SR}	-	Surface roughness correction factor

List of publication and conference presentations

The following journal publications and conference presentations resulted from the research carried out within the scope of this thesis.

Journal publications:

- ***Le, H.**, Penchev, P., Henrottin, A., Bruneel, D., Nasrollahi, V., Ramos-de-Campos, J. A., & Dimov, S. (2020). Effects of Top-hat Laser Beam Processing and Scanning Strategies in Laser Micro-Structuring. Micromachines (Basel), 11(2). https://doi.org/10.3390/mi11020221*

- ***Le, H.**, Karkantonis, T., Nasrollahi, V., Penchev, P., & Dimov, S. (2022). MHz burst mode processing as a tool for achieving removal rates scalability in ultrashort laser micro-machining. Applied Physics A. https://doi.org/10.1007/s00339-022-05864-8*

- ***Le, H.**, Pradhani, C., Penchev, P., Nasrollahi, V., Karkantonis, T., Wang, Y., Dimov, S., & Ramos-de-Campos, J. A. (2022). Laser precession machining of cross-shaped terahertz bandpass filters. Optics and Lasers in Engineering, 149. https://doi.org/10.1016/j.optlaseng.2021.106790*

- ***Le, H.**, Nasrollahi, V., Karkantonis, T., Penchev, P., Marimuthu, S., Crozier, M. and Dimov, S. (2023). Investigation of precession laser machining of microholes in aerospace material. Journal of Laser Applications 35, 012028 https://doi.org/10.2351/7.0000903*

- *Karkantonis, T., Penchev, P., Nasrollahi, V., **Le, H.**, See, T. L., Bruneel, D., Ramos-de-Campos, J. A., & Dimov, S. (2022). Laser micro-machining of freeform surfaces: Accuracy, repeatability and reproducibility achievable with multi-axis processing strategies. Precision Engineering, 78, 233-247. https://doi.org/10.1016/j.precisioneng.2022.08.009*

- *Nasrollahi, V., Penchev, P., Batal, A., **Le, H.**, Dimov, S., & Kim, K. (2020a). Laser drilling with a top-hat beam of micro-scale high aspect ratio holes in silicon nitride. Journal of Materials Processing Technology, 116636. https://doi.org/https://doi.org/10.1016/j.jmatprotec.2020.116636*

Conference presentation

- Industrial Laser Applications Symposium, ILAS, 2019, UK.
- Industrial Laser Applications Symposium, ILAS, 2021, UK.
- World Congress on Micro and Nano Manufacturing, WCMNM, 2019, Raleigh, USA

- World Congress on Micro and Nano Manufacturing, WCMNM, 2021, Bombay, India.
- World Congress on Micro and Nano Manufacturing, WCMNM, 2022, Leuven, Belgium.

CHAPTER 1

INTRODUCTION

1.1. Motivation

The rapid advances in technologies have been changing our lives significantly in the last several decades. Personal devices have been getting more compact and sophisticated by integrating multiple functionalities. This trend has been driving manufacturing companies to design and implement different novel manufacturing solutions to address unceasing growing needs from different markets. Lasers as a processing tool are one of the manufacturing technologies that has been attracting a lot of interest from companies and researchers. It is applied successfully in various application areas, including surface engineering, microfluidic, biotechnology, nanotechnology, energy, defence, etc. This is evident from the number of publications on various laser related topics that were approximately 6.5 million (up to 2022) in which 2 million belongs to laser engineering topic, have been increasing every year while the laser acronym was coined in 1957 [1, 2].

The applications of lasers in materials processing has been constantly increasing for more than six decades since their invention. Lasers, along with the development of many interrelated enabling technologies, have been offering novel solutions for both additive and subtractive manufacturing that are becoming viable alternatives to other conventional and unconventional machining processes, especially at micro-scale, such as mechanical micro-machining and micro-drilling, electro-discharge machining (EDM), electro-chemical machining (ECM) or even photolithography. The key advantages that laser micro-machining offers are relatively fast and non-contact processing, no limitation regarding the processable materials, achievable high precision, reconfigurability and relatively easy to operate [3]. Nowadays, the advancement in laser system technologies offer a higher process controllability and

also flexibility, and thus many different operations, such as cutting, drilling, engraving texturing and structuring can be integrated into a single processing setup. Ultrashort lasers can deliver athermal material processing that is highly desirable in many applications where any negative thermal effects have to be minimised and thus to achieve a higher dimensional and geometrical accuracy and surface integrity. Nevertheless, despite these distinct and very attractive advantages, laser micro-machining still presents some inherent limitations in machining of micro-structures and therefore constrains its micro-manufacturing applications. A critical issue in laser micro processing, especially short and ultrashort laser processing, is much lower removal rate compared to some alternative machining technologies, e.g. mechanical micro-milling and ECM. This consequently impacts the capabilities of this technology, e.g., a limited machinable thickness or long processing times. Therefore, it is not surprising that these open issues have attracted a significant research interest, especially focused on increasing the material removal rates, and thus to be able to achieve a viable micro-machining in the context of different application areas.

An obvious solution to improve the removal rates in laser micro-processing is to increase the average power of employed laser sources. The constant advances in industrial photonics led to the development high power laser source with pulse frequencies up to GHz. For example, ultrashort laser sources with pulse duration of less than several tens of picoseconds can have an average power from few hundred watts to nearly one kilowatt [4-7]. However, increasing in laser power does not always result in a linear improvement of material removal rates. The laser-material interactions are a complex phenomena that involves heating, melting, spallation and phase explosion of materials [8]. As a consequence, there are some typical side effects, such

as material redeposition, plasma and particle shielding or heat accumulation, that normally occur during strong ablation and they can impact the machining process significantly, both in positive and negative ways. In addition, the increase of laser power, e.g. the increase of pulse energy usually leads to poorer quality of micro-structures including edge definitions, surface roughness and cleanness of machined areas. Furthermore, a higher laser intensity leads to a higher wear and degradation of optical components in beam delivery sub-systems. This raises an important question, especially how to deploy effectively high-power laser sources and maximise the achievable removal rates while maintaining, or even improving, the quality of produced micro-structures.

Another challenge in laser micro-machining is associated with the properties of emitted laser irradiation. The majority of laser sources produce a beam with a Gaussian energy distribution. The Gaussian beams offer a peak intensity at the centre of the irradiated area and thus results in a relatively non-uniform processing. This limits the achievable surface quality in laser micro-machining. Another negative side effect, referred to as a tapering effect, on the sidewall of machined micro-structures introduces other processing constraints. This indirectly affects the achievable geometrical accuracy and the scale of this negative effect is close to the laser beam spot size. Many investigations have been focused on developing different micro processing techniques to eliminate this negative side effect. However, majority of them have attempted only to improve the process in specific applications and cannot be applied in general to broaden the laser micro-machining applications. Therefore, the development of generic solutions that can be widely applied to minimise tapering effect and, thus, to

improve the accuracy of laser micro-machining/micro-drilling are required and are highly desirable.

The various open issues in laser micro-machining that were outlined so far, represent the challenges and opportunities that motivate this research. Addressing these challenges can increase the laser processing efficiency and thus to broaden the micro manufacturing applications of this technology. This also promises, indirectly, to make laser material processing more sustainable and environmentally friendly. This is very important, currently and in foreseeable future, and can drive the broader use of this micro-manufacturing technology in different industrial sectors.

1.2. Research aims and objectives

Considering the open issues and challenges in laser micro-machining discussed in the motivation, the overall aim of this PhD research is to advance this technology and achieve, both, quality and process efficiency improvements in producing components/products in different materials. Furthermore, the improvement of the laser micro-processing technology should be achieved with solutions as generic as possible to enable its boarder use in industrial applications. Specifically, different approaches/methods for altering the beam energy distribution, optimising the pulse train energy levels and temporal distributions, and realising complex relative movements between laser beam and workpiece are considered to improve of the laser micro-machining process. The aims of this PhD research are achieved through the following specific objectives:

- ***Objective 1:*** *Investigate systematically the effects of a top-hat energy distribution of laser beams together with different scanning strategies on the*

structural quality and process efficiency in laser micro-machining of silicon wafers. The quality of micro-structures, i.e. HAZ, geometrical accuracy, surface roughness, and ablation efficiency are analysed and compared with what is achievable through processing with Gaussian beams.

- ***Objective 2:*** *Investigate systematically the effects of heat accumulation, plasma shielding and other factors on achievable removal rates in MHz burst mode processing of metals*. Especially, the burst mode is used to split the pulse energy into sub-pulses and thus to utilise fully the available average power and improve the process efficiency.
- ***Objective 3:*** *Investigate a novel laser micro-machining process, called laser precession processing, for fabricating complex "through" microstructures*. The technology was deployed to overcome some inherent limitations of laser micro-machining in producing cross-shaped, free standing THz bandpass filters. The advantages of laser presession micro-machining over alternative technologies, i.e. photolithography, are analysed by assessing accuracy and functional performance of fabricated devices.
- ***Objective 4:*** *Investigate and optimise the precession laser machining process for drilling advanced aerospace materials*. The influence and significance of key process parameters in precession laser drilling of micro-holes are investigated systematically. Furthermore, their effects on a key quality factor, i.e. hole taper angles, are assessed.

1.3. Thesis organization

This thesis was structured into seven chapters. Chapters 1 and 2 introduces the motivation and objectives of this PhD research and reviews the respective state-of-the-

art in the relevant fields. Chapters 3 and 4 are focused on improving the laser micromachining process for producing “blind” structures while Chapters 5 and 6 report research on improving the laser micro-drilling process. Finally, Chapter 7 concludes the thesis. A list of references is provided at the end of each chapter for a convenience in going through the thesis. The order and specific contents of each chapter are described below.

- **Chapter 1** introduces the motivation of this research together with its overall aim and objectives and introduces the thesis structure.
- **Chapter 2** presents the general background in laser micro machining and its applications. A comprehensive review of relevant research in laser micro-machining and micro-drilling is also provided together with an overview of different approaches and methods used for improving process efficiency and processing quality.
- **Chapter 3** presents an investigation into the effects of top-hat laser beam and scanning strategies on quality of microstructure produced on silicon wafer. A typical nanosecond laser source with Gaussian beam was converted into a top-hat one by employing a refractive field mapping beam shaper and microstructures produced using different machining strategies were analysed. The improvements in process efficiency and machining quality, i.e. taper angle, surface roughness and HAZ, were analysed and discussed.
- **Chapter 4** reports a solution for achieving a removal rates’ scalability in ultrashort laser micro machining of metals using a MHz burst mode. The performance and limitations in MHz burst mode processing were analysed and discussed and thus to assess its advantages and limitations. Also, a novel

methodology was proposed and implemented in this chapter to investigate the MHz burst mode machining and quantify the contributions of different factors to the overall process performance.

- **Chapter 5** presents a novel fabrication process, called laser precession machining, to address some key limitations in laser micro processing, i.e. the tapering effect on the side walls of produced microstructures. The capability of this process was demonstrated through the fabrication of THz bandpass filters and an analysis of their functional performance was conducted. The results show the potential of laser precession machining in machining complex through microstructures.
- **Chapter 6** reports an investigation of the laser precession machining process and its application for producing micro holes onto advanced aerospace materials. The effects of three key process parameters and the hole aspect ratio are analysed and discussed. The capabilities and limitations of laser precession machining for producing high aspect-ratio micro holes were studied.
- **Chapter 7** presents the general conclusions and a summary of the main contributions to knowledge of this research and discusses some potential future research directions.

A flowchart is presented at the end of this chapter to visualize the thesis structure including key aspects that are covered in the thesis.

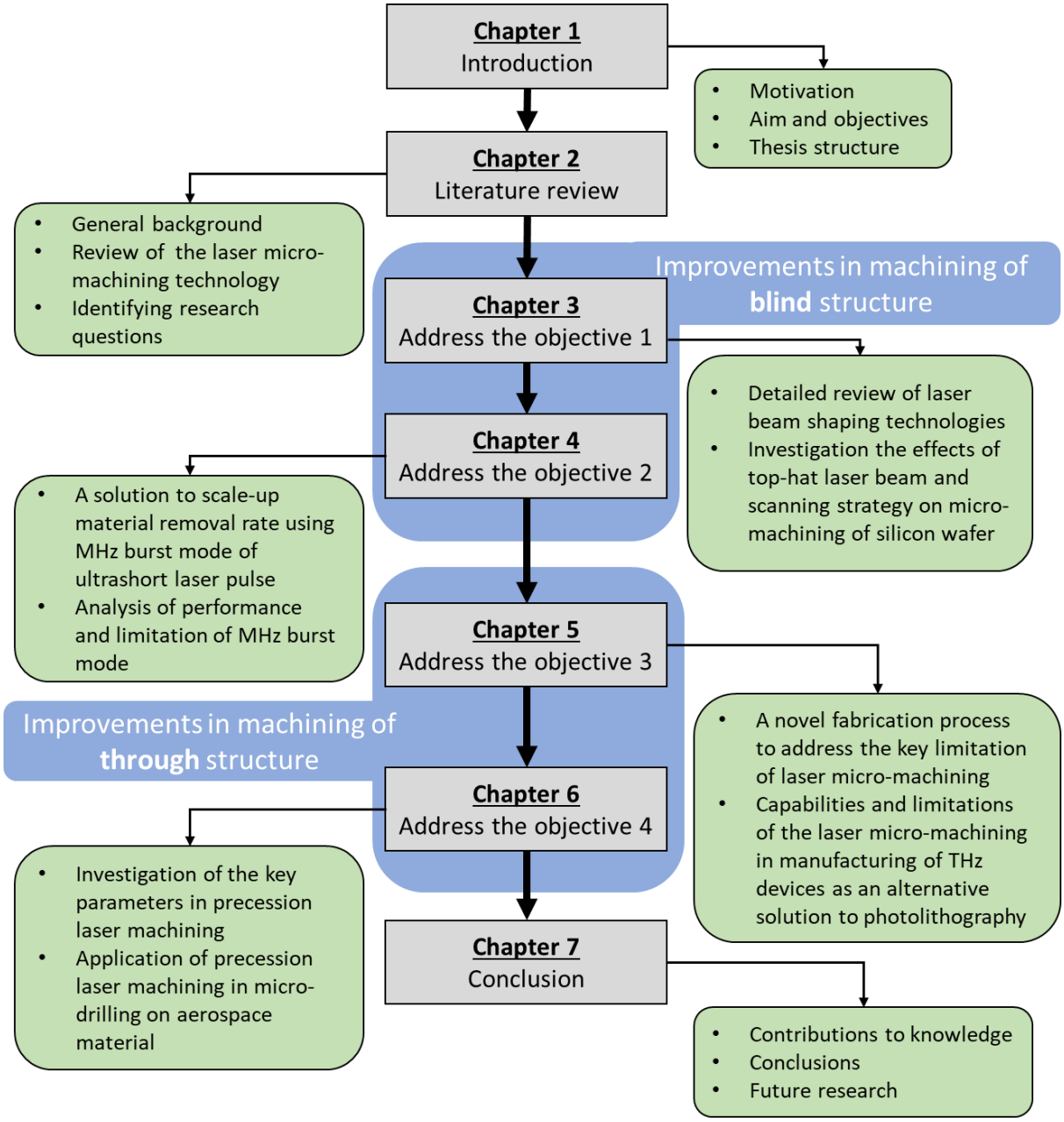
Chapter 1
Introduction
Motivation
Aim and objectives
Thesis structure
Chapter 2
Literature review
General background
Review of the laser micro-machining technology
Identifying research questions
Improvements in machining of blind structure
Chapter 3
Address the objective 1
Detailed review of laser beam shaping technologies
Investigation the effects of top-hat laser beam and scanning strategy on micro-machining of silicon wafer
Chapter 4
Address the objective 2
A solution to scale-up material removal rate using MHz burst mode of ultrashort laser pulse
Analysis of performance and limitation of MHz burst mode
Chapter 5
Address the objective 3
A novel fabrication process to address the key limitation of laser micro-machining
Capabilities and limitations of the laser micro-machining in manufacturing of THz devices as an alternative solution to photolithography
Improvements in machining of through structure
Chapter 6
Address the objective 4
Investigation of the key parameters in precession laser machining
Application of precession laser machining in micro-drilling on aerospace material
Chapter 7
Conclusion
Contributions to knowledge
Conclusions
Future research

References

1. André, P., *On the LASERs bibliometric indicators.* Optical and Quantum Electronics, 2016. **48**(3): p. 1-5.
2. Science, D. *Dimensions*. 2022; Available from: https://app.dimensions.ai.
3. Penchev, P.N., *Reconfigurable laser micro-processing systems: development of generic system-level tools for implementing modular laser micro-manufactoring platforms*. 2016, University of Birmingham.
4. Eidam, T., Hanf, S., Seise, E., Andersen, T.V., Gabler, T., Wirth, C., Schreiber, T., Limpert, J., and Tünnermann, A., *Femtosecond fiber CPA system emitting 830 W average output power.* Optics letters, 2010. **35**(2): p. 94-96.
5. Röser, F., Eidam, T., Rothhardt, J., Schmidt, O., Schimpf, D., Limpert, J., and Tünnermann, A., *Millijoule pulse energy high repetition rate femtosecond fiber chirped-pulse amplification system.* Optics letters, 2007. **32**(24): p. 3495-3497.
6. Finger, J., Kalupka, C., and Reininghaus, M., *High power ultra-short pulse laser ablation of IN718 using high repetition rates.* Journal of materials processing technology, 2015. **226**: p. 221-227.
7. Smrž, M., Novák, O., Mužík, J., Turčičová, H., Chyla, M., Nagisetty, S.S., Vyvlečka, M., Roškot, L., Miura, T., and Černohorská, J., *Advances in high-power, ultrashort pulse DPSSL technologies at HiLASE.* Applied Sciences, 2017. **7**(10): p. 1016.
8. Förster, D.J., Jäggi, B., Michalowski, A., and Neuenschwander, B., *Review on Experimental and Theoretical Investigations of Ultra-Short Pulsed Laser Ablation of Metals with Burst Pulses.* Materials, 2021. **14**(12).

CHAPTER 2

LITERATURE REVIEW

This chapter presents an overview of laser technology and its applications in the manufacturing industry. A review of the most recent research in laser material processing, particularly micro-machining/micro-drilling, is also included to provide an understanding of the technology's present advancements and limits.

2.1. Laser-material interactions

2.1.1. LASER

Laser is an acronym that stands for “Light Amplifications by Stimulated Emission of Radiation”. It was first invented and developed by Theodore H. Maiman in 1960 and it is considered to be one of the most significant inventions in 20th century together with the invention of transistor and computer [1, 2]. A basic structure of a laser source consists of an active medium which is pumped by an energy source (typically light source or electrical current). Thus, the electron energy level of atoms of the active medium is excited from the ground state energy level of E_1 to metastable state energy level of E_2. When the lifetime of the metastable state is over, the electron returns to the ground state and emit one photon with energy level equal to E_2 - E_1. This photon creates a chain reaction of the other atoms to produce photons by similar mechanism. In this way, the number of emitted photons increases exponentially. A part of the spontaneous emission escapes from the active medium and results in laser light [3]. The light emission from a laser source has unique properties that distinguishes laser light to any other light source such as high temporal and spatial coherences, monochromaticity, high directionality, i.e. low divergence, and high brightness, i.e. high emission per unit area [4]. Due to these unique properties, the application of laser can

be found in various fields and including manufacturing, communication, medical treatment, aerospace, metrology, etc. [5-9].

Different perspectives can be used to categorise lasers. The most common method for categorising laser sources is in terms of the active medium, which is essential for producing photon emission. Fig. 2.1 is an illustration of a category of some common industrial laser sources. A laser source's active medium might be in a gaseous, solid, or liquid form and have a variety of chemical compositions.

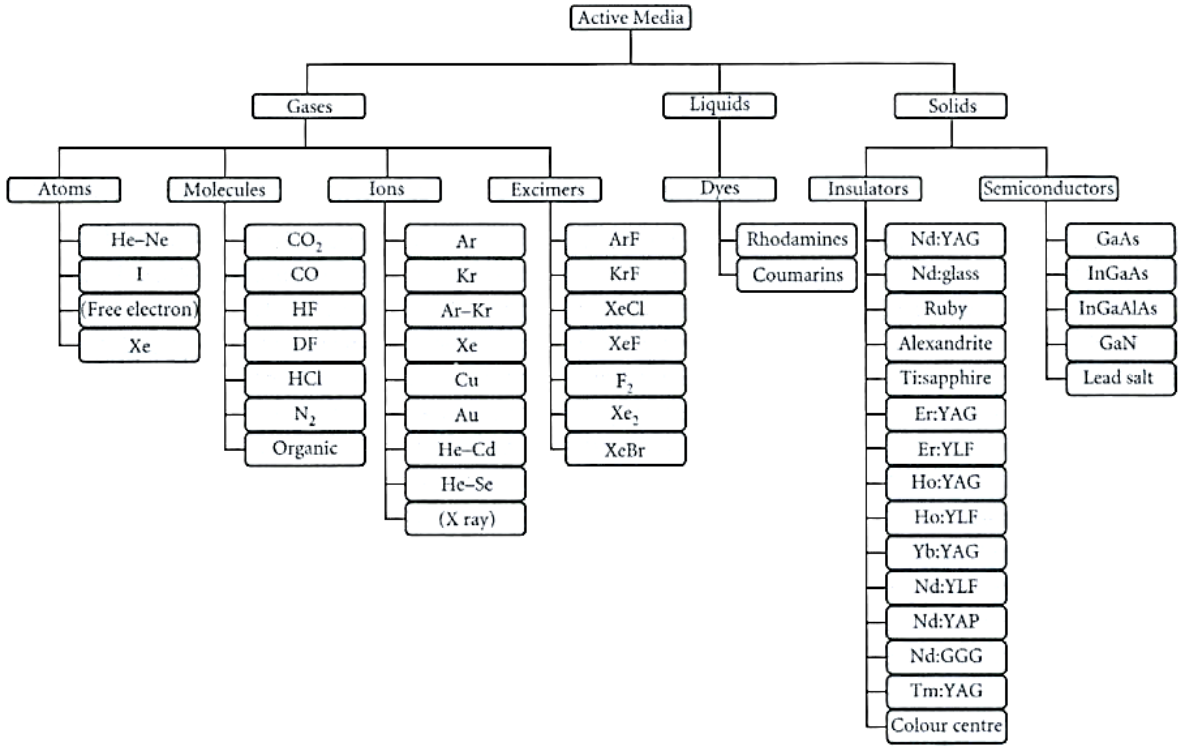

Figure 2.1. *The category of laser for material processing based on active medium [3].*

Other than categorizing laser based on the native of active medium, laser source can also be classified based on the output power, wavelength, output laser mode and application. Current laser sources are able to deliver output power from milliwatts to multi-kilowatts which allows a wide range of applications [10-13]. The wavelength of

laser light can be ultraviolet, visible light, near and far infrared, etc., and advancements in laser technology allows to produce different wavelengths in same laser source [14-16]. Laser operation mode can be either continuous wave (CW) or pulsed. CW lasers result in high continuous power which is advantageous in achieving high removal rate in some subtractive machining applications, e.g. laser cutting of thick materials, or in additive manufacturing [17-19]. Whilst pulsed lasers have more flexibility in controlling the delivering energy and laser-material interaction time, thus, they are typically used to produce high quality structures [16]. There are different applications for laser sources which is briefly presented in Table 2.1.

Table 2.1. Typical applications of laser sources [4]

Laser source	**Applications**
He-Ne	Light pointer, length/velocity measurement, alignment device
Ruby	Metrology, medical application, inorganic material processing
Nd:glass	Length and velocity measurement
Diode	Semiconductor processing, biomedical applications, welding
Carbon dioxide	Material processing, cutting, joining, atomic fusion
Nd:YAG	Material processing, joining, analytical technique
Dye	Isotope separation, pollution detection
Argon ion	Medical applications
Excimer	Material processing, medical applications
Copper	Isotope separation
Krypton ion	Laser light show

Laser provides excellent versatility as a tool for numerous machining operations. This makes laser an innovative solution compared to traditional machining tools such as lathes, milling or drilling machining which are designed to perform a particular job. In the manufacturing sector, the capacity of laser technology to provide high processing speed, accuracy, and quality is appealing. As a result, material processing with lasers has continuously advanced since the introduction of the laser.

2.1.2. Laser-material interactions

The capability of selective removal of material is crucial factor in providing high quality manufacturing at micro scale. Therefore, pulsed lasers are preferable in fabrication of microstructures due to their flexibility in controlling of material removal over CW lasers. In this context, this section focuses on the interaction between laser pulses and solid materials.

There are different physical phenomena that involve in the interaction between the laser irradiation and material surface and they can be classified into absorption, reflection, scattering and transmission [20]. However, only the absorption of laser irradiation contributes to any modification of material [21]. The absorbed energy from laser beam is affected by different factors that belongs to both laser beam and material properties such as laser wavelength and material temperature [22]. The shorter wavelengths of laser emission provide more energetic photons which are easier to be absorbed by electrons than light with longer wavelengths [23]. Whilst, higher temperature of the material leads to an increase of phonon population, thus, electron-phonon energy exchanges are more likely to happen rather than oscillation and radiation of electrons [22, 24]. Consequently, higher temperature of material surface

results in an increase of absorption and a decrease of reflection. Effects of polarisations and incident angle of the laser beam are also significant to the absorptivity of material where there is a large difference between absorptivity of material to s-polarised and p-polarised beam [25]. Another significant factor is the surface roughness of substrate that can create multiple reflection and absorption to enhance the absorptivity of the bulk material [26].

Generally, the absorption of laser energy is transferred into thermal energy and, consequently, leads to heating, melting and vaporisation of material. In particular, when a laser beam irradiates to a metal surface, free electrons absorb energy from photons and oscillates in the electric field of the laser beam [27]. The energy from free electrons is subsequently transferred into lattice of atoms and causes vibration of the lattice system due to electron-phonon coupling [28]. The electron-phonon coupling relaxation time depends on material properties and it is normally from several to tens of picosecond for metal-based materials [29]. The relative difference in time scale between laser pulse duration and electron-phonon coupling relaxation time is critical factor that defines the material removal mechanism. For nanosecond and longer pulses which are extremely longer than the material relaxation time, the kinetic energy from vibration of lattice system is transferred into heat and break the bond between atoms and, consequently, liberates material from bulk substrate [30]. This is called thermal ablation process, i.e. photothermal ablation, which is based on conventional heat conduction, melting, vaporisation, ionisation of material [31]. The removal mechanism of thermal ablation process is illustrated in Fig. 2.2a.

The thermal mechanism is distinct from athermal, i.e. photochemical, mechanism which occurs during ultrashort pulse ablation (Fig. 2.2b) [32]. Specifically, when laser

pulse is shorter than the electron-phonon relaxation time, i.e. typically less than ten picoseconds, and the pulse energy is extremely high, the electron excitations caused by laser photon directly lead to the breaking of the atomic and molecular bonds before electron-phonon coupling happen and introduce high pressure (GHz scale) [33, 34]. Consequently, the ablation takes place before the vibrational energy of the lattice system transfer into heat. Thus, this process can be considered to be non-thermal and it is usually referred as “cold ablation”.

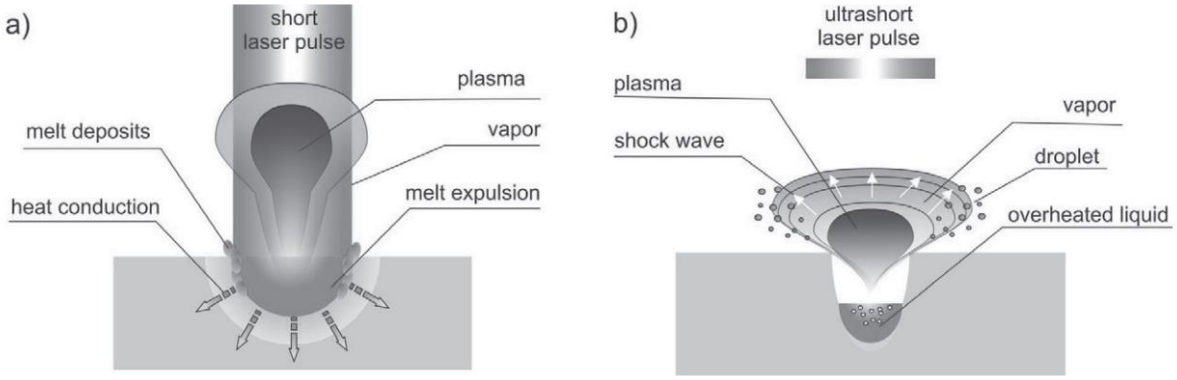

***Figure 2.2**. Diagram of Laser-Matter interactions with (a) short pulse and (b) ultrashort pulse [35].*

Removal of material by laser pulse is characterised by ablation threshold fluence, where fluence is a measure of laser energy per unit area and it is normally expressed in J/cm^2. Ablation of material only occurs when laser fluence is higher than the threshold fluence. This threshold depends on properties of laser emission such as wavelength, pulse duration, number of pulse per spot and material physical properties such as thermal conductivity and surface roughness [36, 37]. There are different methodologies to practically define ablation threshold in short and ultrashort laser

processing of a material [38]. However, the most popular empirical method based on geometrical of the ablated region which was developed by Liu and it is widely used today [39].

2.2. Laser micro-machining platform

2.2.1. Critical components of a laser micro-machining system

Configuration of a laser processing system for micro-machining purposes comprises a number of sub-systems and modules which typically are laser sources, beam delivery sub-systems, workpiece holding devices, gas assisting system, process monitoring and control centre, and power supply system [40]. Fig. 2.3 represents an example of the key sub-systems and components in a laser platform for micro-machining.

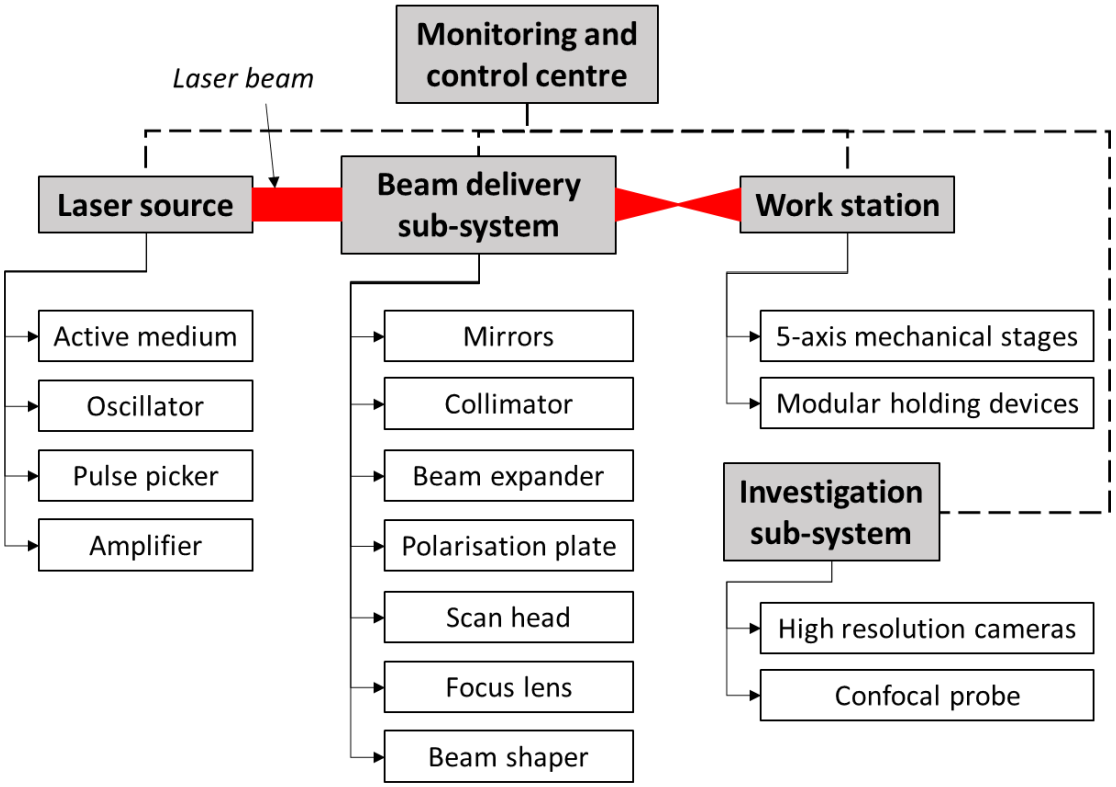

***Figure 2.3**. Schematic diagram of key components in a laser system.*

Laser source plays a role to produce energetic tool, i.e. laser beam, to machine material. While beam delivery system precisely guides, modifies and transforms laser beam into desirable shape and position. On the laser propagation, mirrors are used to change laser beam direction to pass through other optic elements. Collimator is used to reduce the divergence of output beam, thus, to improve the beam quality at the focus position. The beam expander can modify the beam diameter to produce various focused beam spot sizes and indirectly alter the processing fluence. Polarisation plates are used to manipulate the phase of emitted photons to results in different polarisations. Typically, a haft-wave plate is integrated onto beam propagation to provide p- and s- linear polarisations, while a quarter-wave plate is used to provide circular polarisation of the laser beam. Majority of laser sources produce a single Gaussian output beam. However, other beam shapes such as top-hat, airy disc, Bessel or annular, can be attained using beam shaper [41]. Furthermore, advancements in beam shaping technique allow to transform a single laser beam into multiple beams to accelerate the processing time [42]. Scan head normally consists of a set of motorised mirrors to move laser beam optically by deflecting the beam in XY plane to the desirable position. Modern galvanometer scanner can move laser beam up to 20 m/s when combined with F-theta lens [43]. Laser beam for material processing needs to be focused by a lens to reduce beam diameter, thus, to achieve high enough energy density to machine material. The focusing lens also plays an important role in defining working volume of the laser system based on lens's properties, e.g. focal length and field of view.

State-of-the-art laser systems normally consist of 3-axis or 5-axis mechanical stages to realise complex movement and to fabricate 3D structures [44]. The achievable

accuracy of the modern mechanical stages can be better than 1 μm with minimum resolution down to 0.25 μm [45]. Automated mechanical axes together with scan head create great flexibility in manipulation of laser beam for micro-machining purpose. Workpiece holding devices are used to implement various machining configurations of a multi-process manufacturing systems [40]. The investigation sub-system is integrated into the laser system for monitoring the manufacturing process and component calibration. Finally, all of the components in laser system are monitored and controlled by a computational centre which allows to design and implement manufacturing processes [3].

2.2.2. Laser beam characterisation

In order to induce any material modification, the laser beam must be focused to a minimum spot to raise energy density to such a desirable level. Additionally, properties of the laser beam at focus position, i.e. beam waist, directly affect the quality and efficiency of the machining process. Therefore, the focusing region of a laser beam is critical in processing of material. This section introduces some basic laser parameters which are important in understanding and designing of a laser micro-machining process. Fig. 2.4 describes the key spatial parameters of a laser beam at focus position where w_0 is beam radius at the minimum spot, θ is the full beam divergence angle, and z_R is Rayleigh length of the focused beam. Rayleigh length is defined as the distance from beam waist at which beam cross-sectional area doubles along propagation direction [46]. Depth of focus (DOF) of a focused beam is twice of Rayleigh length about the beam waist.

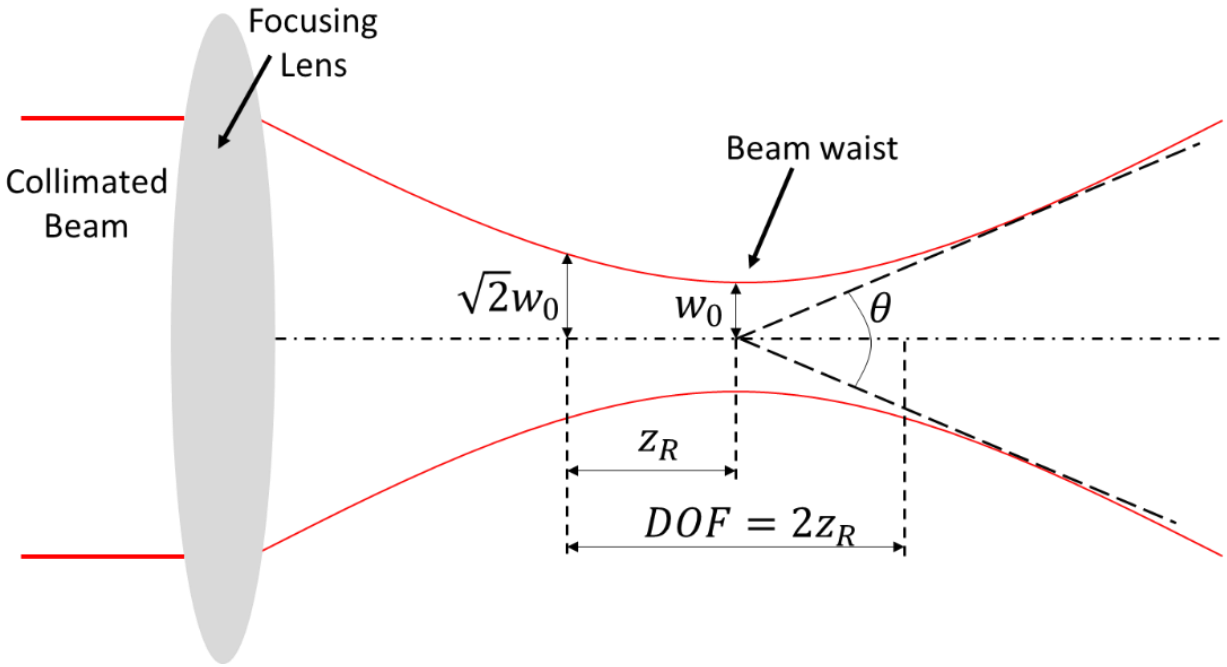

Figure 2.4. *Basic parameters of a focused Gaussian beam.*

The beam waist diameter d and radius w_0 are calculated based on quality factor of the beam M^2, wavelength of laser light λ, focal length of focusing lens D_f and input beam diameter d_0 by following equation:

$$d = 2w_0 = \frac{4M^2\lambda D_f}{\pi d_0} \tag{2.1}$$

The Rayleigh length is:

$$z_R = \frac{\pi w_0^2}{\lambda M^2} \tag{2.2}$$

Hence, the depth of focus DOF can be defined as:

$$DOF = 2z_R = \frac{2\pi w_0^2}{\lambda M^2} = \frac{8M^2\lambda D_f^2}{\pi d_0^2} \tag{2.3}$$

The beam diameter at distance z from beam waist along propagation is defined as:

$$w_z = w_0 \sqrt{1 + \left(\frac{z}{z_r}\right)^2} \tag{2.4}$$

Average fluence F and peak fluence F_{Peak} of a laser pulse are determined by pulse energy E_P and the irradiated area, thus, these fluences at beam waist are:

$$\mathrm{F} = \frac{E_P}{\pi w_0^2} \tag{2.5}$$

$$F_{Peak} = 2F = \frac{2E_P}{\pi w_0^2} \tag{2.6}$$

The laser pulse energy E_P is calculated based on laser average output power P and pulse repetition rate f by following equation:

$$E_P = \frac{P}{f} \tag{2.7}$$

The peak power of a laser pulse P_{Peak} is calculated based on the pulse energy E_P and the pulse duration τ:

$$P_{Peak} = \frac{E_P}{\tau} \tag{2.8}$$

2.2.3. Beam shaping technology

Gaussian is the most popular spatial shape of laser emission for modern laser systems due to its consistency in beam propagation path. However, such intensity profile is not always a beneficial for machining process, therefore, the beam needs to be transformed into other shapes in many applications [47]. Beam shaping solutions normally require integrating an optical sub-system, called beam shaper, onto laser propagation to attain tailored beam profile. Beam shaper technologies fall into two main

categories: multifaceted beam integrators and field mapping employing diffractive or refractive optical elements [48]. Some types of multifaceted beam integrator can be listed as spatial light modulator (SLM) and multiplane light conversion (MPLC) [49]. These techniques mainly focus on splitting and combining of laser beams to customise the beam into complex shapes (e.g. square shape, star shape) using a set micro-lens arrays and binary masks [49, 50]. The advantages of multifaceted beam integrators technique are highly automated and great flexibility in controlling 2D shape of laser beam. However, splitting and combining beams can cause destructive interference and damage beam coherence [51]. The field mapping approach remaps the energy of the Gaussian beam under controlled manner to attain desirable profile using complex optic elements [52]. Diffractive field mapper can be used to transform Gaussian beam into top-hat beam with squared shape, thus, to be beneficial in machining of micro channels [53]. A wide range of beam configuration can be obtained by diffractive optical elements, but the key shortcoming of this technique is large decrease in beam intensity and efficiency due the diffraction. Refractive optical field mapping with high transmittance is suitable for high-power laser beam [54]. The key characteristic of refractive field mapping beam shapers is that they accurately introduce and further compensate for wavefront aberration to change the laser beam profile in a controlled manner. As a result, the output beam is highly collimated with low divergence and the beam consistency is not compromised [55]. Furthermore, the beam shapers based on refractive field mapping have relatively simple design that make them easier to be integrated onto beam propagation [56].

2.2.4. Burst mode of ultrashort pulsed laser systems

The advancements in ultrashort laser technology allow to achieve such high output power and high frequency to upscale the process efficiency of the ultrashort pulsed laser processing [11, 57]. This motivates the development of the accompany technologies including high-speed scanning devices and burst regime of pulses [58]. In recent years, ultrashort pulsed laser sources have emerged and is producing bursts of pulses with temporal distance between pulses in the nanosecond and picosecond scales which equivalent to intra-burst frequency of MHz to GHz scale [59, 60]. Furthermore, advanced laser systems allow great flexibility to adjust of number of pulses per burst and the temporal separation between pulses [61]. A method employing active fibre loop on a fibre chirped pulse amplification system was developed to achieve 72 nanojoule burst of ultrashort pulses with intra-burst frequency of 2.65 GHz and burst repetition rate of 500 kHz [62]. Lasers operated in burst mode can be advantageous to approach GHz frequency and microjoule level pulse energies without demanding average power at kilowatts scale, which is beneficial in some applications [63]. In a recent study, an all-fibre laser system was able to achieve 1.2 GHz burst mode of 473 fs pulses at relatively high average power up to 108 watts [60]. This is very potential tool in micro-machining, frequency metrology and bioimaging due to the capability to achieve high average power and high repetition rate at the same time. Burst-in-burst regime, i.e. biburst, was also developed which is a combination of GHz and MHz burst modes in one system with capability to customise the number of pulses per burst for both GHz and MHz burst [64]. Specifically, a pulse within a 65 MHz burst was able to be divided further up to 25 pulses with 4.88 GHz intraburst frequency.

This regime was proven to improve the throughput and fabrication quality in some materials by taking the advantages of both MHz and GHz burst regimes [65].

2.2.5. State-of-the-art precession laser beam

The capability to manipulate the laser beam is essential to enhance the accuracy of the fabrication process, especially, in eliminating of tapering effect in micro-drilling. This is the main limitation of conventional beam delivery system which normally employing stationary beam with linear mechanical movement or 2D galvanometer scanning. Orbiting the laser beam following precession movement is an attractive solution to achieve zero or negative tapering at sidewall in manufacturing of through structures, and this technique has been developing in the last few years [66]. Table 2.2 summarises the key technical specifications of four commercial precession laser micro-machining systems (numbered from 1 to 4) for micro-drilling and cutting applications. The common feature of these models is the precession motion of the laser beam that has high rotary speed (from 30000 to 48000 rpm) and ability to adjust beam incident angle and focus position. In general, the system number 2, 3 and 4 consist of three linear mechanical axes (X, Y and Z) and two optical axes which are responsible to vary beam incident angle and rotary speed of precession beam. The linear movements in these systems are done by mechanical axes, thus, the dimensional accuracy depends strongly on the mechanical stages. In contrast, the system number 1 consists of 5 mechanical axes (X, Y, Z and A, B) and 4 optical axes that are able to control beam incident angle, focus position and to scan the precession beam in XY plane using scan head. Thus, the dimensional accuracy of system 1 depends on the scan head rather than the mechanical stages. In addition, the system

1 has less freedom in changing beam incident angle but large working field compared to the others due to the ability to scan the precession beam optically.

Table 2.2. Summary of some available precession laser machining systems. Data was collected from companies' websites.

Supplier	**LASEA**	**Scanlab**	**Aerotech**	**Novanta**
Model (Number)	**LS-Precess (1)**	**precSYS (2)**	**AGV5D (3)**	**Precession Elephant 2 (4)**
Wavelengths (nm)	343, 515, 1030	515, 1030 – 1064	515 – 532, 1030 – 1064	515 – 532, 1020 – 1080 1500 – 2100
Maximum input beam size (mm)	6	2.5	2.8	N.A.
Spot size (µm)	35 – 50	8.2 – 20	7 – 15	10 – 30
Maximum input power (W)	100	50	100	N.A.
Maximum pulse energy (µJ)	N.A.	300	400	N.A.
Maximum rotary speed (rpm)	30,000	39,000	48,000	36,000
Polarisation	Linear, circular	Circular	Linear, circular	Linear, circular
Incident angle (degree)	2 - 4	± 7.5	± 9	N.A.
Dynamic focus range (mm)	No	±1	±1	±1
Effective focal length (mm)	50, 100 (lens dependent)	25	N.A.	60, 120
Number of axis	5 mechanical axes 4 optical axes	3 mechanical axes 2 optical axes	3 mechanical axes 2 optical axes	3 mechanical axes 2 optical axes
Working distance (mm)	60 – 110 (lens dependent)	N.A.	4	N.A.
Working field (mm)	25 × 25 mm^2 squared area	2.5 mm diameter circular area	2 mm diameter circular area	N.A.

2.3. Laser processing of materials

2.3.1. Laser micro-machining

Laser micro-machining process is classified as non-microelectromechanical system (non-MEMS) together with micro EDM, mechanical micro-cutting, micro-embossing and micro injection moulding, etc., to distinguish with MEMS or lithography-based technologies (Fig. 2.5) [67]. This process can be defined as a machining process is done using laser which involves removal or modification of material leading to a functional surface or a 3D structure, and the feature dimensions are less than 1 mm [68]. Specifically, laser beam is irradiated to the workpiece surface to selectively ablate

material under a control manner and the process can be further divided into micro-milling, micro-drilling, or scribing, etc. The processing parameters in laser micro-machining can be divided into two categories: laser beam properties and machining strategies. While the quality of a laser micro-machining process is typically assessed by different factors such as surface roughness, geometrical and dimensional accuracies, tapering at sidewall, HAZ, burr and spatter formation, recast layer and redeposition, thermal stress and micro cracks, and removal rate [69].

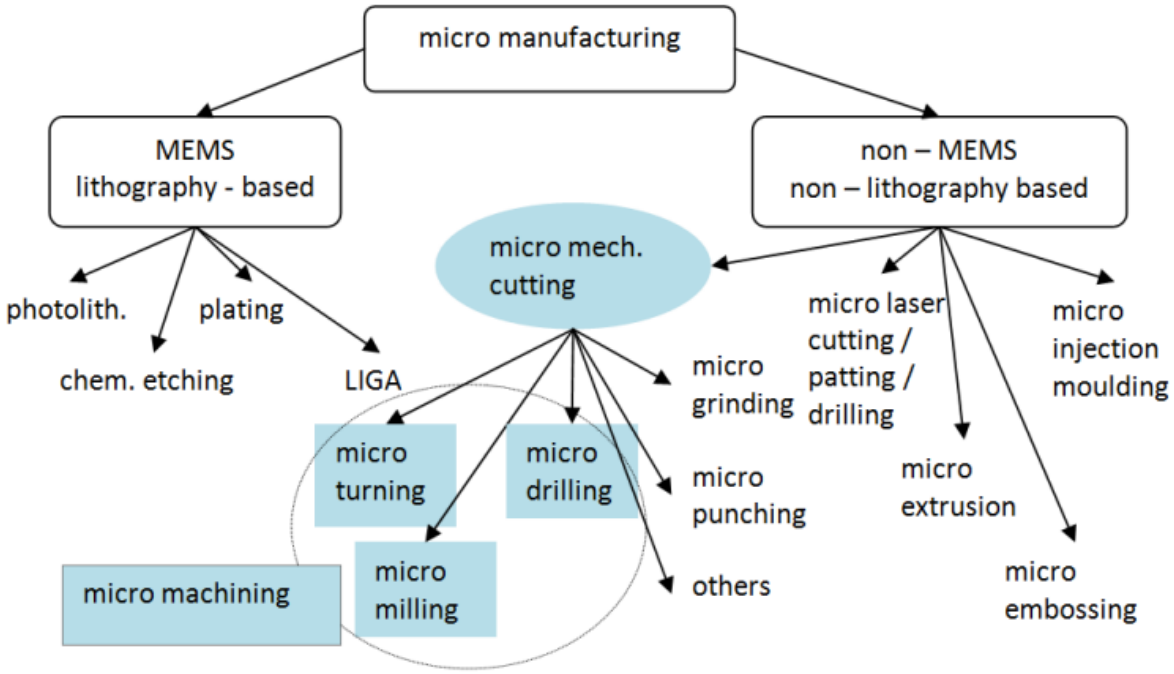

Figure 2.5. *Classification of micro manufacturing techniques [67].*

The first group of programmable parameters belongs to the laser beam which typically are wavelength, pulse energy, pulse duration, pulse repetition rate, fluence, temporal and spatial shapes and polarisation [50, 70, 71]. Gaussian beam is the most popular shape that is widely use in laser systems nowadays due to its self-consistent field distribution along the propagation path and minimum beam distortion when passing

through optics elements in beam delivery system [72, 73]. However, Gaussian distribution presents a peak intensity at the centre and lower intensity at outer part of the irradiated area. Consequently, it results in non-uniform processing and higher HAZ (Fig. 2.6a). Top-hat intensity profile with more even energy distribution of the irradiated area is an option to overcome the inherent shortcomings of Gaussian beam processing, e.g. minimising HAZ, more even ablation and increasing the productivity (Fig. 2.6b) [74, 75]. Other than Gaussian and top-hat beam, higher order of Gaussian beam, i.e. TEM_{mn}, and Bessel beam are also employed in laser micro-drilling and scribing of thin film [76, 77].

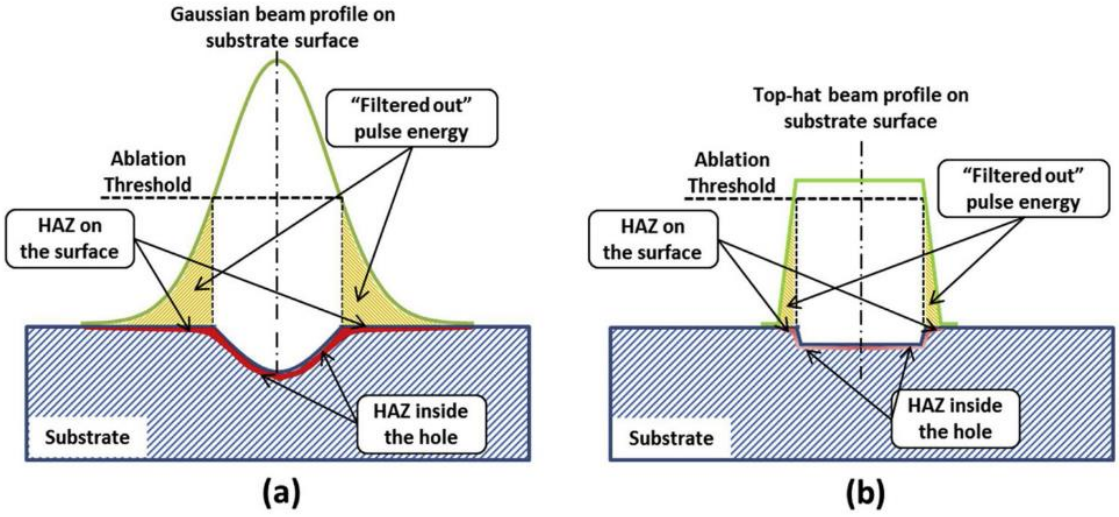

Figure 2.6. *The effect of laser beam intensity distribution on HAZ and ablated shape: (a) Gaussian beam and (b) Top-hat beam [48].*

Pulse energy and fluence are two of the most important parameters in designing a laser micro-machining process which directly impact the fabrication quality and efficiency. Therefore, these factors have been investigated by many studies [78-80]. Pulse energy is a measure of total laser emission over the pulse duration, while fluence refers to the energy density over an irradiated area of an incident pulse, thus, they are

interrelated. Generally, higher laser fluence leads to larger volumetric removal rate of material which is defined by the rate of ablated volume over machining time. This is evidenced by higher laser ablated depth per pulse for higher fluence (Fig 2.7a) [81]. However, the energetic efficiency is actually lowered when fluence exceeds the optimum level. This results in a decrease in specific removal rate (rate of ablated volume over irradiated energy) (Fig. 2.7b and 2.7c) [82, 83]. In particular, the relationship between specific removal rate and fluence in ultrashort pulse processing is described by equation:

$$\frac{dV}{dE} = \frac{1}{2} \cdot \frac{\delta}{F_0} \cdot ln^2\left(\frac{F_0}{F_{th}}\right) \tag{2.9}$$

where: δ is energy penetration depth; F_0 - pulse fluence and F_{th}- ablation threshold. A comprehensive study from Hodgson et al reported the maximum specific removal rate for 22 popular metal based materials achieved by ultrashort pulse processing with ultraviolet and infrared wavelengths [84]. The results showed that the most efficient ablations take place at fluence less than 2 J/cm^2 for all investigated materials which is much lower than achievable fluence level of modern laser systems. The efficient utilisation of high-power laser sources in micro-machining is made difficult by this issue.

Studies have been conducted to optimize the ablation rate of high-power laser sources, i.e. high pulse energy, by different techniques such as using MHz and GHz burst modes and applying novel scanning strategies [85-87]. Butkus et al investigated the influence of burst mode at 62.5 MHz and 5 GHz intraburst frequencies in percussion drilling on Invar foil with ultrashort pulses [61]. The MHz burst mode was able to significantly improve process efficiency for both thin (20 µm) and thick samples (250 µm). While GHz burst mode, when compared to standard kHz processing, produced

higher removal rates for thin substrates and lower removal rates for thick substrates. Lickschat et al proposed a combination of MHz burst of picosecond pulses and GHz burst of femtosecond pulses to benefit from both regimes in fabrication of 3D structure [88]. Specifically, MHz burst was used to enhance the process efficiency in the primary process, while GHz burst was deployed as a secondary process to smoothen the surface fabricated by MHz burst. Adding GHz burst as a secondary process was able to reduce surface roughness significantly from 0.25 – 0.31 µm to 0.13 µm and minimize defects from MHz burst processing such as micro cone structures. Another research also revealed that the advantages of MHz burst to improve material removal rate is more presentative for pulse duration less than 1 picosecond in than pulse duration of 10 picosecond [59]. Incubation effect in GHz burst of femtosecond pulses was investigated by Gaudiuso et al and the results show that the threshold fluence of stainless steel decreases with the increase of number of sub-pulses constituting the GHz burst [89]. It is well proven that burst mode is an attractive solution to scale-up the removal rate by keeping laser fluence close to optimum level and taking the advantages of side effects such as incubation and heat accumulation [90]. However, other machining conditions such as machining strategy have not been investigated in the burst mode of laser processing even though these factors play important roles in removal of material.

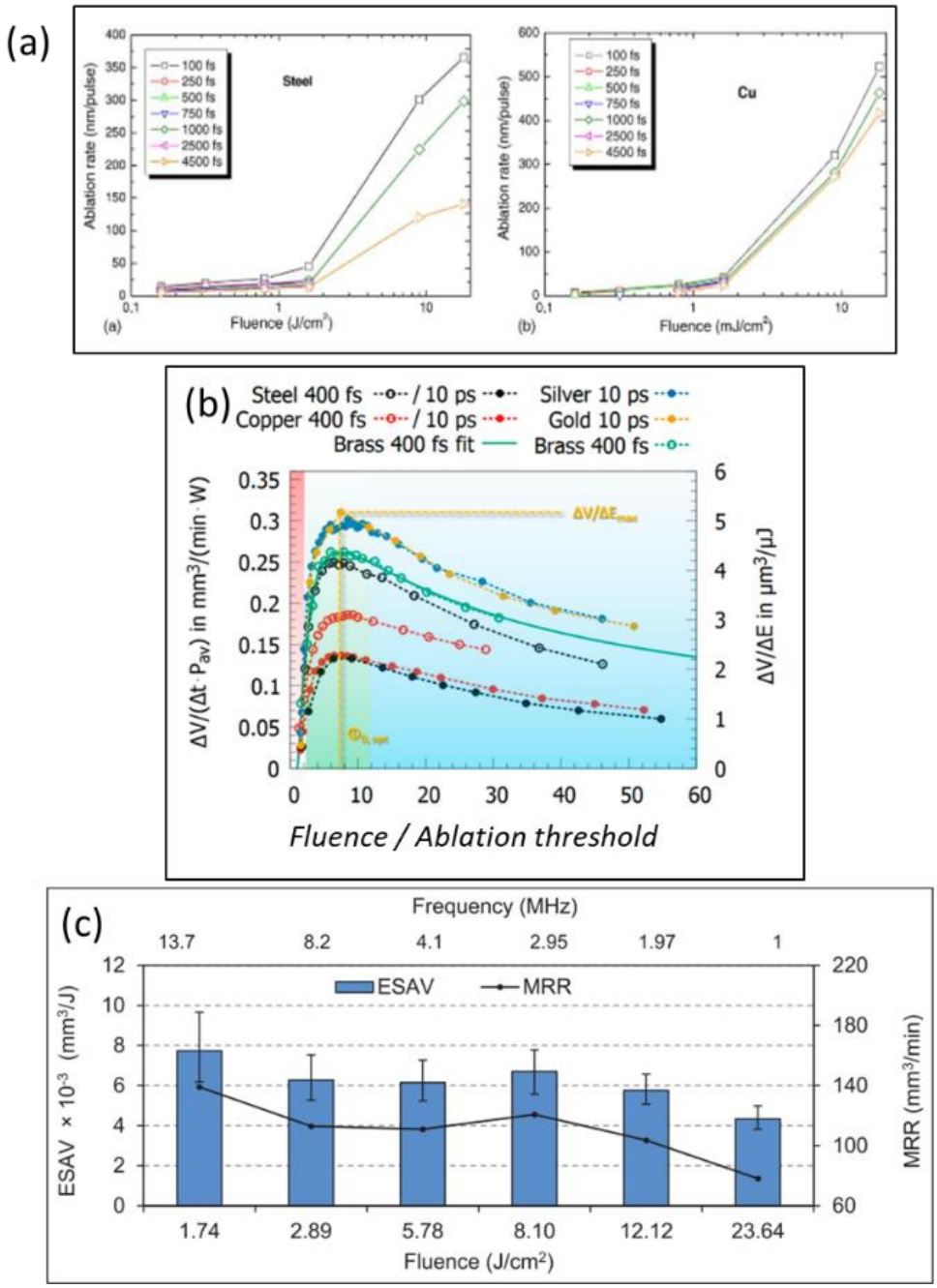

Figure 2.7. *Influence of laser fluence on ablation rates of typical metalic materials: (a) Ablation rate (mm/pulse) as a function of fluence for pulse duration from 100 fs to 4500 fs [91]; (b) Response of specific removal rate (ΔV/ΔE) (µm³/µJ) to the increase of Fluence/Ablation threshold ratio [28]; and (c) Effect of pulse fluence on energy-specific-ablation-volume (ESAV) (mm³/J) and material removal rate (MRR) (mm³/min) on Nickel super alloy [86].*

Heat accumulation is an important side effect during laser ablation in both thermal and athermal processing [92]. A large amount of residual heat during laser ablation can lead to negative effect such as large HAZ, melting and redeposition of material even in ablation with ultrashort pulses. A study from Lickschat et al showed that accumulation of residual heat with other side effects, i.e. plasma formation and interaction between subsequent pulses, impact significantly the ablated volume per pulse in the burst mode processing of stainless steel [59]. The influence of heat accumulation also presents in obtained surface roughness of microstructure. Specifically, lower surface roughness was observed at higher heat accumulation temperature at medium and high scanning speed (greater than 0.1 m/s) [93]. Metzner et al developed a model that considered heat accumulation to simulate laser ablation of chromium alloy with a burst of ultrashort pulses [94]. This study provided numerical simulation of the beneficial role that heat accumulation plays in improving material removal rates. However, the simulation only took temperature into account as the primary reason for ablation caused by residual heat, but other crucial elements like redeposition and plasma shielding were not considered. The contribution of heat accumulation to removal rate of both conventional and burst laser processing is difficult to be quantified due to the complex of laser-material interaction.

The second aspect in controlling laser micro-machining process is machining strategy which usually refers to the relative movements between laser beam and workpiece and these movements can be either 2D or 3D [95]. The laser beam is moved over the defined region to selectively ablate the material when the machining area is larger than the beam spot size, resulting in the production of microstructures. These movements are normally done optically and mechanically using scanning mirror in XY plane and

mechanical stages, respectively [96, 97]. In some state-of-the-art systems, the optical and mechanical motions can be synchronised to machined complex 3D shaped in some applications such as laser turning of symmetrical parts to improve the process efficiency [98]. An example of scanning strategy and different laser beam trajectories in laser micro-milling are presented in Fig. 2.8a and 2.8b. Designing a machining strategy for pulsed laser processing involves different factors such as beam spot size, pulse-to-pulse distance, scanning speed, step-over between scanning lines and direction of scanning vectors, etc.

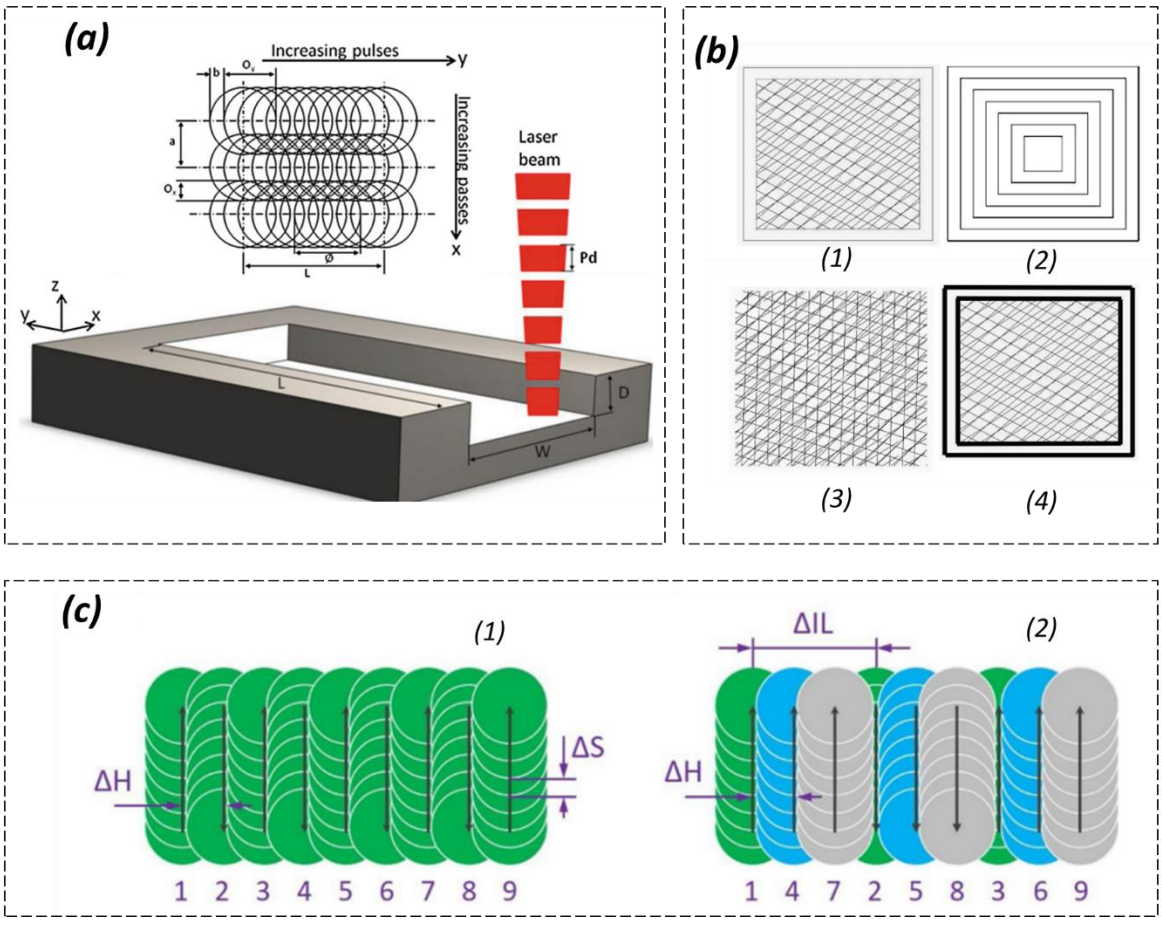

Figure 2.8. (a) *Schematic illustration of scanning strategy for laser micro-milling of 3D structure where a is step-over between adjacent scanning lines, b is pulse-to-pulse distance, O_x and O_y are overlap distances in x and y direction respectively;* ***(b)*** *Different*

laser beam trajectories for laser micro-milling: (1) Random hatching and profile cut along the border, (2) Profile cut only, (3) Random hatching only and (4) Random hatching with enhanced profile cut to produce vertical sidewall; ***(c)*** *Illustration of traditional 2D scanning strategy (1) and novel interlaced scanning strategy where ΔH, ΔS and ΔIL is hatch distance, pulse distance and interlaced distance, respectively [99-101].*

Pulse distance and beam diameter define the overlap between adjacent pulses and this impact the ablation depth directly. Study of Umer et al shows that overlap is the most important factor in response of ablation depth per layer in laser micro-milling of alumina (Fig. 2.9a). The higher overlap level and laser intensity normally result in larger ablation depth due to higher accumulated fluence over an area which is depicted in Fig. 2.9b [93]. However, the high overlap level usually leads to excessive heat accumulation, thus, some negative side effect such as melting and redeposition of material can predominate and result in lower fabrication quality, especially in thermal ablation mechanism. Fig. 2.9c depicts that low overlap level (12.5%) results better surface roughness than high overlap level (85%) when machining steel with IR laser [102]. A novel strategy which interlaced laser beam scanning method was proposed and investigated by Wlodarczyk et al on thick borosilicate glass (Fig. 2.8c) [101]. The removal rate was able to increase more than 4 times and 1.3 times for picosecond processing and femtosecond processing, respectively, when altering from conventional strategy to interlaced strategy. Also, the improvement is removal rate was not in expense of the surface quality. Zemaitis et al developed a theoretical model that based on equation 2.9 to predict ablation efficiency for laser machining of rectangular cavity on copper substrate [103]. Their model takes in to account the decrease in

ablation threshold and saturation of the ablation depth when number of pulses per spot increases, thus, it can be used to examine the influence of scanning strategy and to optimize the ablation rate.

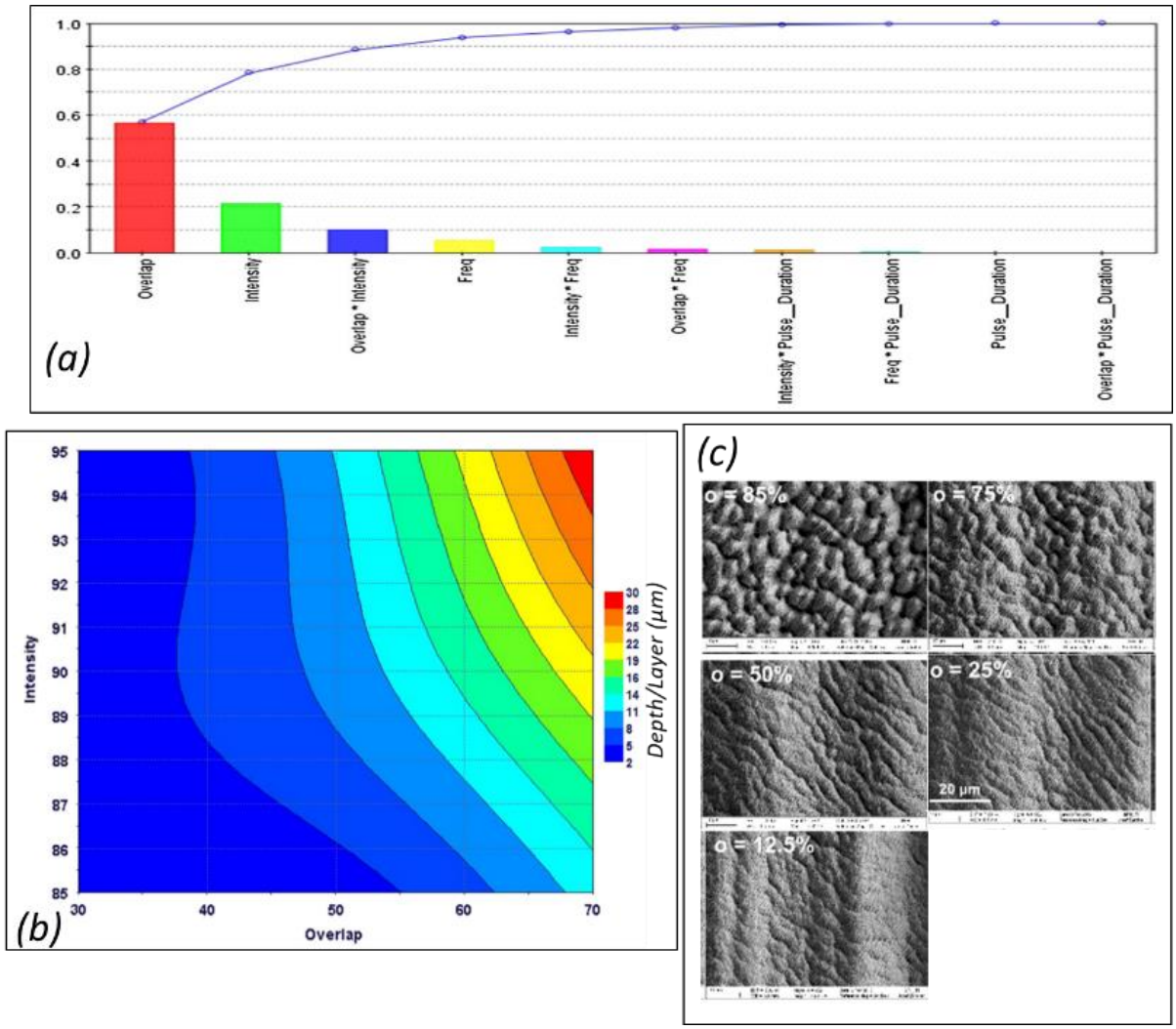

Figure 2.9. *Influence of overlap level in laser micro-machining of alumina with short pulses: (a) Significance of different parameters for ablated depth per layer; and (b) Effect of overlap and laser intensity on ablated depth per layer [102, 104].*

In addition, laser micro-machining is layer-based process where material is removed layer-by-layer. Therefore, the scanning direction between layers and refocusing of laser beam after a number of layers also play an important role in quality of

microstructures, e.g. surface roughness, and process efficiency. Scanning strategy with parallel lines to the lamination direction for the first layer and 45 degree increment in lines direction for the following layers was able to produce minimum surface roughness compared to other strategies, e.g. strategy with identical layers [105].

2.3.2. Laser micro-drilling

Laser micro-drilling can be considered as a particular application of laser micro-machining for high aspect-ratio through structures on materials [106]. The produced micro-structures are usually through circular holes but they can also be more complex shape rather than circular, e.g. squared holes or cross-shaped holes with the size of the features from one micron to several hundred of microns [107, 108]. The advantages of laser micro-drilling over other technologies such as EDM, ECM and electron beam machining (EBM) that it can produce holes on wide range of materials, high productivity, high accuracy, repeatability, and reproducibility [108]. Laser micro-drilling, in particular, can fabricate holes with diameter of less than 10 μm [109]. This is much smaller than the minimum achievable diameter of conventional and EDM micro-drilling which is in the hundreds of micrometer range [110]. Furthermore, micro-drilling using laser beam can be deployed on both conductive and non-conductive material (e.g., metals, polymers, and ceramics). Hence, there is no limitation in machinable material as EDM technology. An essential issue of conventional drilling technology is tool wear, especially, when machining of high strength materials which increase the machining cost and reduce accuracy of the process. This phenomenon is completely avoided with laser micro-drilling due to non-contact property [111]. Therefore, laser micro-drilling is an attractive solution to produce mass production of micro-holes [112]. Some typical drilling techniques of pulsed laser can be listed as Fig. 2.10:

- Single pulse drilling: Drilling by a single pulse. This technique usually employs a single short to long pulse (ns to µs) to drill holes on thick substrate and process throughput is the priority [113].
- Percussion drilling: Drilling by sending multiple pulses to the sample position. This technique is deployed when hole diameter equal to the laser beam spot size [114].
- Trepanning drilling: Laser beam is used to penetrate the substrate first and then cutting along hole profile. This process is normally used when hole diameter is larger than beam spot size [115].
- Helical drilling: Laser beam is moved along hole profile with spiral trajectory into the substrate until hole is penetrated [116]. Similar to trepanning, helical drilling is deployed when hole diameter is larger than beam spot size. However, this process can be performed at higher scanning speed to avoid excessive local heat accumulation, thus, to improve quality and accuracy of fabricated holes.
- Precession drilling (or 5-axis drilling): Drilling with precession movement of laser beam. This technique allows laser beam approach substrate surface at a precise incident angle, thus, to produce hole with zero taper angle [117].

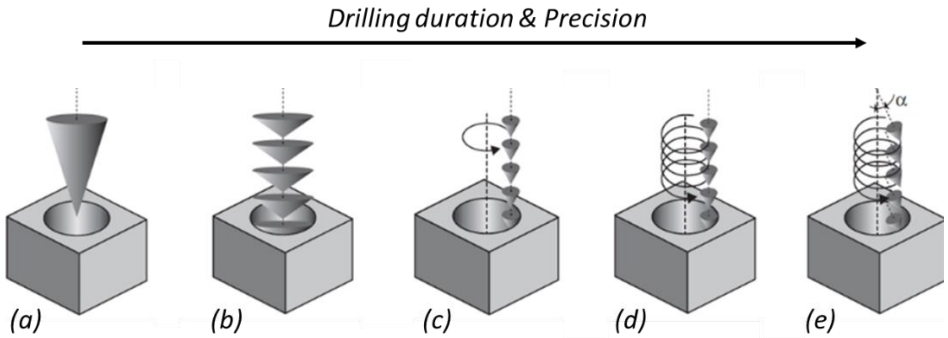

Figure 2.10. *Typical laser drilling techniques: (a) Single pulse drilling, (b) Percussion drilling, (c) Trepanning, (d) Helical drilling and (e) Precession drilling [118].*

Similar to laser micro-machining, the laser parameters and drilling strategies have the most impact on laser micro-drilling. Thus, optimising the processing parameters is an important approach to improve the quality of drilled holes and process throughput [51]. The important controllable parameters in laser micro-drilling are pulse energy, pulse duration, number of pulses, beam quality, wavelength, focus position, polarisation, and beam incident angle, etc. Whilst, the characterisation of laser micro-drilling process is presented by sidewall taper angle, circularity of entrance and exit, HAZ, recast thickness, micro cracks, spatter formation, aspect ratio and process efficiency [119]. Fig. 2.11 is a summary of the significance of different laser processing parameters on characterisation of laser micro-drilling.

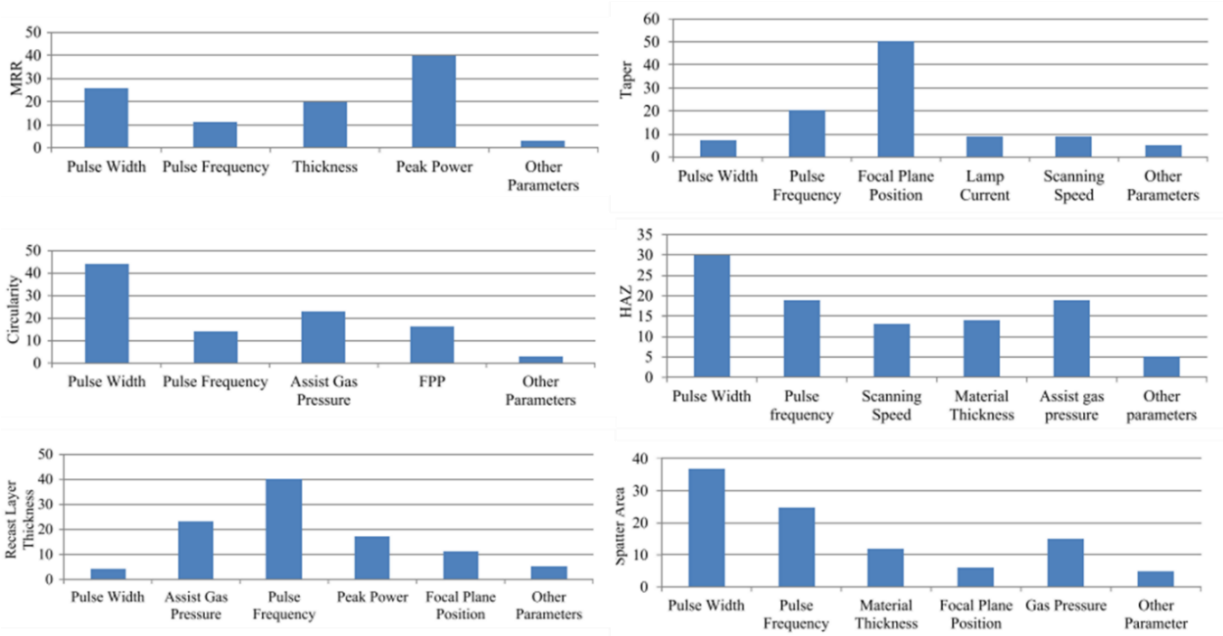

Figure 2.11. *Percentage of contribution of laser processing parameters for different quality factors including material removal rate (MRR), taper angle, hole circularity, heat affect zone (HAZ), thickness of recast layer, and spatter area [106]*

Previous studies showed that shorter pulse duration (µs scale) and lower pulse energy lead to smaller hole diameters at both entrance and exit when drilling with percussion strategy on metallic materials [114]. Furthermore, average taper angle is reduced when drilling with higher number of pulses. However, drilling with long pulses (µs) and high pulse energy (up to 2J) results in thick recast layer and barrel shape inside drilled holes. The increase of hole diameter with the increase of pulse energy and number of pulses is also true for laser micro-drilling with nanosecond pulses [120]. Ultrashort laser processing with femtoseconds to picoseconds pulse durations are used to drill holes with high quality, however, the material removal rate is much lower than short and long pulses [121]. Fig. 2.12 depicts hole opening machined with different pulse duration ranged from short to ultrashort.

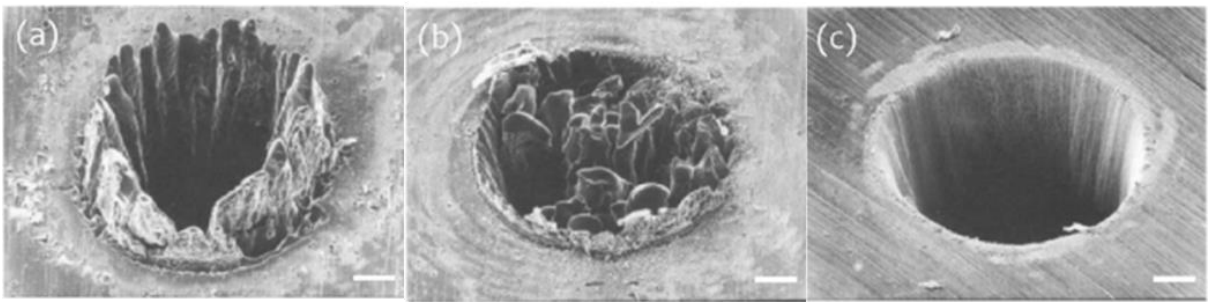

Figure 2.12. *Laser drilling on steel sample at laser wavelength of 780 nm with different pulse durations: (a) 3.3 ns, (b) 80 ps and (c) 200 fs [122].*

Tapering effect at the sidewall of micro holes is a major drawback of the laser micro-drilling which causes difference between entrance and exit diameters of drilled holes. The formation of taper angle is due to the discrepancy in intensity distribution of Gaussian beam and the drop in absorptivity at the sidewall when incident angle of laser beam to the sidewall increases [123]. This effect has gained a lot of attention from researchers to reduce and even eliminate sidewall taper angle, thus, to improve

accuracy of the laser micro-drilling process. As the main cause of taper angle is from Gaussian shape of laser beam, modification of this shape is a straight solution [124]. Top-hat beam shows clear advantages in reducing taper angle and improve hole circularity in drilling high aspect ratio holes with femtosecond pulses (Fig. 2.13). However, it can be seen that top-hat processing results in lower depth of hole compared to Gaussian processing when same number of pulses is performed.

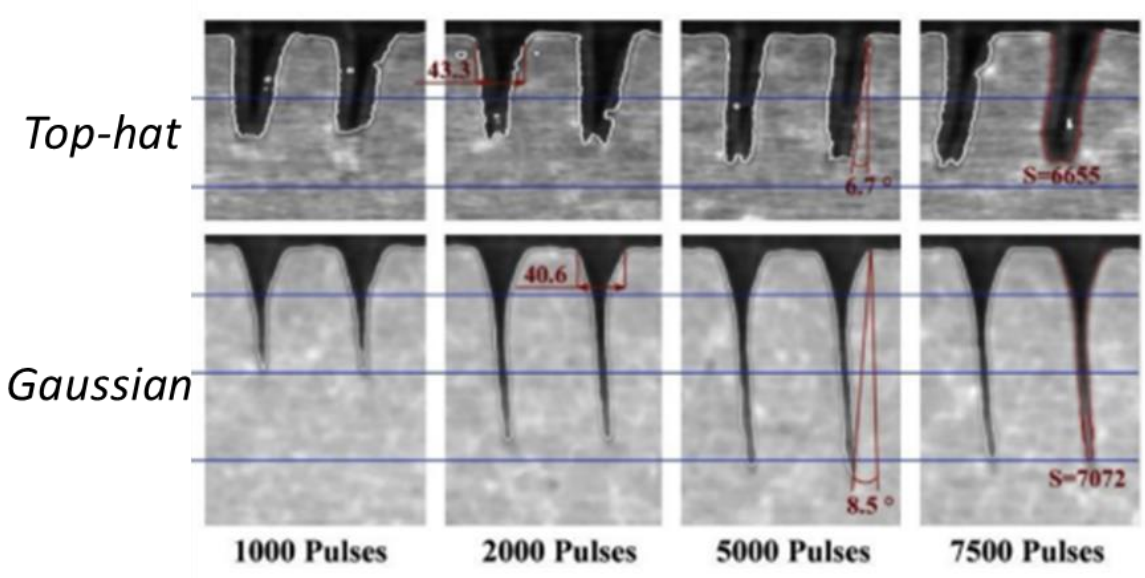

Figure 2.13. *Cross-sectional view of hole drilled by percussion with Top-hat beam and Gaussian beam with different number of 500 fs pulses [48]*

A novel machining route was designed and implemented by Nasrollahi et al to drilled from two side of the substrate to improve the accuracy of micro holes on silicon nitride [125]. The difference between entrance and exit diameter was eliminated. However, tapering effect still exist even it was improved significantly. In addition, this solution requires complex setup and calibration process, and machining time is double compared to laser drilling from one side. Laser micro-drilling with ultrasonic assistance was also proven to reduce taper angle, thus, to reduce the difference between entrance

and exit of micro holes in laser drilling with millisecond pulses [113]. In addition, the employment of ultrasonic assistance also reduces recast layer thickness and micro cracks at hole edge and improve hole circularity in comparison to normal laser micro-drilling [115, 126]. A combination of continuous wave and nanosecond pulse to drill holes on thick substrate was proposed by Jia et al [127]. Specifically, drilling efficiency was improved when nanosecond pulses were employed as a material removal assistance at the centre of processing area. However, the quality of drilled hole was not improved and was mainly affected by the continuous wave laser. Gas can be used as an assisted factor to enhance removal of material in laser micro-drilling of thick substrate [106]. A recent study from Marimuthu et al was successful to produce hole with high aspect ratio of 20 on 10 mm thick substrate using trepanning with different assisted gas [128]. Negative taper angle was achieved when pulse energy was increase. Furthermore, the use of nitrogen and argon to assist drilling process helped to significantly reduce number of pulses to break through the 10 mm substrate compared to the process with oxygen.

Another approach to reduce tapering effect in laser drilling of micro holes is introducing special motions of laser beam, thus, to improve ablation efficiency at the sidewall. Specifically, laser beam approach machining surface at a predefined incident angle is beneficial to effectively ablate material at the sidewall when hole depth increases and, consequently, reduce taper angle. This concept can be achieved through precession motion of the laser beam [129]. Fig. 2.14 illustrates how precession movement of laser beam improve taper angle at the sidewall in laser micro-drilling. The capability of tilted beam and precession beam was demonstrated successfully to minimise tapering effect and achieving vertical sidewall for trepanning and helical drilling in some studies [130,

131]. However, the application of tilted beam was limited to drilling of circular holes for current studies. In addition, the influence of parameters in drilling process have not been systematically investigated and optimized yet.

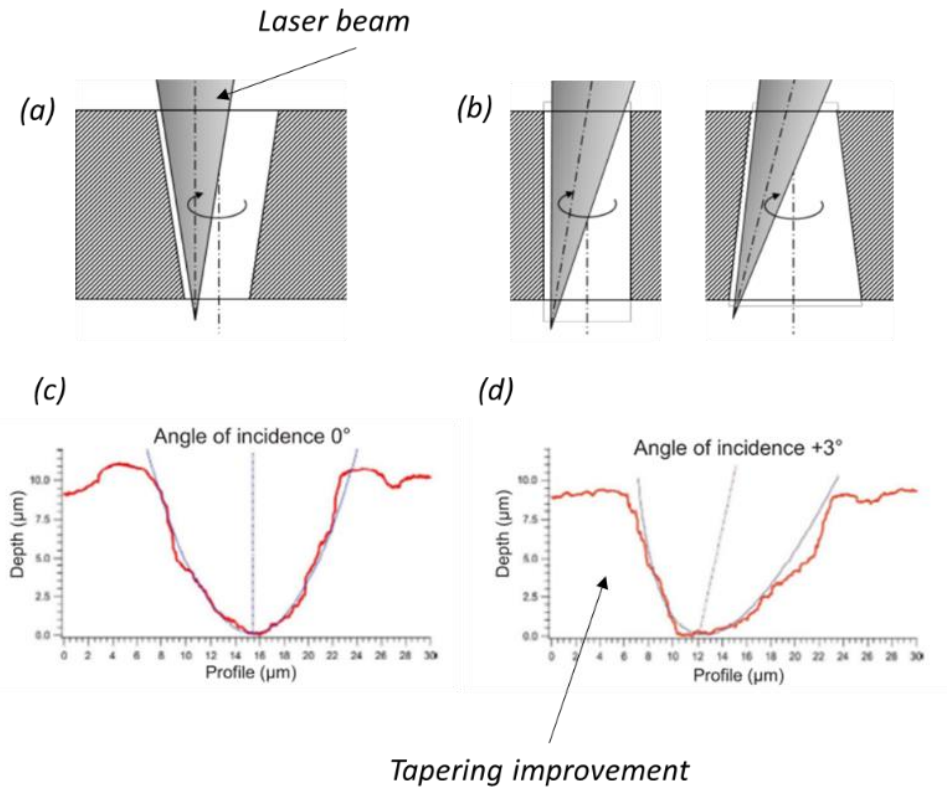

Figure 2.14. *Illustration of relative movement of laser beam to the workpiece and its influence on taper angle: (a) Machining with laser beam normal to the top surface, (b) Machining with precession movement of laser beam, (c) ablation profile of laser beam normal to the top surface, and (d) ablation profile of laser beam with an incident angle [117, 118].*

2.4. Summary of open research issues

Applications of laser micro-machining are becoming increasingly popular in both research and industries. The advancement in laser technology that enables such high-power laser sources necessitates the development of adequate machining procedures to optimize their capabilities, hence broadening the applications of laser micro-machining. The carried-out literature review provides an update on recent research and achievements in laser micro-machining technology, as well as some obstacles and limitations in enhancing quality and process efficiency. Specific open research issues are identified and summarised below:

- The capability of top-hat beam was predominantly demonstrated on micro-drilling of high aspect-ratio holes and scribing of thin films. The dimension of these structures was close to beam spot size, thus, the effect of top-hat beam was clear. However, micro-machining of big structures in comparison to the size of the beam spot, e.g. rectangular shape cavity, should be viewed as a different process that calls for optimization of both processing strategies and process parameters in order to achieve improvement in processing performance.
- The majority of the research focused on demonstrating capability of MHz burst mode in improving material removal rate at relatively low number of pulses per burst. The impact of burst mode with large number of pulses per burst, i.e. tens to hundreds, with high burst energy on ablation process has not been explored. In addition, the effects of heat accumulation, plasma shielding and other factors on specific removal rate of burst processing has not been studied systematically to conclude their contribution to the overall efficiency.

- The capability of precession laser machining to improve geometrical accuracy of microstructure is undeniable. However, until yet, capability demonstration of this technology has been limited to drilling of low aspect-ratio circular holes and cutting of parts. There is lack of demonstration for industrial application to prove its competitiveness with other high-accuracy technology such as photolithography. In addition, the limitations of this technology have not been well identified, thus, to optimize the process and to realise further development.
- Precession laser machining introduces unconventional processing parameters such as incident angle of the precession beam, position of different focuses and angular speed. Furthermore, other typical factors in laser micro-machining, e.g. scanning speed and scanning strategy, have different effects on quality and efficiency of micro fabrication process when compared to standard laser processing. The impact of these unconventional, as well as the change in influence of conventional parameters, has not been systematically investigated. This leads to lack of understanding underlying mechanism of the technology.

References

1. Hecht, J., *A short history of laser development.* Applied optics, 2010. **49**(25): p. F99-F122.
2. Bertolotti, M., *The history of the laser*. 2004: CRC press.
3. Ion, J., *Laser processing of engineering materials: principles, procedure and industrial application*. 2005: Elsevier.
4. Jain, V.K., *Laser Systems and Applications*. 2013: Alpha Science International, Limited.
5. Sahu, R.K., *A review on application of laser tracker in precision positioning metrology of particle accelerators.* Precision Engineering, 2021. **71**: p. 232-249.
6. O'Briant, S.A., Gupta, S.B., and Vasu, S.S., *Laser ignition for aerospace propulsion.* Propulsion and Power Research, 2016. **5**(1): p. 1-21.
7. Yasa, E. and Kruth, J.-P., *Application of laser re-melting on selective laser melting parts.* Advances in Production engineering and Management, 2011. **6**(4): p. 259-270.
8. Barron, J.A., Ringeisen, B.R., Kim, H., Spargo, B.J., and Chrisey, D.B., *Application of laser printing to mammalian cells.* Thin Solid Films, 2004. **453**: p. 383-387.
9. Arnone, D.D., Ciesla, C.M., Corchia, A., Egusa, S., Pepper, M., Chamberlain, J.M., Bezant, C., Linfield, E.H., Clothier, R., and Khammo, N. *Applications of terahertz (THz) technology to medical imaging*. in *Terahertz Spectroscopy and Applications II*. 1999. International Society for Optics and Photonics.
10. Elahi, P., Akçaalan, Ö., Ertek, C., Eken, K., Ilday, F.Ö., and Kalaycoğlu, H., *High-power Yb-based all-fiber laser delivering 300 fs pulses for high-speed ablation-cooled material removal.* Optics Letters, 2018. **43**(3): p. 535-538.
11. Finger, J., Kalupka, C., and Reininghaus, M., *High power ultra-short pulse laser ablation of IN718 using high repetition rates.* Journal of materials processing technology, 2015. **226**: p. 221-227.
12. Martin, P.E., Estival, S., Dijoux, M., de Campos, J.A.R., Kupisiewicz, A., and Braunschweig, R. *High-power femtosecond laser cutting and drilling combining beam-shaping and beam-splitting*. in *Laser Beam Shaping XVIII*. 2018. International Society for Optics and Photonics.
13. Smrž, M., Novák, O., Mužík, J., Turčičová, H., Chyla, M., Nagisetty, S., Vyvlečka, M., Roškot, L., Miura, T., Černohorská, J., Sikocinski, P., Chen, L., Huynh, J., Severová, P., Pranovich, A., Endo, A., and Mocek, T., *Advances in High-Power, Ultrashort Pulse DPSSL Technologies at HiLASE.* Applied Sciences, 2017. **7**(10).
14. Nie, S. and Guan, Y., *Review of UV laser and its applications in micromachining.* Opto-Electronic Engineering, 2017. **44**(12): p. 1169-1179.
15. Zou, J., Ruan, Q., Zhang, X., Xu, B., Cai, Z., and Luo, Z., *Visible-wavelength pulsed lasers with low-dimensional saturable absorbers.* Nanophotonics, 2020. **9**(8): p. 2273-2294.
16. Mishra, S. and Yadava, V., *Laser Beam MicroMachining (LBMM) – A review.* Optics and Lasers in Engineering, 2015. **73**: p. 89-122.
17. García-Moreno, A.-I., Alvarado-Orozco, J.-M., Ibarra-Medina, J., and Martínez-Franco, E., *In-process monitoring of the melt-pool motion during continuous-*

wave laser metal deposition. Journal of Manufacturing Processes, 2021. **65**: p. 42-50.
18. Kumar, S.P., Elangovan, S., Mohanraj, R., and Narayanan, V.S., *Significance of continuous wave and pulsed wave laser in direct metal deposition.* Materials Today: Proceedings, 2021. **46**: p. 8086-8096.
19. Chen, J., An, Q., Ming, W., and Chen, M., *Investigations on continuous-wave laser and pulsed laser induced controllable ablation of SiCf/SiC composites.* Journal of the European Ceramic Society, 2021. **41**(12): p. 5835-5849.
20. Bakhtiyari, A.N., Wang, Z., Wang, L., and Zheng, H., *A review on applications of artificial intelligence in modeling and optimization of laser beam machining.* Optics & Laser Technology, 2021. **135**: p. 106721.
21. Penchev, P.N., *Reconfigurable laser micro-processing systems: development of generic system-level tools for implementing modular laser micro-manufactoring platforms*. 2016, University of Birmingham.
22. Boutalbi, N., Bouaziz, M.N., and Allouche, M., *Influence of temperature-dependent absorptivity on solid surface heated by CO2 and Nd: YAG lasers.* Journal of Laser Applications, 2016. **28**(3): p. 032004.
23. Garban-Labaune, C., Fabre, E., Max, C., Fabbro, R., Amiranoff, F., Virmont, J., Weinfeld, M., and Michard, A., *Effect of laser wavelength and pulse duration on laser-light absorption and back reflection.* Physical Review Letters, 1982. **48**(15): p. 1018.
24. Seibold, G., Dausinger, F., and Huegel, H. *Absorptivity of Nd: YAG-laser radiation on iron and steel depending on temperature and surface conditions*. in *International Congress on Applications of Lasers & Electro-Optics*. 2000. Laser Institute of America.
25. Weber, R., Michalowski, A., Abdou-Ahmed, M., Onuseit, V., Rominger, V., Kraus, M., and Graf, T., *Effects of radial and tangential polarization in laser material processing.* Physics Procedia, 2011. **12**: p. 21-30.
26. Ang, L., Lau, Y., Gilgenbach, R.M., and Spindler, H., *Analysis of laser absorption on a rough metal surface.* Applied physics letters, 1997. **70**(6): p. 696-698.
27. Seely, J.F., *Quantum Theory of Inverse Bremsstrahlung Absorption and Pair Production*, in *Laser Interaction and Related Plasma Phenomena: Volume 3B*, Schwarz, H.J. and Hora, H., Editors. 1974, Springer US: Boston, MA. p. 835-847.
28. Förster, D.J., Jäggi, B., Michalowski, A., and Neuenschwander, B., *Review on Experimental and Theoretical Investigations of Ultra-Short Pulsed Laser Ablation of Metals with Burst Pulses.* Materials, 2021. **14**(12).
29. Yao, Y.L., Chen, H., and Zhang, W., *Time scale effects in laser material removal: a review.* The International Journal of Advanced Manufacturing Technology, 2005. **26**(5-6): p. 598-608.
30. Grigoropoulos, C.P., *Transport in laser microfabrication: fundamentals and applications*. 2009: Cambridge University Press.
31. Russo, R.E., Mao, X., Yoo, J., and Gonzalez, J., *Laser ablation*, in *Laser-induced breakdown spectroscopy*. 2007, Elsevier. p. 41-70.
32. Akman, E., Erdoğan, Y., Bora, M.Ö., Çoban, O., Oztoprak, B.G., and Demir, A., *Investigation of the differences between photochemical and photothermal laser*

ablation on the shear strength of CFRP/CFRP adhesive joints. International Journal of Adhesion and Adhesives, 2020. **98**: p. 102548.
33. Momma, C., Nolte, S., Chichkov, B.N., Alvensleben, F.v., and Tünnermann, A., *Precise laser ablation with ultrashort pulses.* Applied surface science, 1997. **109**: p. 15-19.
34. Wu, C. and Zhigilei, L.V., *Microscopic mechanisms of laser spallation and ablation of metal targets from large-scale molecular dynamics simulations.* Applied Physics A, 2013. **114**(1): p. 11-32.
35. Leitz, K.-H., Redlingshöfer, B., Reg, Y., Otto, A., and Schmidt, M., *Metal ablation with short and ultrashort laser pulses.* Physics Procedia, 2011. **12**: p. 230-238.
36. Hashida, M., Semerok, A., Gobert, O., Petite, G., and Izawa, Y., *Ablation threshold dependence on pulse duration for copper.* Applied surface science, 2002. **197**: p. 862-867.
37. Mustafa, H., Mezera, M., Matthews, D.T.A., and Römer, G., *Effect of surface roughness on the ultrashort pulsed laser ablation fluence threshold of zinc and steel.* Applied surface science, 2019. **488**: p. 10-21.
38. Mustafa, H., Pohl, R., Bor, T., Pathiraj, B., Matthews, D., and Römer, G., *Picosecond-pulsed laser ablation of zinc: crater morphology and comparison of methods to determine ablation threshold.* Optics express, 2018. **26**(14): p. 18664-18683.
39. Liu, J., *Simple technique for measurements of pulsed Gaussian-beam spot sizes.* Optics letters, 1982. **7**(5): p. 196-198.
40. Penchev, P., Dimov, S., Bhaduri, D., and Soo, S.L., *Generic integration tools for reconfigurable laser micromachining systems.* Journal of Manufacturing Systems, 2016. **38**: p. 27-45.
41. Dickey, F.M. and Holswade, S.C., *Beam shaping: a review*, in *Laser Beam Shaping Applications*. 2018, CRC Press. p. 269-305.
42. Cheng, J., Liu, C.-s., Shang, S., Liu, D., Perrie, W., Dearden, G., and Watkins, K., *A review of ultrafast laser materials micromachining.* Optics & Laser Technology, 2013. **46**: p. 88-102.
43. Mincuzzi, G., Audouard, E., Bourtereau, A., Delaigue, M., Faucon, M., Hoenninger, C., Mishchik, K., Rebière, A., Sailer, S., and Seweryn-Schnur, A., *Pulse to pulse control for highly precise and efficient micromachining with femtosecond lasers.* Optics Express, 2020. **28**(12): p. 17209-17218.
44. Boisselier, D., Sankaré, S., and Engel, T., *Improvement of the laser direct metal deposition process in 5-axis configuration.* Physics Procedia, 2014. **56**: p. 239-249.
45. Bhaduri, D., Penchev, P., Dimov, S., and Soo, S.L., *An investigation of accuracy, repeatability and reproducibility of laser micromachining systems.* Measurement, 2016. **88**: p. 248-261.
46. Ji, X. and Dou, L., *Two types of definitions for Rayleigh range.* Optics & Laser Technology, 2012. **44**(1): p. 21-25.
47. Häfner, T., Strauß, J., Roider, C., Heberle, J., and Schmidt, M., *Tailored laser beam shaping for efficient and accurate microstructuring.* Applied Physics A, 2018. **124**(2): p. 111.
48. Nasrollahi, V., Penchev, P., Batal, A., Le, H., Dimov, S., and Kim, K., *Laser drilling with a top-hat beam of micro-scale high aspect ratio holes in silicon nitride.* Journal of Materials Processing Technology, 2020. **281**.

49. Li, J., Tang, Y., Kuang, Z., Schille, J., Loeschner, U., Perrie, W., Liu, D., Dearden, G., and Edwardson, S., *Multi imaging-based beam shaping for ultrafast laser-material processing using spatial light modulators.* Optics and Lasers in Engineering, 2019. **112**: p. 59-67.
50. Tang, Y., Li, J., Zhou, T., Schille, J., Loeschner, U., Perrie, W., Dearden, G., and Edwardson, S., *Dynamic beam shaping with polarization control at the image plane for material processing.* Procedia CIRP, 2018. **74**: p. 581-584.
51. Nasrollahi, V., *Drilling of micro-scale high aspect ratio holes with ultra-short lasers*. 2020, University of Birmingham.
52. Blair, P., Currie, M., Trela, N., Baker, H.J., Murphy, E., Walker, D., and McBride, R. *Field mappers for laser material processing*. in *Laser Resonators, Microresonators, and Beam Control XVIII*. 2016. International Society for Optics and Photonics.
53. Račiukaitis, G., Stankevičius, E., Gečys, P., Gedvilas, M., Bischoff, C., Jäger, E., Umhofer, U., and Völklein, F., *Laser Processing by Using Diffractive Optical Laser Beam Shaping Technique.* Journal of laser micro/nanoengineering, 2011. **6**(1).
54. Laskin, A. and Laskin, V. *πShaper–Refractive beam shaping optics for advanced laser technologies*. in *Journal of Physics: Conference Series*. 2011. IOP Publishing.
55. Laskin, A. and Laskin, V. *Creating round and square flattop laser spots in microprocessing systems with scanning optics*. in *International Congress on Applications of Lasers & Electro-Optics*. 2012. LIA.
56. Delaporte, P., Karnakis, D., and Zergioti, I., *12 - Laser processing of flexible organic electronic materials*, in *Handbook of Flexible Organic Electronics*, Logothetidis, S., Editor. 2015, Woodhead Publishing: Oxford. p. 285-313.
57. Smrž, M., Novák, O., Mužík, J., Turčičová, H., Chyla, M., Nagisetty, S.S., Vyvlečka, M., Roškot, L., Miura, T., and Černohorská, J., *Advances in high-power, ultrashort pulse DPSSL technologies at HiLASE.* Applied Sciences, 2017. **7**(10): p. 1016.
58. Račiukaitis, G., *Ultra-short pulse lasers for microfabrication: A review.* IEEE Journal of Selected Topics in Quantum Electronics, 2021. **27**(6): p. 1-12.
59. Lickschat, P., Metzner, D., and Weißmantel, S., *Burst mode ablation of stainless steel with tunable ultrashort laser pulses.* Journal of Laser Applications, 2021. **33**(2).
60. Liu, Y., Wu, J., Wen, X., Lin, W., Wang, W., Guan, X., Qiao, T., Guo, Y., Wang, W., and Wei, X., *> 100 W GHz femtosecond burst mode all-fiber laser system at 1.0 μm.* Optics Express, 2020. **28**(9): p. 13414-13422.
61. Butkus, S., Jukna, V., Paipulas, D., Barkauskas, M., and Sirutkaitis, V., *Micromachining of Invar Foils with GHz, MHz and kHz Femtosecond Burst Modes.* Micromachines (Basel), 2020. **11**(8).
62. Bartulevicius, T., Madeikis, K., Veselis, L., Petrauskiene, V., and Michailovas, A., *Active fiber loop for synthesizing GHz bursts of equidistant ultrashort pulses.* Optics Express, 2020. **28**(9): p. 13059-13067.
63. Kalaycıoğlu, H., Elahi, P., Akçaalan, Ö., and Ilday, F.Ö., *High-repetition-rate ultrafast fiber lasers for material processing.* IEEE Journal of selected topics in quantum electronics, 2017. **24**(3): p. 1-12.

64. Zemaitis, A., Gaidys, M., Gecys, P., Barkauskas, M., and Gedvilas, M., *Femtosecond laser ablation by bibursts in the MHz and GHz pulse repetition rates.* Opt Express, 2021. **29**(5): p. 7641-7653.
65. Caballero-Lucas, F., Obata, K., and Sugioka, K., *Enhanced ablation efficiency for silicon by femtosecond laser microprocessing with GHz bursts in MHz bursts (BiBurst).* International Journal of Extreme Manufacturing, 2022. **4**(1): p. 015103.
66. Martin, P.-E., Estival, S., Dijoux, M., Laygue, P., Kupisiewicz, A., and Braunschweig, R. *Laser cutting and drilling with zero conicity*. in *Laser-based Micro-and Nanoprocessing XI*. 2017. International Society for Optics and Photonics.
67. Piljek, P., Keran, Z., and Math, M., *Micromachining–review of literature from 1980 to 2010.* Interdisciplinary Description of Complex Systems: INDECS, 2014. **12**(1): p. 1-27.
68. Schaeffer, R., *Fundamentals of laser micromachining*. 2012: CRC press.
69. Sahu, A.K., Malhotra, J., and Jha, S., *Laser-based hybrid micromachining processes: A review.* Optics & Laser Technology, 2022. **146**: p. 107554.
70. Gärtner, E., Polise, V., Tagliaferri, F., and Palumbo, B., *Laser micro machining of alumina by a picosecond laser.* Journal of Laser Micro Nanoengineering, 2018. **13**(2): p. 76-84.
71. Sen, A., Doloi, B., and Bhattacharyya, B., *Parametric influences of fiber laser micro-machining for the generation of micro-channels on PMMA.* Journal of the Brazilian Society of Mechanical Sciences and Engineering, 2020. **42**(8): p. 1-13.
72. Ngcobo, S., Litvin, I., Burger, L., and Forbes, A., *A digital laser for on-demand laser modes.* Nature communications, 2013. **4**(1): p. 1-6.
73. Forbes, A., *Laser beam propagation: generation and propagation of customized light*. 2014: CRC Press.
74. Kim, K.-S., Kim, J.-H., Choi, J.-Y., and Lee, C.-M., *A review on research and development of laser assisted turning.* International Journal of Precision Engineering and Manufacturing, 2011. **12**(4): p. 753-759.
75. Bischoff, C., Jäger, E., and Umhofer, U., *Beam Shaping Optics for Process Acceleration: Increasing the productivity of laser micromachining.* Laser Technik Journal, 2015. **12**(3): p. 53-57.
76. Duocastella, M. and Arnold, C.B., *Bessel and annular beams for materials processing.* Laser & Photonics Reviews, 2012. **6**(5): p. 607-621.
77. Bhuyan, M.K., Courvoisier, F., Lacourt, P.-A., Jacquot, M., Furfaro, L., Withford, M., and Dudley, J., *High aspect ratio taper-free microchannel fabrication using femtosecond Bessel beams.* Optics express, 2010. **18**(2): p. 566-574.
78. Wang, X., Ma, C., Li, C., Kang, M., and Ehmann, K., *Influence of pulse energy on machining characteristics in laser induced plasma micro-machining.* Journal of Materials Processing Technology, 2018. **262**: p. 85-94.
79. Wang, S.Y., Ren, Y., Cheng, C.W., Chen, J.K., and Tzou, D.Y., *Micromachining of copper by femtosecond laser pulses.* Applied Surface Science, 2013. **265**: p. 302-308.
80. Hodgson, N., Steinkopff, A., Heming, S., Allegre, H., Haloui, H., Lee, T.S., Laha, M., and VanNunen, J. *Ultrafast laser machining: process optimization and*

applications. in *Laser Applications in Microelectronic and Optoelectronic Manufacturing (LAMOM) XXVI*. 2021. SPIE.
81. Puoza, J.C., Hua, X., Liu, Q., Kang, Z., and Zhang, P., *Manufacturing of micro-textures on metals by nanosecond laser micromachining.* Advances in Materials and Processing Technologies, 2018. **4**(1): p. 86-99.
82. Kramer, T., Zhang, Y., Remund, S., Jaeggi, B., Michalowski, A., Grad, L., and Neuenschwander, B., *Increasing the specific removal rate for ultra short pulsed laser-micromachining by using pulse bursts.* J. Laser Micro/Nanoeng, 2017. **12**: p. 107.
83. Kramer, T., Neuenschwander, B., Jäggi, B., Remund, S., Hunziker, U., and Zürcher, J., *Influence of pulse bursts on the specific removal rate for ultra-fast pulsed laser micromachining of copper.* Physics Procedia, 2016. **83**: p. 123-134.
84. Hodgson, N., Allegre, H., Starodoumov, A., and Bettencourt, S., *Femtosecond Laser Ablation in Burst Mode as a Function of Pulse Fluence and Intra-Burst Repetition Rate.* Journal of Laser Micro/Nanoengineering, 2020. **15**(3): p. 236 - 244.
85. Holder, D., Weber, R., Röcker, C., Kunz, G., Bruneel, D., Delaigue, M., Graf, T., and Ahmed, M.A., *High-quality high-throughput silicon laser milling using a 1 kW sub-picosecond laser.* Optics letters, 2021. **46**(2): p. 384-387.
86. Marimuthu, S. and Smith, B., *High-Throughput Picosecond Laser Machining of Aerospace Nickel Superalloy.* Proceedings of the Institution of Mechanical Engineers, Part B: Journal of Engineering Manufacture, 2022. **236**(4): p. 363-372.
87. Bonamis, G., Mishchick, K., Audouard, E., Hönninger, C., Mottay, E., Lopez, J., and Manek-Hönninger, I., *High efficiency femtosecond laser ablation with gigahertz level bursts.* Journal of Laser Applications, 2019. **31**(2): p. 022205.
88. Lickschat, P., Metzner, D., and Weißmantel, S., *Manufacturing of high quality 3D microstructures in stainless steel with ultrashort laser pulses using different burst modes.* Journal of Laser Applications, 2021. **33**(4).
89. Gaudiuso, C., Giannuzzi, G., Volpe, A., Lugarà, P.M., Choquet, I., and Ancona, A., *Incubation during laser ablation with bursts of femtosecond pulses with picosecond delays.* Optics express, 2018. **26**(4): p. 3801-3813.
90. Nathala, C.S.R., Ajami, A., Husinsky, W., Farooq, B., Kudryashov, S.I., Daskalova, A., Bliznakova, I., and Assion, A., *Ultrashort laser pulse ablation of copper, silicon and gelatin: effect of the pulse duration on the ablation thresholds and the incubation coefficients.* Applied Physics A, 2016. **122**(2): p. 107.
91. Le Harzic, R., Breitling, D., Weikert, M., Sommer, S., Föhl, C., Valette, S., Donnet, C., Audouard, E., and Dausinger, F., *Pulse width and energy influence on laser micromachining of metals in a range of 100fs to 5ps.* Applied Surface Science, 2005. **249**(1): p. 322-331.
92. Weber, R., Graf, T., Berger, P., Onuseit, V., Wiedenmann, M., Freitag, C., and Feuer, A., *Heat accumulation during pulsed laser materials processing.* Optics express, 2014. **22**(9): p. 11312-11324.
93. Martan, J., Prokešová, L., Moskal, D., Ferreira de Faria, B.C., Honner, M., and Lang, V., *Heat accumulation temperature measurement in ultrashort pulse laser micromachining.* International Journal of Heat and Mass Transfer, 2021. **168**.

94. Metzner, D., Lickschat, P., and Weißmantel, S., *Influence of heat accumulation during laser micromachining of CoCrMo alloy with ultrashort pulses in burst mode.* Applied Physics A, 2020. **126**(2).
95. Batal, A., Michalek, A., Penchev, P., Kupisiewicz, A., and Dimov, S., *Laser processing of freeform surfaces: A new approach based on an efficient workpiece partitioning strategy.* International Journal of Machine Tools and Manufacture, 2020. **156**: p. 103593.
96. Karkantonis, T., Penchev, P., Nasrollahi, V., Le, H., See, T.L., Bruneel, D., Ramos-de-Campos, J.A., and Dimov, S., *Laser micro-machining of freeform surfaces: Accuracy, repeatability and reproducibility achievable with multi-axis processing strategies.* Precision Engineering, 2022. **78**: p. 233-247.
97. Cuccolini, G., Orazi, L., and Fortunato, A., *5 Axes computer aided laser milling.* Optics and Lasers in Engineering, 2013. **51**(6): p. 749-760.
98. Kramer, T., Remund, S., Gafner, M., Zwygart, D., Neuenschwander, B., Holtz, R., Witte, R., and Dury, N., *Novel strategy for ultrafast pulsed laser micromachining of rotational symmetric metallic parts.* Procedia CIRP, 2018. **74**: p. 611-617.
99. Teixidor, D., Grzenda, M., Bustillo, A., and Ciurana, J., *Modeling pulsed laser micromachining of micro geometries using machine-learning techniques.* Journal of Intelligent Manufacturing, 2015. **26**(4): p. 801-814.
100. Petkov, P., Scholz, S., and Dimov, S., *Strategies for material removal in laser milling.* SS Dimov & W. Menz (Eds.) M, 2008. **4**: p. 249-252.
101. Wlodarczyk, K.L., Schille, J., Naumann, L., Lopes, A.A., Bitharas, I., Bidare, P., Dondieu, S.D., Blair, P., Loeschner, U., and Moore, A.J., *Investigation of an interlaced laser beam scanning method for ultrashort pulse laser micromachining applications.* Journal of Materials Processing Technology, 2020. **285**: p. 116807.
102. Jaeggi, B., Remund, S., Streubel, R., Goekce, B., Barcikowski, S., and Neuenschwander, B., *Laser Micromachining of Metals with Ultra-Short Pulses: Factors Limiting the Scale-Up Process.* Journal of Laser Micro/Nanoengineering, 2017. **12**(3).
103. Žemaitis, A., Gaidys, M., Brikas, M., Gečys, P., Račiukaitis, G., and Gedvilas, M., *Advanced laser scanning for highly-efficient ablation and ultrafast surface structuring: experiment and model.* Scientific Reports, 2018. **8**(1): p. 17376.
104. Umer, U., Mohammed, M.K., and Al-Ahmari, A., *Multi-response optimization of machining parameters in micro milling of alumina ceramics using Nd:YAG laser.* Measurement, 2017. **95**: p. 181-192.
105. Campanelli, S.L., Ludovico, A.D., Bonserio, C., Cavalluzzi, P., and Cinquepalmi, M., *Experimental analysis of the laser milling process parameters.* Journal of Materials Processing Technology, 2007. **191**(1-3): p. 220-223.
106. Pattanayak, S. and Panda, S., *Laser beam micro drilling–a review.* Lasers in Manufacturing and Materials Processing, 2018. **5**(4): p. 366-394.
107. Voisiat, B., Indrišiūnas, S., Šniaukas, R., Minkevičius, L., Kašalynas, I., and Račiukaitis, G. *Laser processing for precise fabrication of the THz optics*. in *Laser Applications in Microelectronic and Optoelectronic Manufacturing (LAMOM) XXII*. 2017. International Society for Optics and Photonics.
108. Hasan, M., Zhao, J., and Jiang, Z., *A review of modern advancements in micro drilling techniques.* Journal of Manufacturing Processes, 2017. **29**: p. 343-375.

109. Wang, H.-J. and Yang, T., *A review on laser drilling and cutting of silicon.* Journal of the European Ceramic Society, 2021. **41**(10): p. 4997-5015.
110. Hourmand, M., Sarhan, A.A., and Sayuti, M., *Micro-electrode fabrication processes for micro-EDM drilling and milling: a state-of-the-art review.* The International Journal of Advanced Manufacturing Technology, 2017. **91**(1-4): p. 1023-1056.
111. Calabrese, L., Azzolini, M., Bassi, F., Gallus, E., Bocchi, S., Maccarini, G., Pellegrini, G., and Ravasio, C., *Micro-Milling Process of Metals: A Comparison between Femtosecond Laser and EDM Techniques.* Journal of Manufacturing and Materials Processing, 2021. **5**(4): p. 125.
112. Wang, C., Wang, Q., Qian, Q., and Di, B. *The development of laser drilling: A review*. in *IOP Conference Series: Materials Science and Engineering*. 2020. IOP Publishing.
113. Xia, K., Ren, N., Wang, H., and Shi, C., *Analysis for effects of ultrasonic power on ultrasonic vibration-assisted single-pulse laser drilling.* Optics and Lasers in Engineering, 2018. **110**: p. 279-287.
114. Marimuthu, S., Antar, M., and Dunleavey, J., *Characteristics of micro-hole formation during fibre laser drilling of aerospace superalloy.* Precision Engineering, 2019. **55**: p. 339-348.
115. Shi, C., Ren, N., Wang, H., Xia, K., and Wang, L., *Effects of ultrasonic assistance on microhole drilling based on Nd: YAG laser trepanning.* Optics & Laser Technology, 2018. **106**: p. 451-460.
116. Wang, X., Chen, H., Li, Z., Qin, Y., Zhu, X., Tang, X., and Wen, B., *Helical drilling of carbon fiber reinforced polymer by a femtosecond laser.* Applied Optics, 2022. **61**(1): p. 302-307.
117. Romoli, L., Tantussi, F., and Fuso, F., *Laser milling of martensitic stainless steels using spiral trajectories.* Optics and Lasers in Engineering, 2017. **91**: p. 160-168.
118. Führa, B., Russ, S., Hammers-Weber, P., Diego-Vallejo, D., Kahmann, M., Andreev, A., and Hesse, T. *High precision drilling with ultra-short laser pulses*. in *Proceedings of the Lasers in Manufacturing Conference*. 2017.
119. Gautam, G.D. and Pandey, A.K., *Pulsed Nd: YAG laser beam drilling: A review.* Optics & Laser Technology, 2018. **100**: p. 183-215.
120. Ren, N., Jiang, L., Liu, D., Lv, L., and Wang, Q., *Comparison of the simulation and experimental of hole characteristics during nanosecond-pulsed laser drilling of thin titanium sheets.* The International Journal of Advanced Manufacturing Technology, 2015. **76**(5): p. 735-743.
121. Ancona, A., Döring, S., Jauregui, C., Röser, F., Limpert, J., Nolte, S., and Tünnermann, A., *Femtosecond and picosecond laser drilling of metals at high repetition rates and average powers.* Optics letters, 2009. **34**(21): p. 3304-3306.
122. Piqué, A., Auyeung, R.C., Kim, H., Charipar, N.A., and Mathews, S.A., *Laser 3D micro-manufacturing.* Journal of Physics D: Applied Physics, 2016. **49**(22): p. 223001.
123. Ruf, A., Berger, P., Dausinger, F., and Hügel, H., *Analytical investigations on geometrical influences on laser drilling.* Journal of Physics D: Applied Physics, 2001. **34**(18): p. 2918.

124. Doan, H.D., Naoki, I., and Kazuyoshi, F., *Laser processing by using fluidic laser beam shaper.* International Journal of Heat and Mass Transfer, 2013. **64**: p. 263-268.
125. Nasrollahi, V., Penchev, P., Dimov, S., Korner, L., Leach, R., and Kim, K., *Two-Side Laser Processing Method for Producing High Aspect Ratio Microholes.* Journal of Micro and Nano-Manufacturing, 2017. **5**(4): p. 041006.
126. Xia, K., Wang, H., Ren, N., Ren, X., Liu, D., Shi, C., Li, T., and Tian, J., *Laser drilling in nickel super-alloy sheets with and without ultrasonic assistance characterized by transient in-process detection with indirect characterization after hole-drilling.* Optics & Laser Technology, 2021. **134**: p. 106559.
127. Jia, X., Zhang, Y., Chen, Y., Wang, H., Zhu, G., and Zhu, X., *Combined pulsed laser drilling of metal by continuous wave laser and nanosecond pulse train.* The International Journal of Advanced Manufacturing Technology, 2019. **104**(1): p. 1269-1274.
128. Marimuthu, S., Elkington, H., and Smith, B., *Millisecond fibre laser drilling of thick-section aerospace alloy.* The International Journal of Advanced Manufacturing Technology, 2022: p. 1-11.
129. Bruneel, D., Cangueiro, L., Reed, C., Braunschweig, R., Martin, P.-E., Ramos-de-Campos, J.A., and Kupisiewicz, A. *Optimization of the micromachining process by the simulation of ultrafast laser ablated profiles on metals for different applications*. in *International Congress on Applications of Lasers & Electro-Optics*. 2018. Laser Institute of America.
130. Bechtold, P., Mayer, G., Lühring, P., and Schmidt, M. *Novel System Technology for Trepanning a Laser Beam at Arbitrary Developments of Angle of Incidence and Lateral Focus Position*. in *Key Engineering Materials*. 2012. Trans Tech Publ.
131. Fornaroli, C., Holtkamp, J., and Gillner, A., *Laser-Beam Helical Drilling of High Quality Micro Holes.* Physics Procedia, 2013. **41**: p. 661-669.

CHAPTER 3

EFFECTS OF TOP-HAT LASER BEAM PROCESSING AND SCANNING STRATEGIES IN LASER MICRO-STRUCTURING

Hoang Le [1], Pavel Penchev [1], Anne Henrottin [2], David Bruneel [2], Vahid Nasrollahi [1], Jose A. Ramos-de-Campos [2] and Stefan Dimov [1]

[1]Department of Mechanical Engineering, University of Birmingham, Birmingham B15 2TT, UK

[2]LASEA, Rue des Chasseurs Ardennais 10, 4031 Angleur, Belgium

This research was published as a full-length article in ***Micromachines*** (2020).

Le, H.; Penchev, P.; Henrottin, A.; Bruneel, D.; Nasrollahi, V.; Ramos-de-Campos, J.A.; Dimov, S. Effects of Top-hat Laser Beam Processing and Scanning Strategies in Laser Micro-Structuring. Micromachines 2020, 11, 221. https://doi.org/10.3390/mi11020221

Author Contributions	
Hoang Le **(First Author)**	Conceptualization, Formal analysis, Methodology, Investigation, Validation, Writing–original draft, Writing–review & editing
P. Penchev	Validation
A. Henrottin	Writing–review & editing
D. Bruneel	Writing–review & editing
V. Nasrollahi	Investigation, Writing–review & editing
J. A. Ramos-de-Campos	Writing–review & editing
S. Dimov	Conceptualization, Project administration, Writing–review & editing

Abstract

The uniform energy distribution of top-hat laser beams is a very attractive property that can offer some advantages compared to Gaussian beams. Especially, the desired intensity distribution can be achieved at the laser spot through energy redistribution across the beam spatial profile and, thus, to minimize and even eliminate some inherent shortcomings in laser micro-processing. This paper reports an empirical study that investigates the effects of top-hat beam processing in micro-structuring and compares the results with those obtainable with a conventional Gaussian beam. In particular, a refractive field mapping beam shaper was used to obtain a top-hat profile and the effects of different scanning strategies, pulse energy settings, and accumulated fluence, i.e., hatch and pulse distances, were investigated. In general, the top-hat laser processing led to improvements in surface and structuring quality. Especially, the taper angle was reduced while the surface roughness and edge definition were also improved compared to structures produced with Gaussian beams. A further decrease of the taper angle was achieved by combining hatching with some outlining beam passes. The scanning strategies with only outlining beam passes led to very high ablation rates but in expense of structuring quality. Improvements in surface roughness were obtained with a wide range of pulse energies and pulse and hatch distances when top-hat laser processing was used.

Keywords: beam shapers; top-hat laser beam; gaussian laser beam; micro-structuring; pulse energy; hatch distance; pulse distance

3.1. Introduction

Direct laser micro-structuring is an attractive solution for fabricating micro-scale features due to advantages offered in overcoming some material and dimensional limitations of conventional machining methods. In particular, the inherent capabilities of laser structuring, such as non-contact processing, relatively high ablation rates at micro-scale, good accuracy, and repeatability, makes it a very attractive proposition compared with other competing micro-processing technologies, e.g., mechanical machining and lithography.

Currently, the majority of commercially available laser micro-processing systems employs Gaussian beams (TEM_{00}) due to their intensity profile and their consistency along propagation direction. This makes Gaussian beams much easier to use and calibrate. However, their spatial intensity distribution leads to an energy waste at the "tails" of the beam profiles as the intensity is lower than ablation thresholds and is just sufficient to melt/heat the material. Thus, this increases the heat affected zone (HAZ) while decreasing the processing efficiency of delivered pulse energies. Therefore, an energy redistribution across the beam spatial profile through the use of beam shapers can minimize and even avoid the pulse tail and, thus, achieving the desired intensity distribution at the laser spot [1]. In particular, Gaussian spatial intensity can be transformed into top-hat, donut, or reverse Gaussian distribution by employing beam shapers.

In this context, a uniform spatial intensity, i.e., a top-hat beam profile, can improve the processing condition at the laser spot and lead to higher geometrical accuracy and repeatability, lower surface roughness, and higher laser micro-structuring quality in general. Especially, the top-hat intensity profiles can minimize the recast area, i.e., the

splashes of material at the edges of the structures by reducing HAZ, as most of the energy in the irradiance is over the ablation threshold. In addition, the top-hat beam is expected to improve the resulting surface roughness and reduce taper angles due to the sharp intensity gradient at the pulse tails.

Thus, the objective of this research is the investigation of effects of top-hat beams in laser micro-structuring and compare the resulting structures with those achievable with Gaussian beams. The quality of the structures is studied in terms of HAZ, geometrical accuracy, i.e., taper angle, and surface roughness, while the processing efficiency is considered, too. In addition, the effects of different scanning strategy on structure quality and processing efficiency are analyzed in this research.

3.2. Literature Review of Laser Beam Shaping Application

3.2.1. Gaussian Beam Processing

Gaussian beams have high peak power and if a suitable wavelength is selected any materials can be processed with acceptable quality of resulting structures. Gaussian beams are self-consistent and, thus, the intensity profile is maintained at the same level along the propagation direction and practically beam waist and lens focal plane can be considered coincidental [2]. These attractive properties make them reliable and easy to use and therefore they are widely deployed in many laser processing applications [3]. However, Gaussian distribution partly contributes to the inherent shortcoming of laser micro-machining processes such as tapering effects at side walls and HAZ on the machined parts [4, 5]. The tapering effects are present after most of laser processing applications with Gaussian beams, e.g., drilling [6, 7] or micro-structuring (trenches, 3D structures) [8, 9]. Such draft angles at side walls affect the

geometric accuracy of produced structures and also can impact the functional performance.

The tapering effects of structures can be explained with non-uniform energy distribution of a Gaussian beam that entails non-uniform ablation. The high peak power of Gaussian profiles leads to high ablation rates within only a small area at the center of the beam spots and lower ablation rates (or no ablation) at their surroundings. Thus, it is not possible to have uniform laser-material interactions across the beam spots. This leads to non-uniform laser ablation and formations of recasts when a structures' depth increases, i.e., due to difficulties in evacuating the ablated material, especially in percussion drilling [7]. In addition, there are some other negative side effects in Gaussian beam processing on produced structures such as increased roughness.

At the same time, the demand together with requirements for high accuracy machining are constantly increasing. Furthermore, there is a consistent trend for miniaturization of new and existing devices that drives the advances in laser micro-machining. Efforts to achieve high geometrical accuracy, especially to minimize the tapering effect on side walls of structures fabricated by laser micro-machining, was the focus of many investigations, and different approaches to address this issue were suggested by researchers [10-14]. The main difficulties with these solutions are either the high accuracy requirements for the movements of mechanical stages, or their low repeatability and also their applicability for only specific structures. Laser micro-drilling of holes under flowing water was tried by Wee et al. and compared to those produced in air [15]. Water acted as a coolant and also removed the debris from the processed area and, thus, cleaner holes were produced with smaller draft angles.

3.2.2. Laser Beam Shaping Technology

Beam shapers was considered as an effective generic solution for minimizing the tapering effect because it did not require complex multi-axis processing strategies and at the same time it was relatively easy to integrate into existing laser processing systems. In addition, it was judged that the beam shaping technology led to improvements in laser processing efficiency [16] and quality of produced structures, too.

The latest beam shaping solutions fall into two main groups [1, 17-22], i.e., multifaceted beam integrators based on reflective phase elements and field mapping employing diffractive and refractive optical element. The multifaceted beam integrators can be of different types, e.g., micro-lens arrays, spatial light modulator (SLM), or multi-plane light conversion (MPLC). By employing MPLC based light modulators, laser light can be split and recombined to create different complex shapes such as linearly polarized (LP) modes [23, 24]. A combination of MPLC based light modulators with binary masks was deployed successfully to create complex laser beam shapes [25]. Hafner et al. used liquid crystal on silicon for spatial light modulation (LCoS-SLM) and acousto-optic beam shaping (AOS) to generate flat-top laser profiles that employed them for accurate laser micro-machining [24]. The main shortcoming of beam shapers that involve laser beam splitting and recombining is that they affect the beam consistency and process efficiency and, thus, can be significant drawbacks in laser micro-machining.

At the same time, the field mapping technology employs complex surface optic elements to remap the energy distribution of Gaussian beams in a controlled manner and, thus, achieving a variety of desirable profiles, e.g., such as donut, Airy, top-hat, or reverse Gaussian. There are different types of field mapping beam shapers, e.g.,

single optic field mappers and dual optic field mappers [26]. An important advantage of the field mapping technology is that it can deliver collimated and low divergence output beams [27]. In this way, the beam consistency can be maintained along the propagation direction and, thus, achieving high quality beam profiles at a given plane/distance.

Two types of optical elements are used in field mapping solutions, i.e., refractive optic elements (ROEs) and diffractive optic elements (DOEs). DOEs are typically thin and light weight and therefore the diffractive field mapping has a lower resistance to laser light and can also lead to energy losses [28]. At the same time, small optical elements allow compact beam shapers to be designed that are very suitable for integration in relatively small laser processing systems. The main disadvantage of DOE based field mapping is that resulting beam is very sensitive to any misalignments and the input quality of Gaussian beams. In particular, it was reported that a laser processing system with an integrated DOE based beam shaper to produce a flat-top beam required any angular and liner misalignments between beam and shaper axes to be less than 140 μrad and 25 μm, respectively [29]. This makes the installation and calibration procedures of DOE based field mapping solutions very time consuming and cumbersome.

The other field mapping solution employs ROEs to deflect each pixel on an input plane at a specific angle and, thus, creating a given profile at the image plane [28, 30]. Some advantages of the refractive field mapping are its high transmission efficiency, a relatively simple design that make them easier to manufacture and also ROE based shaper are easier to integrate into existing laser processing systems [31]. In addition, it is important to stress that ROE based beam shapers have a bigger depth of focus,

almost the same as that of Gaussian beams. This makes the setting up of any laser micro-processing operation much easier and at the same time it is a critical requirement in any 3D laser machining. In addition, refractive beam shapers are recommended when a beam spot size of less than 100 μm have be achieved in the focal plane [32].

3.2.3. Application of Top-hat Beams in Laser Micro-machining

The beam shaping technology can be applied to obtain different beam profiles, e.g., such as Bessel, donut (or annular), and top-hat beams, and, thus, addressing specific laser processing requirements [33-37]. The use of top-hat profiles to improve the resulting surface roughness and tapering, has gained a significant attention due to the uniform energy distribution and more efficient processing [38]. Especially, the top-hat laser micro-processing offers important advantages in micro-hole drilling [39], micro-channel scribing [40], and micro-structuring in general. Coutts et al. used nanosecond laser with top-hat profile to drill micro-holes on brass and ceramics substrates [41]. Their research has shown a significant improvement in holes' quality, especially in drilling brass plates compared to a conventional Gaussian profile. In another investigation, a square top-hat beam was used to scribe 150 nm thin films of indium tin oxide using both refractive and diffractive beam shapers [42, 43]. The uniform energy profile of the square top-hat beam allowed for a smaller pulse overlap to be used and this led to nine-fold increase in the scribing speed compared to Gaussian beam processing while achieving a similar quality. In general, the reported studies provided clear evidence about the potential improvements that top-hat processing can offer in laser micro-machining, particularly, in minimizing the side wall taper and surface roughness while improving the processing efficiency.

The beneficial properties of top-hat laser beams were predominantly deployed in drilling micro-holes and also in scribing micro-channels. The sizes of machined holes and channels in these investigations were similar to that of the beam spot size and, thus, the effect of the uniform energy profile in the processing area can be seen clearly. However, micro-machining of large structures in regards to the beam spot size should be considered a different process that requires optimization both in processing strategies and process parameters in order to obtain improvements in processing performance [44]. Thus, it is important to investigate what improvements top-hat laser machining can offer when the technology is used for producing relatively large structures. In this context, this research is an attempt to address the gap in our knowledge about the capabilities that top-hat processing offers in laser micro-machining.

3.3. Methodology

3.3.1. Material

Silicon (Si) wafers with thickness of 500 µm and average surface roughness of approximately 27 nm were used in this empirical study. Laser structuring of silicon gives less recast and debris when compared with those resulting after processing of metal substrates, in particular around the structure edge. Therefore, the structures are usually much better defined and, thus, the measurement uncertainty can be minimized when inspecting them. So, the use of Si wafers provides a better condition to assess the effects of investigated beam intensity profiles. In addition, Si wafers are commonly used in a wide range of industrial applications, e.g., solar cells [45] and electronics circuits.

3.3.2. Laser Source and Beam Delivery System

The structuring experiments were carried out on LS5 LASEA system that integrates a MOPA-based Yb fiber laser with a nominal wavelength of approximately 1064 nm, average power up to 50 W and beam quality factor $M^2 \leq 1.3$. The pulse duration can be varied from 15 to 220 ns with a maximum pulse energy of 0.71 mJ. A nanosecond laser has been employed because it is widely used by industry for micro-structuring because it offers acceptable trade-offs between processing efficiency and a structures' quality. The beam movements were controlled with a Rhothor RTA XY scan head with a positional resolution better than 8 µrad, repeatability less than 15 µrad, and scanning speed up to 2400 mm/s.

A telecentric lens with focal length of 100 mm was integrated in the laser setup that provided a spot size of approximately 50 µm at focal plane and depth of focus of approximately 2.6 mm. The relatively large depth of focus ensures that the top-hat profile is achieved within the effective ablation range of the lens. Furthermore, the beam profile changes, continuously, between top-hat, donut, and Airy profiles along the propagation direction [46]. Therefore, more than one top-hat profile may be obtained within the depth of focus and, thus, such beam delivery setups provide more flexibility. The use of a telecentric lens was essential in this research because the capabilities of a top-hat beam shaper was assessed for performing laser micro-processing operations. Especially, a constant beam path length from the lens to the workpiece surface was maintained and, thus, to have a consistent laser intensity profile at the focal plane, i.e., to keep top-hat profile at the beam waist.

3.3.3. Top-hat Beam Shaper

The refractive field mapping method was employed to change the beam intensity profile from Gaussian to top-hat. This method was selected while taking into account advantages and disadvantages of different beam shaping technologies discussed in Section 2.2 and also the relatively easy integration of ROE based shapers into laser processing systems. An important advantage of the refractive field mapping method is that a top-hat beam can be achieved with a minimum energy loss and misalignment when compared with other methods such as beam truncation with an aperture or using an array of micro-lenses [21]. In addition, the sensitivity of the intensity profile to the shaper's position along the beam path is much less compared with the diffractive field mapping method and this is an important consideration when retrofitting a shaper into existing laser processing systems.

A Focal-πShaper 9_1064 shaper with an optimum wavelength in the range from 1020 to 1100 nm was integrated into the beam delivery system before the XY scan head. The installation and calibration process of the Focal-π Shaper plays a very important role in obtaining good quality beam profile at the lens focal plane. Any small misalignment can contribute to low quality of the top-hat profile at the focal plane. Therefore, a precise alignment procedure was employed to correct the position of the beam shaper stand and, thus, to align it to the beam propagating direction.

The beam profile at the different planes along the propagation direction was measured employing WinCamD-LCM–1" CMOS beam profiler. The input Gaussian beam was transformed into Airy profile, first, after passing through Focal-πShaper as a result of refractive field mapping. Then, through Fourier transformation the intensity profile was converted from Airy to top-hat at the focal plane as shown in Fig. 3.1. This is in

agreement with the theoretical Fourier transformation of Airy intensity profiles along the propagation direction [32, 47]. The top-hat profile shown in Fig. 3.1 is also the best top-hat that can be achieved within depth of focus of the lens. It is important to note that the laser power could decrease because of beam shaper integration into the beam delivery system. Therefore, the laser power was also measured after the focusing lens with laser power meter (Gentec UNO Laser Power Meter). The drop of laser power was compensated by increasing the average power and, thus, maintaining constant power levels during the experiments in this research. The spot sizes of both Gaussian and top-hat beams were kept approximately 50 µm at the focal plane.

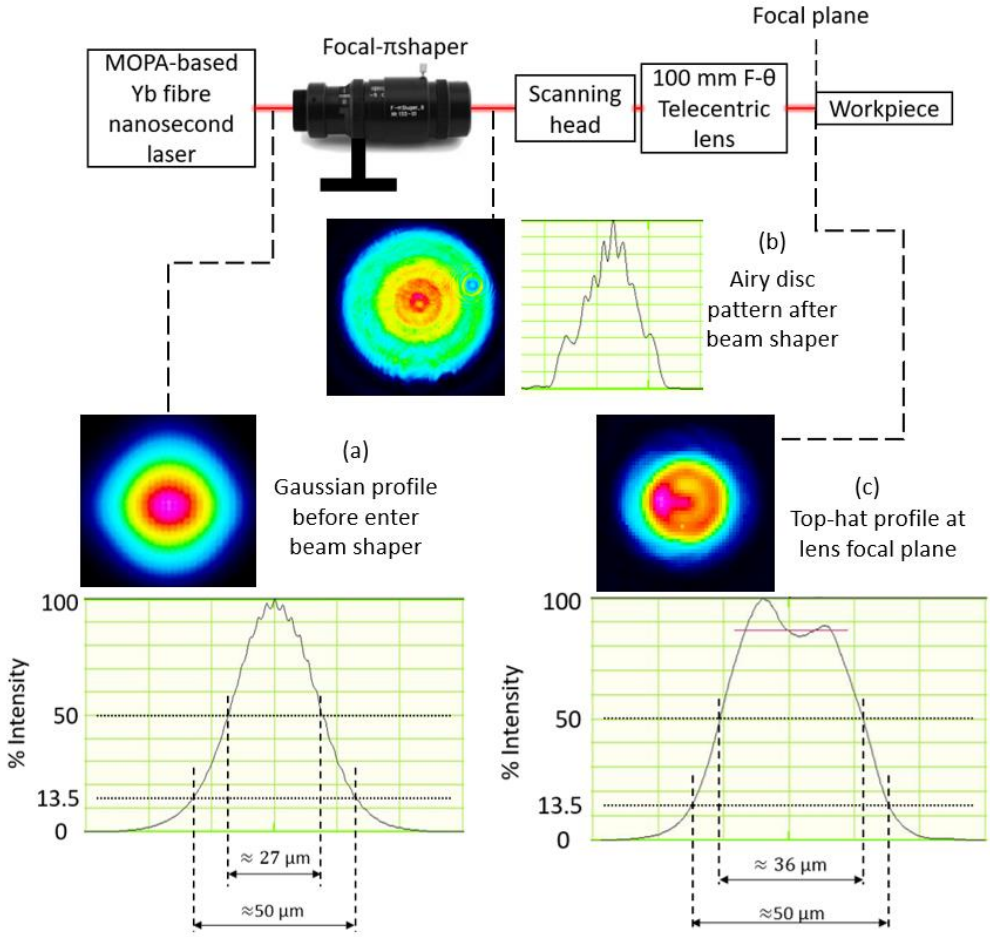

Figure 3.1. *Intensity profiles at different planes along the beam propagation direction: (a) before and (b) after the beam shaper and (c) at the focal plane.*

3.3.4. Design of Experiment

Three sets of experiments were conducted to investigate the capabilities of top-hat laser processing and compare them with the structuring results achievable with Gaussian beam.

3.3.4.1. Structuring with Different Processing Strategies

The structuring quality in this research was assessed based on resulting surface roughness, the tapering effect on the structures' side wall, HAZ, and edge definition. Arrays of square pockets with dimension of 1.5 by 1.5 mm^2 were produced with Gaussian and top-hat beams on Si wafers by applying the process settings in Table 3.1. The pulse distance (P_d) was maintained the same, 10 µm, by adjusting pulse frequency (f) and/or scanning speed (v) by using the following equation:

$$P_d = v/f \quad (1)$$

The optimal hatch and pulse distances to achieve a good surface quality was determined after conducting some initial structuring trials. Three scanning strategies as depicted in Fig. 3.2 were considered in producing the pockets layer by layer, i.e.:

(a) Hatching with 45-degree angular shift between layers;

(b) Reduction outlining from outside to inside;

(c) A combination of hatching and five outlining passes after each layer.

The laser delays were optimized to achieve the best possible structuring quality [9]. Five pockets were produced with each strategy and the processing parameters in Table 3.1 and the average results were analyzed in this research. These parameters were chosen based on some initial trials. The focal plane is kept at the workpiece surface throughout the experiments.

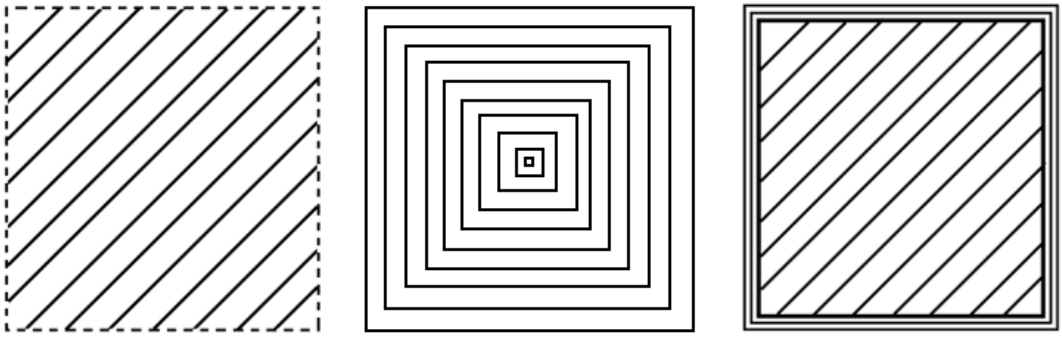

Figure 3.2. *Laser scanning strategies: (a) hatching with 15 µm step over between the passes and 45 degrees shifts between the layers; (b) reduction outlining with 15 µm step over between the passes; and (c) a combination of (a) and (b).*

Table 3.1. Laser processing parameters.

Parameter	Unit	Value
Power	W	22.5
Pulse energy	mJ	0.15
Pulse duration	ns	65
Frequency	kHz	150
Scanning speed	mm/s	1500
Number of layer		30

3.3.4.2. Structuring with Varying Hatching and Pulse Distances

The effects of top-hat profile on ablation rates, specially the pocket depth, and the resulting surface roughness on pocket bottoms were investigated by varying pulse and hatching distances. In particular, the pulse distance was varied in the range from 5 to 14.3 µm by increasing the scanning speed from 750 to 2150 mm/s while keeping the pulse frequency constant at 150 kHz. This helps to avoid the effect of frequency variation which is outside the scope of this study. At the same time, the hatching distance was varied from 5 to 25 µm with an increment of 5 µm as shown in Table 3.2. The structures were fabricated with the hatching (a) strategy, especially with only

hatching passes, while other parameters were kept the same as given in Table 3.1. Both Gaussian and top-hat beams were used to compare the results. Five pockets were produced with each process setting and the average results were analyzed. A full list of conducted experiments is presented in Appendix 1.

Table 3.2. Pulse and hatching distances and pulse energies used in the second and third sets of experiments.

Scanning Speed (mm/s)	**750**	**950**	**1150**	**1350**	**1550**	**1750**	**1950**	**2150**
Equivalent pulse distance (µm)	5.00	6.33	7.67	9.00	10.33	11.67	13.00	14.33
Hatching distance (µm)	5, 10 , 15, 20 ,25							
Pulse energy (mJ)	0.040	0.081	0.120	0.161	0.200	0.238	0.256	

3.3.4.3. Structuring with Varying Pulse Energies

Arrays of square pockets were produced with Gaussian and top-hat beams while pulse energies were varied in the range from 0.04 to 0.256 mJ. Especially, the pulse energies were varied by changing laser power settings while the pulse frequency was kept constant at 150 kHz. This set of experiments were conducted again with the first structuring strategy and also the process settings in Table 3.1 were used with a hatch distance of 15 µm. As in other experiments, five pockets were produced with each process setting and the average results were analyzed.

3.3.5. Inspection

The structured Si wafers were cleaned in an ultrasonic bath and then inspected with a focus variation microscope system (Alicona G5) and a scanning electron microscope (SEM) system (JEOL JCM-6000). All pockets in the three sets of experiments were

scanned with the same resolution settings to obtain their 3D profiles by Alicona G5. The surface roughness was measured over a square area of 700 by 700 μm^2 at the center of the pockets' bottom that was smaller than the minimum required by the standard to measure the true roughness. However, the objective of this research was to compare the structuring performance of top-hat and Gaussian beams and therefore it was more important to keep measurement conditions identical.

The roughness was measured at the centers of fabricated structures to avoid any negative effects near the pockets' edges, especially due to the side walls' tapering, recasts, or beam deflection effect, which can lead to a lower surface quality. Such side effects may prevent judging correctly about the true effects of these two different beam profiles. The taper angles were considered the deviations of the side wall profiles from the normal to the structured planar surface.

3.4. Results and Discussion

3.4.1. Structuring with Different Processing Strategies

3.4.1.1. Quality of Structures

The inspection results from structures produced with three different processing strategies are provided in Table 3.3. In general, the use of the top-hat beam led to lower surface roughness, i.e., S_a. In particular, the improvements in surface quality compared with that achieved with the Gaussian beam were 15% and 21% in case of the hatching (a) and hatching with outlining (c) strategies, respectively. There was only a small increase of surface roughness (3%) when the top-hat beam with the reduction outlining strategy (b) was used to produce the pockets. The uniform intensity distribution of the top-hat beam, especially the much reduce energy tail, led to a more

even material ablation within the beam spot area and also there was less recast around the processed area. In addition, the drop of peak power when the Gaussian profile was transformed into a top-hat one while keeping the pulse energy the same led to a reduction of the average surface roughness. Roughness was improved with all three processing strategies while the average depth of the pocket decreased only marginally, in the range from 0.5% to 1.6%. This marginal decrease of the ablation rate can be compensated easily with small increases of pulse energy that should not have any impact on resulting roughness.

With both beam profiles, there was a tendency surface roughness to increase closer to pockets' walls. This can be explained with the changes in the evacuation conditions for the ablated material and also due to some beam shadowing effects closer to the walls. Recast formation along the walls together with some processing debris could also be contributing to the high roughness.

Table 3.3. Inspection results of the structures produced with three processing strategies.

Processing strategy	Gaussian			Top-hat		
	Roughness S_a	Depth	Taper angle	Roughness S_a	Depth	Taper angle
	µm	µm	Degree	µm	µm	Degree
(a)	1.05 ± 0.05	187	15.19 ± 2.02	0.89 ± 0.02	184	12.92 ± 0.85
(b)	2.62 ± 0.09	175	16.92 ± 1.61	2.69 ± 0.08	174	16.22 ± 1.86
(b)	1.12 ± 0.05	186	3.02 ± 0.46	0.89 ± 0.02	185	6.09 ± 1.85

The tapering effect in laser micro-processing is a major shortcoming, thus, minimizing and eliminating it is a challenge. The results in Table 3.3 clearly show that the top-hat processing had a beneficial effect on the taper angle along the pockets' side walls. In particular, the taper angle was reduced by 2.3° (14.9%) and 0.7° (4.1%) in case of the hatching (a) and reduction outlining (b) strategies, respectively. However, the hatching with outlining (c) strategy with Gaussian beam led to a significantly smaller tapering effect along the side wall, i.e., approximately 50% less that the taper angle obtained with the top-hat profile. This could be explained with the high peak power of the Gaussian beam that led to higher ablation rates at the center of the beam spot. This led to a better material removal along the side walls, especially after the outlining passes along the walls.

The edge definition is also an important factor affecting the structuring quality that should be considered when comparing the pockets produced with both beam intensity profiles and the considered three processing strategies. Fig. 3.3 depicts the edge quality achieved with both beam profiles and three processing strategies. The effect on HAZ cannot be seen clearly and the recast formations at the edges are quite similar for the structures produced with both beam profiles. As expected, distinctly cleaner and sharper edges were created with strategy (c) due to the additional outlining passes and the corrugated effect along the side wall (as shown in Fig. 3.3a, 3.3b, 3.3d and 3.3e) was eliminated.

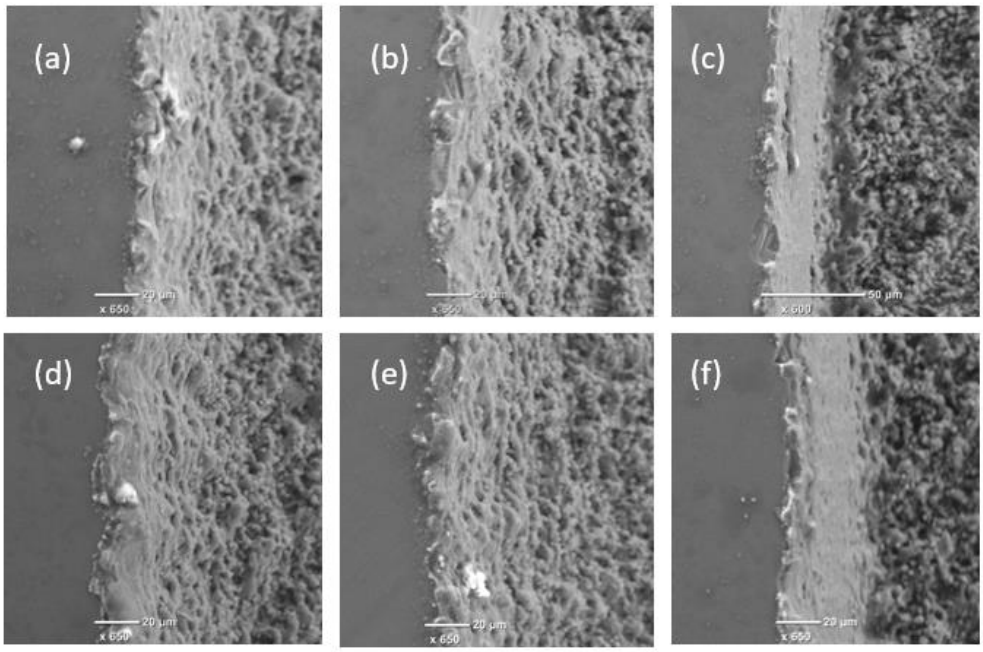

Figure 3.3. *SEM images of the pocket edges produced with Gaussian (top) and top-hat (bottom) beams and the three strategies, respectively: Hatching (a) and (d), reduction outlining (b) and (e), and hatching with outlining (c) and (f).*

The sharpness of pocket corners was again strongly dependent on scanning strategy. Much better definition of the corner was achieved with hatching (a) and hatching with outlining (c) strategies compared with the reduction outlining one (b) as shown in Fig. 3.4. The relatively poor corner definition resulting after strategy (b) can be attributed to some dynamic effects of the scan head at high speed when sharp changes in the beam movement directions are required. The effects of the top-hat processing on structuring quality are not as well pronounced as those on surface integrity. Especially, this is the case because such effects are highly dependent on the quality of the top-hat beam. The laser system used to conduct the experiments was not designed to integrate a beam shaper. Therefore, the quality of the top-hat beam achieved on this system might be affected by the employed manual procedures to retrofit and then to calibration the

beam shaper. The beam shaper may work better on laser system, which is designed to install beam shaper, thus, to give better top-hat beam.

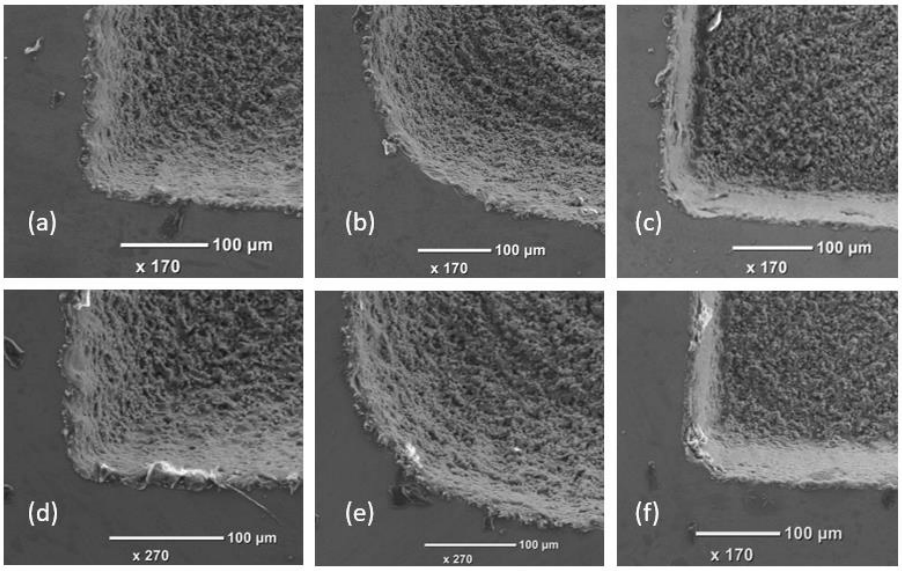

Figure 3.4. *The sharpness of pocket corners achieved with Gaussian (top) and top-hat (bottom) beams and the three strategies, respectively: Hatching (a) and (d), reduction outlining (b) and (e), and hatching with outlining (c) and (f).*

The three investigated scanning strategies in this research had a clear impact on structure quality but also on their morphology. Cross-sectional views of the structures produced with the top-hat beam with these three strategies are presented in Fig. 3.5. The best side walls in regard to the taper angle and the sharpness of the bottom corners were achieved with strategy (c) as was discussed above. In addition, the reduction outlining (b) strategy led to a significant deviation from the nominal pocket profile. In particular, the central part of the pocket was deeper as shown in Fig. 3.5 because of the heat accumulation effect that led to high ablation rates there. This phenomenon occurs when laser passes are too close to each other. In addition, when outlining square trajectories become smaller at the center part, the scanner cannot

reach the designated speed. Thereby, the actual overlap in center area is greater than the outer area. This partly contributed to higher ablation rate at center of the structure. However, it can be minimized by increasing pulse and hatching distances at central of the pocket. The accuracy of the pockets was much better when hatching (a) and hatching with outlining (c) strategies were used as shown in Fig. 3.5.

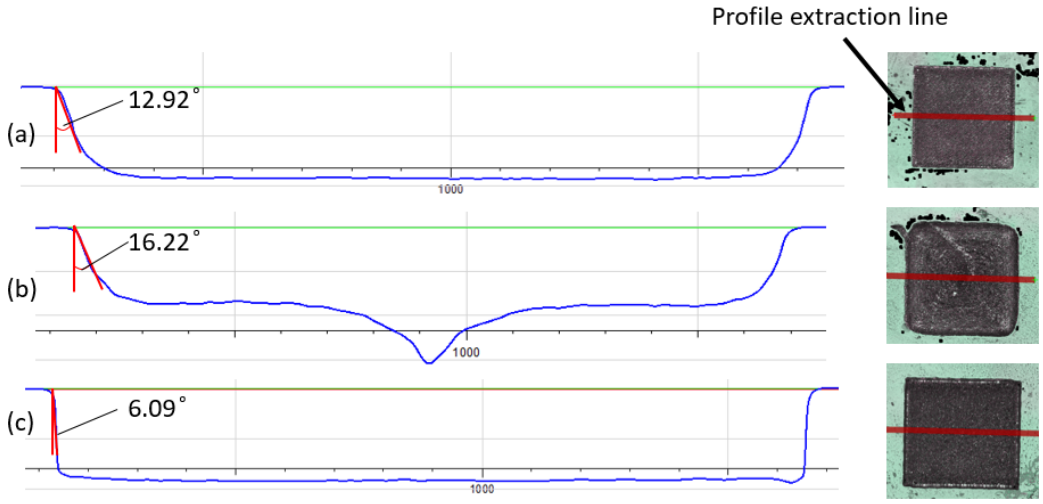

Figure 3.5. *Representative cross sections of pockets produced with top-hat beam (pulse energy 0.15 mJ, hatch distance 15 µm, pulse distance 10 µm, and frequency 150 kHz) and the three strategies, respectively: (a) hatching, (b) reduction outlining, and (c) hatching and outlining.*

3.4.1.2. Process Efficiency

The ablation rates were assessed based on the actual thickness of each processed layer and, thus, to compare the impact of beam profiles and also the respective three processing strategies (see Table 3.4). The ablation rates achieved with the top-hat beam were nearly equal (98% to 99.5%) to those achieved with Gaussian beam when the same pulse energy of 0.15 mJ was applied. The drop of peak power when structuring with top-hat beam led only to marginal reduction in ablation rates.

Theoretically, the lower peak power of top-hat beams should lead to some reductions of ablation rates. However, at the same time the top-hat profile leads to bigger beam spot area with fluence levels higher than the ablation threshold compared to Gaussian one. Thus, larger overlaps of effective ablation areas can be achieved with the top-hat beam when pulse and hatch distances are similar as shown in Fig. 3.6. Consequently, the heat accumulation phenomena affects a bigger area in case of top-hat processing where decreases ablation threshold [48] and, thus, leads to a better ablation efficiency. This compensates to larger extend the decrease of ablation rates in top-hat processing due to the drop of pulse peak intensity. It is evident from the experimental results that the heat accumulation effect can bring an important advantage in laser micro-processing, especially improvements in ablation rates can be achieved without sacrificing either structuring or surface quality.

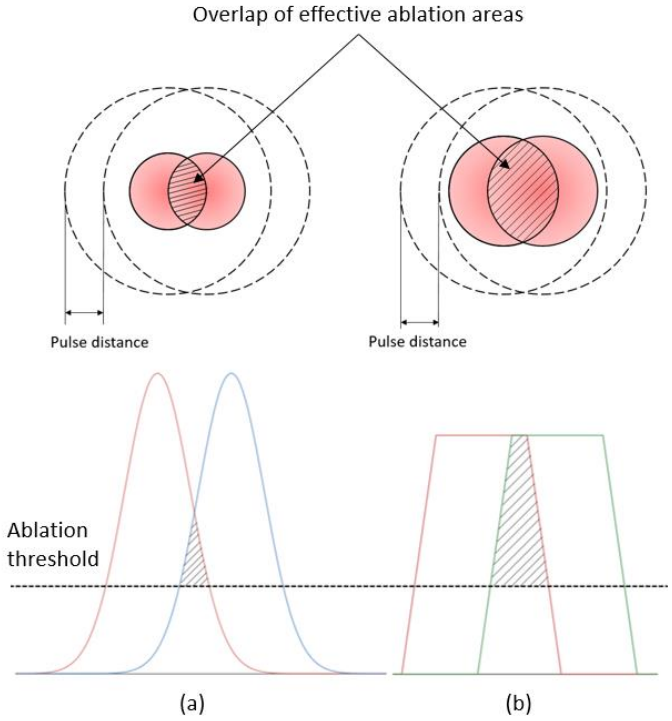

Figure 3.6. *Overlaps of effective ablation areas achievable with Gaussian (a) and top-hat (b) beams with similar pulse and hatch distances.*

Hatching with outlining (c) strategy led to the best taper angle and good average surface roughness (see Table 3.4). As stated in Section 4.1.1, outlining passes reduced the tapering effect but this was in expense of processing efficiency as they were additional to the hatching ones. It is important to note that the structuring efficiency, the achievable ablation rates, of silicon wafers is relatively good compare with some metals, e.g., stainless steel or copper-based alloys. Therefore, only five outlining passes were necessary after the hatching ones for each layer. However, if a material with lower ablation rates is used, e.g., stainless steel, the processing time will increase even further as more outlining passes will be required when hatching with outlining (c) strategy is employed. At the same time, this increase of processing time can be minimized due to bigger effective ablation areas achievable with top-hat profiles and also by increasing the pulse distance, e.g., by increasing the scanning speed and hatch distance. Therefore, the use of top-hat beams can expand the parameters' domain that should be considered when optimizing the process, especially by taking into account the trade-offs between processing efficiency and structuring quality.

Table 3.4. Ablation rates and processing times achievable with the investigated 3 processing strategies.

Scanning Strategy	Ablation Rate (μm/layer)		Processing Time (30 layers) [s]
	Gaussian	Top-hat	
(a)	6.23	6.13	10.7
(b)	5.83	5.80	3.7
(c)	6.20	6.17	12.23

When the reduction outlining (b) strategy was used, the ablation depth per layer was lower, i.e., 94%–95% lower, compared with other two strategies but at the same time the processing efficiency increased approximately three times even though the total

beam path lengths were equal across the three strategies. The increase of processing time can be explained with the employed laser delays during the hatching passes that are necessary for achieving a good structuring accuracy while they are not necessary for the outlining passes in (b) strategy. However, as discussed before this high processing efficiency achieved with the reduction outlining strategy was in expense of structuring quality as discussed in Section 4.1.1. Thus, again it can be reiterated that there is a potential for further improvements of processing efficiency when top-hat beams are used by developing new structuring strategies that can combine the capabilities of hatching and outlining passes while taking into account the trade-offs associated with quality.

3.4.2. Structuring with Varying Hatching and Pulse Distances

The effects of varying pulse and hatching distances with the hatching (a) strategy on resulting surface roughness and ablation rates were investigated. Contour plots that depicts the roughness levels achieved across the considered pulse and hatching distances with both beam profiles are given in Fig. 3.7. The highest roughness was obtained when the pulse distance was in the range from 10.5 to 14.5 µm while the hatch distance was higher than 15 µm for both beam profiles. However, it should be mentioned that the increase of roughness with these process settings was less in case of the top-hat beam. The high roughness can be explained with relatively small pulse overlaps at these settings and as consequence of this the processing was not uniform while the heat accumulation was the relatively low, that also led to low processing efficiency. At the same time, the other extreme, i.e., too small pulse distances of less than 6 µm, also led to high roughness with both beam profiles. In this case, the heat accumulation was too much and led to more debris and recasts in the processed area.

Overall, the top-hat beam provided a lower roughness than the processing with Gaussian beam for most of investigated process settings. Thus, if a given roughness should be achieved, the processing with top-hat beam will offer more flexibility, especially processing with higher pulse and hatch distances, and, thus, a higher processing efficiency. Likewise, it should be stated that roughness lower than 0.8 µm was achieved with top-hat beam when the pockets were produced with pulse and hatch distances in the range from 13 to 14.5 µm and from 10 to 15 µm, respectively, while such lower roughness was not achieved with Gaussian beam. It is important to note that the hatch areas in Fig. 3.7 depict regions where the accumulated laser fluence increased to such a level in the conducted experiments that it was sufficient to penetrate the workpiece.

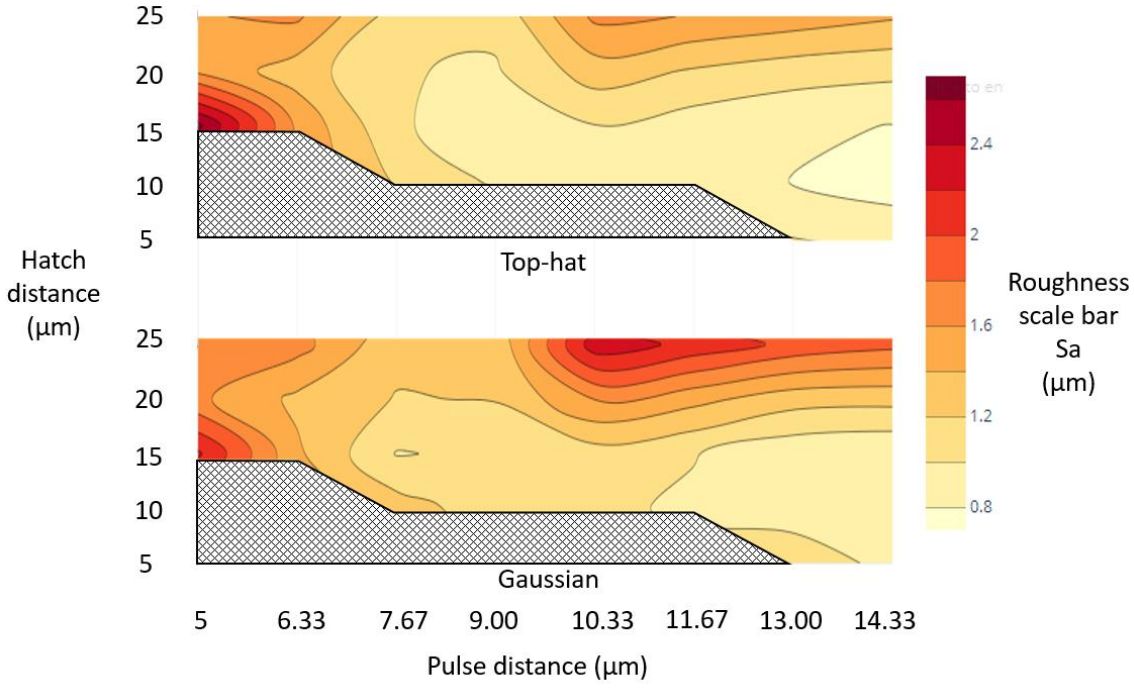

Figure 3.7 *Roughness contour plots of pockets produced with top-hat and Gaussian beams and considered hatch and pulse distances (pulse length 65 ns, frequency 150 kHz, and pulse energy 1.5 mJ).*

3.4.3. Structuring with Varying Pulse Energies

The effects of varying pulse energies on structuring performance with both beam profiles were investigated, too. Especially, the impact of increasing pulse energies in the range from 0.04 to 0.256 mJ on resulting roughness and structuring efficiency is depicted in Fig. 3.8. Two distinct processing regimes were identified when the effects of pulse energy on surface roughness were analyzed. The first regime was present when laser intensity was not sufficient and melting and boiling dominated in the interaction area. The second one was triggered when the intensity reached the required level for consistent ablation that led to a linear increase of material removal with the increase of pulse energy. The surface roughness was the highest, i.e., S_a of 1.7 µm, at the lowest pulse energy of 0.04 mJ, dropped to 0.9 µm at 0.08 mJ and then increased almost linearly to reach S_a of 1.6 µm at 0.256 mJ when the structuring was carried out with Gaussian beam.

A different surface response in regard to the resulting roughness was observed when the structuring was performed with a top-hat beam and the same range of pulse energies were investigated. Especially, roughness was S_a of 2.83 µm at the lowest pulse energy setting of 0.04 mJ and then initially increased to peak with S_a of 3.81 µm at E_p = 0.08 mJ. Next, roughness dropped to the lowest S_a value of 0.9 µm at 0.12 mJ and then again increased almost linearly to S_a of 1.6 at the highest pulse energy setting of 0.256 mJ. At the low pulse energy settings (first processing regime), the laser intensity was only sufficient for melting or partly boiling the substrate material that can explain the higher resulting roughness. The transition from first to second regime led to the lowest roughness that was achieved at different pulse energy levels for the two

considered beam profiles, especially at lower setting for the Gaussian beam of 0.08 mJ while pulse energy of 0.12 mJ was required for the top-hat one.

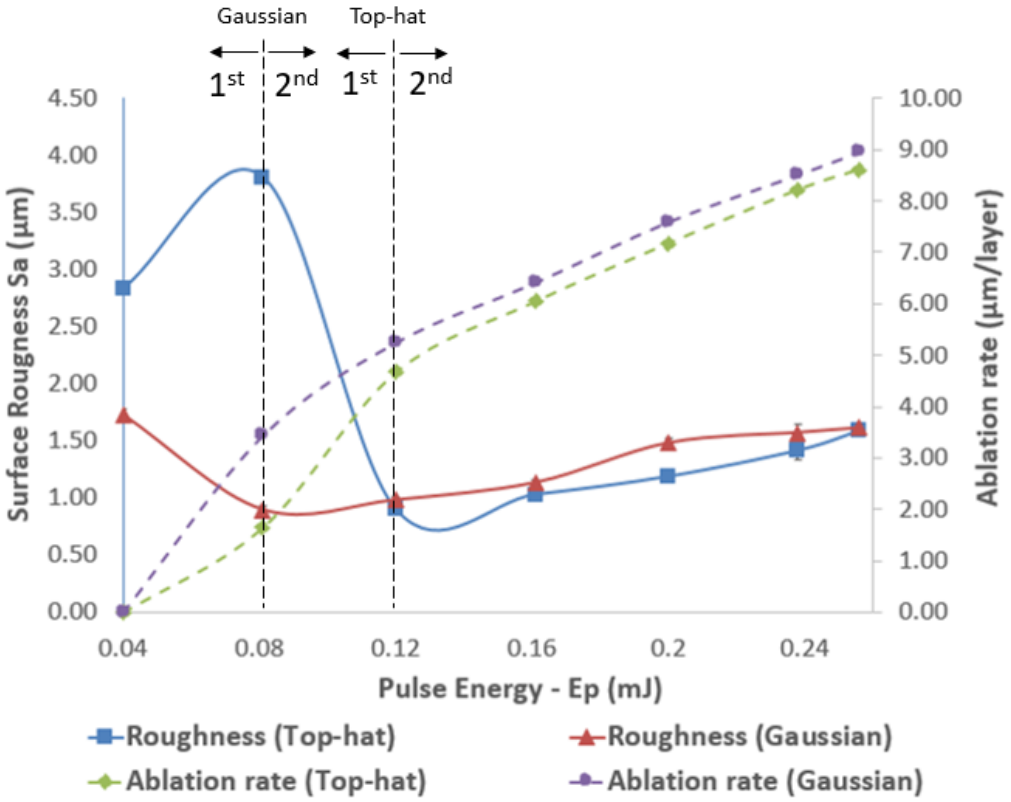

Figure 3.8. *The effects of varying pulse energy on surface roughness and processing efficiency achievable with Gaussian and top-hat beams (pulse length 65 ns, frequency 150 kHz, pulse distance 10 µm, and hatch distance 15 µm).*

The ablation rates at the lowest pulse energy settings of 0.04 mJ were zero for both Gaussian and top-hat beam. When the pulse energy increased to 0.08 mJ, there was some ablation with both Gaussian and top-hat beams, especially 3.44 and 1.65 µm/layer, respectively. The processing efficiency of the top-hat beam was less than

half of that achieved with Gaussian beam while the Sa roughness values reached the two extremes, i.e., the highest (3.81 μm) and the lowest (0.89 μm), respectively. The high roughness values achieved with the top-hat beam can be explained with the relatively low peak power that was not sufficient to have a stable ablation process and therefore led to some recasts and melted material in the processed areas.

At the same time, when the pulse energy excessed 0.12 mJ, the structures fabricated with the top-hat beam had consistently a better surface roughness compared to that achieved with Gaussian beam. In particular, the improvements in surface roughness varied in the range of 1%–2% at 0.256 mJ to almost 20% at 0.2 mJ when the pulse energy was varied from 0.12 mJ to 0.256 mJ. The average roughness improvement in this pulse energy range was 9.5%. Regarding the processing efficiency, the ablation rates achieved with the top-hat beam was 89% at 0.12 mJ to 97% at 0.238 mJ of the respective ones obtained with Gaussian beam. Thus, it can be stated that the ablation rates of top-hat beam were getting close to those achieved with Gaussian beam when pulse energy was increased. Thus, taking into account the bigger parameter domain that should be considered in optimizing the top-hat structuring process it should be possible to achieve a better surface roughness with a comparable processing efficiency to that achieved with Gaussian beam.

3.5. Conclusion

The paper reports an investigation into the effects of beam intensity profiles and scanning strategies in laser micro-structuring. The resulting surface and structuring quality together with processing efficiency were compared when the other process parameters were kept the same. The result shows that the top-hat processing can lead

to improvements both in surface roughness and structuring quality. Especially, the top-hat processing resulted into a decrease of the taper angle on the side walls of the structures in the range from 4% to 15% when only hatching and reduction outlining strategies were used. The tapering effect was smaller with Gaussian beam only when hatching with additional outlining passes were used. However, it is worth stressing that the improvements in surface roughness and the tapper angle achieved with the top-hat beam were not in expense of processing efficiency. In particular, the ablation rates were nearly the same with both beam intensity profiles or just marginally worst with the top-hat beam. The hatching strategy with some additional outlining passes resulted in a very good surface roughness and the lowest taper angle along the side walls with both beam profiles. The use of only outlining passes improved the processing efficiency almost three times but this was in expense of surface and structuring quality. The effects of top-hat structuring when varying pulse energy and hatch and pulse distances were also investigated. The top-hat structuring led to a better surface and structuring quality when pulse energy higher than 0.12 mJ were used while the processing efficiency was almost the same. The dependence of surface quality on set hatch and pulse distances showed that a better surface quality in a bigger parameters' domain can be achieved with a top-hat beam. In addition, a given pre-defined surface roughness can always be achieved with a better processing efficiency when the structuring is performed with a top-hat beam.

Funding and Acknowledgments

The research was supported by two H2020 Factory of the Future projects, "Modular laser based additive manufacturing platform for large scale industrial applications"

(MAESTRO, Grant agreement number 723826) and “High-Impact Injection Moulding Platform for mass-production of 3D and/or large micro-structured surfaces with Antimicrobial, Self-cleaning, Anti-scratch, Anti-squeak and Aesthetic functionalities” (HIMALAIA, Grant agreement number 766871). Also, the research was carried out with the framework of the regional ESIF project “Smart Factory Hub” (SmartFub).

References

1. Homburg, O. and Mitra, T. *Gaussian-to-top-hat beam shaping: an overview of parameters, methods, and applications*. in *Laser Resonators, Microresonators, and Beam Control XIV*. 2012. International Society for Optics and Photonics.
2. Laskin, A., Bae, H., Laskin, V., and Ostrun, A., *Beam shaping of focused beams for microprocessing application.*
3. Booth, H., *Recent applications of pulsed lasers in advanced materials processing.* Thin Solid Films, 2004. **453**: p. 450-457.
4. Ahn, S., Hwang, D.J., Park, H.K., and Grigoropoulos, C.P., *Femtosecond laser drilling of crystalline and multicrystalline silicon for advanced solar cell fabrication.* Applied Physics A, 2012. **108**(1): p. 113-120.
5. Ruf, A., Berger, P., Dausinger, F., and Hügel, H., *Analytical investigations on geometrical influences on laser drilling.* Journal of Physics D: Applied Physics, 2001. **34**(18): p. 2918.
6. Jackson, M.J. and O'Neill, W., *Laser micro-drilling of tool steel using Nd:YAG lasers.* Journal of Materials Processing Technology, 2003. **142**(2): p. 517-525.
7. Nasrollahi, V., Penchev, P., Jwad, T., Dimov, S., Kim, K., and Im, C., *Drilling of micron-scale high aspect ratio holes with ultra-short pulsed lasers: Critical effects of focusing lenses and fluence on the resulting holes' morphology.* Optics and Lasers in Engineering, 2018. **110**: p. 315-322.
8. Bhaduri, D., Penchev, P., Dimov, S., and Soo, S.L., *An investigation of accuracy, repeatability and reproducibility of laser micromachining systems.* Measurement, 2016. **88**: p. 248-261.
9. Penchev, P., Dimov, S., Bhaduri, D., Soo, S.L., and Crickboom, B., *Generic software tool for counteracting the dynamics effects of optical beam delivery systems.* Proceedings of the Institution of Mechanical Engineers, Part B: Journal of Engineering Manufacture, 2017. **231**(1): p. 48-64.
10. Auerswald, J., Ruckli, A., Gschwilm, T., Weber, P., Diego-Vallejo, D., and Schlüter, H., *Taper Angle Correction in Cutting of Complex Micro-mechanical Contours with Ultra-Short Pulse Laser.* 2016.
11. Wang, X.C., Zheng, H.Y., Chu, P.L., Tan, J.L., Teh, K.M., Liu, T., Ang, B.C.Y., and Tay, G.H., *High quality femtosecond laser cutting of alumina substrates.* Optics and Lasers in Engineering, 2010. **48**(6): p. 657-663.
12. Ghoreishi, M., Low, D.K.Y., and Li, L., *Comparative statistical analysis of hole taper and circularity in laser percussion drilling.* International Journal of Machine Tools and Manufacture, 2002. **42**(9): p. 985-995.
13. Penchev, P., Shang, X., Dimov, S., and Lancaster, M., *Novel manufacturing route for scale up production of terahertz technology devices.* Journal of Micro and Nano-Manufacturing, 2016. **4**(2): p. 021002.

14. Nasrollahi, V., Penchev, P., Dimov, S., Korner, L., Leach, R., and Kim, K., *Two-Side Laser Processing Method for Producing High Aspect Ratio Microholes.* Journal of Micro and Nano-Manufacturing, 2017. **5**(4): p. 041006.
15. Wee, L.M., Ng, E.Y.K., Prathama, A.H., and Zheng, H., *Micro-machining of silicon wafer in air and under water.* Optics & Laser Technology, 2011. **43**(1): p. 62-71.
16. Shealy, D.L. and Hoffnagle, J.A., *Laser beam shaping profiles and propagation.* Applied Optics, 2006. **45**(21): p. 5118-5131.
17. Dickey, F.M. and Holswade, S.C., *Gaussian laser beam profile shaping.* Optical Engineering, 1996. **35**(11): p. 3285-3296.
18. Dickey, F.M., Weichman, L.S., and Shagam, R.N. *Laser beam shaping techniques*. in *High-Power Laser Ablation III*. 2000. International Society for Optics and Photonics.
19. Yura, H.T. and Rose, T.S., *Gaussian beam transfer through hard-aperture optics.* Applied Optics, 1995. **34**(30): p. 6826-6828.
20. Dickey, F.M., *Laser beam shaping: theory and techniques*. 2014: CRC press.
21. Laskin, A. and Laskin, V. *πShaper–Refractive beam shaping optics for advanced laser technologies*. in *Journal of Physics: Conference Series*. 2011. IOP Publishing.
22. Sanner, N., Huot, N., Audouard, E., Larat, C., Loiseaux, B., and Huignard, J.-P., *Programmable spatial beam shaping of a 100 kHz amplified femtosecond laser.* Optics Letters, 2005. **30**: p. 1479-1481.
23. Labroille, G., Denolle, B., Jian, P., Genevaux, P., Treps, N., and Morizur, J.-F., *Efficient and mode selective spatial mode multiplexer based on multi-plane light conversion.* Optics Express, 2014. **22**(13): p. 15599-15607.
24. Häfner, T., Strauß, J., Roider, C., Heberle, J., and Schmidt, M., *Tailored laser beam shaping for efficient and accurate microstructuring.* Applied Physics A, 2018. **124**(2): p. 111.
25. Li, J., Tang, Y., Kuang, Z., Schille, J., Loeschner, U., Perrie, W., Liu, D., Dearden, G., and Edwardson, S., *Multi imaging-based beam shaping for ultrafast laser-material processing using spatial light modulators.* Optics and Lasers in Engineering, 2019. **112**: p. 59-67.
26. Blair, P., Currie, M., Trela, N., Baker, H.J., Murphy, E., Walker, D., and McBride, R. *Field mappers for laser material processing*. in *Laser Resonators, Microresonators, and Beam Control XVIII*. 2016. International Society for Optics and Photonics.
27. Laskin, A. and Laskin, V. *Variable beam shaping with using the same field mapping refractive beam shaper*. in *Laser Resonators, Microresonators, and Beam Control XIV*. 2012. International Society for Optics and Photonics.

28. Umhofer, U., Jäger, E., and Bischoff, C., *Refractive and diffractive laser beam shaping optics: High end components for material processing.* Laser Technik Journal, 2011. **8**(3): p. 24-27.
29. Račiukaitis, G., Stankevičius, E., Gečys, P., Gedvilas, M., Bischoff, C., Jäger, E., Umhofer, U., and Völklein, F., *Laser Processing by Using Diffractive Optical Laser Beam Shaping Technique.* Journal of laser micro/nanoengineering, 2011. **6**(1).
30. Laskin, A. and Laskin, V. *Imaging techniques with refractive beam shaping optics*. in *Laser Beam Shaping XIII*. 2012. International Society for Optics and Photonics.
31. Delaporte, P., Karnakis, D., and Zergioti, I., *12 - Laser processing of flexible organic electronic materials*, in *Handbook of Flexible Organic Electronics*, Logothetidis, S., Editor. 2015, Woodhead Publishing: Oxford. p. 285-313.
32. Laskin, A. and Laskin, V. *Creating round and square flattop laser spots in microprocessing systems with scanning optics*. in *International Congress on Applications of Lasers & Electro-Optics*. 2012. LIA.
33. Bhuyan, M.K., Courvoisier, F., Lacourt, P.-A., Jacquot, M., Furfaro, L., Withford, M., and Dudley, J., *High aspect ratio taper-free microchannel fabrication using femtosecond Bessel beams.* Optics express, 2010. **18**(2): p. 566-574.
34. Duocastella, M. and Arnold, C.B., *Bessel and annular beams for materials processing.* Laser & Photonics Reviews, 2012. **6**(5): p. 607-621.
35. Doan, H.D., Naoki, I., and Kazuyoshi, F., *Laser processing by using fluidic laser beam shaper.* International Journal of Heat and Mass Transfer, 2013. **64**: p. 263-268.
36. Sanner, N., Huot, N., Audouard, E., Larat, C., and Huignard, J.P., *Direct ultrafast laser micro-structuring of materials using programmable beam shaping.* Optics and Lasers in Engineering, 2007. **45**(6): p. 737-741.
37. Matsuoka, Y., Kizuka, Y., and Inoue, T., *The characteristics of laser micro drilling using a Bessel beam.* Applied Physics A, 2006. **84**(4): p. 423-430.
38. Li, B., Xiong, S., and Zhang, Y., *Fresnel diffraction model for mode-mismatched thermal lens with top-hat beam excitation.* Applied Physics B, 2005. **80**(4): p. 527-534.
39. Nasrollahi, V., Penchev, P., Batal, A., Le, H., Dimov, S., and Kim, K., *Laser drilling with a top-hat beam of micro-scale high aspect ratio holes in silicon nitride.* Journal of Materials Processing Technology, 2020: p. 116636.
40. Wehrmann, A., Puttnins, S., Hartmann, L., Ehrhardt, M., Lorenz, P., and Zimmer, K., *Analysis of laser scribes at CIGS thin-film solar cells by localized electrical and optical measurements.* Optics & Laser Technology, 2012. **44**(6): p. 1753-1757.
41. Coutts, D., Withford, M., Piper, J., Rutterford, G., Bell, A., and Knowles, M. *Generation of flat-top focussed beams for percussion drilling of ceramic and*

metal. in *International Congress on Applications of Lasers & Electro-Optics*. 2002. LIA.
42. Rung, S., Rexhepi, M., Bischoff, C., and Hellmann, R., *Laserscribing of thin films using top-hat laser beam profiles.* Journal of Laser Micro Nanoengineering, 2013. **8**(3): p. 309.
43. Rung, S., Barth, J., and Hellmann, R., *Characterization of laser beam shaping optics based on their ablation geometry of thin films.* Micromachines, 2014. **5**(4): p. 943-953.
44. Mishra, S. and Yadava, V., *Laser Beam MicroMachining (LBMM) – A review.* Optics and Lasers in Engineering, 2015. **73**: p. 89-122.
45. Engelhart, P., Harder, N.P., Grischke, R., Merkle, A., Meyer, R., and Brendel, R., *Laser structuring for back junction silicon solar cells.* Progress in Photovoltaics: Research and Applications, 2007. **15**(3): p. 237-243.
46. Laskin, A. and Laskin, V. *Refractive field mapping beam shaping optics: important features for a right choice*. in *Proc. ICALEO*. 2010.
47. Kanzler, K.J. *Transformation of a gaussian laser beam to an Airy pattern for use in focal plane intensity shaping using diffractive optics*. in *Laser Beam Shaping II*. 2001. International Society for Optics and Photonics.
48. Sun, Z., Lenzner, M., and Rudolph, W., *Generic incubation law for laser damage and ablation thresholds.* Journal of Applied Physics, 2015. **117**(7): p. 073102.

CHAPTER 4

MHZ BURST MODE PROCESSING AS A TOOL FOR ACHIEVING REMOVAL RATES SCALABILITY IN ULTRASHORT LASER MICRO-MACHINING

Hoang Le [1], Themistoklis Karkantonis [1], Vahid Nasrollahi [1], Pavel Penchev [1] and Stefan Dimov [1]

[1]Department of Mechanical Engineering, University of Birmingham, Birmingham B15 2TT, UK

This research was published as a full-length article in ***Applied Physics A: Material Science & Processing*** (2022).

Le, H., Karkantonis, T., Nasrollahi, V. et al. MHz burst mode processing as a tool for achieving removal rates scalability in ultrashort laser micro-machining. Appl. Phys. A 128, 711 (2022). https://doi.org/10.1007/s00339-022-05864-8

Author Contributions	
Hoang Le **(First Author)**	Conceptualization, Formal analysis, Methodology, Investigation, Validation, Writing–original draft, Writing–review & editing
Themistoklis Karkantonis	Investigation
Vahid Nasrollahi	Writing–review & editing
Pavel Penchev	Methodology
Stefan Dimov	Conceptualization, Project administration, Writing–review & editing

Abstract

The average power of ultrashort laser source has been increasing continuously and therefore solutions are required to employ fully these technology advances for improving the ablation efficiency in laser micro-processing. The use of burst mode processing is one of the solutions that has attracted a significant research and industrial interest in the last decade. A novel empirical methodology is proposed and implemented in this research to assess the MHz burst mode impact on the specific removal rate (SRR) and processing efficiency in ultrashort laser micro-machining. Especially, the capability of the MHz burst mode processing is investigated to scale up SRRs achievable on copper and stainless steel while utilising fully the available maximum pulse energy and average laser power. The results showed that the MHz burst mode offer a significant SRR scalability potential that can be attributed to beneficial near optimum fluence level and other side effects such as heat accumulation. Also, it is evidenced from the obtained results that the surface quality attained with the burst mode processing was comparable to that achieved with the single pulse processing and even better at some specific process settings. Thus, the obtained SRR improvements were not in expense of the surface quality and the MHz bust mode processing represents a promising solution to employ fully the constantly increasing average power in ultrashort laser processing operations.

Keywords: laser processing, burst mode, specific removal rate, pulse distance, surface quality.

4.1. Introduction

Over the last decade, the rapid development in laser technology enabled the development of higher power ultrashort pulsed laser sources that can meet the requirements of micro-machining processes. In particular, a higher process efficiency and/or material removal rates have been achieved by employing such lasers [1, 2]. Generally, a higher pulse energy (i.e. pulse fluence) leads to higher removal rates, which is usually quantified with the removed volume per processing time or feeds [3, 4]. In contrast, specific removal rate (SRR) is commonly used to judge about the ablation efficiency of ultrashort pulse lasers. In reality, this process parameter is dependent on the pulse fluence and can be calculated using the following equation [5]:

$$SRR = \frac{dV}{dE} = \frac{1}{2} \cdot \frac{\delta}{F_0} \cdot ln^2\left(\frac{F_0}{F_{th}}\right) \quad (1)$$

where: δ is energy penetration depth; F_0 - pulse fluence and F_{th}- ablation threshold. As can be judge from Eq. (1) and also some other reported studies [6-8], a relatively high ultrashort pulse fluence (ten times higher than the ablation threshold) reduces the specific removal rate, i.e. the removal volume per unit energy. This is attributed to the significant pulse energy losses into heat diffusion and ionisation instead of using it

only for material sublimation [9]. At the same time, when ultrashort pulse fluence much higher than the ablation threshold is used, this lead to some negative side effects, i.e. melting and re-solidification of material, which can reduce the overall process efficiency [10]. To address these limitations, burst mode processing has been investigated as one of potential solutions to attain a higher processing flexibility and control during the laser irradiation. By applying the burst mode processing, a single ultrashort pulse can be split into a train of smaller sub-pulses and thus each of them can have a fluence closer to the optimum value [11, 12]. In this way, it can be extrapolated, theoretically, that the maximum available output power could be utilised while maintaining SRR of a single pulse at its optimum value. In addition, the use of burst mode allows a higher repetition frequency between sub-pulses that can be up to MHz and GHz scales. As a result, different advantages associated with the burst mode processing were reported, i.e. significant improvement in removal rate and surface quality simultaneously, especially in the case of GHz bursts [13-15].

Over the last few years, many studies have investigated the capabilities of the burst mode regime for ultrashort laser micro-processing. For instance, its benefits in the laser machining processes have been demonstrated for different type of materials, such as metals, ceramics and transparent materials [16-18]. Jaeggi et al. reported that the removal rates achieved with 3 sub-pulses burst mode processing of aluminium and copper were higher than those obtained with a single pulse within a certain fluence

range; while, the 2 sub-pulses burst mode did not show any advantages over the single pulse processing [19]. This phenomenon can be attributed to the shielding effect and the material redeposition on the surface [9, 20]. Similar results were also reported by other researchers, especially confirming the high efficiency achievable with 3 sub-pulses burst mode on copper and stainless steel [21]. However, delivering a train of sub-pulses with a temporal distance of nanoseconds led to SRR reduction in the case of gold and silver regardless of the number of sub-pulses compared to the single pulse processing [21].

Applying a femtosecond MHz burst mode for welding of glass was reported in another study [22]. It was shown that the burst mode did not have a positive effect on enlarging the heat affected zone (HAZ) into the longitudinal dimension, which is desirable in welding of glass. However, the HAZ increase in the vertical dimension was reported to create a longer filamentation inside the glass with the same delivered energy as the single pulse welding. The use of Bessel beam in the MHz burst mode was reported in another study, especially to drill micro-hole onto a thin AF32 glass with the objective to increase the drilling speed [23]. However, the burst mode led to strong thermal side effects that induced cracks at the edges of micro-holes, although the sub-pulse energy in the burst was less than that used in the single pulse drilling. In addition, the fluence level and temporal distance between sub-pulses strongly affected the laser-material interactions and consequently the process efficiency and the hole quality. The laser

wavelength was another important parameter that influenced the performance in the burst mode processing. In particular, the use of the burst mode with an infrared laser showed clear advantages over a green laser processing in regard to the removal rate achieved on metals and semiconductors [19, 24]. Though, the energy penetration depth in the green laser regime was greater than that achieved with the infrared laser.

Different effects can be obtained by varying the temporal distance between the sub-pulses. In ultrashort laser micro-machining, GHz burst mode was used not only to increase the material removal rate but also to improve the quality of the machined structures [16, 25]. More specifically, surface roughness was significantly reduced when the GHz burst mode was used as a post-processing step to clean the surface, e.g. to remove micro-scale recasts and micro cone structures from the machined surface [26]. The GHz burst of femtosecond pulses also resulted in cleaner entrance when drilling micro-holes onto invar foils, however when applying on thick substrates the process efficient was impacted dramatically [27]. On the contrary, the MHz burst mode processing improved the removal rate, because it led to an increase of the heat accumulation [28]. However, this removal rate improvement came at the expense of the surface quality. Especially, the micro-structures fabricated using the MHz burst mode led to a significant residual heat and thus the overall quality was similar to that achieved in nanosecond laser processing [29]. Nevertheless, the MHz burst mode processing with a temporal sub-pulse distance of few nanoseconds had be employed

in some applications to smoothen surfaces at low fluence level [30]. Combinations of GHz and MHz burst mode processing were proposed as a potential solution to benefit from the advantages offered by both processes [31-34]. Although, the reported results showed that there were no efficiency gains in comparison to the single pulse mode, the surface roughness was improved and did not depend on the number of processed layers.

The conducted literature review led to the conclusion that the influence of the burst mode was strongly dependant on the specific application and how its effects were investigated. Some researchers argued that the burst mode performance should be compared with that of a single pulse processing, i.e. with the same pulse energy, and a similar intensity per area [16, 21]. At the same time, the burst mode delivers a train of sub-pulses and therefore its impact on the processing performance comes mainly from the optimum fluence level applied and the change in ablation mechanism, i.e. the incubation effect led to the ablation threshold decrease and heat accumulation due to high repetition rate. Though, few studies employed the burst mode to reduce the sub-pulse fluence to near optimum levels for a given material and hence to increase the removal rate [11, 35].

So, it could be stated that the removal rate improvements can be attributed to different factors, especially the set sub-pulse fluence, the induced incubation effects and the heat accumulation due to multiple sub-pulses within a single pulse/burst. The impact

of the heat accumulation on removal rates has been reported to be significant, because it could either raise the surface temperature to the material vaporization point or lead indirectly to material redeposition due to the residual heat [36-38]. However, the effects of heat accumulation, plasma shielding and other factors on the overall specific removal rate have not been studied systematically, while this is very important for assessing and judging conclusively about their contributions. In addition, the increase of sub-pulses in a burst from tens to hundreds, especially when a relatively high pulse energies are available at certain frequencies, has not be studied, i.e. the number of sub-pulses in the reported investigations was limited to less than 30. Also, the negative effects of plasma shielding on ablation process have not been studied, especially, when pulse-to-pulse and sub-pulse shielding are simultaneously present as it is the case in burst mode applied. Especially, laser induced plasma plume can have a significant impact by blocking/shielding the energy of subsequent pulses and sub-pulses in a burst and thus to reduce the ablation efficiency [39, 40].

This research reports a systematic investigation into the impact of the heat accumulation and other factors on achievable removal rates in MHz burst mode processing. Especially, the benefits and some intrinsic side effects were studied in MHz burst mode processing and the achieved performance were compared with the single pulse one. In this way, the improvements in the machining performance have been quantified and the achievable SRR scalability with the MHz burst mode

processing is discussed. The next section describes the empirical methodology employed in this research and then the obtained results are discussed, and conclusions are made.

4.2. Materials and methodology

4.2.1. Laser source and burst mode generation

The experiments were carried out on LASEA LS-4 workstation that integrates a diode-pumped ultrashort laser source Yuja from Amplitude Systems with an average power of 10 W and can provide a tuneable pulse duration from less than 500 fs to 10 ps. The laser source has a central wavelength of 1030 µm and beam quality M^2 is better than 1.2. The maximum pulse energy after the focusing lens was 90 µJ at a frequency of 100 kHz in the utilised laser system. The final output beam had a diameter of 30 µm at the focus plane and a circular polarisation. The burst mode of the laser source is generated through oscillator at 40 MHz and a pulse picker as shown in Fig. 4.1a. This results in a minimum temporal distance of 25 ns between sub-pulses in the burst mode (equivalent to intra-burst frequency f_{IB} = 40 MHz). Therefore, the maximum number of sub-pulses per burst can be up to 400. The pulse/burst energy is set when the burst mode is triggered. This means that the energy of a single pulse and the respected burst are the same and equal to the number of sub-pulses per burst (N_b) multiplied by the sub-pulse energy (Fig. 4.1a and 4.1b), theoretically. In fact, the energy distribution across the sub-pulses is not even, due the gain saturation effect of amplifiers [41].

However, this is an intrinsic property of the laser source and its impact on experimental results can be considered marginal and thus could be ignored. Therefore, it is assumed in this research that the burst energy was distributed equally between the sub-pulses.

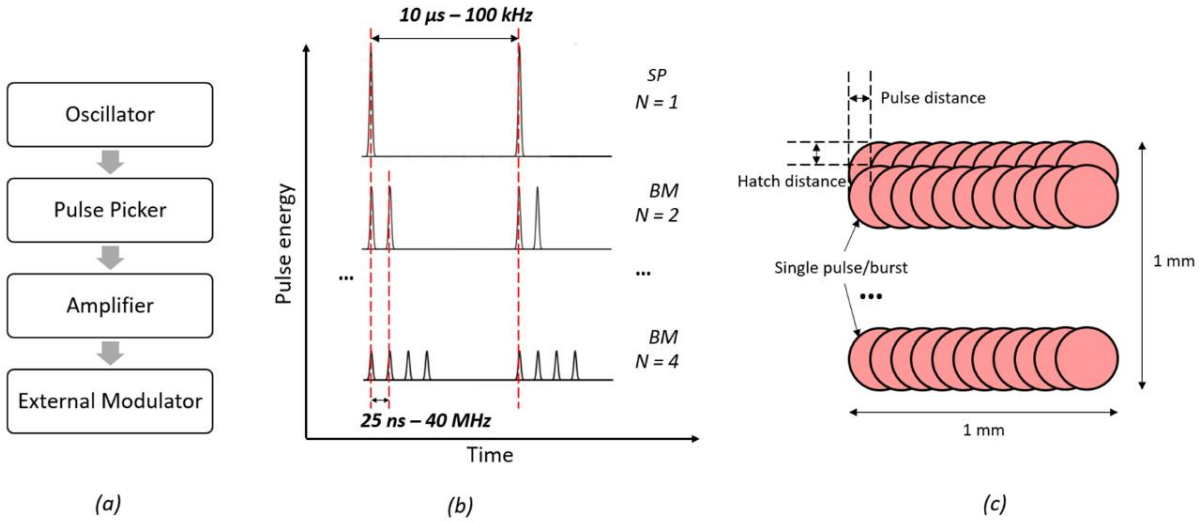

Figure 4.1. *The burst mode processing: (a) schematic of the burst mode generation; (b) the energy distribution in single pulse (SP) and burst mode (BM); and (c) the machining strategy used to process pockets.*

4.2.2. Specific removal rates

The aim of this research was to investigate the scalability achievable with the burst mode processing at high average laser power. Therefore, the maximum available laser power of 10 W was deployed in all experimental trials, i.e. pulse frequency (f_p) was fixed at 100 kHz while the pulse and the burst energy (E) 90 µJ. This represents a peak fluence of 25.5 J/cm^2 per single pulse and per burst, too, that was calculated as follows:

$$F = \frac{2E}{\pi R^2} \tag{2}$$

where: R is the radius of laser spot at the focal plane. The number of sub-pulses per burst was varied from 2 to 400 hundred and the results were compared with those obtained with a single pulse. The pulse overlap was varied from approximately 33% to 99% by varying the scanning speed in the range from 2000 mm/s to 20 mm/s and was calculated using the following equation:

$$\%Overlap = \frac{A}{\pi R^2} \times 100\% \tag{3}$$

where: A is the intersection area between two pulses (or bursts). The area A was calculated based on the relative spatial distance between two pulses (or bursts) and the laser spot size using the following equation:

$$A = 2R^2 cos^{-1}\left(\frac{d}{2R}\right) - d\sqrt{R^2 - \frac{d^2}{4}} \tag{4}$$

where: d is the pulse (or burst) spatial distance calculated based on the used scanning velocity and pulse frequency, i.e. $d = v/f_p$; and R - the radius of the laser spot. In fact, there is a certain special distance between sub-pulses in a burst, too, due to the constant beam motion. However, this value is much small (the maximum sub-pulse distance is 50 nm at scanning speed (v) of 2000 mm/s and intra-burst frequency (f_b) of 40 MHz and, thus, has been considered neglectable in this study.

The removal rate was also investigated for four different pulse durations within the laser source available range, i.e. 500 fs, 1 ps, 5 ps and 10 ps, to investigate the effects of different laser-material interaction times on the processing performance in burst mode. A summary of various process parameters used in this experimental study are given in Table 4.1. A high purity copper (99%) and stainless-steel grade 316 substrates were chosen to conduct the experiment due to the significant difference in their thermal conductivity and also their wide use in many industrial applications.

Table 4.1. Summary of various process parameters varied in this research.

	Various Parameters									
Scanning speed [mm/s]	20	60	100	140	200	400	800	1200	1600	2000
Overlap level [%]	99	98	96	95	93	87	73	60	47	33
Pulse duration [ps]	0.5, 1, 5 and 10									
Number of sub-pulses/burst	1, 2, 3, 5, 10, 15, 20, 50, 100, 200 and 400									

Squared pockets with an area of 1 × 1 mm^2 were ablated onto copper and stainless steel substrates employing single mode and burst mode processing with process settings in Table 4.1. A full list of conducted experiments is presented in Appendix 2. The distinctly different thermal conductivity of the two materials allowed the incubation effects in the burst mode processing to be investigated. The machining strategies utilised in the experiments together with its respective variables are provided in Fig. 4.1c. The pulse distance was varied from 0.2 µm to 20 µm by controlling the scanning

speed, while the hatch distance (D_h) was maintained the same, 10 µm, and ten layers were ablated from each of the pockets.

The measurement of the ablated pockets was carried out with Alicona G5 system employing the its VolumeMeasurement module [42, 43]. The ablated volume (V) was measured by fitting a reference plane on the top of the calibrated 3D form of the sample's surface and then the removed volume below this plane was calculated as depicted in Fig. 4.2. Five measurements were taken on a representative crater and a pocket to assess the uncertainty associated with the measurement procedure. Especially, the Type A measurement uncertainties of obtained volumetric data about ablated craters and pockets was determined to be 3 and 106×10^3 µm^3, which represents 0.73 and 0.14% of the mean values, respectively [44].

SRR was calculated by using Eq (4). This quantifying approach was considered to offer a basis for a fair assessment of the achievable processing scalability with different number of sub-pulses in a burst in comparison to the results obtained with the single pulse processing.

$$SRR = \frac{V_a}{E \times N_{Total}^{p}} = \frac{V_a}{E \times N_{Line}^{p} \times N_{Line} \times N_{Layer}}$$

$$= \frac{V_a}{E \times {1000}/{d} \times {1000}/{D_h} \times 10} \quad [\mu m^3/\mu J] \tag{5}$$

where: V_a is the ablated volume; N_{Total}^{p} – the total delivered pulses; N_{Line}^{p} – the number pulses per line; N_{Line} – the number of lines and N_{Layer} – the number of layers.

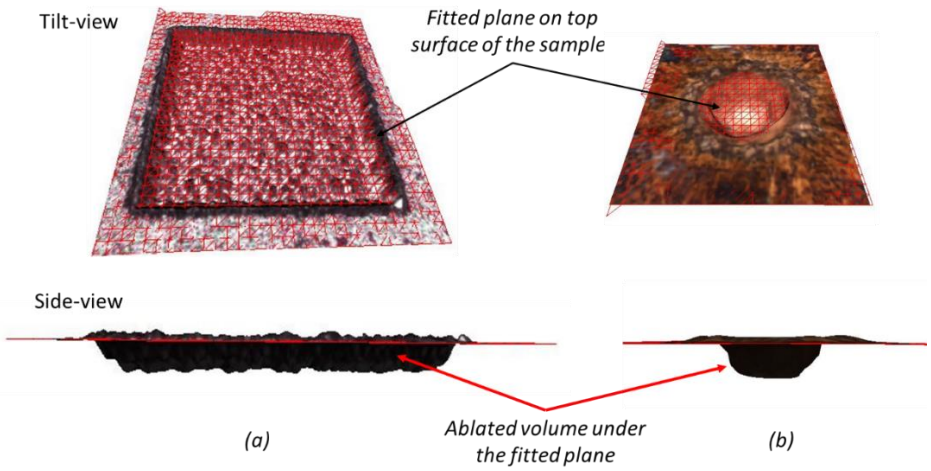

Figure 4.2 *The measurement of ablated volumes using Alicona G5 system: (a) an ablated pocket and (b) a single shot crater.*

4.2.3. Heat accumulation and other effects

A method for analysing heat accumulation and other effects such as the material redeposition and plasma shielding in the burst mode processing, especially how to determine their advantageous and negative effects on SRRs under varying machining conditions, is proposed in this section. The method analyses the contributions of main factors affecting the removal rates and the proposed approach is presented in Fig. 4.3.

The overall SRRs achievable employing single pulse (SRR_{Total}^{sp}) and burst mode (SRR_{Total}^{BM}) processing are considered to include the material ablated directly with the delivered pulse/burst energy and also additional volumes as a result of the heat accumulation, both in single pulse and burst mode processing. The processing condition in such single shot machining can be considered representative of single

pulse one without any heat accumulation impact and pulse-to-pulse plasma shielding. At the same time a single burst can be considered as burst mode processing with heat accumulation effect on SRRs just due to the sub-pulse train. Especially, this is the heat accumulation effect just due to intra-burst frequency that leads to incubation effects and reduction of ablation threshold, consequently, that is discussed later. At the same time, the plasma shielding due to the sub-pulse trains can be considered as an inherent property in the burst mode processing. This is because the temporal distance and the energy distribution between sub-pulses are fixed (for a certain number of sub-pulse) while the spatial sub-pulse distance is neglectable. This material removal mechanism is considered as a direct laser ablation in the analysis and is distinguished from the overall heat accumulation effects due to the trains of pulses and bursts deployed during the whole machining process. Therefore, by comparing SRRs calculated based on a single shot crater with those for the whole process, it will be possible to assess the impact of various factors leading to heat accumulation and thus to judge about the ablation efficiency. The respective volumes of removed material are calculated employing the measurements and the SRR calculation described in Section 2.2.

In the single pulse processing, SRRs due to the direct laser ablation (SRR^{sp}) is calculated based on the volume ablated with a single pulse. The contribution of the heat accumulation (SRR_{HA}^{sp}) is attributed to the incubation effects due to the delivery of a pulse train per spot that leads to a decrease of ablation threshold and residual heat,

and thus further material removal [45]. Therefore, SRR_{HA}^{sp} can be estimated based on the difference between SRR_{Total}^{sp} and SRR^{sp}.

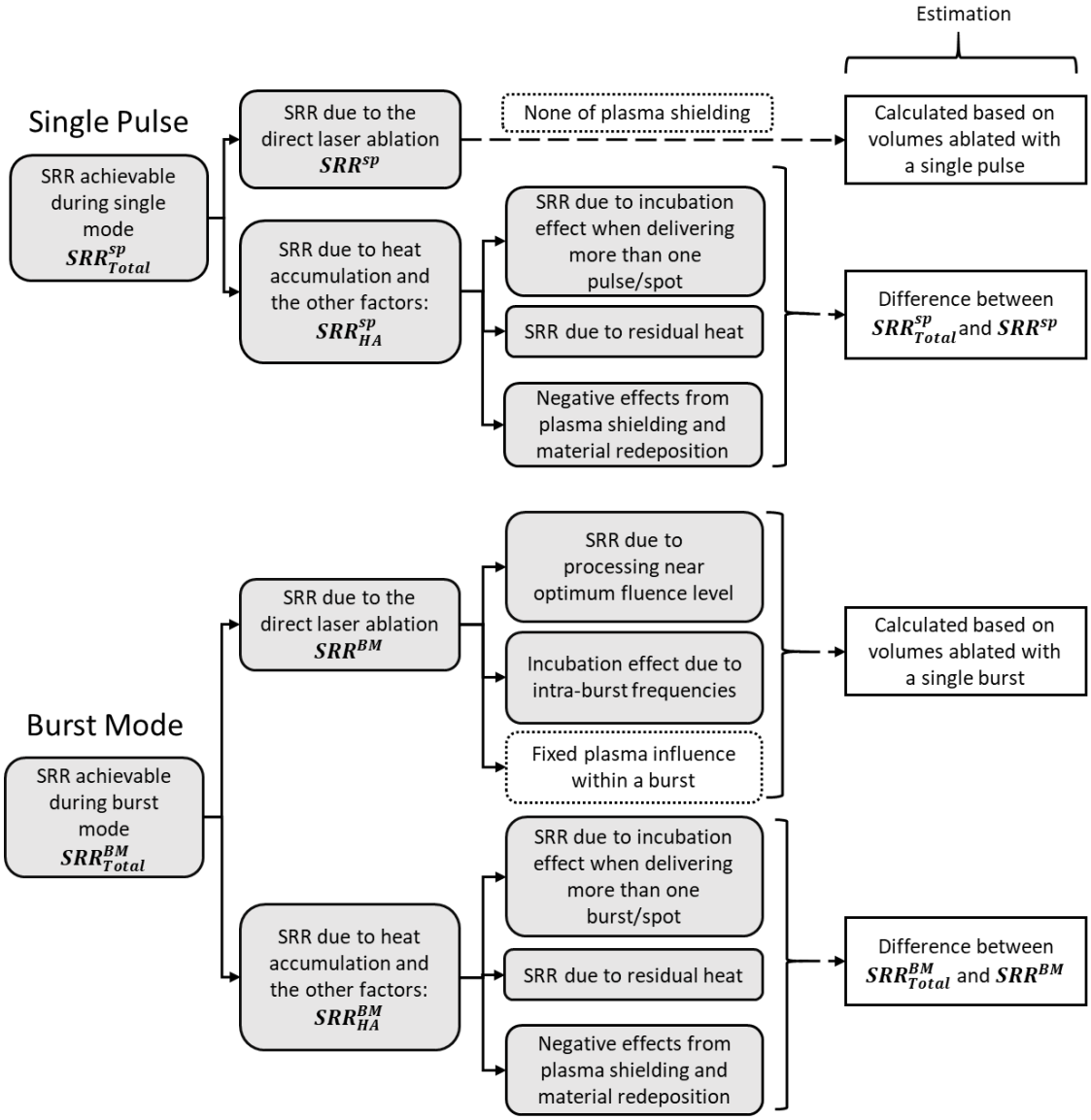

Figure 4.3. *Methodology for analysing the contributions of the main factors affecting the material removal in single pulse (top) and the burst mode (bottom) processing.*

In the burst mode processing, SRR due to the direct laser ablation (SRR^{BM}) is the sum of the SRR achievable when sub-pulses with near optimum fluence levels are used

and SRR due to the intra-burst frequency and the resulting from this incubation effects. Similarly, to the single pulse processing, $SRR^{BM}$is calculated based on the volume ablated with a single burst. In this case, the contribution of the heat accumulation (SRR_{HA}^{BM}) is again attributed to the incubation effects as more than one burst is delivered per spot and ultimately leads to residual heat and further material removal. So, SRR_{HA}^{BM} can be estimated based on the difference between SRR_{Total}^{BM} and SRR^{BM}.

It is important to state that there are some assumptions in the proposed method about other factors that can affect the removal rates. For example, the effects from any changes of absorption coefficient can be considered neglectable compared to those directly associated with the heat accumulation.

There are three possible cases that should be considered in assessing the heat accumulation and other effects in calculating SRRs. Especially, the following three cases should be considered in burst mode processing:

1. $SRR_{Total}^{BM} > SRR^{BM}$

   Hence, $SRR_{HA}^{BM} > 0$, and $SRR_{HA}^{BM} = SRR_{Total}^{BM} - SRR^{BM}$

   The heat accumulation has a beneficial influence over the negative effects of the pulse-to-pulse plasma shielding and redeposition effects and leads to SRR improvements.

2. $SRR_{Total}^{BM} = SRR^{BM}$

   Hence, $SRR_{HA}^{BM} = 0$

The heat accumulation does not have any positive impact. In this case it can be assumed that the plasma shielding and material redeposition offset any contributions from the heat accumulation.

3. $SRR_{Total}^{BM} < SRR^{BM}$

   Hence, $SRR_{HA}^{BM} < 0$

   Any positive impact of the heat accumulation on the material removal process is offset by plasma shielding and material redeposition due to an excessive accumulated fluence and residual heat.

4.2.4. Surface roughness

A comparison of surface quality achievable with single pulse and MHz burst mode processing while using the same experiments, i.e. the pockets ablated with the processing parameters in Table 4.1 and the same number of layers, was conducted. Generally, the increase of ablated layers leads to a lower surface quality due to changes of surface morphology after each layer. The formation of some other surface structures such as pin holes or micro cone shapes can also be expected after layer-based processing. Taking this into account, the use of MHz burst mode processing can be beneficial as less layers would be required to achieve the same depth as that in the single pulse processing, i.e. due to the expected higher SRR, and thus the surface quality can be improved, too.

Therefore, similar pockets to those produced with the burst mode processing and 10 ablation layers were machined with the single pulse mode but with different numbers of layers, defined experimentally to achieve the same depth. The surface roughness was measured at the bottom of the ablated pockets and the obtained results were compared. SEM images were taken using Jeol JCM6000 system at 15 kV acceleration voltage and magnification of 220 times.

4.3. Results and Discussion

4.3.1. Ablation threshold

The ablation threshold for 500 fs pulses was determined when performing single pulse and burst mode processing using Liu's method [46], while the number of sub-pulses was varied from 2 to 400. The measured radiuses of the craters to calculate the ablation threshold as a function of the burst sub-pulse number is provided in Fig. 4.4. The ablation threshold attained for copper with the burst mode processing was higher than that achieved with the single pulse when the processing was conducted with up to 10 sub-pulses. Only when more than 10 sub-pulses per burst were applied, the ablation threshold of copper was lower than that for the single pulse process. In contrast, the ablation threshold in the case of stainless steel was lower for all the burst regimes in comparison to the single pulse processing. This reduction was attributed to the incubation effect, which was more pronounced in the MHz burst mode processing of stainless steel because its low thermal conductivity (14 - 16.3 $Wm^{-1}K^{-1}$) compared

with copper (386 $Wm^{-1}K^{-1}$) [47, 48]. Thus, more residual heat was retained locally and partly contributed to the achieved material sublimation rate. This also can explain why a stainless steel ablation was present even at 400 sub-pulses per burst whilst any noticeable ablation on copper occurred only below 100 sub-pulses.

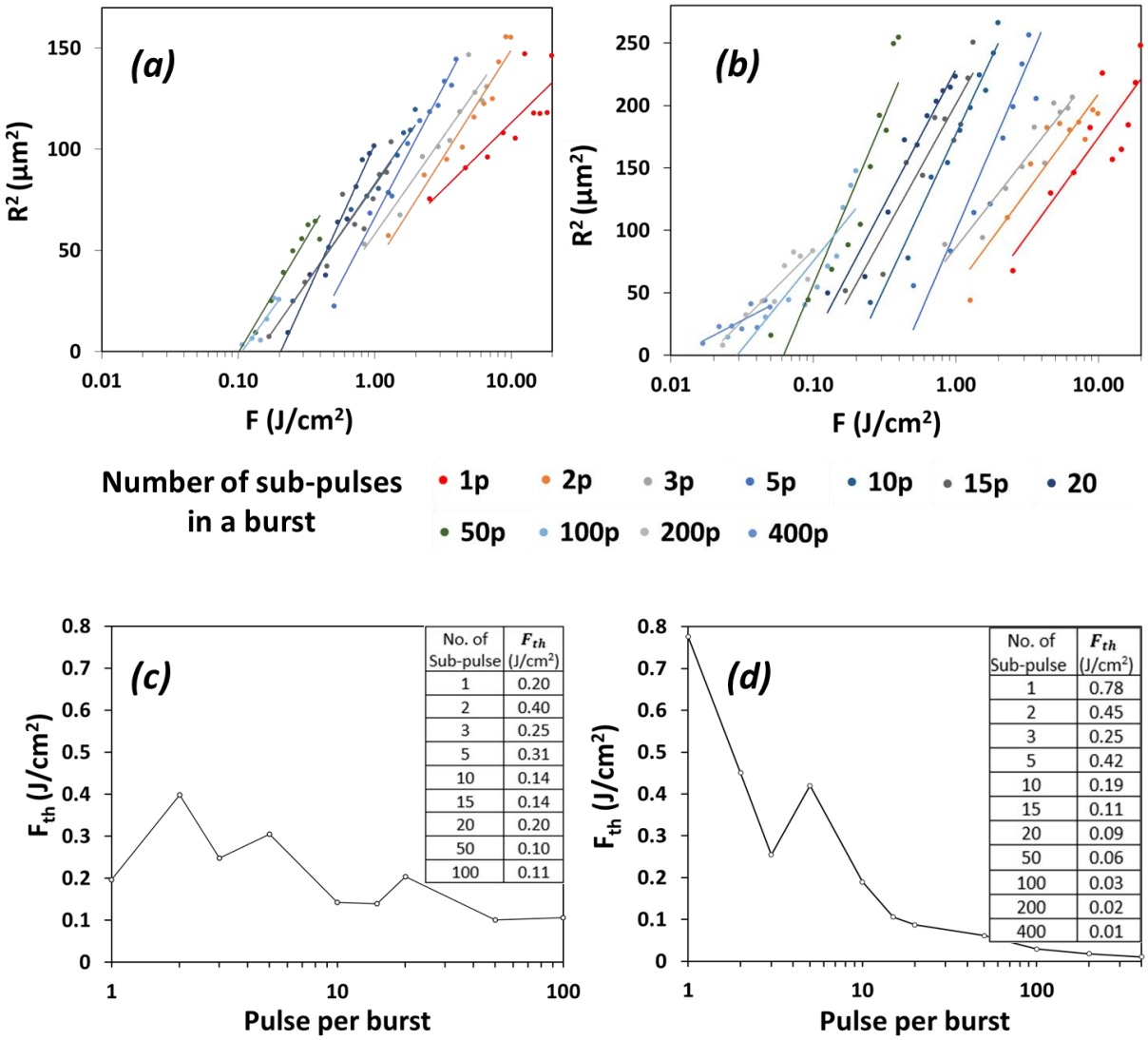

Figure 4.4. *R^2 of craters as a function of fluence (top) and the ablation threshold fluence (F_{th}) changes when the MHz burst mode was applied with different numbers of*

sub-pulses and pulse duration of 500 fs (bottom) to process: (a) and (c) Copper and (b) and (d) 316 stainless steel.

Note: The burst mode ablation threshold was quantified taking into account the total fluence of a single burst rather than the fluence of a sub-pulse.

A closer look at ablated craters after single pulse and burst mode processing of copper and stainless steel is provided in Fig. 4.5. Even though the total delivered energy was the same, the crater depth dramatically increased as the number of sub-pulses increased from 1 to 20 and from 1 to 50 on copper and stainless steel, respectively. The maximum depth of the single-burst crater was obtained at 10 and 20 sub-pulse per burst for copper and stainless steel, respectively. It is worth noting that in case of copper the increase of the ablation threshold when the number of sub-pulses was less than 10 did not result in lowering the removal rates for the single-burst craters (see Fig. 4.5). Therefore, the most likely reason for this phenomenon is the heat accumulation the train of sub-pulses as it can compensate the increase of the ablation threshold and even to improve further SRRs. However, the ablation efficiency was reduced significantly when the number of sub-pulses increased beyond 20 and 50 for copper and stainless steel, respectively. This is because sub-pulse fluence was much lower than ablation threshold and the heat incubation was not sufficient to impact the ablation performance.

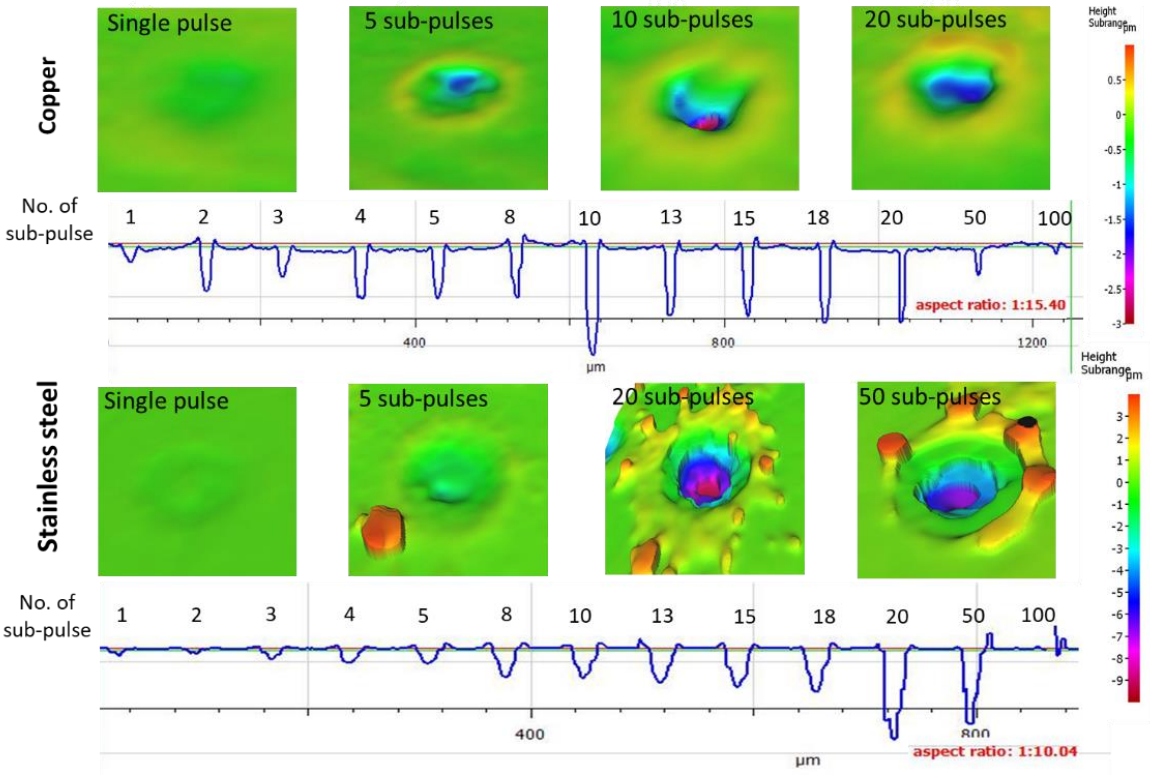

Figure 4.5. *3D surface scans and cross-sectional profiles of craters produced with single pulse and burst mode processing and pulse duration of 500 fs while varying the number of sub-pulses for copper (top) and stain less steel (bottom).*

Note: Craters' cross-sectional profile was further magnified and the respective aspect ratios provided in the figure.

4.3.2. Specific removal rates

4.3.2.1. Copper

SRRs achieved on copper as a function of pulse distances in single pulse and burst mode processing while using four different pulse durations are presented in Fig. 4.6. The ablation rates obtained with single pulse processing are highlighted in red. The

removal rates were significantly improved when MHz burst mode processing was applied with varying number of sub-pulses, but this was not the case across all pulse distances investigated in this research. In general, the interdependences of SRRs on pulse/burst distances were changing across the following three ranges: i) smaller pulse distances in the range from 0.2 µm to 1 µm; ii) intermediate pulse distances (from 1 µm to 4 µm) presented in Fig. 4.6b, 4.6d, 4.6f and 4.6h; and iii) higher pulse distances (greater than 4 µm) presented in Fig. 4.6a, 4.6c, 4.6e and 4.6g. In the 1st range, where the pulse/burst overlap was more than 96%, the single pulse mode resulted in better SRRs compared to the results obtained with any burst mode processing across all four pulse durations. It can be stated that the accumulated fluence from a single pulse train led to a less residual heat and plasma shielding due to much lower pulse frequency, and thus to less redeposition of material and hence a cleaner ablation. In addition, the plasma plume had a noticeable impact at intra-burst frequency (40 MHz) as the sub-pulse energy was absorbed by plasma plume and led to a reduced ablation efficiency. At the same time, SRRs increased quickly with the increase of the pulse distance for both single pulse and burst mode processing except for 10 ps in a single mode, where SRR was relatively stable.

The 2nd range of pulse distances covered the processing condition where the pulse overlaps were from 87 to 95%. In this range, SRRs for most burst mode regimes increased dramatically with the decrease of the pulse overlaps and exceeded SRRs

achieved with the single mode when the pulse distance was higher than 1.4 μm. Thus, beneficial processing conditions were created that facilitated the material removal/ejection from the ablation area and therefore less material redeposition and cleaner ablation was obtained when the distance between the bursts increased. Also, it should be noted that plasma shielding effect tended to decrease when pulse/burst distance increased. And, this had an evident impact that made the benefits of processing at near optimum fluence more pronounced and led to the SRR increase. The SRRs achieved with the single pulse processing reached their maximum values (see Table 4.2) and decreased marginally when the pulse distance increased across all four pulse durations. Comparing the results obtained with the different pulse durations, bursts with number of sub-pulses from 3 to 20 resulted in higher removal rates for 500 fs and 1 ps pulses. At the same time, higher SRRs were achieved even with 100 sub-pulses per burst at 5 ps and 10 ps pulse durations when compared with the results obtained with the single pulse processing.

Finally, the 3rd range covered pulsed distances where the pulse overlaps was less than 87%, i.e. the pulse distances were higher than 4 μm. In this case, the advantages of the burst mode were more pronounced as shown in Fig.4.6a, 4.6c, 4.6e and 4.6g and SRRs kept increased significantly to reach their maximum values. They were higher than those obtained with the single pulse and the burst mode with the number of sub-pulses from 3 to 50 (in case of 500 fs and 1ps pulses) and from 3 to 100 (for 5 ps and

10 ps pulses). Specifically, SRRs achieved with the burst mode reached the maximum values of 3.7 $\mu m^3/\mu J$, 4 $\mu m^3/\mu J$, 5.4 $\mu m^3/\mu J$ and 4.6 $\mu m^3/\mu J$ for 500 fs, 1 ps, 5 ps and 10 ps pulse durations, respectively (see Table 4.2). These maximum SRRs were achieved at 15 sub-pulses, especially when the processing was performed with near optimum fluence levels of 1.7 J/cm^2 for 500 fs and 1 ps pulses. These results are very close to what has been reported by other researchers [49]. And, it was evident from the results in Table 4.2 that the optimum fluence level tended to decrease to approximately 1.3 J/cm^2 that was achieved at 20 sub-pulses with the longer durations of 5 and 10 ps. In addition, it is important to note that SRRs plateaued and were not anymore dependent on the increase of the pulse distances, when they became higher than 4 µm and 8 µm. Especially, this was achieved when the pulse overlaps were less than 87% and 73% for the pulse durations of 500 fs and 1 ps and 5 and 10 ps, respectively. This indicated that the negative side effects, such as plasma shielding and redeposition of material, had declined and became steady in this range of pulse distances.

The observed changes of SRRs across the three ranges of pulse distances are in good agreement with the results reported in another investigation [50]. The maximum SRRs were achieved with the burst mode when a relatively higher number of sub-pulses, i.e. from 15 to 50 sub-pulses, across the investigated pulse distances and pulse durations was used and thus to benefit fully from the available maximum pulse energy of 90 µJ

in this study. In addition, the maximum SRR in machining micro-structures on copper substrates was attained at different number of sub-pulses per burst compared to the results obtained with the single burst of 10 sub-pulses. This indicates that the performance improvements in the MHz burst mode processing can be achieved at specific machining conditions in regard to the accumulated fluence and sub-pulses' fluence levels. Therefore, it is important to investigate these conditions systematically and thus to identify the respective limits and thus to benefit fully from the capabilities that the burst mode processing offers. Also, the similarities of the copper response to burst mode processing with 500 fs and 1 ps and 5 ps and 10 ps pulse durations should be noted.

Table 4.2. Maximum SRRs achieved on copper with single pulse and burst mode processing at four different pulse durations.

Pulse duration	*Regime*	*Maximum SRR ($\mu m^3/\mu J$)*	*Number of sub-pulses*	*Sub-pulse fluence (J/cm^2)*	*Pulse distance (μm)*	*Overlap level (%)*
500 fs	*Single pulse*	*1.8*	*1*	*25.5*	*2*	*93*
	Burst mode	*3.7*	*15*	*1.7*	*16*	*47*
1 ps	*Single pulse*	*1.6*	*1*	*25.5*	*1*	*96*
	Burst mode	*4.0*	*15*	*1.7*	*16*	*47*
5 ps	*Single pulse*	*1.2*	*1*	*25.5*	*0.6*	*98*
	Burst mode	*5.4*	*20*	*1.3*	*20*	*33*
10 ps	*Single pulse*	*0.7*	*1*	*25.5*	*0.6*	*98*
	Burst mode	*4.57*	*20*	*1.3*	*20*	*33*

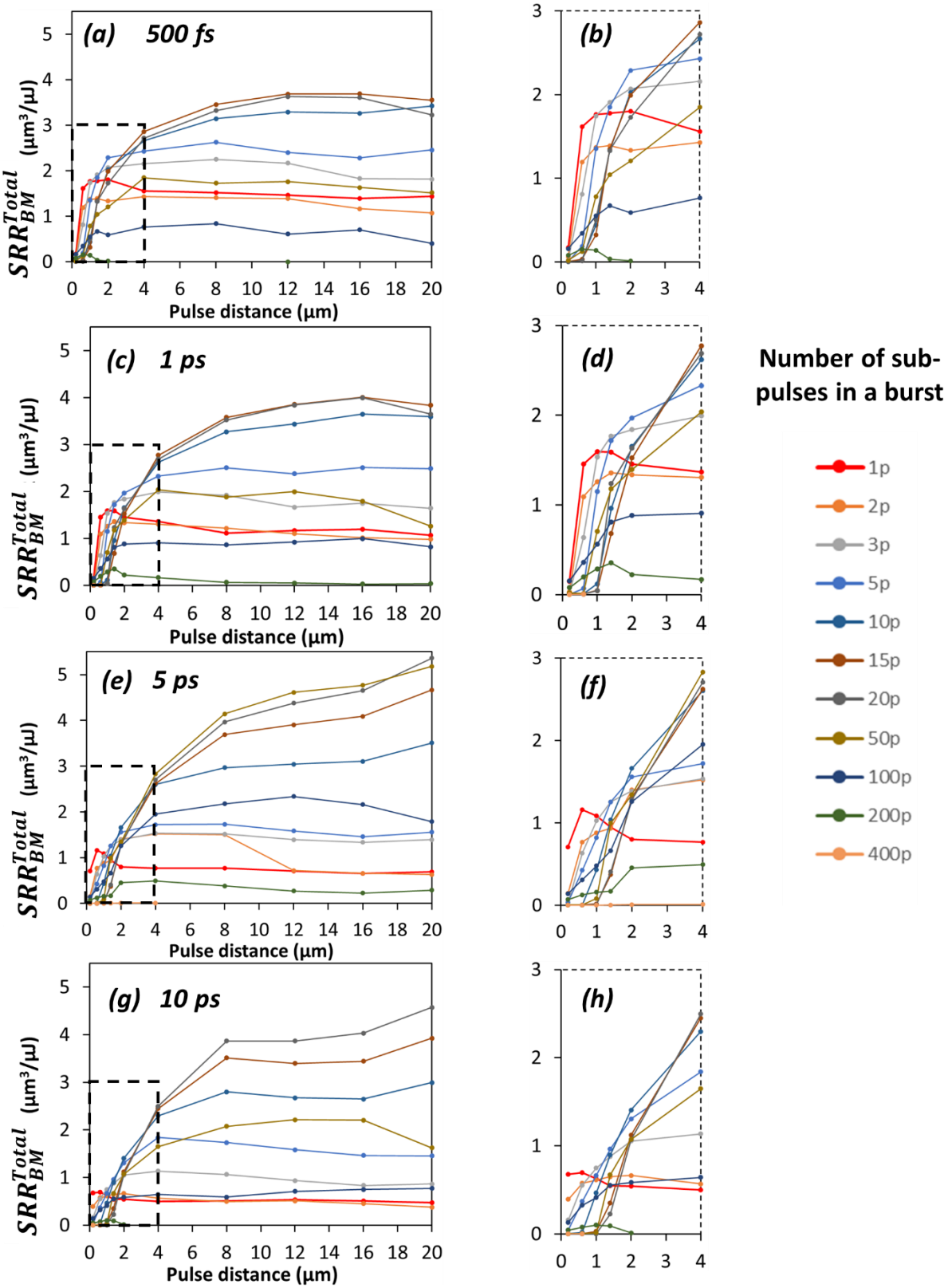

Figure 4.6. *SRRs as a function of pulse distances in single pulse (red line) and burst mode processing of copper with four different pulse durations: (a), (c), (e) and (g)*

SRRs achieved with pulse/burst distances up to 20 µm and pulse durations of 500 fs, 1 ps, 5 ps and 10 ps, respectively; (b), (d), (f) and (h) a closer look at SRRs achieved with pulse/burst distances of less than 4 µm for 500 fs, 1 ps, 5 ps and 10 ps, respectively.

Note: 1p denotes one sub-pulse per burst which denote a single pulse processing while 2p,3p, …, 400p – a burst mode processing with an increasing sub-pulse number per burst.

4.3.2.2. Stainless steel

SRRs as a function of the pulse/burst distances in the single pulse and burst mode processing of stainless steel (grade 316) at the same four pulse durations are shown in Fig. 4.7. It can be immediately noted that the advantages of the burst mode processing over the single pulse one are more pronounced compared to copper.

The dependences of SRRs on stainless steel in the burst mode processing with varying pulse distances (or overlap) were changing across the following two ranges. The first range includes pulse distances from 0.2 µm to 4 µm while the second one those in excess of 4 µm. Within the first range, SRRs achieved with the single pulse processing reached its maximum values and then plateaued with any further pulse distance increases at all four pulse durations. Again, there were similarity in the material response to SRRs achieved at pulse durations of 500 fs and 1 ps and pulse duration

of 5 ps and 10 ps, respectively. The single pulse processing resulted in higher SRRs at 500 fs and 1 ps (maximum value around 1 $\mu m^3/\mu J$) pulse durations compared to relatively low values obtained at 5 ps and 10 ps (maximum SRRs from 0.3 to 0.4 $\mu m^3/\mu J$) across all pulse distances investigated in this research (Table 4.3). The SRRs achieved with the burst mode with the sub-pulse number in the range from 50 to 200 were higher than those achieved with the single pulse process, even at the lowest pulse-to-pulse distance of 0.2 µm, across all four pulse durations (Fig. 4.7b, 4.7d, 4.7f and 4.7h). The sub-pulse fluence at 50 to 200 sub-pulses per burst was in the range from 0.1 to 0.5 J/cm^2. This low fluence level led to a less pronounced plasma shielding at high overlap levels (more than 98% for pulse-to-pulse distances lower than 0.2 µm) and thus the ablation process was more efficient. An efficient ablation with the single pulse processing was achieved only when the pulse distances was greater than 0.6 µm and SRRSs were higher compared with the values obtains with burst distances up to 1.4 µm at 500 fs and 1 ps pulse durations. SRRs achieved with the burst mode increased dramatically when pulse/burst distances were higher than 1.4 µm and then plateaued when they exceeded 4 µm, due to the reduction of plasma shielding. However, the SRR increase was not always steady as there were some sudden fluctuations, e.g. when the number of sub-pulses in the burst were 50, 100, 200, 300 and 400. This can be attributed to some alterations in the surface morphology, which led to sudden change in the absorption coefficient and therefore SRRs were affected

strongly. Despite such SRR uncertainties at some burst mode processing conditions, the advantages over the single pulse processing were dominant on stainless steel across all four pulse durations. The optimum fluence level was 0.5 J/cm^2 that was achieved with 50 sub-pulses per burst while the maximum SRRs across the four pulse durations were in the range from 4.9 µm^3/µJ to 5.7 µm^3/µJ (see Table 4.3). An efficient ablation was achieved even with 300 or 400 sub-pulses per burst when the sub-pulse fluence was much lower than the ablation threshold. This can be explained with the heat incubation affects that are discussed in the next section. Contrary to what was observed for copper, the pulse duration did not affect the optimum fluence on stainless steel, as the maximum SRRs were achieved with the same fluence across all four pulse durations. In addition, the highest SRRs on stainless steel were attained with 500 fs pulses, while for copper it was with 5 ps ones.

Table 4.3. Maximum SRRS achieved on stainless steel with single pulse and burst mode processing at four different pulse durations.

Pulse duration	*Regime*	*Maximum SRR (µm^3/µJ)*	*Number of sub-pulses*	*Sub-pulse fluence (J/cm^2)*	*Pulse distance (µm)*	*Overlap level (%)*
500 fs	*Single pulse*	*1.0*	*1*	*25.5*	*1*	*96*
	Burst mode	*5.7*	*50*	*0.5*	*12*	*60*
1 ps	*Single pulse*	*0.9*	*1*	*25.5*	*1*	*96*
	Burst mode	*5.5*	*50*	*0.5*	*12*	*60*
5 ps	*Single pulse*	*0.4*	*1*	*25.5*	*1*	*96*
	Burst mode	*5.2*	*50*	*0.5*	*12*	*60*
10 ps	*Single pulse*	*0.3*	*1*	*25.5*	*0.2*	*99*
	Burst mode	*4.9*	*50*	*0.5*	*12*	*60*

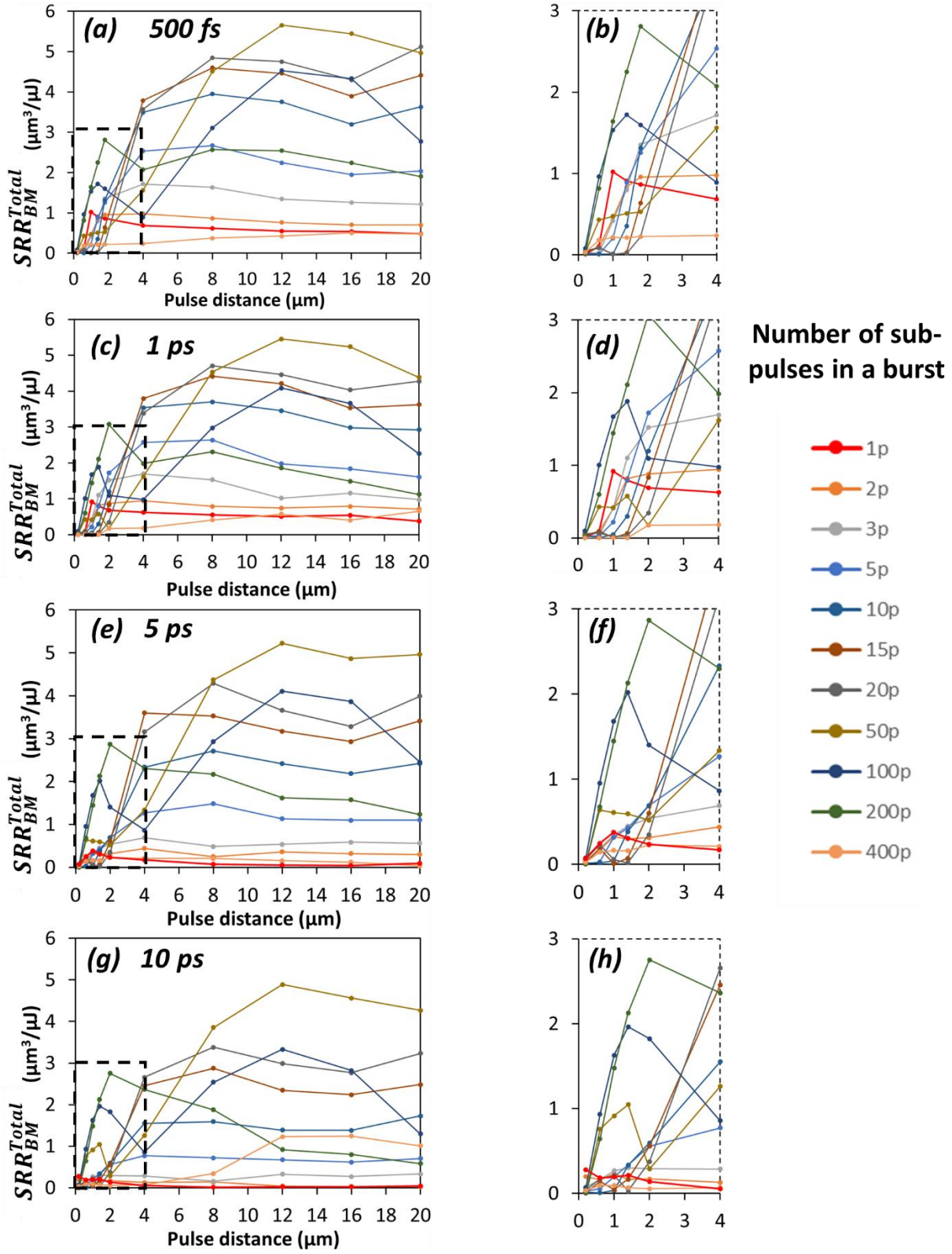

Figure 4.7. *SRRs as a function of pulse/burst distances in single pulse (red line) and burst mode processing on stainless steel with four different pulse durations: (a), (c),*

(e) and (g) SRRs at 500 fs, 1 ps, 5 ps and 10 ps, respectively; (b), (d), (f) and (h) a closer look of SRRs achieved with pulse/burst distances of less than 4 µm at 500 fs, 1 ps, 5 ps and 10 ps, respectively.

4.3.3. Heat accumulation effects

As discussed in Section 3.2, there were some similarities in the two materials' SRR response at 500 fs and 1 ps and 5ps and 10 ps pulse durations when the effects of the increasing pulse/burst distances were analysed. Therefore, a further investigation was conducted only at two pulse durations, i.e. 500 fs and 5 ps. In addition, the analysis was carried out for only four pulse/burst distances, i.e 1.4 µm, 4 µm, 12 µm and 20 µm, which covered the three and two specific processing ranges for copper and stainless steel, respectively, as discussed previously. The heat accumulation influence was studied for both, single pulse and burst mode processing with numbers of sub-pulses increasing from 2 to 400.

4.3.3.1 Copper

Fig. 4.8 depicts SRRs obtained on copper with four different pulse distances while the number of sub-pulses per burst had been increasing. These SRRs were then compared with calculated ones from a single spot crater with an increasing number of sub-pulses. In case of 500 fs processing on copper (Fig. 4.8a), SRRs calculated based on the ablated pockets were higher than the values achieved for the reference single crater with one (single pulse) and two sub-pulses per burst. The other burst mode

regimes led to lower SRRs compared to those achieved on the single crater across all four analysed pulse distances. It should be noted that the negative side effects from the plasma shielding and the material redepositing when processing pockets were dominant over any positive ones from the heat accumulation. Especially, the heat accumulation had a positive impact only in the single pulse and burst mode processing of copper with only two sub-pulses. The maximum SRR of 6.2 µm^3/µJ was achieved with a single burst of 10 sub-pulses.

As expected, the positive influence of the heat accumulation was more pronounced with 5 ps pulses on copper (Fig. 4.8b). SRRs achieved on the ablated pockets were slightly higher than those calculated for the single crater with the number of sub-pulses less than 3 and the pulse distance of less than 4 µm. However, SRRs on copper increased significantly when the number of sub-pulses exceeded 50, especially for pulse distances higher than 4 µm. For example, SRR_{Total}^{BM} of 5.2 µm^3/µJ and SRR^{BM} of 1 µm^3/µJ were achieved with 50 sub-pulses per burst and 20 µm pulse/burst distance. Therefore, this significant SRR increase on copper can be attributed explicitly to the heat accumulation effect, i.e. the increase of SRR_{HA}^{BM} to 4.2 µm^3/µJ. Especially, this big difference in SRR achieved with a single burst can be attributed not only to heat accumulation but also the declining negative effects of plasma shielding when the sub-pulse energy decreased.

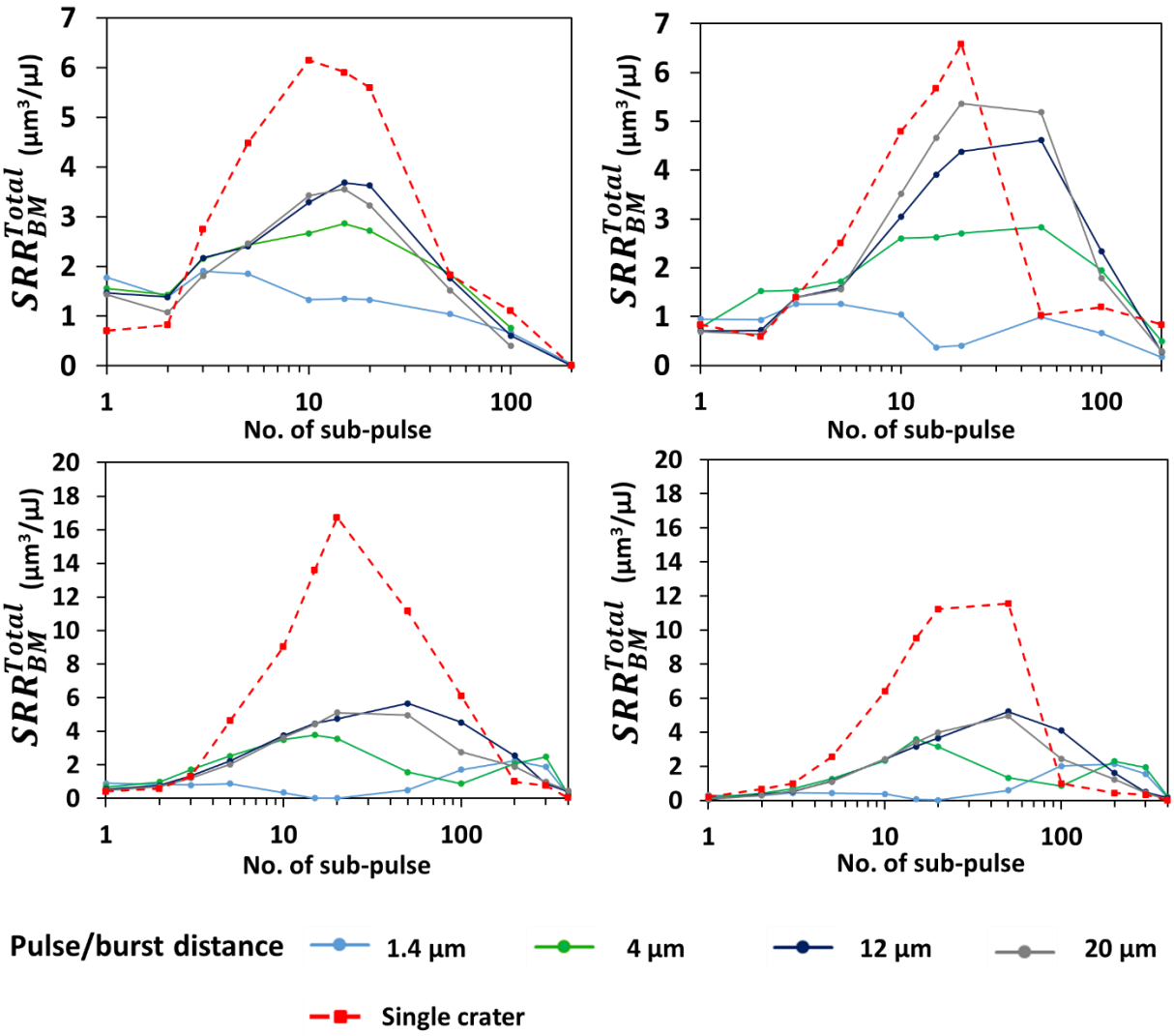

Figure 4.8. *SRRs as a function of number of sub-pulses per burst for pockets machined with four different pulse/burst distances, i.e. overlap levels, for two different pulse durations and materials: (a) Copper, 500 fs; (b) Copper, 5 ps; (c) Stainless steel, 500 fs and (d) Stainless steel, 5 ps.*

Note: The reference single crater curve shows the calculated SRRs from a single shot crater with an increasing number of sub-pulses.

4.3.3.2 Stainless steel

The plasma shielding in 500 fs processing led to predominantly negative effects on stainless steel (Fig. 4.8c and 4.8d). There were not significant differences between SRRs achieved on ablated pockets when compared with the single crater results obtained with up to 4 sub-pulses for both investigated pulse durations ($SRR_{Total}^{BM} = SRR^{BM}$). The processing conditions in this case can be considered to strike a balance between the advantages associate with the heat accumulation on SRRs and the negative ones due to the plasma shielding and material redepositing effects. When the number of sub-pulses increased and was in the range from 5 to 100, the plasma shielding and material redeposition started to dominate due to the plasma excitation by subsequent sub-pulses [51]. Therefore, SRRs attained on processed pockets were much lower than those achieved on the single spot crater. The positive impact of the residual heat on stainless steel could only be observed when the number of sub-pulses exceeded 200 and 100 at 500 fs and 5 ps pulse durations, respectively. Similar to the copper response at 5 ps pulse duration, the positive influence of heat accumulation in burst mode processing of stainless steel started to become noticeable when the number of sub-pulses per burst exceeded 100.

In addition, the SRR results obtained on stainless steel and also on copper at different processing conditions (see Fig. 4.8) revealed that SRRs increased with the increase of the pulse/burst distance, i.e. when the respective overlap levels decreased. Also, it

was confirmed that SRRs increased when the number of sub-pulses used led to a near optimum fluence as discussed in the previous section. This is indicative of some interdependences between the pulse/burst overlap level and the optimum number of sub-pulses on both materials. Thus, it can be stated that relatively low pulse/burst overlap levels require a higher number of sub-pulses to attain the maximum SRR values.

4.3.4. Surface roughness

The effects on surface roughness were investigated at only two pulse durations. i.e. 500 fs and 5 ps, due to the discussed similarity between SRRs achieved with 1 ps and 10 ps pulses, respectively, in Section 3.2. Three different scanning speeds, i.e. 500 mm/s, 1000 mm/s and 1500 mm/s, were investigated that led to pulse distances of 5 µm, 10 µm and 15 µm, respectively. In addition, two burst settings of 15 and 50 sub-pulses were selected for the conducted experiments on copper and stainless steel, respectively, because one of the highest SRRs were achieved with them (see Section 3.2). Also, it is important to note that it was necessary to ablate more than 10 layers when the single pulse processing was used, as presented in Table 4.4, and thus to achieve a similar depth with the two processing regimes as shown in Fig. 4.9a and 4.9b.

Table 4.4. The number of layers required to achieve similar pocket depths with the selected two pulse durations and three scanning speeds.

Scanning speed (mm/s)	Regime	Number of layers			
		500 fs		5 ps	
		Copper	Stainless steel	Copper	Stainless steel
500	Single pulse	20	30	30	58
	Burst mode	10	10	10	10
1000	Single pulse	27	77	53	195
	Burst mode	10	10	10	10
1500	Single pulse	30	90	75	240
	Burst mode	10	10	10	10

Fig. 4.9c and 4.9d present the surface roughness measurements on copper and stainless steel after undergoing processing with the two pulse durations. The respective surface morphologies achieved with the two processing modes are shown in Fig. 4.10. A marginally lower surface roughness was achieved on copper with the 500 fs burst mode processing at 500 mm/s and 1000 mm/s, whilst the surface quality was similar at 1500 mm/s as shown in Fig. 4.9c. The difference in surface quality was more pronounced at 5 ps processing of copper. The roughness values obtained with the burst mode were two times higher than those achieved with the single pulse processing at the lower scanning speed of 500 mm/s. Nevertheless, the burst mode resulted in a significantly smaller roughness at the higher scanning speeds of 1000 and 1500 mm/s.

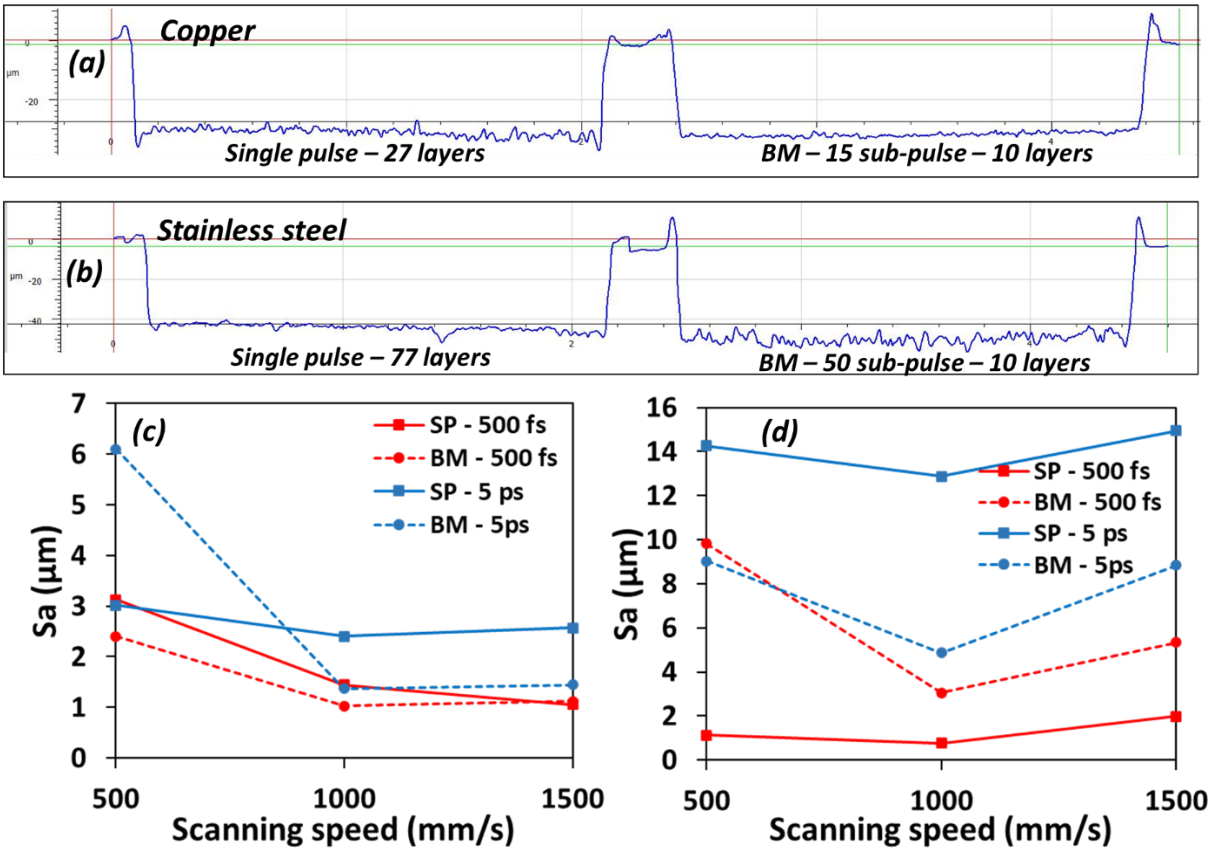

Figure 4.9. *The surface roughness results: (a) and (b) representative cross-sectional profiles of ablated pockets with a similar depth but achieved with different numbers of lasers when the two processing modes were used on copper and stainless steel with 500 fs pulse duration and 1000 mm/s scanning speed; and (c) and (d) surface roughness (Sa) measurements at the bottom of the ablated pockets produced with the two processing modes and the two pulse durations on copper and stainless steel, respectively.*

Based on the results obtained on stainless steel, the pulse duration had a clear influence on surface quality (see Fig. 4.9d). In particular, a significant increase in surface roughness was observed when the pulse duration increased from 500 fs to 5

ps in the single pulse processing whilst the roughness differences were marginal on the pockets produced with the burst mode processing at the investigated two pulse durations. The MHz burst mode did not lead to any improvements in surface roughness across all three scanning speeds at 500 fs pulse duration. Whereas, the burst mode with 5 ps pulses had a significant positive impact on surface quality across all investigated scanning speeds. The biggest reduction of surface roughness achieved with the burst mode in comparison to that obtained with the single pulse processing was observed at 1000 mm/s, i.e. 10 µm pulse distance, with 5 ps pulses, i.e. a reduction from 13 µm to 5 µm was achieved. It should be stressed that having a significantly smaller number of ablated layers in the burst mode, i.e. especially when processing stainless steel, did not only lead to a better surface quality, but also reduced the overall processing time, substantially. Considering the industry requirements for a viable ultrashort laser processing, especially higher SRRs, the use of the MHz burst mode can help to broaden the industrial applications of this technology.

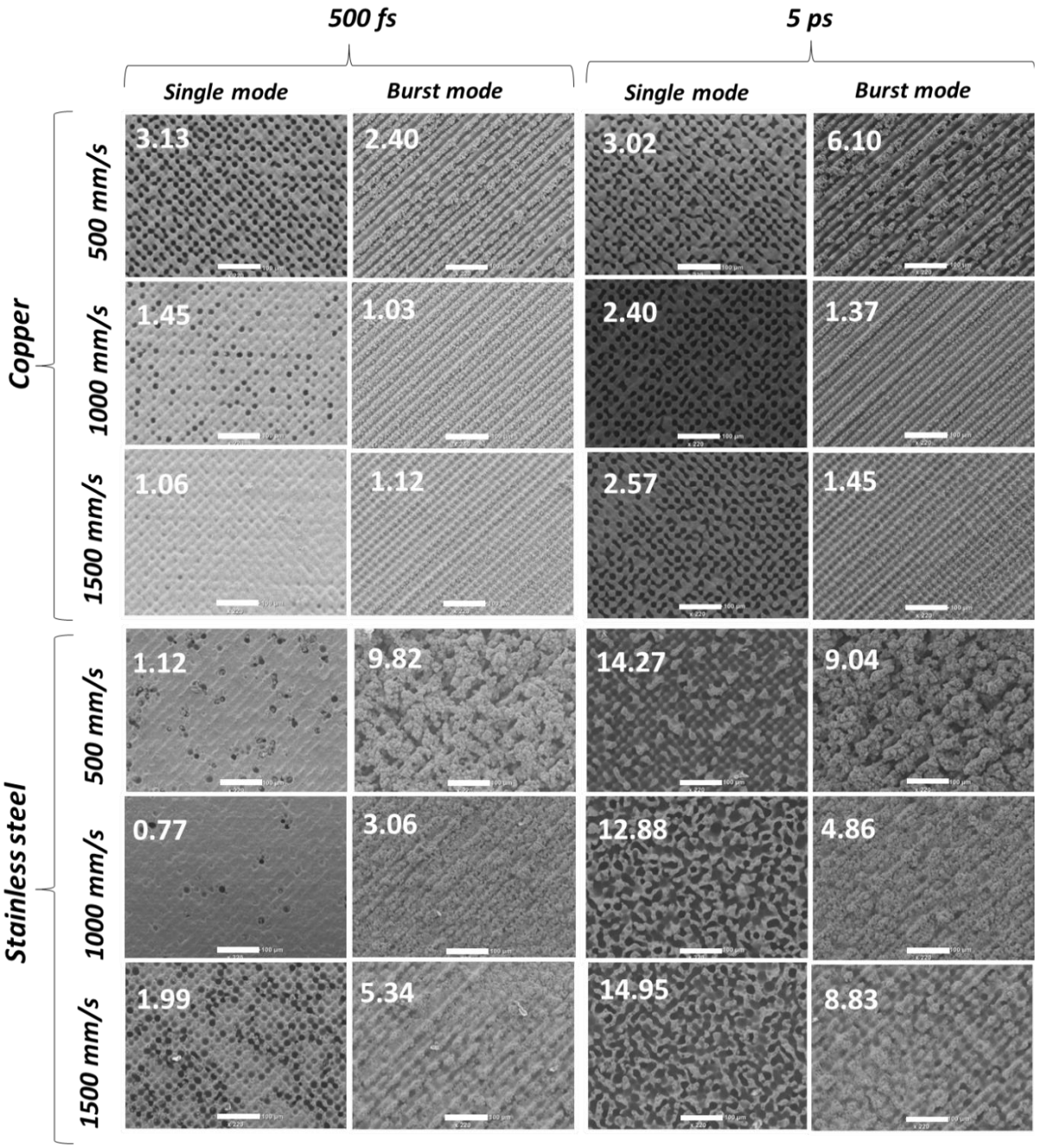

Figure 4.10. *SEM micrographs taken at the bottom surfaces of ablated pockets with the investigated two pulse durations and three scanning speeds on copper (left) and stainless steel (right). It is important to note that the depth of the pockets was kept the same but different number of layers was used to achieve this with the two processing regimes.*

Note: The numbers with the white colour denote the surface roughness (µm). Scale bar: 100 µm.

The surface morphology of ablated pockets are shown in Fig. 4.10. The burst mode processing minimised and also eliminated the micro pinhole formation, especially, on copper with both pulse durations. However, the higher ablation rate achieved with the burst mode led to the appearance of a different surface morphology, i.e. some line-like patterns. This reflects the scanning path used to process the last layer, and the same patterns were also observed on stainless steel. The effect of heat accumulation in the burst mode was more pronounced on stainless steel. There was a clear redepositing of an ablated material that led to the formation non-uniform micro-structures at the bottom surface of the pockets. Again, this can be explained with the lower thermal conductivity of stainless steel compared to copper.

4.4. Conclusions

The capability of the MHz burst mode processing was investigated in this research as a means to increase SRRs achievable in laser micro-machining on copper and stainless steel while utilising fully the available maximum pulse energy. Specifically, the experiments were conducted with a relatively high pulse fluence, i.e. 25.5 J/cm^2, and four different pulse durations, i.e. from 500 fs to 10 ps. The results showed that the MHz burst mode processing has clear advantages in regard to achievable SRRs and thus to utilise fully the available average power. These removal rate improvements

can be explained with the near optimum fluence levels of sub-pulses and beneficial heat accumulation effects in the burst mode compared to those in the single pulse processing. Especially, high SRRs were achieved with a relatively higher number of sub-pulses per burst, e.g. 15 to 20 and 20 to 50 on copper and stainless steel, respectively. However, the results also showed that the ablation efficiency improvements achievable with the burst mode can only be obtained under some specific processing conditions. Sustained high SRRs with the burst mode were achieved when the pulse overlap was relatively small, i.e. less than 87%. Especially, the highest SRRs achieved on copper and stainless steel were 5.4 $\mu m^3/\mu J$ (with 20 sub-pulses, 33% pulse overlap and 5 ps pulse duration) and 5.7 $\mu m^3/\mu J$ (at 50 sub-pulse, 60% pulse overlap and 500 fs pulse duration), respectively. There were similarities in the SRR dependence on the number of sub-pulses per burst when relatively low and high pulse durations, i.e. 500 fs and 1 ps, and 5 and 10 ps, respectively, were used.

In addition, a novel empirical approach is implemented in this research to assess the heat accumulation effects on SRRs in the burst mode processing. In general, the heat accumulation effects were predominantly advantageous both at relatively small (from 1 to 3) or high (above 100) number of sub-pulses per burst. The results clearly show the potential of the MHz mode processing for improving SRRs and reducing the machining time in ultrashort laser machining and structuring. In addition, it is worth

noting that the surface quality attained with the burst mode processing was comparable to that achieved with the single mode and even better with some specific process settings. Thus, it can be concluded that the obtained SRR improvements were not in expense of the surface quality and thus it will be possible to benefit fully from the constantly increasing pulse energies and average power in ultrashort laser processing operations.

Acknowledgement

The authors would like to acknowledge the collaboration with LASEA SA, Belgium within the framework of the ESIF project “Smart Factory Hub” (SmartFub). The project was also partly supported by the Manufacturing Technology Centre (MTC).

References

1. Finger, J., Kalupka, C., and Reininghaus, M., *High power ultra-short pulse laser ablation of IN718 using high repetition rates.* Journal of materials processing technology, 2015. **226**: p. 221-227.
2. Smrž, M., Novák, O., Mužík, J., Turčičová, H., Chyla, M., Nagisetty, S.S., Vyvlečka, M., Roškot, L., Miura, T., and Černohorská, J., *Advances in high-power, ultrashort pulse DPSSL technologies at HiLASE.* Applied Sciences, 2017. **7**(10): p. 1016.
3. Mishra, S. and Yadava, V., *Laser Beam MicroMachining (LBMM) – A review.* Optics and Lasers in Engineering, 2015. **73**: p. 89-122.
4. Cheng, J., Liu, C.-s., Shang, S., Liu, D., Perrie, W., Dearden, G., and Watkins, K., *A review of ultrafast laser materials micromachining.* Optics & Laser Technology, 2013. **46**: p. 88-102.
5. Kramer, T., Neuenschwander, B., Jäggi, B., Remund, S., Hunziker, U., and Zürcher, J., *Influence of pulse bursts on the specific removal rate for ultra-fast pulsed laser micromachining of copper.* Physics Procedia, 2016. **83**: p. 123-134.
6. Neuenschwander, B., Kramer, T., Lauer, B., and Jaeggi, B. *Burst mode with ps- and fs-pulses: Influence on the removal rate, surface quality, and heat accumulation*. in *Laser Applications in Microelectronic and Optoelectronic Manufacturing (LAMOM) XX*. 2015. International Society for Optics and Photonics.
7. Jaeggi, B., Neuenschwander, B., Remund, S., and Kramer, T. *Influence of the pulse duration and the experimental approach onto the specific removal rate for ultra-short pulses*. in *Laser Applications in Microelectronic and Optoelectronic Manufacturing (LAMOM) XXII*. 2017. International Society for Optics and Photonics.
8. Žemaitis, A., Gaidys, M., Gečys, P., Račiukaitis, G., and Gedvilas, M., *Rapid high-quality 3D micro-machining by optimised efficient ultrashort laser ablation.* Optics and Lasers in Engineering, 2019. **114**: p. 83-89.
9. Amouye Foumani, A., Förster, D.J., Ghorbanfekr, H., Weber, R., Graf, T., and Niknam, A.R., *Atomistic simulation of ultra-short pulsed laser ablation of metals with single and double pulses: An investigation of the re-deposition phenomenon.* Applied Surface Science, 2021. **537**: p. 147775.
10. Förster, D.J., Jäggi, B., Michalowski, A., and Neuenschwander, B., *Review on Experimental and Theoretical Investigations of Ultra-Short Pulsed Laser Ablation of Metals with Burst Pulses.* Materials, 2021. **14**(12).
11. Knappe, R., Haloui, H., Seifert, A., Weis, A., and Nebel, A. *Scaling ablation rates for picosecond lasers using burst micromachining*. in *Laser-based Micro-and Nanopackaging and Assembly IV*. 2010. International Society for Optics and Photonics.

12. Hodgson, N., Steinkopff, A., Heming, S., Allegre, H., Haloui, H., Lee, T.S., Laha, M., and VanNunen, J. *Ultrafast laser machining: process optimization and applications*. in *Laser Applications in Microelectronic and Optoelectronic Manufacturing (LAMOM) XXVI*. 2021. International Society for Optics and Photonics.
13. Kerse, C., Kalaycıoğlu, H., Elahi, P., Çetin, B., Kesim, D.K., Akçaalan, Ö., Yavaş, S., Aşık, M.D., Öktem, B., and Hoogland, H., *Ablation-cooled material removal with ultrafast bursts of pulses.* Nature, 2016. **537**(7618): p. 84.
14. Elahi, P., Akçaalan, Ö., Ertek, C., Eken, K., Ilday, F.Ö., and Kalaycoğlu, H., *High-power Yb-based all-fiber laser delivering 300 fs pulses for high-speed ablation-cooled material removal.* Optics Letters, 2018. **43**(3): p. 535-538.
15. Gaudiuso, C., Giannuzzi, G., Volpe, A., Lugarà, P.M., Choquet, I., and Ancona, A., *Incubation during laser ablation with bursts of femtosecond pulses with picosecond delays.* Optics express, 2018. **26**(4): p. 3801-3813.
16. Lickschat, P., Demba, A., and Weissmantel, S., *Ablation of steel using picosecond laser pulses in burst mode.* Applied Physics A, 2017. **123**(2).
17. Gärtner, E., Polise, V., Tagliaferri, F., and Palumbo, B., *Laser micro machining of alumina by a picosecond laser.* Journal of Laser Micro Nanoengineering, 2018. **13**(2): p. 76-84.
18. Esser, D., Rezaei, S., Li, J., Herman, P.R., and Gottmann, J., *Time dynamics of burst-train filamentation assisted femtosecond laser machining in glasses.* Optics express, 2011. **19**(25): p. 25632-25642.
19. Jaeggi, B., Remund, S., Zhang, Y., Kramer, T., and Neuenschwander, B., *Optimizing the Specific Removal Rate with the Burst Mode Under Varying Conditions.* Journal of Laser Micro/Nanoengineering, 2017. **12**(3).
20. Förster, D.J., Faas, S., Gröninger, S., Bauer, F., Michalowski, A., Weber, R., and Graf, T., *Shielding effects and re-deposition of material during processing of metals with bursts of ultra-short laser pulses.* Applied Surface Science, 2018. **440**: p. 926-931.
21. Kramer, T., Zhang, Y., Remund, S., Jaeggi, B., Michalowski, A., Grad, L., and Neuenschwander, B., *Increasing the specific removal rate for ultra short pulsed laser-micromachining by using pulse bursts.* J. Laser Micro/Nanoeng, 2017. **12**: p. 107.
22. Javaux, C., Mishchik, K., Dematteo-Caulier, O., Skupin, S., Chimier, B., Duchateau, G., Bourgeade, A., Hönninger, C., Mottay, E., and Lopez, J. *Effects of burst mode on transparent materials processing*. in *Laser-based Micro-and Nanoprocessing IX*. 2015. International Society for Optics and Photonics.
23. Belloni, V., Sabonis, V., Di Trapani, P., and Jedrkiewicz, O., *Burst mode versus single-pulse machining for Bessel beam micro-drilling of thin glass: Study and comparison.* SN Applied Sciences, 2020. **2**(9): p. 1-12.

24. Neuenschwander, B., Jaeggi, B., Foerster, D.J., Kramer, T., and Remund, S., *Influence of the burst mode onto the specific removal rate for metals and semiconductors.* Journal of Laser Applications, 2019. **31**(2): p. 022203.
25. Bonamis, G., Mishchick, K., Audouard, E., Hönninger, C., Mottay, E., Lopez, J., and Manek-Hönninger, I., *High efficiency femtosecond laser ablation with gigahertz level bursts.* Journal of Laser Applications, 2019. **31**(2): p. 022205.
26. Lickschat, P., Metzner, D., and Weißmantel, S., *Manufacturing of high quality 3D microstructures in stainless steel with ultrashort laser pulses using different burst modes.* Journal of Laser Applications, 2021. **33**(4): p. 042002.
27. Butkus, S., Jukna, V., Paipulas, D., Barkauskas, M., and Sirutkaitis, V., *Micromachining of Invar Foils with GHz, MHz and kHz Femtosecond Burst Modes.* Micromachines (Basel), 2020. **11**(8).
28. Martan, J., Prokešová, L., Moskal, D., Ferreira de Faria, B.C., Honner, M., and Lang, V., *Heat accumulation temperature measurement in ultrashort pulse laser micromachining.* International Journal of Heat and Mass Transfer, 2021. **168**.
29. Domke, M., Matylitsky, V., and Stroj, S., *Surface ablation efficiency and quality of fs lasers in single-pulse mode, fs lasers in burst mode, and ns lasers.* Applied Surface Science, 2020. **505**: p. 144594.
30. Michalowski, A., Nyenhuis, F., and Kunz, G., *Smooth Surfaces by Pulsed Laser Processing with Bursts: Making use of the effects of successive pulses.* PhotonicsViews, 2020. **17**(3): p. 42-45.
31. Žemaitis, A., Gaidys, M., Gečys, P., Barkauskas, M., and Gedvilas, M., *Novel ultrafast laser ablation by biburst in MHz and GHz pulse repetition rate.* arXiv preprint arXiv:2011.14770, 2020.
32. Metzner, D., Lickschat, P., and Weißmantel, S., *Optimization of the ablation process using ultrashort pulsed laser radiation in different burst modes.* Journal of Laser Applications, 2021. **33**(1).
33. Zemaitis, A., Gaidys, M., Gecys, P., Barkauskas, M., and Gedvilas, M., *Femtosecond laser ablation by bibursts in the MHz and GHz pulse repetition rates.* Opt Express, 2021. **29**(5): p. 7641-7653.
34. Caballero-Lucas, F., Obata, K., and Sugioka, K., *Enhanced ablation efficiency for silicon by femtosecond laser microprocessing with GHz bursts in MHz bursts (BiBurst).* International Journal of Extreme Manufacturing, 2022. **4**(1): p. 015103.
35. Lickschat, P., Metzner, D., and Weißmantel, S., *Burst mode ablation of stainless steel with tunable ultrashort laser pulses.* Journal of Laser Applications, 2021. **33**(2).
36. Neuenschwander, B., Jaeggi, B., Zavedeev, E., Arutyunyan, N., and Pimenov, S., *Heat accumulation effects in laser processing of diamond-like nanocomposite films with bursts of femtosecond pulses.* Journal of Applied Physics, 2019. **126**(11): p. 115301.

37. Metzner, D., Lickschat, P., and Weißmantel, S., *Laser micromachining of silicon and cemented tungsten carbide using picosecond laser pulses in burst mode: ablation mechanisms and heat accumulation.* Applied Physics A, 2019. **125**(7).
38. Cangueiro, L., Ramos-de-Campos, J.A., and Bruneel, D., *Prediction of Thermal Damage upon Ultrafast Laser Ablation of Metals.* Molecules, 2021. **26**(21): p. 6327.
39. Penczak, J., Kupfer, R., Bar, I., and Gordon, R.J., *The role of plasma shielding in collinear double-pulse femtosecond laser-induced breakdown spectroscopy.* Spectrochimica Acta Part B: Atomic Spectroscopy, 2014. **97**: p. 34-41.
40. Tan, S., Wu, J., Zhang, Y., Wang, M., and Ou, Y., *A model of ultra-short pulsed laser ablation of metal with considering plasma shielding and non-Fourier effect.* Energies, 2018. **11**(11): p. 3163.
41. Thurow, B.S., Satija, A., and Lynch, K., *Third-generation megahertz-rate pulse burst laser system.* Applied optics, 2009. **48**(11): p. 2086-2093.
42. Chowdhury, M., Bose, B., Yamamoto, K., Shuster, L., Paiva, J., Fox-Rabinovich, G., and Veldhuis, S., *Wear performance investigation of PVD coated and uncoated carbide tools during high-speed machining of TiAl6V4 aerospace alloy.* Wear, 2020. **446**: p. 203168.
43. Leksycki, K. and Królczyk, J.B., *Comparative assessment of the surface topography for different optical profilometry techniques after dry turning of Ti6Al4V titanium alloy.* Measurement, 2021. **169**: p. 108378.
44. Metrology, J.C.f.G.i., *Evaluation of measurement data—Guide to the expression of uncertainty in measurement.* JCGM, 2008. **100**(2008): p. 1-116.
45. Sun, Z., Lenzner, M., and Rudolph, W., *Generic incubation law for laser damage and ablation thresholds.* Journal of Applied Physics, 2015. **117**(7): p. 073102.
46. Liu, J., *Simple technique for measurements of pulsed Gaussian-beam spot sizes.* Optics letters, 1982. **7**(5): p. 196-198.
47. Eshkabilov, S., Ara, I., Sevostianov, I., Azarmi, F., and Tangpong, X., *Mechanical and thermal properties of stainless steel parts, manufactured by various technologies, in relation to their microstructure.* International Journal of Engineering Science, 2021. **159**: p. 103398.
48. Carvill, J., *3 - Thermodynamics and heat transfer*, in *Mechanical Engineer's Data Handbook*, Carvill, J., Editor. 1993, Butterworth-Heinemann: Oxford. p. 102-145.
49. Hodgson, N., Allegre, H., Starodoumov, A., and Bettencourt, S., *Femtosecond Laser Ablation in Burst Mode as a Function of Pulse Fluence and Intra-Burst Repetition Rate.* Journal of Laser Micro/Nanoengineering, 2020. **15**(3): p. 236 - 244.
50. Žemaitis, A., Gaidys, M., Brikas, M., Gečys, P., Račiukaitis, G., and Gedvilas, M., *Advanced laser scanning for highly-efficient ablation and ultrafast surface structuring: experiment and model.* Scientific Reports, 2018. **8**(1): p. 17376.

51. Semerok, A. and Dutouquet, C., *Ultrashort double pulse laser ablation of metals.* Thin solid films, 2004. **453**: p. 501-505.

CHAPTER 5

LASER PRECESSION MACHINING OF CROSS-SHAPED TERAHERTZ BANDPASS FILTERS

Hoang Le [1], Chandrasekhar Pradhani [2], Pavel Penchev [1], Vahid Nasrollahi [1], Themistoklis Karkantonis [1], Yi Wang [2], Stefan Dimov [1] and Jose A. Ramos-de-Campos [3]

[1] Department of Mechanical Engineering, University of Birmingham, Birmingham B15 2TT, UK

[2] Department of Electronic, Electrical and Systems Engineering, University of Birmingham, Birmingham B15 2TT, UK.

[3] LASEA S.A., Liège Science Park, Rue Louis Plescia 31, 4102 Seraing, Belgium.

This research was published as a full-length article in ***Optics and Lasers in Engineering*** (2022).

Le, H., Pradhani, C., Penchev, P., Nasrollahi, V., Karkantonis, T., Wang, Y., Dimov, S., & Ramos-de-Campos, J. A.. Laser precession machining of cross-shaped terahertz bandpass filters. Optics and Lasers in Engineering, 149 (2022).

Https://doi.org/10.1016/j.optlaseng.2021.106790

Author Contributions	
Hoang Le **(First Author)**	Conceptualization, Formal analysis, Methodology, Investigation, Validation, Writing–original draft, Writing–review & editing
C. Pradhani	Formal analysis, Validation, Writing–review & editing
P. Penchev	Methodology
V. Nasrollahi	Writing–review & editing
T. Karkantonis	Writing–review & editing
Y. Wang	Investigation, Validation
S. Dimov	Project administration, Writing–review & editing
J. A. Ramos-de-Campos	Writing–review & editing

Abstract

The laser micro-machining technology is an attractive alternative to conventional photoresist-based technologies for manufacturing terahertz (THz) cross-shaped mesh filters. It can address some limitations related to filter's quality, process complexity, unit cost and available materials. However, there are also open issues associated with the laser micro-machining technology that have to be addressed. In particular, some intrinsic characteristics of laser micro-machined structures, i.e. the side-wall tapering, that impact both achievable geometrical and dimensional accuracy and the filters' performance. This research proposes a novel fabrication process, called laser precession machining, that addresses some of the key laser micro-machining limitations in producing THz mesh filters. It employs an ultrafast laser and a "precess" module to vary the beam incident angle and thus to minimise the taper angle on the sidewalls of the filters' cross-shaped through holes. A significant reduction of this negative tapering effect was achieved on micro-structures produced with this new method that led to a significant improvement of filters' performance. The filters' performance was compared with the simulation results and they were in good agreement. X-ray photoelectron spectroscopy (XPS) analysis was carried out to analyse the effects of laser precession machining on the composition of copper substrates as a potential factor affecting the filters' performance.

Keywords: Terahertz, Cross-shaped, Mesh Filter, Laser Micro-machining, Precession, Tapering Effect.

5.1. Introduction

The interests in developing and implementing terahertz (THz) technology have been growing consistently in the last decade with a wide range of applications offering unique capabilities [1]. The THz emission frequency covers the gap between the microwave and infrared radiation in the electromagnetic spectrum, ranging from 0.1 to 10 THz that is equivalent to wavelength from 3 mm to 30 μm and exists in non-ionizing form [2, 3]. Applications of the terahertz radiation can be found in various areas, such as biomedical imaging, cancer detection, food and water inspection, radars, security and astronomy [4-9]. One of the key components in many THz communication systems are the frequency restricting components that act as filters in selecting one or more target frequency bands [10, 11]. A typical example of such components are the frequency selective surfaces which are formed of two-dimensional arrays of through structures onto a thin substrate, also known as mesh filters [12]. One popular through structure of the THz mesh filters are cross-shaped holes with critical dimensions such as length, width and periodicity [13, 14]. Consequently, the performance of cross-shaped THz mesh filters is very sensitive to their geometrical accuracy [15]. Therefore, the technologies used for their manufacture normally require a very high accuracy and repeatability [16].

Photolithography that employs SU-8 photoresist has been used to manufacture THz components and frequency selective surfaces [17, 18]. This technology typically produces components with a very high geometrical accuracy, especially in regard to the taper angle on the micro-structures' sidewall, that affects the mesh filters' performance. This is an important prerequisite for achieving a good mesh filter's performance, i.e. transmitting only the selected frequencies with minimum insertion losses, as these THz device's characteristics are very sensitive to any dimensional variations. However, photolithography also has some intrinsic shortcomings, in particular it can only process photoresist materials with their limited mechanical, thermal and electrical properties. SU-8 is an epoxy-based photoresist with Young's modulus in range of 2.92 to 4.95 GPa that is far lower when compared with metallic substrates [19]. In addition, SU-8 has a high electrical resistivity and therefore the photoresist-based manufacturing technologies for producing THz devices have to include a metallisation step.

There are other manufacturing technologies of producing frequency selective surfaces such as electron-beam lithography, nanoimprint lithography, deep reactive ion etching and inkjet printing [20-22]. These technologies again require an additional metallisation step, as with the case of photolithography. Hard substrates are usually required to reinforce the mesh filters fabricated with them. Another common limitation of these technologies is that they are capital intensive and therefore are mostly viable for

relatively large batch sizes while the unit costs are still relatively high due to the use of clean room manufacturing technologies.

In this context, laser-based micro machining offers unique advantages compared to photoresist-based manufacturing technologies, especially for producing THz frequency selective surfaces. It is a direct write and non-contact process and can be used to structure almost any material [23]. Therefore, the researchers have started looking at employing this technology for fabricating THz communication components [24-28].

Table 5.1. A comparison of manufacturing capabilities of laser-based and photoresist-based micro-manufacturing technologies [29].

Manufacturing solutions	***Photoresist-based***	***Laser-based***
Geometrical complexity	*2.5D*	*3D*
Requirement for secondary processes	*Mask production; Coatings*	*No*
Assembly operations	*Required*	*No*
Material requirements	*Photoresists*	*No limitations*
Vulnerability to design changes	*High*	*Low*
Environment impact	*Chemical usage*	*No*
Process flexibility	*Low*	*High*

Table 5.1 compares the capabilities of photoresist-based technologies against laser-based ones for producing THz devices. It can be clearly seen that laser-based micro-machining systems offer important advantages and also flexibility in their manufacture. The achievable accuracy with state-of-the-art laser micro-machining systems can be better than 4 μm and thus is becoming comparable to what can be attained employing

photolithography [30]. The production costs can be reduced, too, with the use of laser direct fabrication of THz devices as it will be possible to avoid post-processing steps. The attractive capabilities of laser micro-machining systems, such as non-contact 3D processing and abilities to structure directly metallic substrates, can also underpin the development of novel THz device's designs.

However, the laser micro-machining technology still has some inherent limitations that can affect the manufacturing process and thus the performance of THz mesh filters. In particular, the tapering effect on structure's sidewalls is a challenge that limits the achievable geometrical and dimensional accuracy in producing through structures [31, 32] and thus the achievable aspect-ratios in producing the functional features of THz mesh filters. Most of the THz mesh filters fabricated by laser micro-machining so far were produced using relatively thin substrates (a thickness of less than 50 μm) [33, 34] and therefore the tapering effect had a relatively small impact on their dimensional accuracy. The thermal side effects, such as the heat affected zone and the formation of recasts around the features, have been the other issues that have affected negatively the achievable accuracy when micro structures have to be produced [35]. Furthermore, laser micro-machining systems are more suitable for producing small batches of components. However, in general, it is a scalable technology that with some process setting up automation can be made suitable for a serial manufacture, too. For example, this can be achieved by developing specialised work-holding devices [36]

and capitalising on the latest advances in ultra-short pulse technology, both on constantly increasing the average power of femtosecond laser sources and optical solutions for beam splitting and shaping [37].

Taking into account the advantages and limitations of laser-based micro-machining, this research reports a feasibility study in the use of this technology for producing THz devices, especially THz mesh filters. The specific objective is to investigate the capabilities of a novel laser micro-machining technology, called precession laser micro-machining, for producing cross-shaped, free-stranding THz mesh filters out of metal materials directly without requiring any dielectric substrates. We also choose to demonstrate the capability of lasing processing by machining a ‘thick’ mesh filter structure [10] which presents additional fabrication challenges. In particular, a precession module was integrated into a reconfigurable workstation to control the incident angle of the laser beam. In this way, it was possible to control the beam incident angle and thus to minimise and potentially eliminate the negative tapering effect on accuracy of microstructures. The feasibility study was conducted by manufacturing THz mesh filters with different dimensions and aspect-ratios for their critical features, and thus to demonstrate the capabilities of this novel laser micro-machining process. As a reference for comparison purposes, another recently reported approach for minimising the tapering effect, called two-side laser micro-machining [38], was employed to fabricate the same THz mesh filters. The geometrical and

dimensional accuracy together with the respective performance of produced filters were analysed and conclusions made about the capabilities of the proposed manufacturing approach.

5.2. Materials and methods

5.2.1. Cross-shaped terahertz mesh filters

Two designs of terahertz mesh filters were used to investigate the manufacturing capabilities of the proposed laser precession micro-machining method. Both filters were designed to allow frequency of 0.3 THz (300 GHz) to pass through them. The first mesh filter design (Design 1) is a single-pole filter that transmits only one peak frequency, while the second mesh filter design (Design 2) is a two-pole filter with increased frequency selectivity. The difference in their required transmission performance leads to differences in the dimensions of these two filter designs. In general, the functional feature of the two filters are arrays of cross-shaped through holes with dimensions as shown in Fig. 5.1. The sidewalls of the cross-shaped holes are normal to the mesh filter surface. In particular, Design 1 includes an array of 14×14 cross-shaped holes that cover a square area of 8.65 mm × 8.65 mm, while Design 2 is an array of 28×28 holes that covers an area of 26.21 mm × 26.21 mm. The designed thickness of the two THz mesh filters is also different, 300 and 670 μm for the single-pole and the two-pole filters, respectively. Taking into account the sizes of the cross-

shaped holes and the thicknesses of the substrates, the aspect-ratios that have to be achieved are 1:4.76 and 1:2.18 for Design 1 and Design 2, respectively.

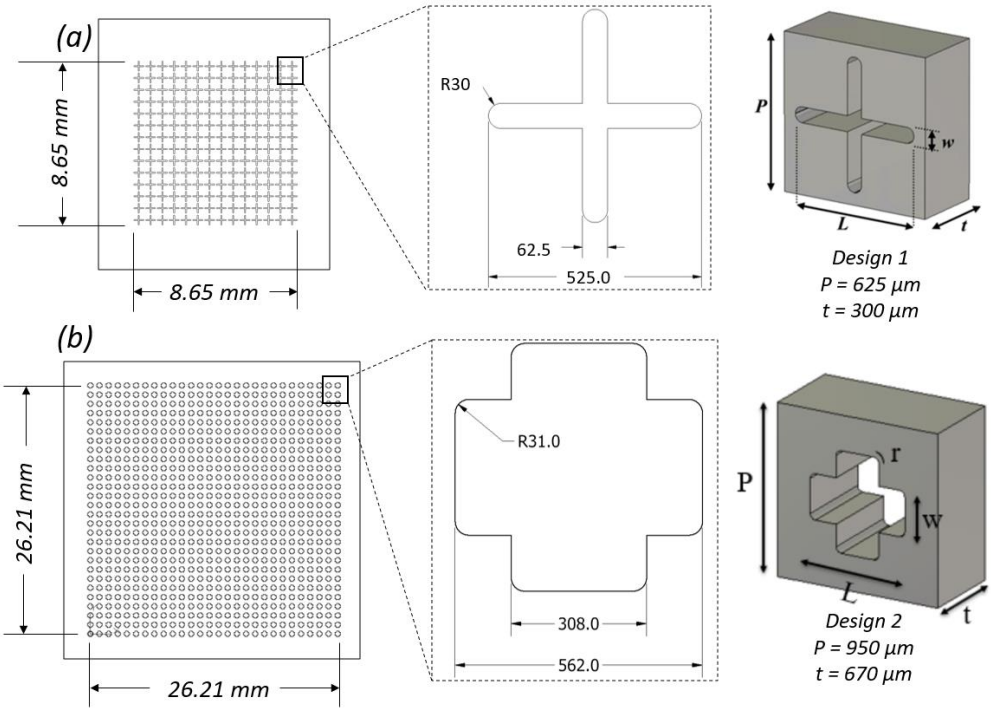

Figure 5.1 *The two THz mesh filter designs: (a) Design 1 and (b) Design 2.*

Note: the dimensions of cross-shaped holes are given in micrometers and P is the hole's preriodicity, L – the hole's length, w – the hole's width, R – the fillets' radiusm at the hole's corners and t – the thickness.

99.9% purity copper was chosen as a substrate material. Copper has a very low resistivity and therefore the need for any coatings will be minimised or even eliminated. Additionally, the copper substrates are sufficiently rigid and therefore no reinforcement is required, too. This is another advantage of THz filters machined from copper substrates compared to the photoresist-based manufacturing approaches as any risks

from damage during storage, transportation and installation can be reduced and even fully eliminated.

5.2.2. Laser micro-machining system

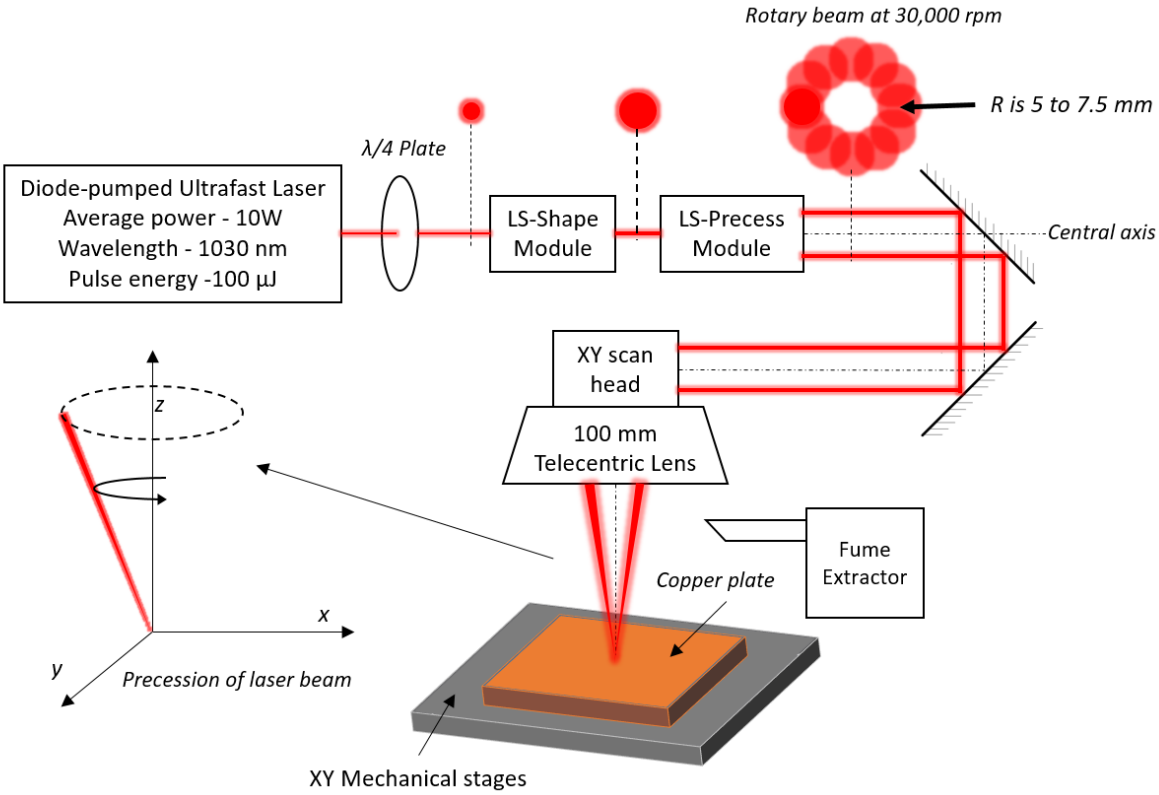

Figure 5.2. *A schematic representation of the laser micro-machining setup.*

Note: R is the beam offset from the central axis.

The THz mesh filters were fabricated using a LASEA LS-4 workstation that integrates a sub-picosecond laser source, YUJA from Amplitude Systemes, with wavelength of 1030 nm and pulse duration of 390 femtoseconds for athermal/"cold" processing. A schematic representation of the laser micro-machining setup is provided in Fig. 5.2. The maximum average laser power after the focusing lens was 8W and thus the pulse

energy was 80 μJ at a repetition rate of 100 kHz. By using the maximum average power available, the highest possible material removal rate was used to minimise the processing time. An ultrafast laser processing was preferred in this research in order to produce mesh filters with high dimensional accuracy and quality [39]. A quarter waveplate was integrated into the beam delivery sub-system to carry out the machining with a circularly polarised beam and thus to achieve an even ablation at the focal plane [40].

The beam delivery sub-system consists of two modules, i.e. LS-shape and LS-precess. The LS-shape module is used to condition the beam and control basic laser beam properties, in particular the laser power and beam diameter. The LS-precess module is critical for realising a precession laser processing. Especially, the module allows a parallel offset and rotation of the laser beam about the beam central axis with a maximum speed of 30,000 rpm (more details are provided in Section 2.3). The laser beam is then steered with X and Y deflectors before the focusing telecentric lens with focal length of 100 mm and thus to achieve beam spot size of approximately 30 μm at the focal plane. The workpiece is placed on a stack of X and Y direct-drive linear stages with accuracy of ±1 μm and repeatability of ±0.4 μm. Each individual cross-shaped hole was machined by using only the X and Y beam deflectors while the mechanical stages were used to reposition the beam for machining the arrays of holes. Therefore, the accuracy and repeatability of the stages was important in ensuring the required

periodicity between cross-shaped holes. A fume extractor was used to evacuate any debris from laser-material interaction area and thus to minimise the contamination of the machined copper substrates.

5.2.3. Precession laser machining

The LS-precess module allows a beam offset in the range from 5 to 7.5 mm while the beam remains parallel to the original central axis [41]. Then, the laser beam is rotated at high speed (up to 30,000 rpm) to create a donut ring with a diameter from 10 to 15 mm after the LS-precess module. The precession movement of the laser beam after the focusing lens is created by focusing the donut ring with a telecentric lens as depicted in Fig. 5.3. When the beam is offset and parallel to its central axis, the angle between the approaching beam and the first surface of the telecentric lens is no longer normal. Consequently, the output beam approaches the workpiece surface with a controllable attack angle (Fig. 5.3a). The attack angle with the used LS-precess module can be varied from 2.9 to 4.3 degree and depends on the size of the donut ring before the focusing lens. However, there is another constraint associated with the scan head aperture, especially the maximum diameter of the donut ring is limited by the aperture size (20 mm in the used experimental setup). Therefore, the diameter of the donut ring was kept at 12 mm approximately and thus to maximize the attack angle while avoiding any potential clipping of the rotating laser beam at the scan head aperture. This resulted in a beam attack angle of 3.46 degree after the telecentric lens.

The advantages of using an incident beam that is not anymore normal to the focal plane and at the same time rotates at high speed are to ablate the material at the holes' sidewall more efficiently. This is very important when high aspect ratio structures have to be produced and the evacuation of the ablated material becomes much more difficult. Using this technique, through structures with vertical sidewalls or even a negative taper angle can be produced as shown in Fig. 5.3b.

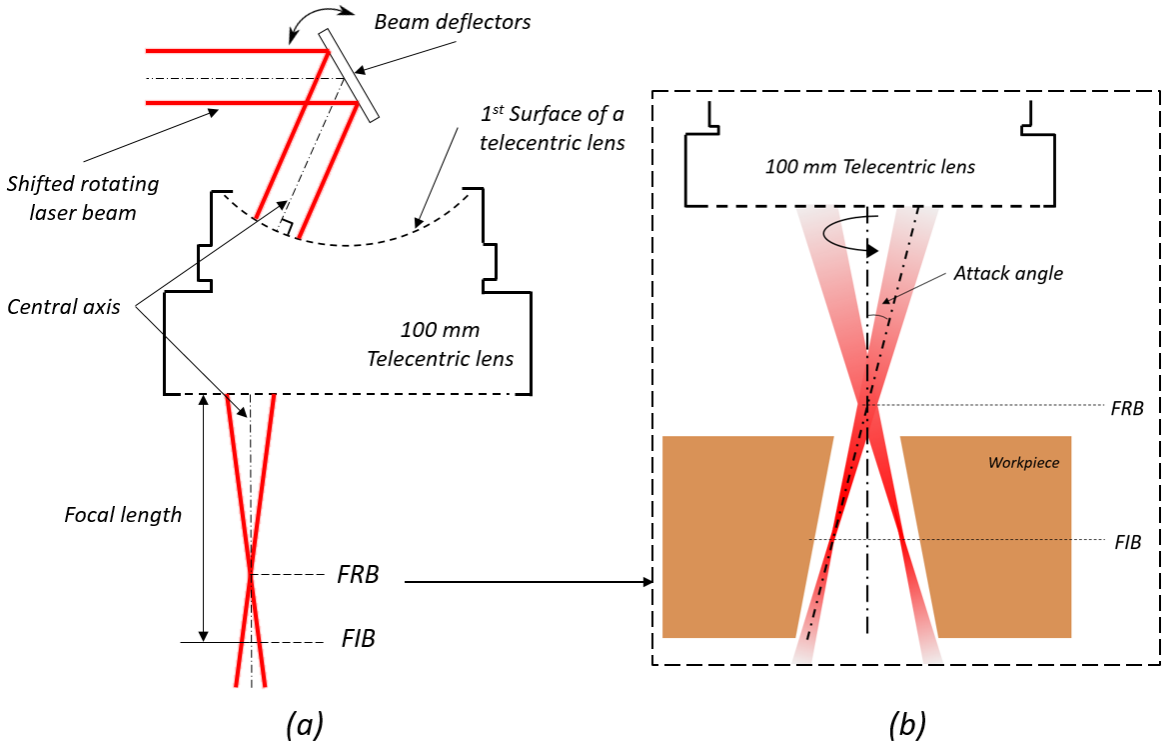

Figure 5.3. *A schematic representation of laser beam precession movements: (a) the precession movement of the laser beam created by focusing the rotating beam, (b) zero or negative tapering effect achievable with a precession laser beam.*

Note: FIB - the focus of the "individual" laser beam at the focal plane of the telecentric lens; FRB – the intersection point of the rotating beam that is along the central axis.

The cross-shaped holes of the THz filters were fabricated by employing a precession laser beam. The scanning speed of the laser beam is synchronised with its rotational speed and therefore has to be reduced significantly compared to the speeds normally used when a precession movement is not required. Especially, the scanning speed should be less than 50 mm/s during precession processing and thus to achieve a sufficient overlapping between the beam loops and so to ablate the material efficiently along the structure profiles. This is the main limitation of the precession laser processing technology. However, it is feasible to increase the scanning speed by increasing simultaneously the beam rotational speed as there is a linear interdependence between them.

A layer-based machining strategy was used to produce the cross-shaped holes. Two different scanning speeds were used to achieve an efficient material removal and produce holes with smooth edges. In particular, by trials, two scanning speeds were selected, 20.5 and 12 mm/s, and the resulting beam paths are presented in Fig. 5.4. Nine passes with the faster scanning speed were required to achieve good overlaps between the pulses and the beam loops and to machine the copper substrates, efficiently, and remove most of the material. Then, additional four finishing passes with the lower speed were necessary to clean the holes' edges/kerfs and also to reduce further the taper angle on the sidewalls. The use of the slower scanning regime allowed the striation effects at the holes' edges to be eliminated, especially by reducing the

distance between the precession beam loops. Thus, it was possible to produce cutting kerfs with straight and well-defined edges by employing two scanning regimes.

In addition, the initial trials had shown that the scanning direction of the precession laser beam affected the edge quality. Therefore, the outer part of the precession loops was along the edges of the holes as shown in Fig. 5.4a and 5.4b and as a result structures with well-defined and smooth edges were produced. Finally, the conducted trials have also shown that the cross-sectional profile of the holes should be outlined three times per layer to facilitate a proper material evacuation with the increase of the hole's depth. Especially, the holes' kerfs were widened by conducing three outlining cuts per layer with a step-over distance between them of 50 um as shown in Fig. 5.4c and 5.4d and Fig. 5.5a and 5.5c.

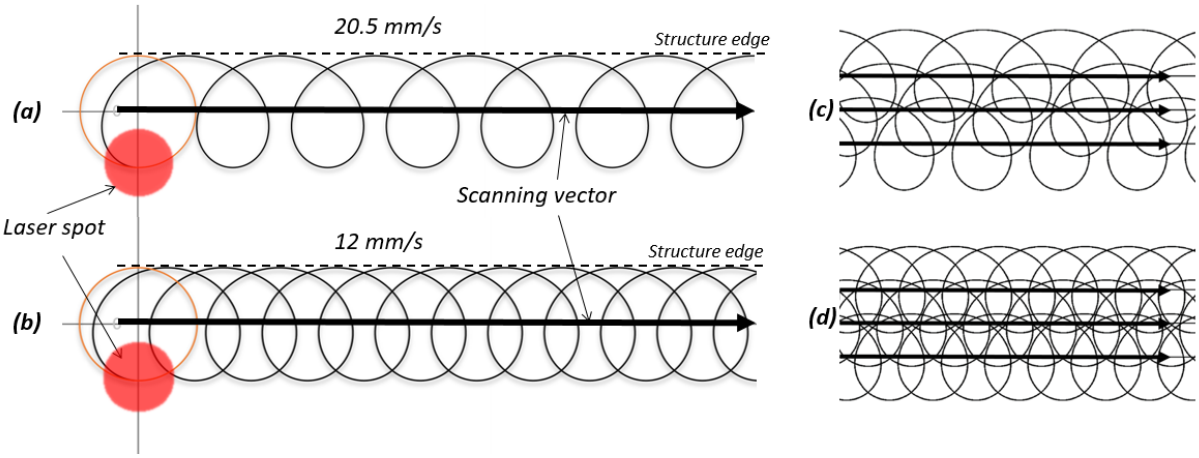

Figure 5.4. *The beam paths for the two different scanning speeds: (a) a single pass with the faster scanning speed, 20.5 mm/s; (b) a single pass with the slower scanning*

speed, 12 mm/s; (c) multiple passes with the faster scanning speed; and (d) multiple passes with the slower scanning speed.

So, the precession machining strategy implemented for producing the two filter designs required three outlining cuts and each of them included nine passes with the higher scanning speed and four more with the lower speed, hence thirteen passes per cut and thirty-nine ones in total for each layer. FIB was kept at the top surface of the substrate at the start of the machining cycles and then moved down 100 µm at each layer. Three layers were required for the Design 1 filter while six layers were necessary to produce the Design 2 as showed in Fig. 5.5b and 5.5d.

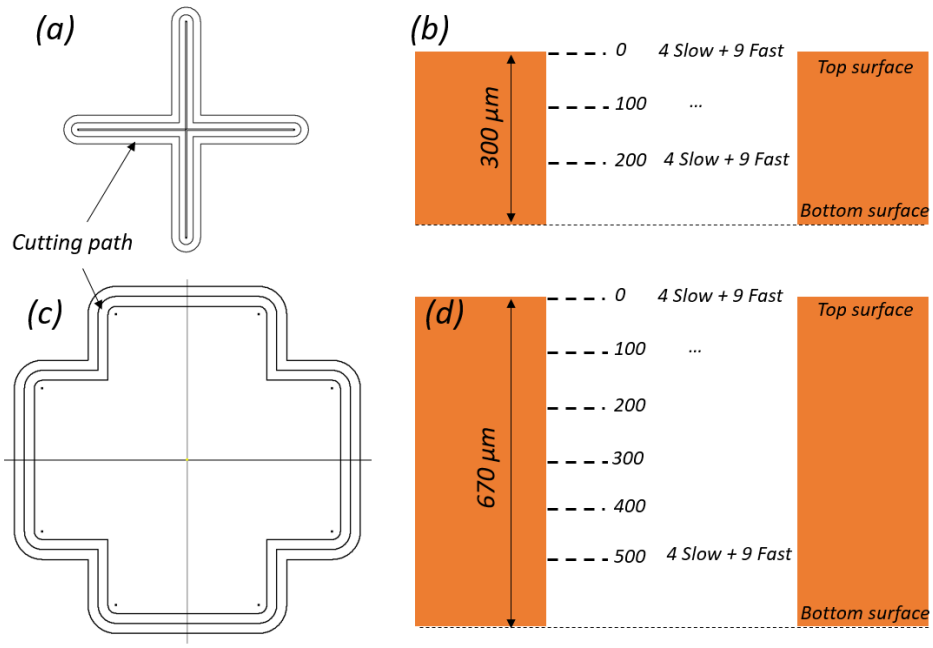

Figure 5.5. *The layer-based machining strategies used to produce the cross-shaped holes: (a) and (c) the three cutting paths with a step-over of 50 µm used to machine each layer of the single-pole and two-pole filters, respectively; (b) and (d) the layers*

per cut with their 4 slow and 9 fast passes required in machining the holes of the single-pole and two-pole filters, respectively.

The final step of the fabrication process was the cleaning of the samples in an ultrasonic bath with acetone for 10 minutes. This step was necessary in order to remove any debris inside the cross-shaped holes that can affect the performance of THz filters.

5.2.4. Two-side laser machining

As it was stated, the two THz filter designs were also fabricated using the two-side laser processing method proposed by Nasrollahi et al. [38]. The samples fabricated with this method were used as references and their performance was compared with the filters produced using the precession machining regime. Again, an ultrafast (femtosecond) laser source was used to produce the filters while the same circular polarization, 100 mm telecentric focusing lens and mechanical stages as those used in implementing the precession machining method were utilised. Especially, a mechanical rotary stage with accuracy of 29 μrad was employed to rotate the workpiece at 180 degree as required by the two-side method. Trials were conducted to find a suitable processing window for machining the filter holes with a comparable edge definition and dimensional accuracy to those achieved with the precession method. The maximum pulse energy was set at 80 uJ and achieve an accumulated fluence of 8.2 J/cm^2. In addition, a hatching strategy with a step-over distance of 10

μm was deployed to produce the holes. The pulse repetition rate was kept the same, 100 kHz, as in the precession method while the maximum possible scanning speed, 2000 mm/s, was used in order to minimise the processing time.

5.2.5. Measurements

5.2.5.1. Dimensional measurements

Dimensional analysis was carried out by using a focus variation microscope, ALICONA G5. The critical dimensions of the two filter designs were analysed. In particular, the length and width of the cross-shaped holes, the taper angle at the sidewalls and the holes' periodicity (the distance between holes) were measured.

The dimensions of cross-shaped holes were measured at nine different places over the machined areas and the average values were used to analyse the accuracy and repeatability achieved in the laser machining operations. The three-dimensional profiles/morphology of the cross-shaped holes was reconstructed by conducting focus variation measurements and thus to establish the taper angle on the holes' sidewall.

The thickness and the surface roughness of as-received substrates before the laser machining operation were also measured as they are factors affecting the performance of THz filters. The results of these measurements are provided in Table 5.2.

Table 5.2: The as-received thickness and surface roughness of the substrates used to produce the filters with the two laser micro-machining methods.

THz mesh filter design	***Design 1***		***Design 2***	
	Sample 1	***Sample 2***	***Sample 3***	***Sample 4***
Method	*Two-side*	*Precession*	*Two-side*	*Precession*
True thickness (µm)	*290-320*	*280-310*	*640-660*	*650-670*
Surface roughness S_a (µm)	*0.817*	*0.641*	*0.501*	*0.879*

Notes: the thickness of the substrates was measured with a calliper while their surface roughness with the Alicona G5 system

5.2.5.2. Performance measurements and simulations

The functionality of the THz mesh filters was assessed with a free space Quasi-Optic system that employs a vector network analyzer (VNA), illustrated in Fig. 5.6. It covers the range of 220 GHz to 325 GHz in this measurement [10, 42]. The performance of THz mesh filters was assessed by measuring S-parameters that characterize their reflection and transmission in the frequency domain [43]. In particular, the S11 parameter designates the impedance matching of the filter while the S21 parameter assesses the insertion loss of the signal when it passes through the frequency selective component. These parameters are measured in decibels [dB]. An ideal THz mesh filter should transmit a wave signal at 300 GHz with a zero insertion loss.

The filters' performance was simulated by using the CST MICROWAVE STUDIO® software [44]. The electric and magnetic walls were chosen to be the opposite

boundary pairs in order to model the unit cell. The resonant frequency of the unit cell was calculated by employing the full Floquet modal expansion and periodic boundaries. The efficient electric conductivity was calculated and included into the simulation [45]:

$$\sigma_{eff} = \frac{\sigma_0}{K_{SR}^2}$$

where σ_0 is theoretical electric conductivity of smooth surface material (5.87×10^7 S/m) and K_{SR} is surface roughness correction factor.

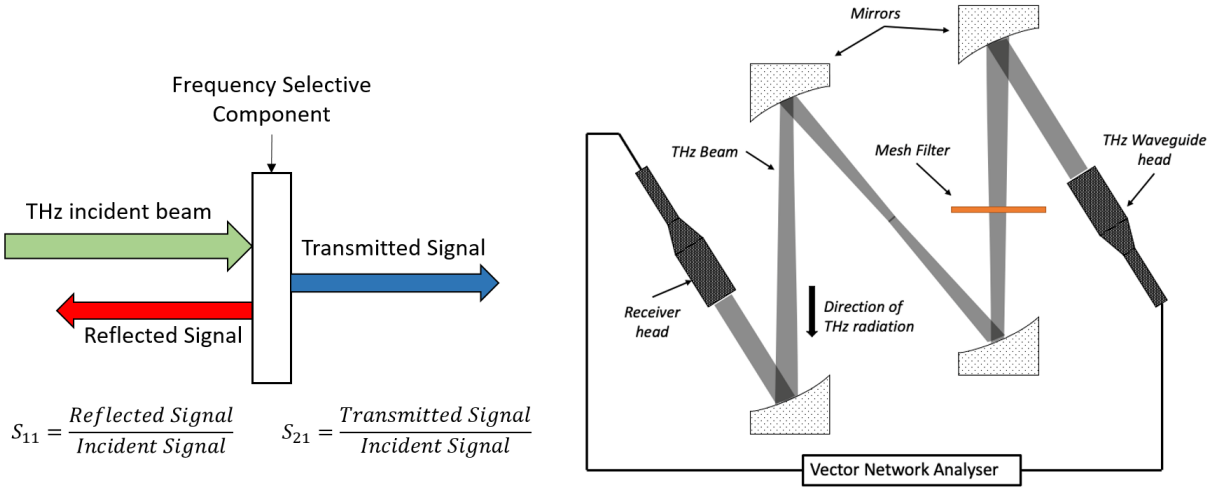

Figure 5.6. *A schematic representation of a frequency selective components with respective S11 and S21 parameters (Left) and a schematic diagram of the free space Quasi-Optic system used to assess the THz mesh filter's performance (Right).*

5.2.5.3. X-ray photoelectron spectroscopy analysis

X-ray photoelectron spectroscopy (XPS) analysis was performed on a Thermo Fisher Scientific K-alpha^{+} spectrometer. Samples were analysed using 100 µm spot mode of a micro-focused monochromatic Al x-ray source (14 W). The data was recorded at pass energies of 150 eV for the survey scans and 40 eV for the high resolution scan with 1 eV and 0.1 eV step sizes, respectively. Data analysis was performed in CasaXPS using a Shirley type background and Scofield cross sections, with an energy dependence of -0.6.

5.3. Results and discussions

5.3.1. Dimensional accuracy

Four samples of the THz mesh filters were fabricated by employing the two laser micro-machining approaches, i.e. two-side and precession laser micro-machining, described in Section 2. Sample 1 (S1) and S2 are single-pole filters, while S3 and S4 are two-pole ones. The two-side laser machining approach was employed to produce S1 and S3 while S2 and S4 were produced with the precession laser machining method.

Representative images of the two prototype mesh filters are provided in Fig. 5.7. In general, the ultrafast laser processing of copper substrates results in relatively clean structures with well-defined edges, i.e. neither observable re-cast at the edges nor apparent surface contaminations.

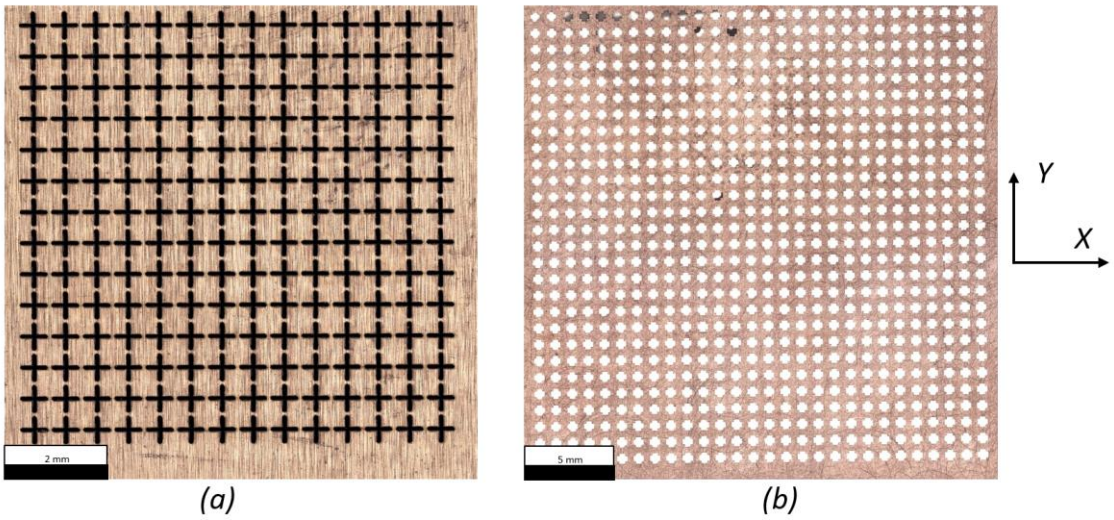

Figure 5.7. *Representative images of the two THz filter designs produced employing the precession method: (a) Design 1 (Single-pole) and (b) Design 2 (Two-pole).*

5.3.1.1. Taper angle analysis

The precession laser machining method led to better results with regard to the geometrical accuracy of the cross-shaped holes. Table 5.3 provides the measurement results, showing the reduction of the tapering effect at the sidewall in comparison to the two-side method. The average taper angle was reduced 2.6 times from 4.1 degree to 1.6 degree for the single-pole filter (Design 1). A bigger reduction of the taper angle was achieved for the two-pole filter, i.e. from 11.5 degree to 1.9 degree (6.1 times). In addition, it is important to note that this improvement was not at the expense of total machining time in spite of the fact that the precession machining process was not optimised. Especially, the machining times of S1 and S2 were the same while there was an increase of only 2 hours for S4 in comparison to S3.

Table 5.3: Average taper angles at the sidewalls of the two THz mesh filter designs with the machining times

THz mesh filter designs	***Design 1***		***Design 2***	
	S1	***S2***	***S3***	***S4***
Method	*Two-side*	*Precession*	*Two-side*	*Precession*
Taper angle [deg.]	*4.1*	*1.6*	*11.5*	*1.9*
Total machining time [hr]	*6*	*6*	*24*	*26*

The edge definition and the morphology of the holes produced with the two methods is depicted in Fig. 5.8. The sidewalls can be clearly seen in the front and back views for the holes produced with the two-side method (Fig. 5.8a and 5.8b). In contrast, the entrances (front view) were cleaner and very sharp exits (back view) were achieved on the cross-shaped holes produced with the precession laser machining method (Fig. 5.8e and 5.8f).

One of the advantages of the precession laser processing comes from the use of multiple cuts and the layer-based machining strategy. The outlining cuts in laser micro-machining have a proven positive effect on the resulting edge quality [31]. In addition, the beam precession loops in the four slow passes not only led to a further material ablation, but also helped to smooth the hole's edges. It is also important to stress that the holes were produced from one side only and the three outlining cuts with the slow and fast scanning speeds were sufficient to evacuate all ablated material efficiently. There were not visible debris or recasts at the hole's entrances. As a result, a very

good edge definition at the hole's exits were achieved and there were no evidence of a heat effected zone around them. The constructed sidewalls and extracted profiles of S1 and S2 with the focus variation method (Fig. 5.8c, 5.8d, 5.8g and 5.8h) depict a clean and well-defined sidewall for the holes produced with the precession laser machining method.

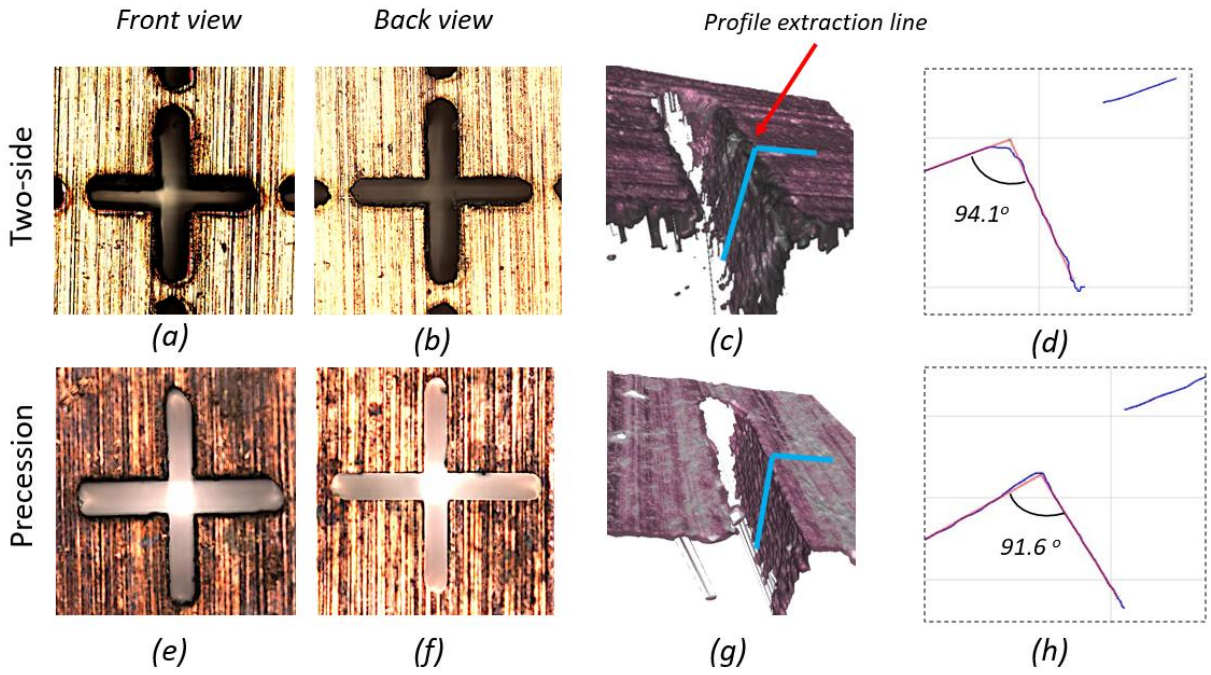

Figure 5.8. *The cross-shaped holes of the single-pole filter fabricated by the two methods. The first row depicts a hole produced with the two-side method while the second one with the precession method, in particular: (a) and (e) the front views; (b) and (f) the back views; the reconstructed sidewalls in (c) and (g), and extracted profiles in (d) and (h).*

The taper angle reduction is much more pronounced on the cross-shaped holes of the two-pole filters because the thickness of the copper substrates are more than twice higher than those used in the single pole ones. Fig. 5.9a and 5.9b depict clearly the sidewalls in the front and back views and the high taper angle and the narrowing effect in the middle of the through holes produced with the two-side method. In addition, the extracted profile in Fig. 5.9d shows that the taper angle increases with the increase of the depth. This results in large dimensional deviations of the hole's length and width and also a large geometrical deviation from the nominal vertical sidewalls.

In contrast, there are no apparent tapering effect on the sidewalls of the entrance and exit (Fig. 5.9e and 5.9f) of the hole machined with the precession method. This is similar to what was achieved for the holes of the single-pole filters. In fact, the taper angle decreased more than 6 times for the THz mesh filter fabricated with the precession laser beam. Furthermore, the precession method produced holes with straight walls and a consistent taper angle throughout their full depth. These is a clear evidence of the attained efficient material removal with the multiple cuts and the layer-based machining strategy. This is also evident from the uniform ablation that was maintained with the increase of the hole depth.

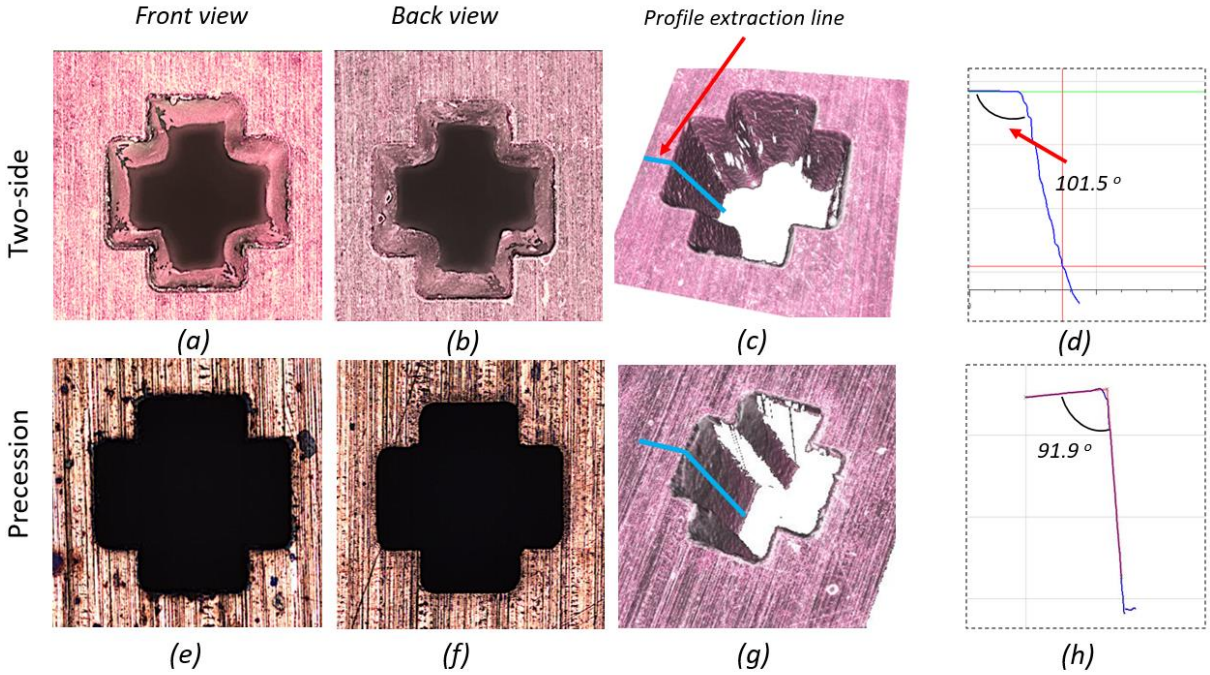

Figure 5.9. *The cross-shaped holes of the two-pole filter fabricated with the two methods. The first row depicts a hole produced with the two-side method while the second one with the precession method, in particular: (a) and (e) the front views; (b) and (f) the back views; the reconstructed sidewalls in (c) and (g), and extracted profiles in (d) and (h).*

Fig. 5.10 shows the cross-shaped hole's morphology obtained with by two-side method. The narrowing of the hole at the middle is an inherent issue associated with the two-side method. This is the result of the tapering effect that is common for any structure machined with a normal incident beam. This effect can be almost fully eliminated when the structurers are machined with a precession beam which leads to a significant increase of their accuracy, both dimensional and geometrical. It is worth

stating that the taper angle could even be eliminated through a further optimisation of the precession machining process.

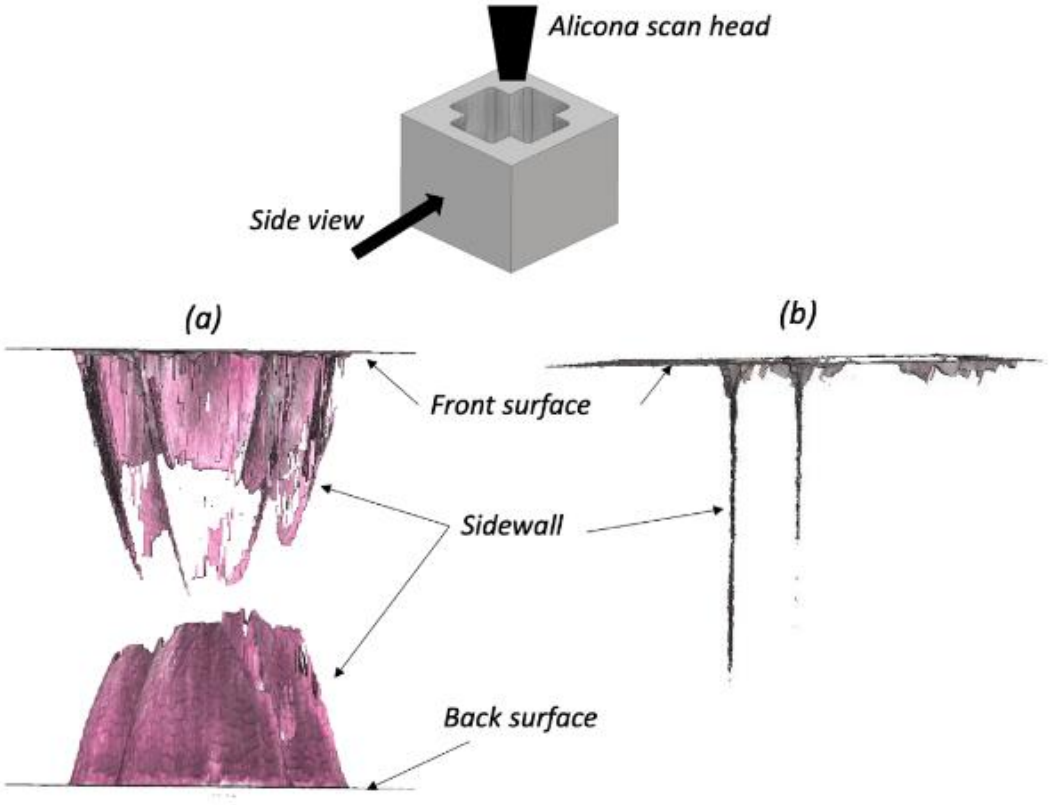

Figure 5.10. *A comparison of hole's morphologies obtained with the two laser machining methods: (a) the narrowing effect in the two-side method; and (b) the straight vertical cuts along the hole profile produced with the precession method that define the sidewalls.*

5.3.1.2. Dimensions in XY plane

Table 5.4 and Table 5.5 provide the dimensional measurements in both X and Y directions that includes the hole's length, width and periodicity of all samples. It can be seen in Table 5.4 that length and width of the S1 holes are generally bigger than those

of S2 in X and Y, and also on both sides of the single-pole filter. The average deviations from the nominal dimensions on the front side were from 29 µm to 52 µm for S1 and from -1 µm to 31 µm for S2. In the case of S1, there was a slight increase of the size of the cross-shaped holes due to the relatively high aspect ratio of almost 1:5. In general, the deviations are more pronounced on the front side in comparison with the dimensional measurements obtained on the back side of the single-pole filters produced with both methods.

The results obtained on S3 and S4 were different, and they are provided in Table 5.5. The deviations from the nominals were higher for the two-pole filter fabricated with the precession method compared to those on the S3 filter produced with the two-side one. In particular, the average deviation from the nominal values were in the range from 84 µm to 101 µm on the entrance side and from 45 µm to 48 µm on the exit side of S4. While on S3 fabricated with the two-side method, the deviations were smaller on both sides, especially from -10 µm to 23 µm and -10 µm to 24 µm on the front and the back sides, respectively. However, the better accuracy in XY plane achieved with the two-side method did not lead to a smaller taper angle (as discussed in Section 4.1.1) or more importantly to a better filter's performance. This will be discussed in Section 3.2. In general, the variation of S2 and S4 dimensions were smaller on the exit side in comparison with the values obtained on the entrance side of the filters produced with the precession method.

The sources of errors in the two-side method were discussed in details in another research [38]. The deviation between measurements and the nominals of the filters fabricated with the precession method can be attributed to several reasons. First, the ellipticity of the laser beam played a role and has led to deviations of the dimensions in X and Y plane. In fact, the maximum difference between the biggest and smallest diameter of the laser beam was 10 µm during the machining process. This difference can be reduced by calibrating the laser beam and/or compensating this error by making adjustments in the machining strategy in X and Y directions. The second reason is the larger divergence of the focused precession beam than that of the “conventional” laser beam. Therefore, the precession beam is more sensitive to variations of the focal distance, e.g. due to any flatness deviations of the substrates used to produce the filters. The negative effects associated with this error source can be minimised by improving the quality of as-received workpieces and by employing appropriate holding devices during the machining process. The third reason is non-optimized machining strategy and processing parameters that were used to produce the filters with the precession method. In particular, the negative effects of multiple cuts and passes on dimensional accuracy in the layer-based machining strategy can be minimised by optimising the process and by introducing compensations to the X and Y dimensions. In addition, the errors associated with the used telecentric lens to focus the precession laser beam should be investigated and taken into account in optimizing the process.

Finally, the repeatability of beam deflectors and the uncertainty associated with the measurements also contributed to the obtained deviations from the nominals.

The periodicity deviations from the nominal values of S1 and S2 are in the range from 0.7 to 1.3 μm and they were less than those on S3 and S4 (from 1.3 to 1.7 μm). This can be explained with the smaller number of cross-shaped holes and thus the machining fields of S1 and S2 are smaller and less prepositional movements with the mechanical stages are required. Consequently, the accumulated errors as a result of these repositioning movements are smaller. At the same time, the better periodicity obtained with the precession method can be explained with the machining of the filters from one side only and thus avoiding the alignment error in the two-side method. It should also be noted that the cleaner and better-defined edges obtained with the precession method have reduced the uncertainty in the conducted dimensional measurements.

Table 5.4. Dimensional measurements of the single-pole THz mesh filters (S1 and S2) produced with the two machining methods.

Dimensional measurements		Nominal dimensions [μm]	Average Value [μm]		Average deviations from nominals and standard deviation of measurements [μm]	
			S1	S2	S1	S2
Technique			Two-side	Precession	Two-side	Precession
Front side	Length X	525	554	539	29 ± 4.4	14 ± 2.2
	Length Y	525	577	556	52 ± 3.3	31 ± 3.7
	Width X	62.5	108	62	45 ± 2.9	-1 ± 3.0
	Width Y	62.5	111	77	49 ± 5.7	14 ± 6.2
Back side	Length X	525	557	520	32 ± 3.8	-5 ± 2.2
	Length Y	525	561	523	36 ± 2.2	-2 ± 3.3
	Width X	62.5	93	56	31 ± 3.7	-7 ± 1.4
	Width Y	62.5	81	64	19 ± 1.8	1 ± 3.8
	Periodicity X	625	625	625	1.3 ± 1.7	0.7 ± 0.8
	Periodicity Y	625	626	626	1.2 ± 1.3	1.2 ± 1.0

Table 5.5. Dimensional measurements of the two-pole THz mesh filters (S3 and S4) produced with the two machining methods.

Dimension measurements		Nominal dimensions [μm]	Average Value [μm]		Average deviations from nominals and standard deviation of measurements [μm]	
			S3	S4	S3	S4
Technique			Two-side	Precession	Two-side	Precession
Front side	Length X	562	585	647	23 ± 3.1	85 ± 8.6
	Length Y	562	552	662	-10 ± 4.4	100 ± 4.7
	Width X	308	329	392	21 ± 2.3	84 ± 9.6
	Width Y	308	298	409	-10 ± 4.7	101 ± 3.6
Back side	Length X	562	586	607	24 ± 2.6	45 ± 6.3
	Length Y	562	552	610	-10 ± 3.5	48 ± 6.1
	Width X	308	330	353	22 ± 2.0	45 ± 6.6
	Width Y	308	296	355	-12 ± 4.0	47 ± 4.9
	Periodicity X	950	951	951	1.5 ± 1.9	1.5 ± 1.8
	Periodicity Y	950	950	951	1.7 ± 2.2	1.3 ± 1.5

Note: The positive values and negative values denote that the measured dimensions are larger or smaller than the nominal values, respectively.

5.3.2. Performance of THz mesh filters

The ultimate assessment and comparison of THz mesh filters produced with the two-side and the precession methods can be obtained by analyzing their functional performance, i.e. the S-parameters obtained with the free space Quasi-Optic system. In particular, measurement results obtained at two orientations of S2, S3 and S4 were analysed. Firstly, the filters were measured at their original orientation. Then, the filters were rotated by 90 degree to repeat the measurements. The filter's performance was analysed and recorded, again.

Fig. 5.11 shows the measurement results of single-pole filters fabricated with the two different machining methods. It can be seen in Fig. 5.11a that the S1 filter fabricated with the two-side method provide a single pole (S11 parameter) but the peak of the resonance frequency was shifted to the right of the simulation ones. Fig. 5.11b depicts a closer look at the S21 parameter that assesses the insertion loss of the filter, in particular the minimum loss of the S1 filter was 3.9 dB. The high-than-expected insertion loss can be attributed to the low dimensional accuracy achieved by the two-side method, especially, the narrowing effects in the middle of the S1 cross-shaped holes. In contrast, the performance of the S2 filter was much better, especially the single pole frequency (S11) was sharply defined as shown in Fig. 5.11c. The resonance frequency was slightly shifted to the lower frequencies in comparison to the simulation results. The offset was around 3 GHz that was equivalent to 1% error. The

closer look at the S21 parameter in Fig. 5.11d shows a minimum insertion loss of 0.8 dB when the filter was measured at its original reference orientation. The bandwidth was also closer to the S2 simulation results.

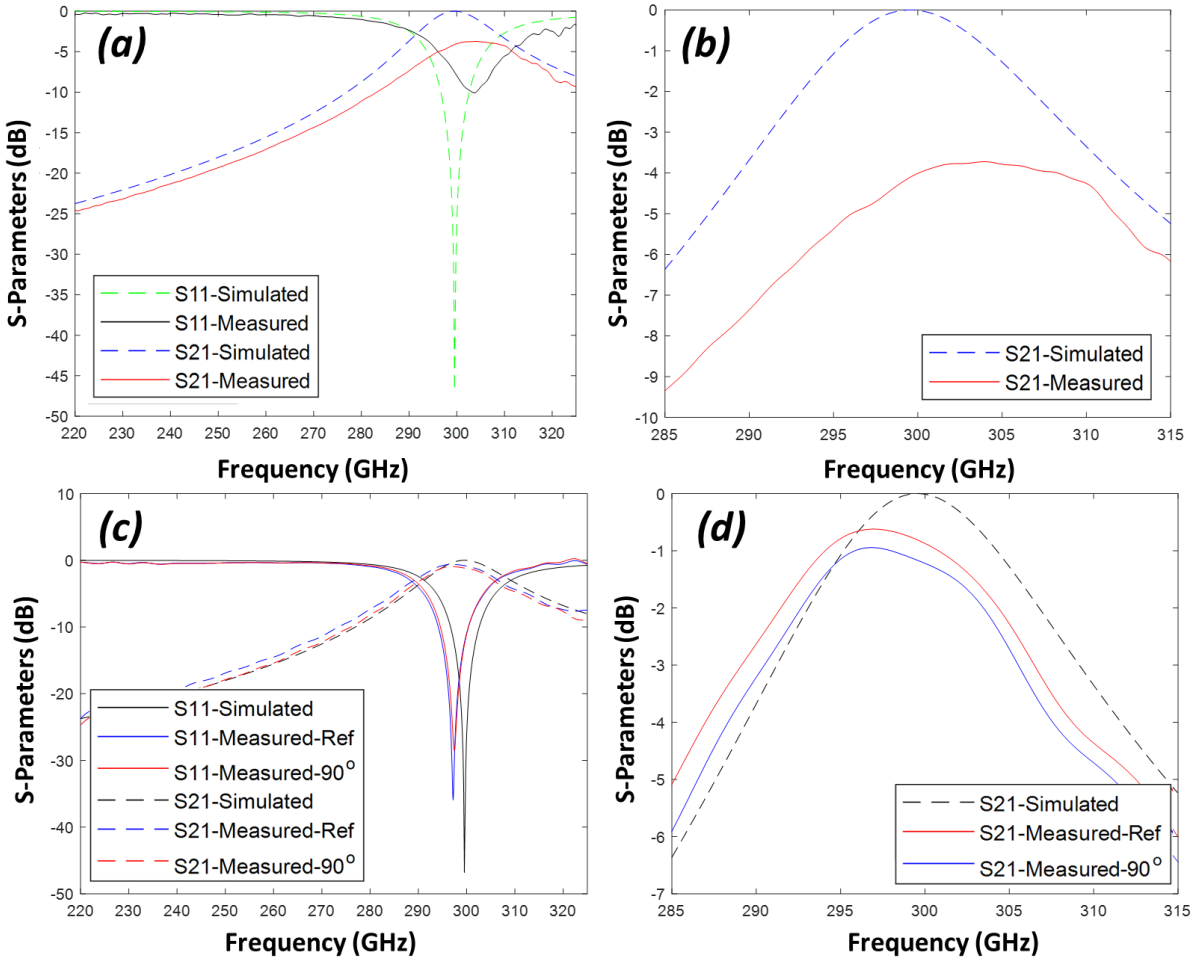

Figure 5.11. *The performance characteristics of* ***single-pole*** *filters: (a) S11 and S21 parameters of the S1 filter; (b) the closer look at the S21 parameter of the S1 filter; (c) the S11 and S21 parameters of the S2 filter; (d) a closer look at the S21 parameter of the S2 filter.*

The performance of the two-pole filters is depicted in Fig. 5.12. Again, the performance of the filter fabricated with the two-side method (S3) was not satisfactory due to the large deviations from the nominal dimensions. The S11 measurements did not show two well defined poles and there was a significant shift of 10 GHz to the higher frequency as shown in Fig. 5.12a. The minimum insertion loss was 4.6 dB and the bandwidth was much smaller than the simulation results (Fig. 5.12b). On the other hand, the S11 and S21 characteristics of the S4 filter were in good agreement with the simulation results as depicted in Fig. 5.12c. The two poles of the 2nd-order filter can be clearly seen and one of the poles coincides exactly with the simulated frequency of 300 GHz. The S21 measurements showed a minimum loss of 0.8 dB for both S4 orientations (Fig. 5.12d). In addition, the S4 bandwidth was very close to the simulation results but was slightly shifted to the lower frequencies.

It can be clearly seen that the S2 and S4 filters provided similar results with their two different orientation that indicates a consistent performance. The shifting of frequency (S11) can be attributed to the difference between designed and actual thickness of the filter [12]. Other factors discussed in Section 3.1.2 can affect the performance of the THz mesh filters, too, such as the flatness of the substrates, some oxidation of copper as a result of the laser-material interactions in not controlled environment which will be discussed next.

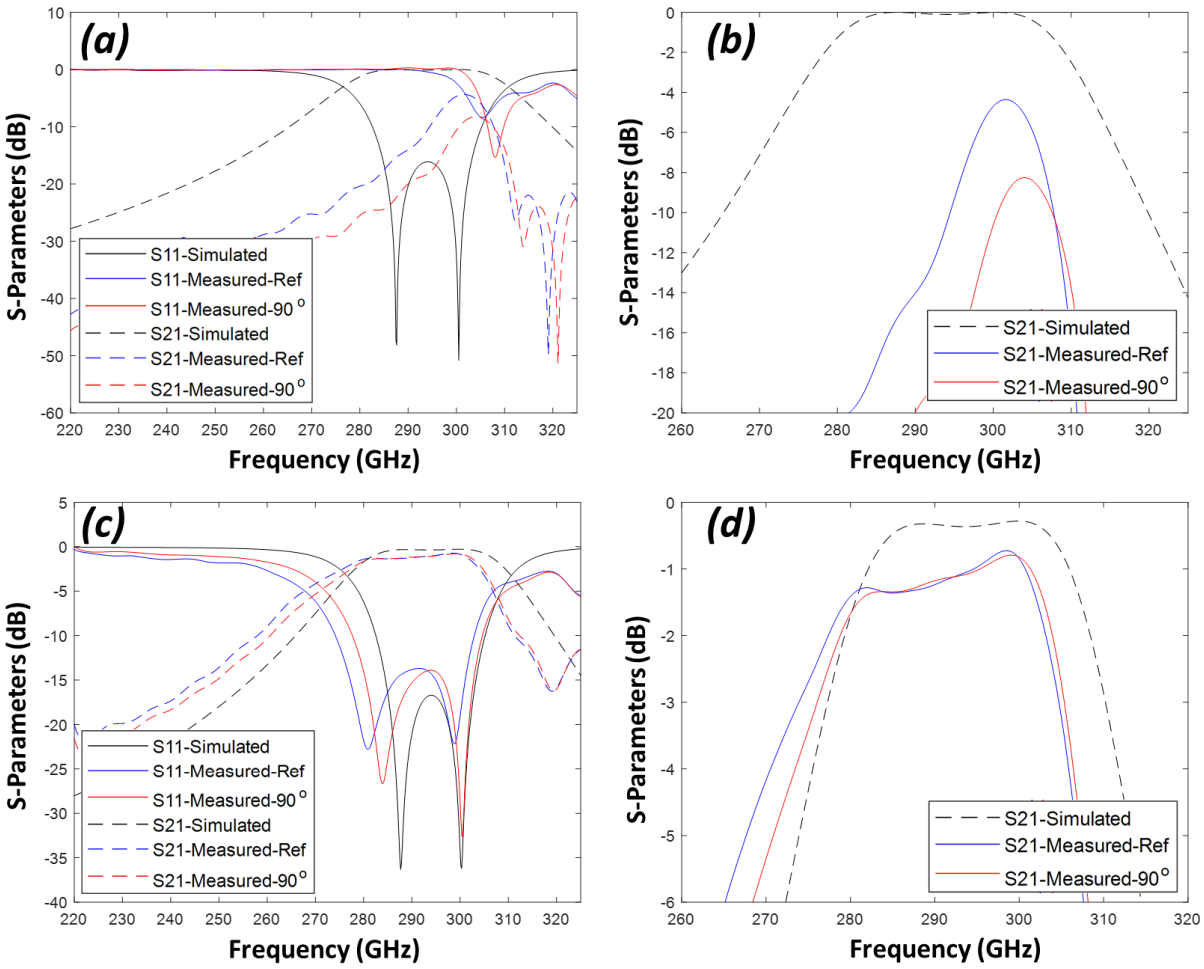

Figure 5.12. The performance characteristics of **two-pole** filters: (a) S11 and S21 parameters of the S3 filter; (b) the closer look at the S21 parameter of the S3 filter; (c) the S11 and S21 parameters of the S4 filter; (d) a closer look at the S21 parameter of the S4 filter.

5.3.3. Oxidation and XPS analysis

An investigation of potential side-effects due to the laser machining process of copper substrates in not controlled environment was conducted as this may have negative effects on filters' performance. An XPS analysis of the front side surface (unprocessed

area) and the sidewall surface (processed area) of the cross-shaped holes machined with the precession method was conducted to look for potential changes in surface chemistry, especially copper oxidation. The XPS spectra in Fig. 5.13 and extracted atomic concentration in Table 6 show the presence of Cu 2p which signify the formation of copper oxides at both front side and sidewall surface [46]. The high-resolution normalized XPS spectra of Cu 2p (3/2 and 1/2) are depicted in Fig. 5.13c. The contribution of copper (I) oxide (Cu_2O) was more pronounced on the unprocessed area (the front side surface) with a peak position at around 933 eV, which indicates the formation of a native oxide layer onto the surface due to its exposure to ambient air. On the other hand, the processed area (the sidewall surface) had significant contributions of both copper (I) oxide (Cu_2O) and copper (II) oxide (CuO) components, which can be validated with the satellite features at 943 eV and the broader peak shape. This is in good agreement with the indirect ratio of oxygen/copper, which can be used to judge about the surface's oxidation level [47].

Table 5.6. The composition of a copper substrate after precession laser machining

Analysed area	*Atomic concentration of found elements (%)*				
	Cu 2p (3/2)	***O 1s***	***C 1s***	***Ca 2p***	***Si 2p***
Front side	*1.79*	*12.30*	*81.51*	*0.62*	*3.78*
Sidewall	*1.28*	*11.53*	*83.39*	*1.50*	*2.30*

In particular, this ratio increased from 6.87 to 9.01 (calculated from Table 5.6) when the material was subjected to laser machining. Therefore, it can be concluded that the

heat accumulation during laser precession processing of copper led to some material oxidation and this is in spite of the use of ultrashort pulses. The formation of copper oxide is undesirable and can affect the THz filter's performance because this is a non-conductive compound. Thus, the copper oxidation could contribute to the higher-than-expected insertion loss of THz filters produced by the precession laser machining method. This negative side effect can be minimised and even eliminated by conducting the laser processing in control environments.

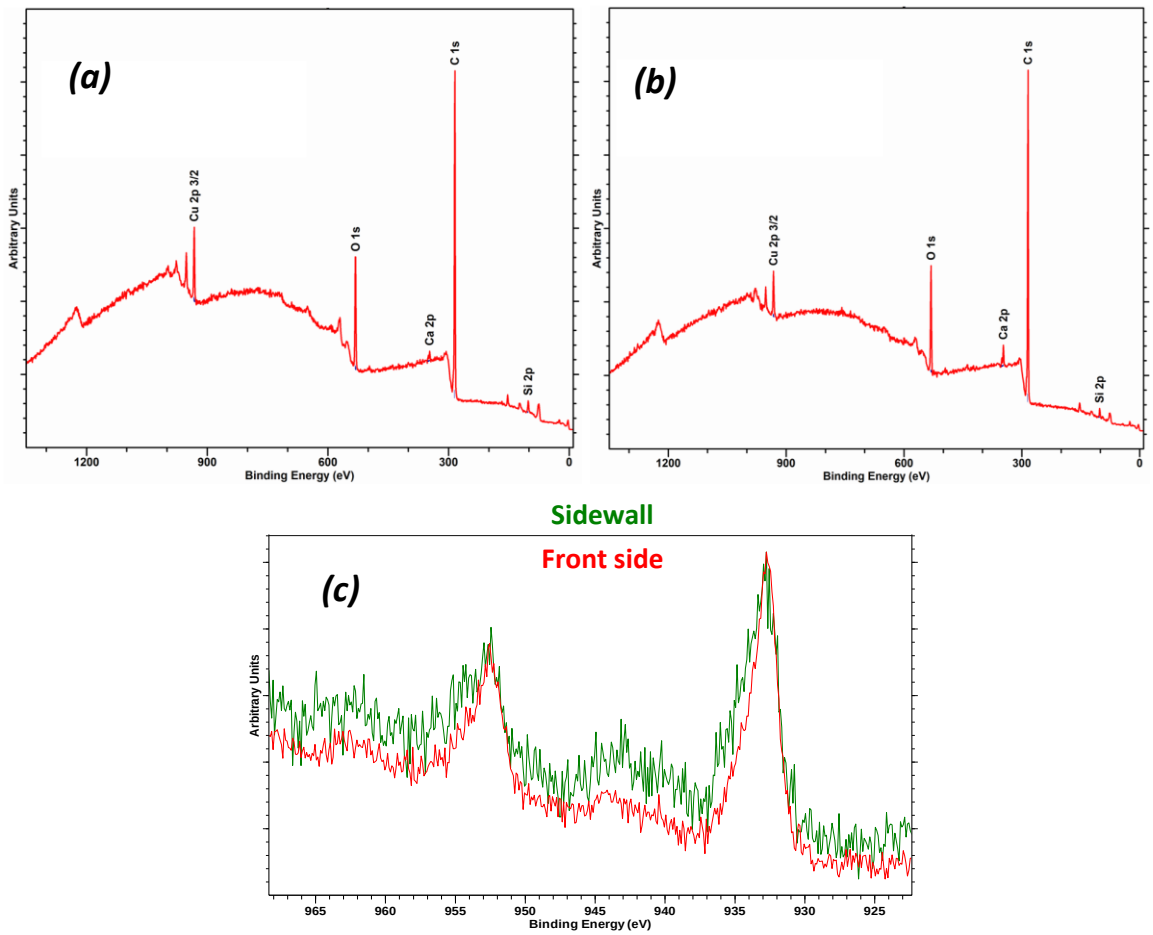

Figure 5.13. *The XPS analysis of a two-pole filter after precession machining: (a) XPS spectra of front side surface (unprocessed area); (b) XPS spectra of sidewall surface*

(processed area); (c) High-resolution normalized spectra of Cu 2p as obtained for front side surface (red) and sidewall surface (green).

The analysis also showed high concentration of carbon compared to copper and oxygen. The deposition of carbon can be partly the result of contamination during the cleaning process and partly due to absorption of organic compounds in an ambient environment [48, 49]. Traces of other elements such as calcium and silicon were also identified, which could be due to some other sources of contamination, e.g. fingerprints. However, the contribution of carbon and other elements was minor and hence should not have a significant impact on the filters' functionality.

5.4. Conclusions

This study investigates a manufacturing route for producing THz mesh filters that employed a novel laser micro-machining technology, especially by machining directly relatively thick copper substrates. The method proposed in this research is called laser precession machining and it can be considered an alternative to photoresist-based fabrication technologies. Two different designs of cross-shaped THz mesh filters with thickness of 300 µm and 670 µm were successfully fabricated by laser precession machining of copper substrates. The drawback of conventional laser micro-machining processes, i.e. the tapering effect on sidewalls, was overcome by controlling the incident/attack angle of the precession process and implementing an appropriate machining strategy. In particular, the material along the cross-shaped holes of the

filters was ablated efficiently by employing a layer-based machining strategy with multiple cuts and passes at each layer and thus to reduce the taper angle on the sidewalls. In this way, it was possible to reduce the taper angle by 3 times (from 4.1 to 1.6 degree) and 6 times (from 11.5 degree to 1.9 degree) in producing the through cross-shaped holes of single-pole and two-pole filters, respectively, compared to the reference two-side method. It is important to note that this was not achieved at the expense of the machining times, which were comparable for the two methods. However, there were some relatively large dimensional deviations of the cross-shaped holes in the XY plane for the THz filters fabricated with the precession method. These can be attributed to the ellipticity of the laser beam, the sensitivity of the precession beam to any focal distance variations and the non-optimized laser precession machining process that was utilised. This shortcoming can be minimised or even eliminated by optimizing the precession machining process and by introducing some compensations to the XY dimensions in the machining strategy.

Nevertheless, the performance of the THz mesh filters that were produced had clearly demonstrated the process potential in spite of employing a sub-optimal machining strategy. The S-parameters, i.e. S11 and S21, of the single-pole filter were very closed to the simulation results, with only 3 GHz offset that is equivalent to 1% error. The two-pole filter provided two clear reflection zeros (transmission poles) while one of them was at the designed frequency of 300 GHz. The insertion loss of the filters was 0.8 dB.

The loss in the transmission was mostly due to some deviations from the nominal dimensions of the machined cross-shaped holes and the formation of copper oxide at sidewall during the laser precession process. However, it is important to reiterate that this was a feasibility study and a thorough process optimisation can address the accuracy issues and improve the performance of THz mesh filters further.

Acknowledgement

XPS data collection was performed at the EPSRC National Facility for XPS (‘HarwellXPS’), operated by Cardiff University and UCL, under contract No. PR16195. The use of the 1.1 THz vector network analyser was funded by the EPSRC Strategic Equipment grant EP/P020615/1. Authors would like to thank Professor Michael Lancaster (University of Birmingham) for his supervision and doctor Stephen Hanham (University of Birmingham) for his help in measurements of the samples.

References

1. Siegel, P.H., *THz technology: An overview*, in *Terahertz Sensing Technology: Volume 1: Electronic Devices and Advanced Systems Technology*. 2003, World Scientific. p. 1-44.
2. Pawar, A.Y., Sonawane, D.D., Erande, K.B., and Derle, D.V., *Terahertz technology and its applications.* Drug invention today, 2013. **5**(2): p. 157-163.
3. Cherkasova, O.P., Serdyukov, D.S., Ratushnyak, A.S., Nemova, E.F., Kozlov, E.N., Shidlovskii, Y.V., Zaytsev, K.I., and Tuchin, V.V., *Effects of Terahertz Radiation on Living Cells: a Review.* Optics and Spectroscopy, 2020. **128**(6): p. 855-866.
4. Ren, A., Zahid, A., Fan, D., Yang, X., Imran, M.A., Alomainy, A., and Abbasi, Q.H., *State-of-the-art in terahertz sensing for food and water security–A comprehensive review.* Trends in Food Science & Technology, 2019. **85**: p. 241-251.
5. Nagashima, T., Tani, M., and Hangyo, M., *Polarization-sensitive THz-TDS and its application to anisotropy sensing.* Journal of Infrared, Millimeter, and Terahertz Waves, 2013. **34**(11): p. 740-775.
6. Wang, K., Sun, D.-W., and Pu, H., *Emerging non-destructive terahertz spectroscopic imaging technique: Principle and applications in the agri-food industry.* Trends in Food Science & Technology, 2017. **67**: p. 93-105.
7. Guerboukha, H., Nallappan, K., and Skorobogatiy, M., *Toward real-time terahertz imaging.* Advances in Optics and Photonics, 2018. **10**(4): p. 843-938.
8. Lindley-Hatcher, H., Stantchev, R.I., Chen, X., Hernandez-Serrano, A.I., Hardwicke, J., and Pickwell-MacPherson, E., *Real time THz imaging—opportunities and challenges for skin cancer detection.* Applied Physics Letters, 2021. **118**(23).
9. Zaytsev, K.I., Dolganova, I.N., Chernomyrdin, N.V., Katyba, G.M., Gavdush, A.A., Cherkasova, O.P., Komandin, G.A., Shchedrina, M.A., Khodan, A.N., Ponomarev, D.S., Reshetov, I.V., Karasik, V.E., Skorobogatiy, M., Kurlov, V.N., and Tuchin, V.V., *The progress and perspectives of terahertz technology for diagnosis of neoplasms: a review.* Journal of Optics, 2020. **22**(1).
10. Wang, Y., Yang, B., Tian, Y., Donnan, R.S., and Lancaster, M.J., *Micromachined thick mesh filters for millimeter-wave and terahertz applications.* IEEE Transactions on Terahertz Science and Technology, 2014. **4**(2): p. 247-253.
11. Gavdush, A.A., Chernomyrdin, N.V., Lavrukhin, D.V., Cao, Y., Komandin, G.A., Spektor, I.E., Perov, A.N., Dolganova, I.N., Katyba, G.M., Kurlov, V.N., Ponomarev, D.S., Skorobogatiy, M., Reshetov, I.V., and Zaytsev, K.I., *Proof of concept for continuously-tunable terahertz bandpass filter based on a gradient metal-hole array.* Opt Express, 2020. **28**(18): p. 26228-26238.

12. Melo, A.M., Gobbi, A.L., Piazzetta, M.H., and Da Silva, A.M., *Cross-shaped terahertz metal mesh filters: Historical review and results.* Advances in Optical Technologies, 2012. **2012**.
13. Demirhan, Y., Alaboz, H., Ozyuzer, L., Nebioğlu, M.A., Takan, T., Altan, H., and Sabah, C., *Metal mesh filters based on Ti, ITO and Cu thin films for terahertz waves.* Optical and Quantum Electronics, 2016. **48**(2): p. 170.
14. Porterfield, D.W., Hesler, J., Densing, R., Mueller, E., Crowe, T., and Weikle, R., *Resonant metal-mesh bandpass filters for the far infrared.* Applied Optics, 1994. **33**(25): p. 6046-6052.
15. Ferraro, A., Zografopoulos, D.C., Caputo, R., and Beccherelli, R., *Broad-and narrow-line terahertz filtering in frequency-selective surfaces patterned on thin low-loss polymer substrates.* IEEE Journal of selected topics in quantum electronics, 2017. **23**(4): p. 1-8.
16. Wang, Q., Gao, B., Raglione, M., Wang, H., Li, B., Toor, F., Arnold, M.A., and Ding, H., *Design, fabrication, and modulation of THz bandpass metamaterials.* Laser & Photonics Reviews, 2019. **13**(11): p. 1900071.
17. Yang, H., Dhayalan, Y., Shang, X., Lancaster, M.J., Liu, B., Wang, H., Henry, M., and Huggard, P.G., *WR-3 waveguide bandpass filters fabricated using high precision CNC machining and SU-8 photoresist technology.* IEEE Transactions on Terahertz Science and Technology, 2018. **8**(1): p. 100-107.
18. Ao, T., Xu, X., Gu, Y., Chen, Z., Jiang, Y., Li, X., Lian, Y., Wang, F., He, Q., and Chen, Z., *Terahertz band-pass filters based on fishnet metamaterials fabricated on free-standing SiNx membrane.* Optics Communications, 2017. **405**: p. 22-28.
19. Chung, S. and Park, S., *Effects of temperature on mechanical properties of SU-8 photoresist material.* Journal of Mechanical Science and Technology, 2013. **27**(9): p. 2701-2707.
20. Puscasu, I., Boreman, G., Tiberio, R., Spencer, D., and Krchnavek, R., *Comparison of infrared frequency selective surfaces fabricated by direct-write electron-beam and bilayer nanoimprint lithographies.* Journal of Vacuum Science & Technology B: Microelectronics and Nanometer Structures Processing, Measurement, and Phenomena, 2000. **18**(6): p. 3578-3581.
21. Dickie, R., Cahill, R., Fusco, V., Gamble, H.S., and Mitchell, N., *THz Frequency Selective Surface Filters for Earth Observation Remote Sensing Instruments.* IEEE Transactions on Terahertz Science and Technology, 2011. **1**(2): p. 450-461.
22. Sushko, O., Pigeon, M., Donnan, R.S., Kreouzis, T., Parini, C.G., and Dubrovka, R., *Comparative Study of Sub-THz FSS Filters Fabricated by Inkjet Printing, Microprecision Material Printing, and Photolithography.* IEEE Transactions on Terahertz Science and Technology, 2017. **7**(2): p. 184-190.

23. Piqué, A., Auyeung, R.C., Kim, H., Charipar, N.A., and Mathews, S.A., *Laser 3D micro-manufacturing.* Journal of Physics D: Applied Physics, 2016. **49**(22): p. 223001.
24. Voisiat, B., Indrišiūnas, S., Šniaukas, R., Minkevičius, L., Kašalynas, I., and Račiukaitis, G. *Laser processing for precise fabrication of the THz optics*. in *Laser Applications in Microelectronic and Optoelectronic Manufacturing (LAMOM) XXII*. 2017. International Society for Optics and Photonics.
25. Voisiat, B., Bičiūnas, A., Kašalynas, I., and Račiukaitis, G., *Band-pass filters for THz spectral range fabricated by laser ablation.* Applied Physics A, 2011. **104**(3): p. 953-958.
26. Shang, X., Penchev, P., Guo, C., Lancaster, M.J., Dimov, S., Dong, Y., Favre, M., Billod, M., and De Rijk, E., *W-Band Waveguide Filters Fabricated by Laser Micromachining and 3-D Printing.* IEEE Transactions on Microwave Theory and Techniques, 2016. **64**(8): p. 2572-2580.
27. Manikandan, E., Sreeja, B.S., Radha, S., Duraiselvam, M., Gupta, A., and Prabhu, S. *Microfabrication of terahertz frequency-selective surface by short- and ultrashort laser ablation*. 2018. SPIE.
28. Born, N., Gente, R., Al-Naib, I., and Koch, M., *Laser beam machined free-standing terahertz metamaterials.* Electronics Letters, 2015. **51**(13): p. 1012-1014.
29. Penchev, P., Shang, X., Dimov, S., and Lancaster, M., *Novel manufacturing route for scale up production of terahertz technology devices.* Journal of Micro and Nano-Manufacturing, 2016. **4**(2): p. 021002.
30. Bhaduri, D., Penchev, P., Dimov, S., and Soo, S.L., *An investigation of accuracy, repeatability and reproducibility of laser micromachining systems.* Measurement, 2016. **88**: p. 248-261.
31. Le, H., Penchev, P., Henrottin, A., Bruneel, D., Nasrollahi, V., Ramos-de-Campos, J.A., and Dimov, S., *Effects of Top-hat Laser Beam Processing and Scanning Strategies in Laser Micro-Structuring.* Micromachines, 2020. **11**(2): p. 221.
32. Fornaroli, C., Holtkamp, J., and Gillner, A., *Laser-Beam Helical Drilling of High Quality Micro Holes.* Physics Procedia, 2013. **41**: p. 661-669.
33. Esakkimuthu, M., Suseela, S.B., Sankararajan, R., Gupta, A., Rana, G., and Prabhu, S., *Laser patterning of thin film copper and ITO on flexible substrates for terahertz antenna applications.* Journal of Laser Micro Nanoengineering, 2017. **12**(3): p. 313-321.
34. Lin, Y., Yao, H., Ju, X., Chen, Y., Zhong, S., and Wang, X., *Free-standing double-layer terahertz band-pass filters fabricated by femtosecond laser micro-machining.* Optics Express, 2017. **25**(21): p. 25125-25134.

35. Faisal, N., Zindani, D., Kumar, K., and Bhowmik, S., *Laser micromachining of engineering materials—a review.* Micro and Nano Machining of Engineering Materials, 2019: p. 121-136.
36. Penchev, P., Dimov, S., Bhaduri, D., and Soo, S.L., *Generic integration tools for reconfigurable laser micromachining systems.* Journal of Manufacturing Systems, 2016. **38**: p. 27-45.
37. Martin, P.E., Estival, S., Dijoux, M., de Campos, J.A.R., Kupisiewicz, A., and Braunschweig, R. *High-power femtosecond laser cutting and drilling combining beam-shaping and beam-splitting*. in *Laser Beam Shaping XVIII*. 2018. International Society for Optics and Photonics.
38. Nasrollahi, V., Penchev, P., Dimov, S., Korner, L., Leach, R., and Kim, K., *Two-Side Laser Processing Method for Producing High Aspect Ratio Microholes.* Journal of Micro and Nano-Manufacturing, 2017. **5**(4): p. 041006.
39. Petkov, P., Dimov, S., Minev, R., and Pham, D.T., *Laser milling: pulse duration effects on surface integrity.* Proceedings of the Institution of Mechanical Engineers, Part B: Journal of Engineering Manufacture, 2008. **222**(1): p. 35-45.
40. Nolte, S., Momma, C., Kamlage, G., Ostendorf, A., Fallnich, C., von Alvensleben, F., and Welling, H., *Polarization effects in ultrashort-pulse laser drilling.* Applied Physics A, 1999. **68**(5): p. 563-567.
41. Estival, S., Martin, P.-e., and Kupisiewicz, A., *Machining device*. 2019, US Patents.
42. Ridler, N., Clarke, R., Salter, M., and Wilson, A. *Traceability to national standards for S-parameter measurements in waveguide at frequencies from 140 GHz to 220 GHz*. in *2010 76th ARFTG Microwave Measurement Conference*. 2010. IEEE.
43. Horibe, M. and Kishikawa, R., *Metrological traceability in waveguide S-parameter measurements at 1.0 THz band.* IEEE Transactions on Instrumentation and Measurement, 2013. **62**(6): p. 1814-1820.
44. Jayawardene, M. and Vardaxoglou, Y., *3-D EM Simulation of Infinite Periodic Arrays and Finite Frequency Selective Horns.*
45. Hammerstad, E. and Jensen, O. *Accurate models for microstrip computer-aided design*. in *1980 IEEE MTT-S International Microwave Symposium Digest*. 1980. IEEE.
46. Long, J., Zhong, M., Fan, P., Gong, D., and Zhang, H., *Wettability conversion of ultrafast laser structured copper surface.* Journal of Laser Applications, 2015. **27**(S2): p. S29107.
47. Giannuzzi, G., Gaudiuso, C., Di Mundo, R., Mirenghi, L., Fraggelakis, F., Kling, R., Lugarà, P.M., and Ancona, A., *Short and long term surface chemistry and wetting behaviour of stainless steel with 1D and 2D periodic structures induced by bursts of femtosecond laser pulses.* Applied Surface Science, 2019. **494**: p. 1055-1065.

48. Yang, Z., Tian, Y., Zhao, Y., and Yang, C., *Study on the Fabrication of Super-Hydrophobic Surface on Inconel Alloy via Nanosecond Laser Ablation.* Materials (Basel), 2019. **12**(2).
49. Gaddam, A., Sharma, H., Karkantonis, T., and Dimov, S., *Anti-icing properties of femtosecond laser-induced nano and multiscale topographies.* Applied Surface Science, 2021. **552**.

CHAPTER 6

INVESTIGATION OF PRECESSION LASER MACHINING OF MICRO-HOLES ON AEROSPACE MATERIAL

Hoang Le [1], Vahid Nasrollahi [1], Themistoklis Karkantonis [1],

Pavel Penchev [1], Sundar Marimuthu [2] and Stefan Dimov [1]

[1] Department of Mechanical Engineering, University of Birmingham, Birmingham B15 2TT, UK

[2] The Manufacturing Technology Centre Ltd, Coventry, CV7 9JU, UK

This research was published as a full-length article at ***Journal of Laser Applications***.

Le, H., Nasrollahi, V., Karkantonis, T., Penchev, P., Marimuthu, S., Crozier, M. and Dimov, S. (2023). Investigation of precession laser machining of microholes in aerospace material. Journal of Laser Applications 35, 012028 https://doi.org/10.2351/7.0000903

Author Contributions	
Hoang Le **(First Author)**	Conceptualization, Methodology, Experiment, Formal analysis, Investigation, Validation, Writing–original draft, Writing–review & editing,
V. Nasrollahi	Methodology, Validation
T. Karkantonis	Writing–review & editing
P. Penchev	Writing–review & editing
S. Marimuthu	Investigation, Writing–review & editing
S. Dimov	Conceptualization, Project administration, Writing–review & editing

Abstract

Sidewall tapering is one of the main limitations in ultrashort pulse (USP) laser machining and is associated with the beam shape and self-limiting effect. Laser processing with a precession beam is a potential solution to overcome this limitation. A study into the effects of precession parameters on the taper angle in micro-hole drilling of Nickel alloy is reported in this paper. The effects of three key precession parameters, i.e. incident angle, relative distance between the focuses of the precession and individual beams and scanning speed have been investigated in detail. Experiments were performed to drill through holes with aspect ratios up to 20:1 and diameters ranging from 100 µm to 500 µm over 0.6 mm to 2 mm thick Nickel alloy substrates. Experiment results showed that all the considered parameters/factors were significant and affected the hole tapering in different ways. In addition, there were important interaction effects between two of the factors, i.e. incident angle and focus position, in some cases. The optimal parameters to minimise tapering effect are suggested and the mechanism is discussed in detail. The precession laser machining showed clear advantages in overcoming the limitations to associated with the conventional USP laser machining. Fabricating micro-holes with high geometrical accuracy, i.e. with straight side walls and zero taper angles, is feasible with the use of precession beam. The results clearly show the potential of precession laser processing and the capabilities that the technology can offer for a range of laser micro-machining

applications in different industries, such as microelectronics, automotive and aerospace.

Keywords: Precession, Ultrashort Pulse Laser, Micro-hole, Optimization, Nickel Alloys.

6.1. Introduction

The use of laser micro-machining technology for hole drilling has widely been known in manufacturing industry, especially, when quality and accuracy are the main requirements [1]. Typical applications of laser micro-drilling can be found in numerous fields such as microfluidic, biomedical, and microelectronic devices or automotive and aerospace components [2-5]. Generally, key technical requirements in laser micro-drilling are the hole's aspect ratio, geometrical and dimensional accuracy and the overall process efficiency. Also, the quality of laser drilled micro-holes can be impacted by the heat affected zone and redepositions of material that typically appear at entrance of the holes [6]. At the same time, the process efficiency is mainly assessed either by the material removal rate or machining time. Due to constant advancements in laser technology and beam delivery sub-systems, different approaches/methods have been developed and deployed to improve the laser micro-drilling process. Especially, there are two main approaches to improve the laser micro-machining process, i.e. through changes of laser beam properties (e.g. energy, shape and pulse duration) or relative movements between laser beam and workpiece. In case of pulsed

lasers, micro-drilling can be performed with various pulse durations, from ultrashort to short or long pulse widths. Short and long laser pulses with widths from sub-nanosecond to millisecond, usually used for achieving high removal rates at the expense of machining quality [7, 8], like thermal damage. On the contrary, USP lasers are preferred when high quality holes are required because the ablation mechanism is almost athermal and the heat affected zone would be minimal [9, 10]. Changing the beam spatial profile through beam shaping is also a potential solution for minimising any negative tapering effects in micro holes that are laser drilled [11]. Apart from the Gaussian beam profile that is widely used, a top-hat (or flat-top) beam is used for improving the processing quality and efficiency, i.e. for reducing the taper angles and increasing material removal rates [12]. In addition, it should be noted that the beam polarisation, pulse repetition rates and fluence levels are also process variables that affect the laser micro-drilling operations [13].

The second approach widely used to improve the micro drilling process is through the introduction of a beam motion and thus to achieve more efficient and precise ablation. Especially, relative movements between beam and workpiece are employed in laser micro-drilling that are usually implemented through scanning strategies and by varying the incident/attacking angle of the laser beam. Typical scanning strategies used for laser micro-drilling operations are single pulse drilling, hatching, percussion, helical drilling and trepanning [6, 14-16]. Single pulse drilling and percussion drilling are

generally employed when a hole diameter equal to the beam spot size is required, whereas the other strategies are applied for hole diameters larger than the beam spot size. The helical drilling and trepanning strategies are used to distribute laser energy evenly along the hole contour and thus to ablate material only in those areas rather than to ablate all material within the holes as it is the case in hatching ones. As a result, these drilling strategies can reduce the taper angle with the increase of the hole depth and can minimise the machining time. Despite the different scanning strategies were studied and applied on USP laser micro-machining, these solution still cannot eliminate completely the tapering effect in laser micro-drilling or micro-milling and thus to enable the manufacture of vertical wall due to the inherent properties of Gaussian laser beams [17, 18].

The tapering effect is mostly attributed to the increase in the size of laser-material interaction zone, at the side wall, and the self-limiting effect leading to drop of fluence levels and low ablation efficiency, consequently [19, 20]. Therefore, a rational solution to overcome this issue is to increase the ablation efficiency, i.e. the laser fluence, at the side walls of micro-holes. However, to achieve this, the laser beam should not be normal to the substrate surface anymore and instead should be approaching at a given incident angle, for example the beam can perform relative precession movements in regard to the workpiece [21]. Such precession movements can be performed by either the workpiece or the beam. The latter is preferable because it can offer a higher

flexibility and can be executed more efficiently. Currently, there are commercial laser systems on the market that offer such capabilities, i.e. beam precession movements for improving micro-drilling and cutting processes [22-26]. There are some common key parameters in such precession processing systems, such as incident angle, linear and rotary speed of the precession beam together with its focusing position. However, the role and significance of these parameters and their interactions in precession micro-drilling have not been investigated systematically and thus there is a significant knowledge gap in this topic.

Therefore, this study investigates the underlying mechanism of the precession laser processing with the objective to understand the laser micro-drilling process in more details. The influence of key precession parameters are investigated systematically and their effects on laser micro-drilling process are analysed. A popular aerospace alloy, i.e. nickel-based super alloy C263, has been selected to carry out this empirical research and thus the results are of a specific interest to aerospace applications of micro-drilling process. However, C263 is an alloy and has similar mechanism with other metal-based materials in laser ablation, therefore, the conclusions made could be considered more generic, especially about the precession micro-drilling capabilities, and can inform other potential applications of this technology [27-29].

6.2. Methodology and materials

6.2.1. Laser micro-machining system

The research reported in this study was carried out on LASEA LS-4 laser processing workstation that integrates a diode-pumped pulsed laser source with pulse duration of approximately 500 fs at central wavelength of 1030 nm. The athermal ablation mechanism of this USP laser source allows laser processing with almost negligible negative side effects and therefore the effects of different parameters on quality of produced micro-structures can be seen clearer. The same pulse energy at the workpiece, i.e. 60 µJ at a frequency of 100 kHz, was used in all experiments. The laser pulse energy was controlled based on applied frequency and laser power after the focusing lens measured by a power meter. The beam had a circular polarisation and was focused through a telecentric lens with focal distance of 100 mm onto a spot size of 30 (measured by camera-based beam profiler) µm and the peak fluence was 16.98 J/cm^2 at the focal plane. A simplified diagram of the laser processing workstation is provided in Fig. 6.1.

The precession movements of the laser beam after the focusing lens are produced by a module, called LS-Precess, which is integrated into the beam delivery sub-system between the beam conditioning module and the XY scan head. The precession laser machining principals are described in details in [30, 31]. The rotary speed of the precession beam after the focusing lens can be varied from 0 to 3141 rad/s. However,

only the maximum rotary speed was used in this experimental study to achieve the highest possible machining efficiency on this laser processing workstation.

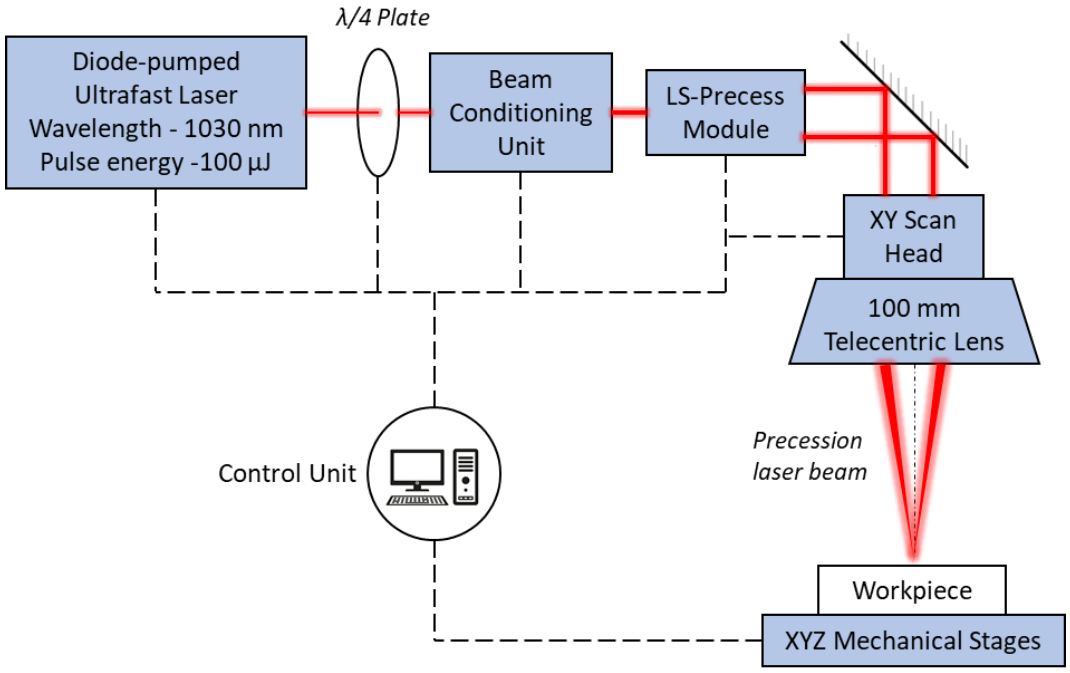

Figure 6.1. *Diagram of the laser processing workstation with its key components.*

The two important precession parameters investigated in this research are illustrated in Fig. 6.2. The first key parameter is the incident angle of the laser beam, which is defined by the angle between the beam and the central axis of the focusing lens. The incident angle can be varied on the LS4-workstation in the range from 2.86 to 4.27 degree by changing the diameter of the precession beam before the focusing lens with the LS-Precess module, as shown in Fig. 6.2a and 6.2b [30]. However, there was a clipping of the precession beam at the entrance of the scan head when the incident angle was greater than 3.56 degree. Thus, to avoid the significant drop of laser power

and the deterioration of beam quality after the focusing lens, the incident angle was varied from 2.86 to 3.56 degree, only.

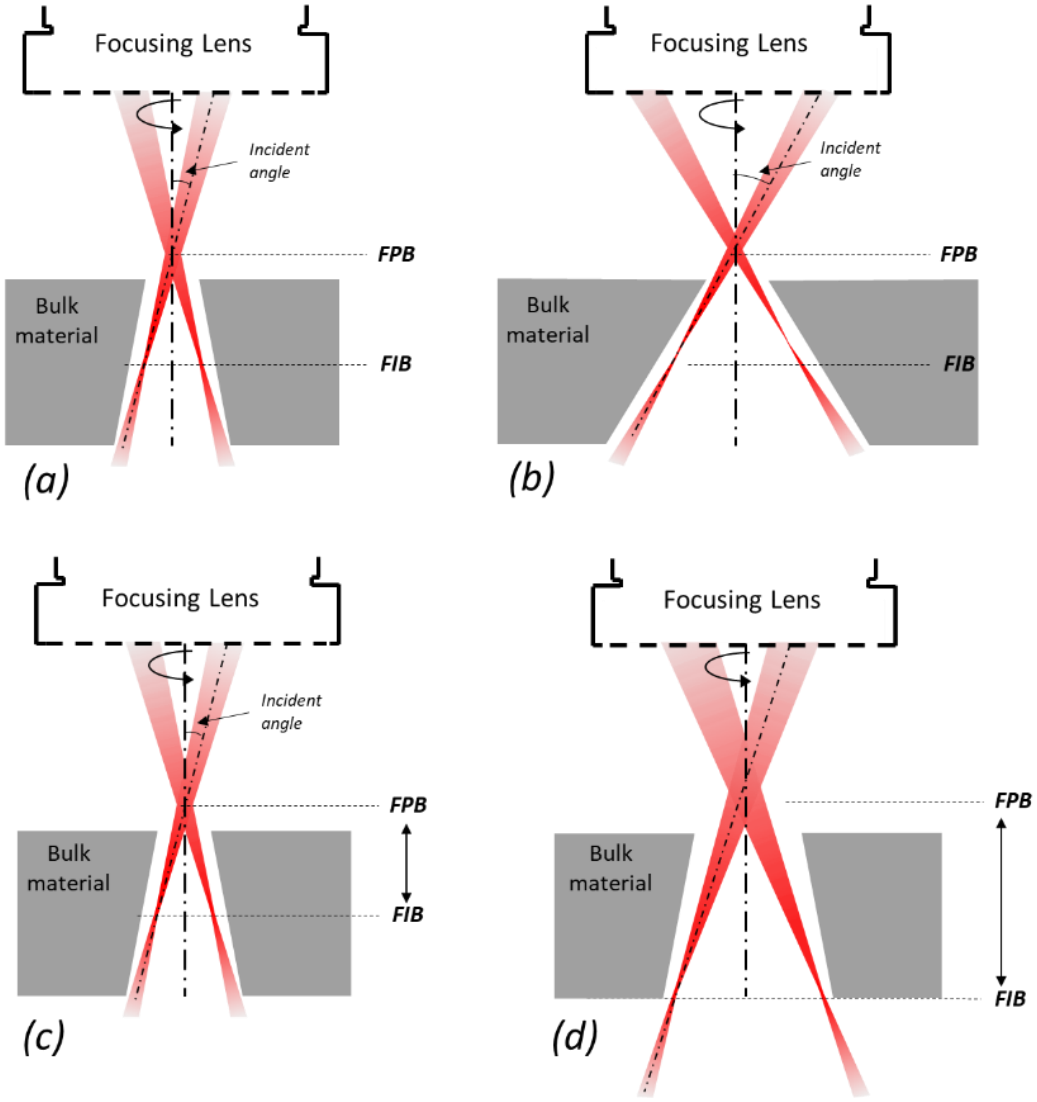

Figure 6.2. *An Illustration of the precession laser beam in interaction with material while varying key processing parameters: (a) small incident angle; (b) large incident angle; (c) small FPB-FIB distance, and (d) large FPB-FIB distance.*

Note: FPB refers to the Focus of the Precession Beam while FIB is the Focus of the Individual Beam.

The interdependence between the incident angle and the diameter of the precession beam is depicted in Fig. 6.3. This functional dependence can potentially affect the drilling process when relatively thick substrates are machined using bigger incident angles while the precession beam is translated downward. Consequently, the beam could be partially blocked by the structure edge and therefore the design of an appropriate machining strategy is essential for a successful micro-drilling operation.

The second key parameter investigated in this study is the distance between the Focus of the Precession Beam (FPB) and the Focus of the Individual Beam (FIB) (Fig. 6.2c and 6.2d). FPB is the point along the focusing lens axis where the precession beam has the smallest diameter while FIB is the beam focus where the laser fluence reaches the highest value. Therefore, the FPB-FIB distance plays an important role in achieving the required dimensional accuracy together with a higher ablation efficiency. It is possible to vary the FPB-FIB distance from 400 to 900 µm, approximately, on the LS4 workstation and its variation does not affect the precession beam diameter. However, a reduction of laser power was observed when the FPB-FIB distance had been increasing.

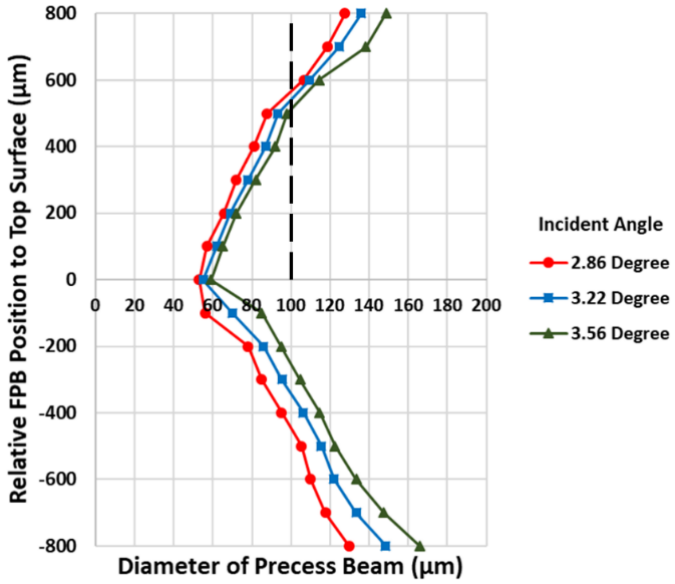

Figure 6.3. *Measured diameters of the precession beam with three different incident angles at different positions along the focusing lens axis. Precession beam diameters were measured experimentally by machining straight lines on a silicon wafer with a single pass at different FPB positions. The beam diameter is determined by the width of machined lines.*

The third key parameter investigated in this research was the linear scanning speed of the precession beam. The precession beam path is a combination of its circular and linear scanning motion that leads to a spiral trajectory. As the beam rotational speed is usually kept at its maximum value, the scanning speed is an essential factor for controlling the overlap level between laser pulses. Thus, the resulting trepanning strategy allows the removal rate together with the edge definition of micro-structures [32] to be controlled. The effects of scanning speed on the beam path and the pulse overlap level is depicted in Fig. 6.4.

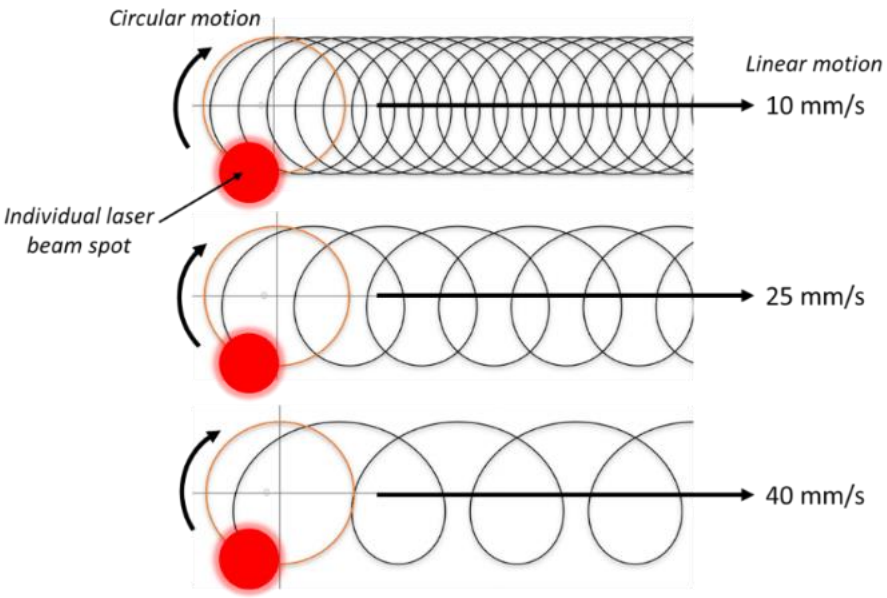

Figure 6.4. *The laser beam paths with different scanning speeds when FIB is at the top surface of the workpiece.*

6.2.2. Materials

The precession laser micro-drilling was investigated and optimised for a Nickel-based super alloy, i.e. C263, that is well known for its high strength and excellent resistance to oxidation under extreme working conditions [33, 34]. These properties make C263 an ideal material for producing different components for turbine applications, e.g. in aerospace and powerplants [35]. Laser micro-drilling is a desirable solution to manufacture feature, such as cooling holes on turbine blades. Especially, the high precision and accuracy that can be achieved with precession laser processing can offer performance and quality improvements of such functional features for turbine applications. Nickel-based super alloy C263 plate with thicknesses from 0.6 mm to 2 mm was used in the experiments of this research.

6.2.3. Design of experiment (DoE)

6.2.3.1. Machining strategies

The precession drilling strategies were investigated on the machining of holes with three diameters, i.e. 100 µm, 250 µm and 500 µm, on C263 plates with three thicknesses, 0.6 mm, 1 mm, and 2 mm. Different precession drilling strategies were required to produce those holes on the samples due to differences in their diameters and sample thickness (or holes' aspect ratio). Therefore, initial trials were conducted to identify suitable strategies and define the parameter range for this research.

The precession drilling strategies for different hole diameters and substrate thicknesses were designed to be as simple as possible for execution and the differences between them to be minimal in order to minimise their influence on the machining results. Therefore, a family of outlining strategies was employed to machine the holes with different diameters as depicted in Fig. 6.5. The laser beam spot size was taken into account in adjusting the outlining diameters with the objective to machine holes as close as possible to the target dimensions. In general, the thicker samples required a high number of FPB adjustments, referred to layers of outlining passes in this research, for refocus the precession laser beam and thus to maintain an efficient laser ablation at a higher hole depth. Especially, as it was already stated, plates with three thicknesses were used, i.e. 0.6, 1 and 2 mm, and their holes were

produced with one layer (Layer 1), three layers (Layers 1 to 3) and 5 layers (Layers 1 to 5), respectively.

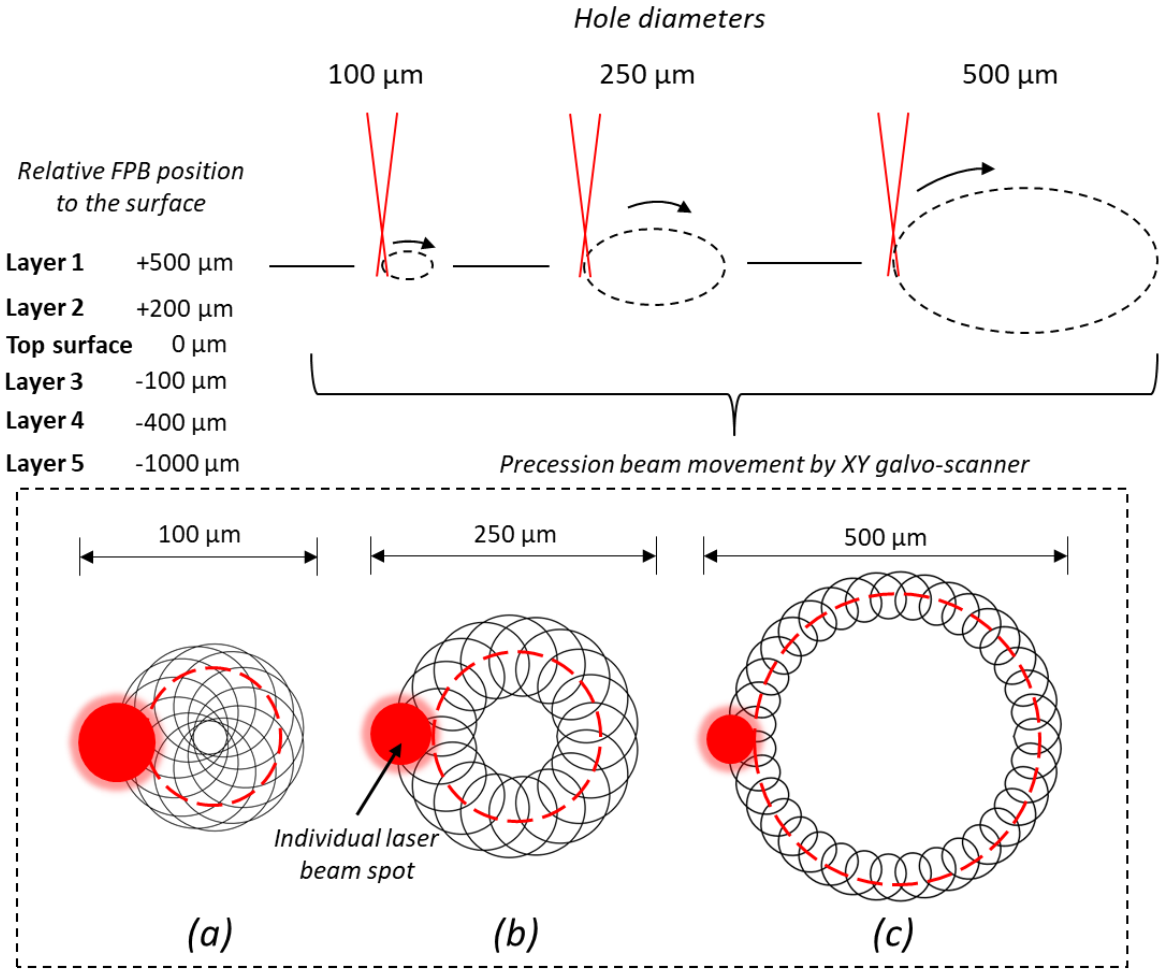

Figure 6.5. *Top: the family of precession strategies used to drill micro-holes with different diameters in the plates with three thicknesses. Bottom: the paths of the individual beam (black line) and the precession beam (red dashed line) when drilling holes with different diameters: (a) 100 µm, (b) 250 µm and (c) 500 µm. Note: The beam spot size in figures (a)-(c) are the same for different diameters in reality.The difference in spot size in figure is for illustration purpose.*

The number of passes per layer in the outlining strategies was kept the same, 500 passes for each layer. The respective paths of the precession beam when machining different diameters are illustrated in Fig. 6.5a-c. The relative offset positions of different layers from the top surface of the plates are also provided in Fig. 6.5. Especially, the offset of the first layer or FPB in the outlining strategies was at 500 µm above the samples and thus FIB was close to the plate top surface. In this way, there was an efficient laser ablation at the 1st layer, and thus the production of micro-holes with clean openings.

6.2.3.2. Full factorial experimental design

The three independent parameters investigated in this study were the incident angle, the FPB-FIB distance and the scanning speed. A full factorial experimental design was used to analyse the effects of these key precession processing parameters and their interactions on the taper angle of the drilled holes together with their respective quality. The parameter ranges and their levels were narrowed down based on some initial drilling trials that produced successfully holes with acceptable quality. Especially, the maximum range of incident angles available on the LS4 workstation, i.e. from 2.86 to 3.56 degree, was used. At the same time, the FPB-FIB distance in the range from 400 and 600 µm and scanning speeds up to 40 mm/s were identified as an effective processing domain for precession drilling of the holes. A further increase of the FPB-FIB distance led to a significant power drop of the output beam. The parameter domain

considered in this study is provided in Table 6.1. In addition, for a reference, holes were produced by conventional laser micro-machining, i.e. helical drilling, to compare and quantify the advantages of the precession laser processing. In the conventional laser drilling, the laser beam was kept normal to the plate surface with the use of a telecentric focusing lens and the beam was moved with the scanning head, only. A strategy with hatch distance of 5 μm was deployed to remove all of the material inside the holes. Scanning speed was set to be 1000 mm/s and pulse frequency of 100 kHz. A similar layer arrangement and pulse energy to precession machining was used in the conventional laser machining. Each layer was repeated 100 times before laser was refocused to the next layer.

Table 6.1. The precession drilling parameters together with their respective three levels as used in the full factorial experiments

Factors	**Unit**	**Value**		
		Level 1	Level 2	Level 3
Incident angle	Degree	2.86	3.22	3.56
FPB-FIB distance	μm	400	500	600
Speed	mm/s	10	25	40
No. of experiment with precession beam	**243**			
No. of experiment with conventional beam	**9**			
Total No. of experiment	**252**			

6.2.4. Measurement and data analysis

The important output results from the conducted study were the taper angles of the produced micro-holes. The angles were calculated based on the difference between entrance and exit diameters of the drilled holes. The measurements of the hole entrances and exits were conducted on Alicona G5 system with x20 magnification. Scanning electron microscopy (SEM) images of the holes were taken, too, by using a JCM6000 system. Finally, X-ray computed tomography was used to analyse the machined sample with 5.1 µm resolution, 100 kV voltage and 10 µA current. The experimental results were analysed with the Minitab statistics software to determine the effects of considered three process variables together with their interacts on taper angles of produced holes.

6.3. Results and discussion

6.3.1. The effects of key parameters

Taper angles obtained on the drilled holes are reported in Table 6.2 together with taper angles attained with the reference process, i.e. employing conventional laser micro-machining. The smallest taper angles obtained for each hole diameter and substrate thickness are highlighted in grey. Note that the smallest taper angle in this research is the one closest to zero and not the one which has the absolute smallest value.

It is clear from the obtained results that the investigated key parameters, i.e. substrate thicknesses and hole diameters, had different effects. Fig. 6.6 presents how the taper angle responded to these parameter variations. Pareto charts were also used to quantify the relative importance of these key parameters and their interaction effects on resulting taper angles based on their standardised effects (see Fig. 6.6). The reference line to analyse the factors' effects was drawn using Lenth's method in Minitab with a significance level of 0.05 [36].

Table 6.2. Taper angles attained in the experiments

Order	Incident angle [Degree]	FPB-FIB [µm]	Speed [mm/s]	Nickel alloy C265 substrate thickness [mm]								
				0.6			1			2		
				Hole diameter [µm]			Hole diameter [µm]			Hole diameter [µm]		
				100	250	500	100	250	500	100	250	500
1	2.86	400	10	1.30	1.47	0.95	0.55	0.54	0.21	1.61	1.46	1.66
2	2.86	400	25	1.79	1.68	1.55	0.56	0.69	0.73	1.72	1.76	2.27
3	2.86	400	40	2.22	2.23	3.57	0.72	0.77	1.65	1.95	2.05	2.97
4	2.86	500	10	0.91	0.83	0.36	0.31	0.31	0.00	1.75	1.53	1.58
5	2.86	500	25	1.55	1.42	1.11	0.29	0.34	1.14	1.88	1.86	2.21
6	2.86	500	40	1.77	2.06	3.74	0.61	0.44	1.55	1.99	2.31	2.83
7	2.86	600	10	0.81	0.89	0.08	0.13	0.48	0.02	1.98	1.59	1.40
8	2.86	600	25	1.11	0.88	1.06	0.24	0.43	1.96	2.02	1.87	1.85
9	2.86	600	40	1.47	1.11	4.31	0.46	0.44	1.85	2.14	2.28	2.35
10	3.22	400	10	1.12	1.43	0.75	0.36	0.46	0.50	1.89	1.46	1.57
11	3.22	400	25	1.50	1.92	1.23	0.57	0.58	0.75	1.88	1.66	1.80
12	3.22	400	40	1.92	2.45	3.80	0.70	0.65	2.01	2.05	1.94	2.46
13	3.22	500	10	0.83	1.33	0.27	0.23	0.31	0.12	1.98	1.34	1.48
14	3.22	500	25	1.22	1.59	1.12	0.20	0.34	1.01	2.18	1.55	1.75
15	3.22	500	40	1.55	2.02	4.04	0.41	0.42	2.26	2.25	1.94	2.38
16	3.22	600	10	0.87	0.85	-0.06	0.01	0.06	-0.03	1.87	1.24	1.28
17	3.22	600	25	0.97	0.99	0.93	0.10	0.22	1.08	2.15	1.43	1.54
18	3.22	600	40	1.18	1.59	4.31	0.45	0.19	2.40	2.29	1.74	2.28
19	3.56	400	10	1.68	1.20	0.60	0.42	0.69	0.30	1.90	1.22	1.59
20	3.56	400	25	1.54	1.31	0.90	0.55	0.77	1.62	2.14	1.58	1.88
21	3.56	400	40	2.05	1.90	3.35	0.66	0.88	2.21	2.25	1.92	2.45
22	3.56	500	10	1.14	0.93	-0.20	0.22	0.13	0.26	1.78	1.28	1.56
23	3.56	500	25	1.12	0.65	0.87	0.27	0.30	1.48	2.08	1.66	1.70
24	3.56	500	40	1.64	1.54	3.94	0.32	0.40	2.59	2.27	1.82	2.33
25	3.56	600	10	0.94	0.41	-0.13	0.00	0.16	-0.07	1.96	1.11	1.23
26	3.56	600	25	1.11	0.59	0.79	0.14	0.22	0.55	2.20	1.54	1.58
27	3.56	600	40	1.39	1.07	3.36	0.24	0.42	2.68	2.35	1.76	2.20
Conventional laser drilling				2.51	2.34	2.81	2.50	2.93	3.29	2.41	2.77	3.22

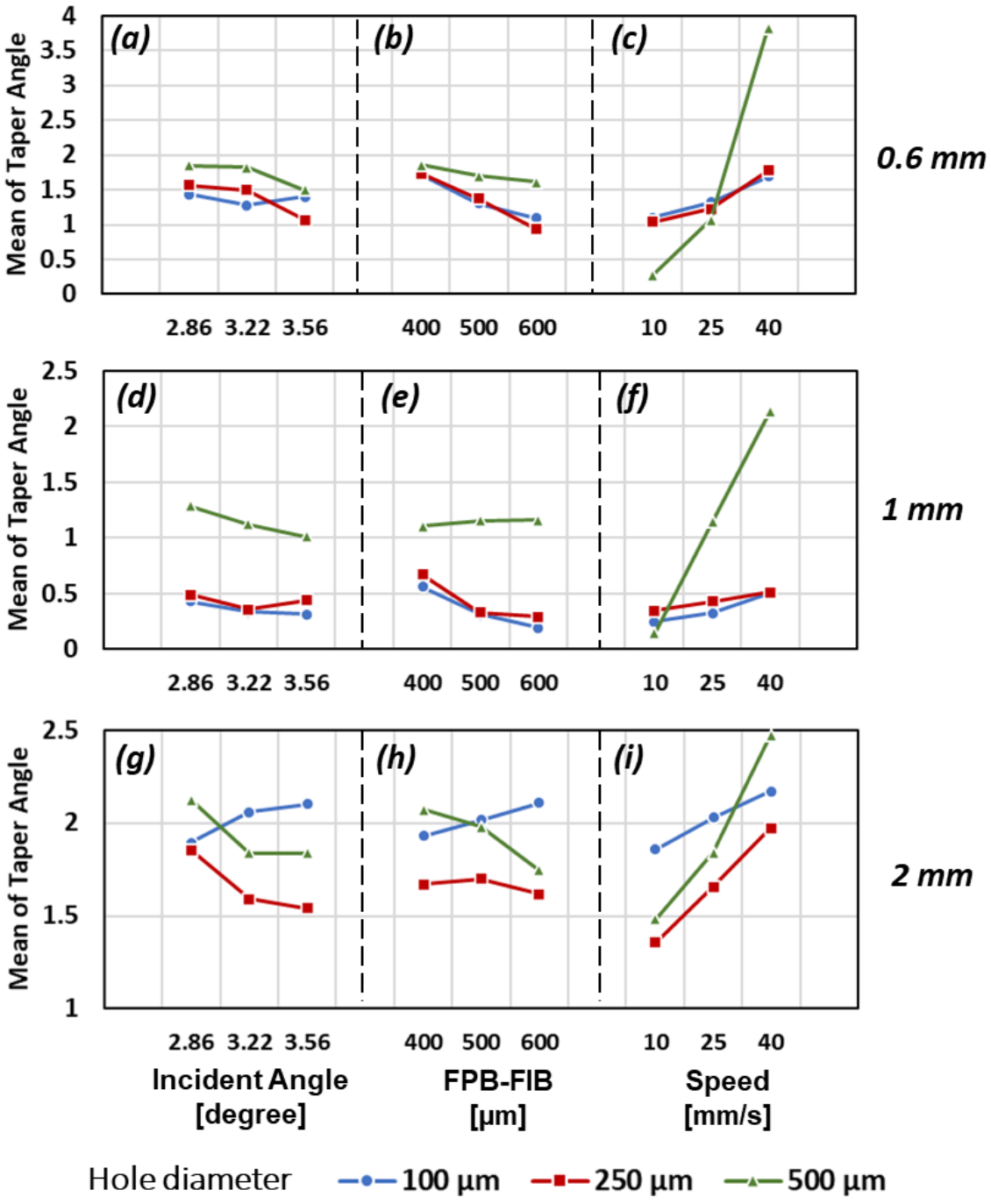

Figure 6.6. *The mean values of taper angles (degree) in regard to the parameter changes in precession drilling holes with diameters ranging from 100 µm to 500 µm on three substrate thicknesses: (a)-(c) 0.6 mm thickness, (d)-(f) 1 mm thickness and (g)-(h) 2 mm thickness.*

6.3.1.1. The effects of incident angle

Fig. 6.6a, 6.6d and 6.6g depicts the effects of incident angle on the taper angle of micro-holes drilled into 0.6 mm, 1 mm, and 2 mm substrates, respectively. It can be seen that the increase of incident angle led to a small/marginal decrease of taper angle in most of the cases. A bigger incident angle led to a bigger attacking angle in regard to the hole axis and side wall, too. Consequently, the laser beam spot area is reduced while fluence increases which resulted in a more efficient ablation and a smaller taper angles can be achieved along the hole's side walls [37]. However, this is not the case for 100 µm hole drilled onto the 2 mm substrate, where the holes' aspect ratio was 20:1, and the increase of incident angle led to a higher average taper angle. In this case, the precession beam was partially clipping the hole's entrance when larger incident angle was applied, especially, when FPB was moved downward with a small entrance of just 100 µm. Especially, it can be seen in Fig. 6.3 that the precession beam diameter was larger than 100 µm at more than 500 µm offset from the FPB position. This led to clipping of the precession beam at 100 µm entrance when FPB was more than 500 µm below the substrate top surface. In case of 250 µm hole onto 1 mm and 2 mm thickness and 500 µm hole onto 2 mm thickness, the response of taper angle mean value stabilised at the medium incident angle of 3.22 degree, thus, any further increases led to only marginal improvements. Nevertheless, incident angle was found to be a statistically significant factor for all hole diameters except for 500 µm holes

drilled into the 1 mm substrate (see Fig. 6.7f), where only scanning speed had a significant influence. However, the significance of incident angle was much less than that of scanning speed and the FPB-FIB distance.

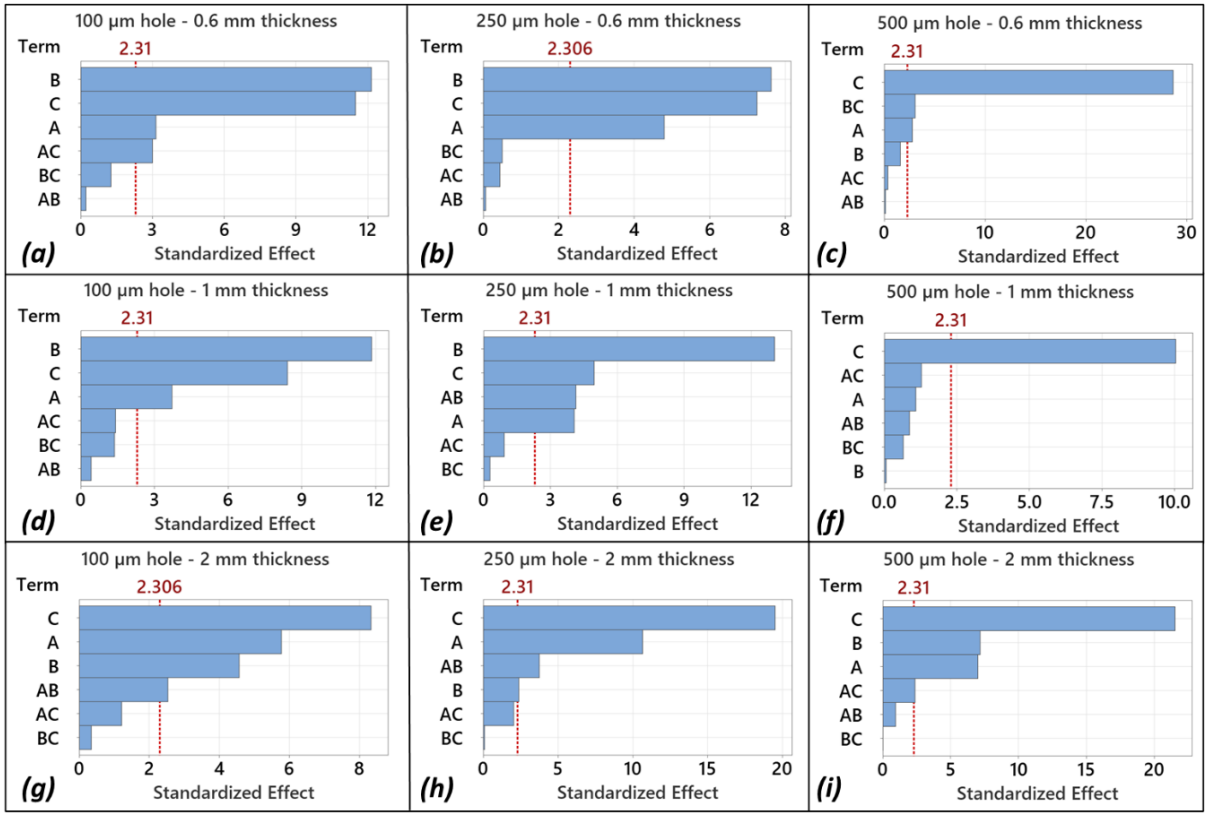

Figure 6.7. *Pareto charts on the significance of the investigated three factors, i.e. incident angle (A), the FPB-FIB distance (B) and scanning speed (C) when drilling holes onto: (a) - (c) 0.6 mm substrate, (d) - (f) 1 mm substrate, and (g) - (i) 2 mm substrate.*

6.3.1.2. The effects of FPB-FIP distance

The effects of the FPB-FIB distance on taper angle are presented in Fig. 6.6b, 6.6e and 6.6h. Specifically, the mean value of resulting taper angles decreased with the

increase of the FPB-FIB distance and reached a minimum value at the FPB-FIB distance of 600 µm for most of the investigated diameters and substrate thicknesses. Positioning FPB at 500 µm above the substrate surface for the 1st layer led to FIB position of 100 µm, 0 and -100 µm, respectively, when the FPB-FIB distance was varied from 400 to 600 µm. The ablation efficiency declined with the increase of hole aspect ratios as can be expected and this could be attributed also to the processing with an offset from FIB. This was more pronounced when FIB was positioned at 100 µm, i.e. FPB-FIB distance of 400 µm. Focusing the beam below the substrate surface (-100 µm) improved the ablation response and material removal when the hole depths increased, especially when there was no beam refocusing (machining of 0.6 mm substrates). Thus, it can be stated that some beneficial effects on taper angle was achieved, indirectly.

Furthermore, the relationship between taper angle and the FPB-FIB distance were close to linear compared to the effects of incident angle. In contrast, 100 µm holes drilled on 2 mm substrate showed an opposite effect on taper angle, especially the larger FPB-FIB distance led to a higher tapering effect (Fig. 6.6h). At the same time, the mean value of taper angle was almost unaffected by the FPB-FIB distance when drilling 500 µm holes onto 1 mm substrates (Fig. 6.6e and 6.7f).

The Pareto chart (Fig. 6.7a, 6.7b, 6.7d and 6.7e) showed that the FPB-FIB distance was the most important factor when drilling 100 µm and 250 µm holes onto 0.6 mm

and 1 mm substrates. The interaction effect of incident angle and the FPB-FIB distance (AB) was also significant in drilling 100 µm holes onto 2 mm substrates and 250 µm holes onto 1 mm and 2 mm substrates (Fig. 6.7e, 6.7g and 6.7h).

Fig. 6.8 shows the X-ray cross-sectional views of drilled holes onto the substrates with different thicknesses. It is operant that the precession machining with an USP laser produces holes with almost no evidence of any abnormal material redeposition inside the holes. The obtained side walls were straight and consistent across the holes drilled onto 0.6 mm and 1 mm substrates and thus a better geometrical accuracy was achieved compared with the conventional drilling process. Whilst, the holes drilled onto 2 mm substrates exhibited a sudden reduction in the holes' diameter near their exits (Fig. 6.8g, 6.8h and 6.8i). This is due to the reduced ablation efficiency with the depth increase and hence the increase of aspect ratio. Although the beam was translated down into the material to assist the material removal, this also led to a partial clipping of the laser beam as discussed in Section 3.1.1. However, the precession drilling still led to clear improvements when compared with the results obtained with the conventional laser drilling (Fig. 6.8j and 6.8k). In addition, the FPB-FIB distance did not affect the entrance diameter of the hole.

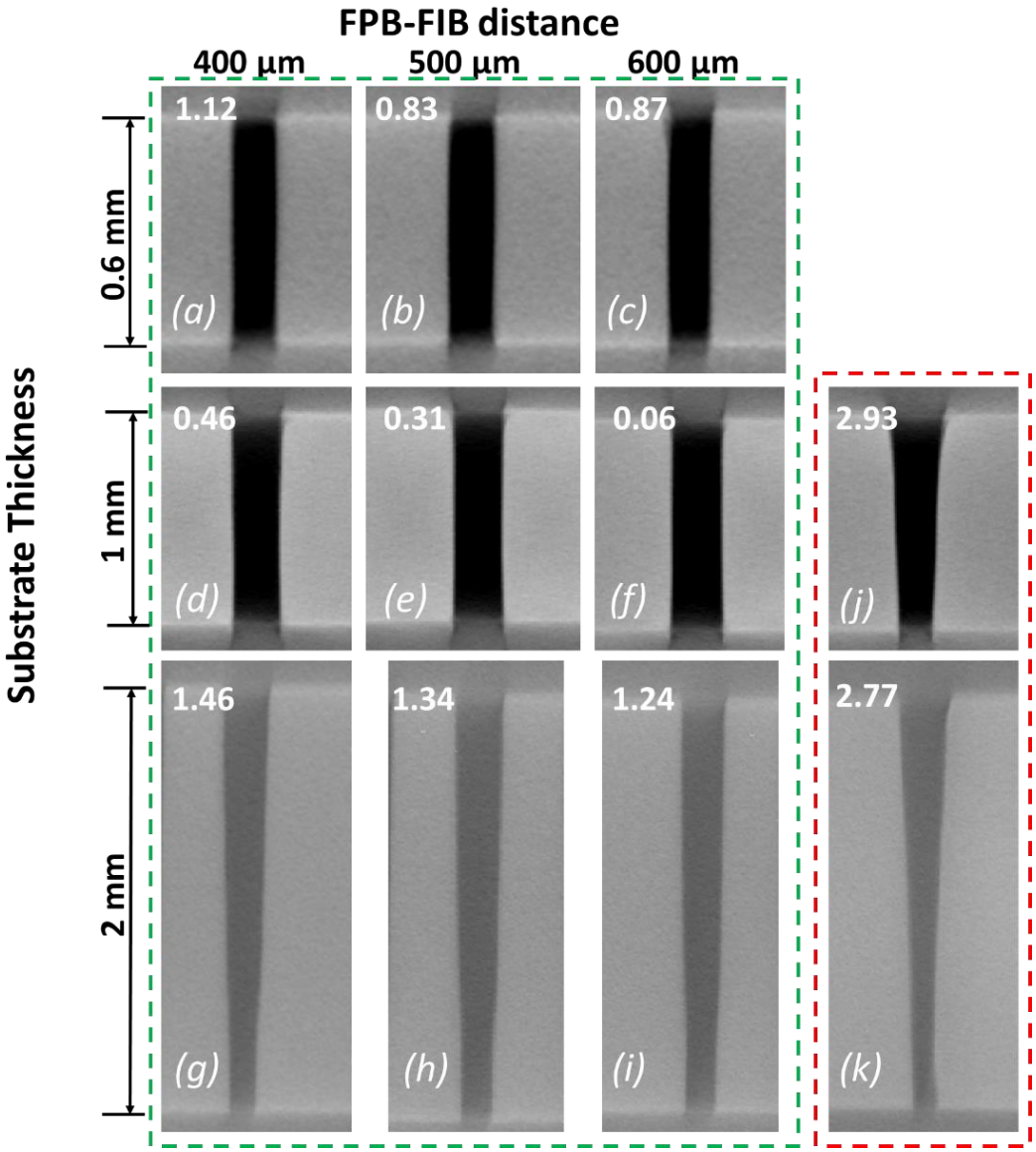

Figure 6.8. *X-ray cross-sectional views of holes produced by precession (green dashed line) and conventional (red dashed line) drilling onto the substrates with three thicknesses and varying FPB-FIB distances: (a)-(c): 100 µm holes onto 0.6 mm substrate; (d)-(f) 250 µm holes on 1 mm substrate; (g)-(i) 250 µm holes on 2 mm substrate; (j) and (k): 250 µm holes on 1 mm and 2 mm substrates, respectively. All holes were drilled with incident angle of 3.22 degree and scanning speed of 10 mm/s. Corresponding taper angle of each hole is showed in top left corner of each image.*

6.3.1.3. The effects of scanning speed

The effects of scanning speed on taper angle were the most pronounced among the investigated three factors. Consistent trends were observed for the three hole diameters and substrate thicknesses used in the research. Fig. 6.6c, 6.6f and 6.6i shows that the increase of scanning speed led to higher mean values of taper angle in all cases. This effect on taper angle was opposite to the general trend attained when increasing, both, incident angle and the FPB-FIP distance. This can be attributed to the interdependence between accumulated fluence and scanning speed. Especially, a higher speed at a constant repetition rate (100 kHz) resulted in lower pulse overlap level and less accumulated pulse energy when the same scanning strategies were executed. It is worth noting that the effect of scanning speed on taper angle was the most linear one among the investigated three precession drilling parameters.

Furthermore, the effect of scanning speed was much more pronounced in the case of 500 µm holes across all three substrate thicknesses. Fig 6.5a-c show that the beam paths in case of 100 µm and 250 µm hole diameters were much closer to each other compared to 500 µm hole. In fact, the employed beam paths covered almost entirely the hole's area (100% of hole's area) and all material inside the holes was removed in the case of 100 and 250 µm holes (Fig. 6.9a and 6.9b). At the same time, the beam paths covered much smaller percentage of hole's area (39% of hole's area) and removed only outer material of 500 µm holes and left a "core" inside (Fig. 6.9c). In

addition, the beam passes in the layers for the smaller diameter holes required a shorter scanning time. As a result, this led to some heat accumulation and its impact on the ablation process was less affected by the varying scanning speed when machining smaller holes. Contrarily, the larger holes required a longer time for each beam pass in the layers and thus there was more time for heat conduction into the material to take place. Consequently, the effect of scanning speed on ablation efficiency was much higher and therefore led to a significant increase of taper angle. Especially, the steep increase of taper angle from approximately 0.25 to 3.8 degree with the increase of scanning speed from 10 to 40 mm/s, respectively, on 0.6 mm substrate (see Fig. 6.6c) is another strong evidence of the heat conduction impact on the ablation process and consequently on taper angle.

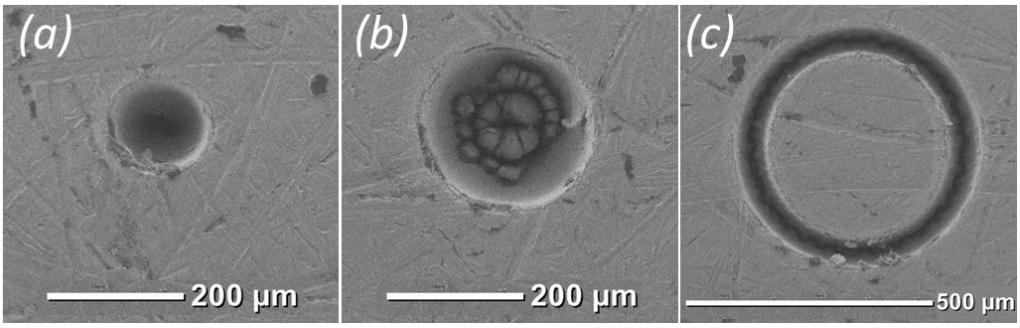

Figure 6.9. *The hole's opening produced by employed strategies for different diameters: (a) 100 µm, (b) 250 µm and (c) 500 µm.*

Scanning speed was one of the most significant factors in five cases (Fig. 6.7c, 6.7f, 6.7g, 6.7h and 6.7i) and was always into the top two most important factor across the three hole diameters and substrate thicknesses. In addition, it can be seen from Fig.

6.6 and Fig. 6.7 that the impact of speed on 100 µm and 250 µm diameter were quite similar for all three substrate thicknesses. At the same time, the influence of scanning speed strongly dominated the effects of other two factors in drilling 500 µm holes. Especially, scanning speed was the only factor that had a significant impact on tapering effect when drilling 500 µm hole onto 1 mm substrates (Fig. 6.7f). In addition, the interaction effect of scanning speed and incident angle (AC) was found to be significant only in drilling 100 µm hole onto 0.6 mm substrate.

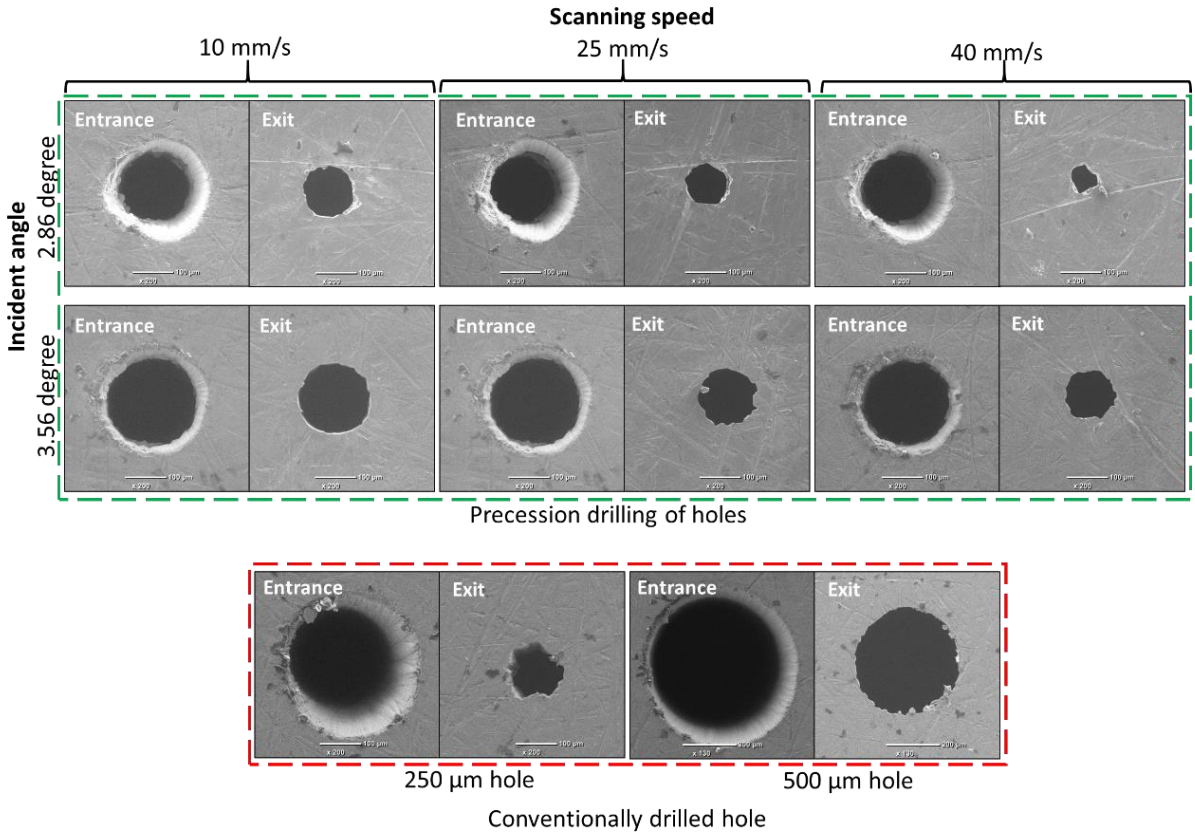

***Figure 6.10**. Entrances and exits of 250 µm holes produced by precession drilling while the FPB-FIB distance fixed at 600 µm and different scanning speeds and incident angles on 2 mm substrate (green dashed line). Entrances and exits of 250 µm and 500*

µm holes drilled onto 2 mm substrate with the conventional laser drilling process (red dashed line).

Some examples depicting the effects of scanning speed and incident angle on holes' entrances and exits are presented in Fig. 6.10. Scanning speed did not have a noticeable effect on hole entrances. The scanning speeds investigated in this research were sufficient to achieve the accumulated fluence necessary for producing holes with clean entrances, even at the highest scanning speed of 40 mm/s. However, a clear reduction of exit diameters can be seen when the speed increased from 10 mm/s to 40 mm/s regardless of incident angles. At the same time, the effect of incident angle on taper angle was confirmed, i.e. when the increase of incident angle led to larger exit diameters (see Fig. 6.10), while the hole entrances were also affected. Especially, incident angle of 3.56 degree led to a better edge definition and slightly bigger entrance than incident angle of 2.86 degree. In general, the dimensional accuracy and circularity of holes produced by precession drilling was better than those produced with the conventional laser drilling process.

6.3.2. Process optimisation

The optimal parameters for precession drilling holes with a minimised taper angle onto the C263 substrates with three different thicknesses are provided in Table 6.3. The minimum taper angles for all three hole diameters and substrate thicknesses were achieved at scanning speed of 10 mm/s. This underlines the importance of speed, i.e.

the pulse overlap levels in precession laser machining, on improving the ablation efficiency due to the higher heat accumulation at the low speed.

Table 6.3. The optimum values of investigated precession drilling parameters for producing micro-holes with a minimum taper angle onto the C263 substrates with the three different thicknesses.

Thickness [mm]	Target hole diameter [µm]	Optimum key parameters			Obtained taper angle
		Incident angle [Degree]	FPB-FIB [µm]	Speed [mm/s]	
0.6	100	2.86	600	10	0.81
	250	3.56	600	10	0.41
	500	3.22	600	10	-0.06
1	100	3.56	600	10	0.00
	250	3.22	600	10	0.06
	500	3.56	600	10	-0.07
2	100	2.86	400	10	1.61
	250	3.56	600	10	1.11
	500	3.56	600	10	1.23

The higher FPB-FIB distances of 600 µm were also important for attaining a minimum taper angle. At the same time, higher incident angles are beneficial in precession drilling bigger holes, while the machining of smaller ones requires a carefully consideration of the trade-offs between incident angle and the interaction effects between other parameters. Fig. 6.11 shows the entrances and exits of the holes machined with the optimal precession parameters. The impact of the substrate thickness is very well pronounced in case of 100 µm holes, where the exit diameter decreased significantly with the thickness increase from 1 mm to 2 mm, and the precession drilling process managed to penetrate only barely 2 mm substrate. Thus,

the high aspect ratios in drilling thicker substrates are still a challenge even when precession laser machining is employed. Based on the conducted empirical study, the substrate thickness of 1 mm can be considered the upper limit for achieving a zero-taper angle with the precession drilling process.

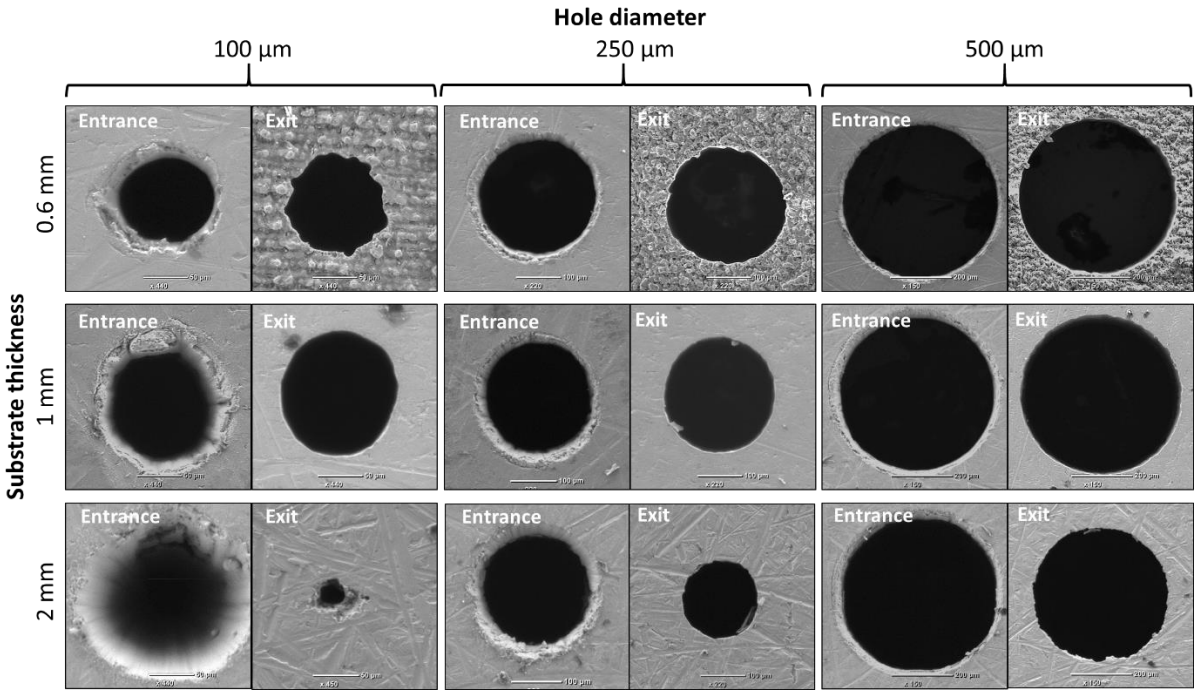

Figure 6.11. *The holes' entrances and exits when the minimum taper angles were achieved by the precession drilling process on the three investigated substrate thicknesses.*

6.4. Conclusion

The results reported in this study provides an insight into capabilities and limitations of precession laser machining, both in general about the effects of key precession processing parameters on dimensional and geometrical accuracy of micro-holes and

also about one specific application, i.e. drilling of Nickel alloy C263. The precession drilling of holes with diameters from 100 to 500 µm onto substrates with thicknesses up to 2 mm, aspect ratios up to 20:1, were investigated. The effects of three key parameters, i.e. incident angle, FPB-FIB distance and scanning speed, in precession laser drilling were analysed. The taper angle of the micro-holes was used as a key output quality factor to determine the effects of the investigated three parameters. The results showed that all three parameters affected the precession drilling process but to different extends.

Generally, the increase of incident angle and the FPB-FIB distance led to a taper angle reduction in most of the cases. In contrast, the increase of scanning speed entailed a taper angle increase. However, the precession drilling process was affected by a beam clipping at the hole entrance when machining high aspect ratio hole or thicker substrates. This beam clipping affected the ablation efficiency with the increase of the hole depth and led to a taper angle increase. Nonetheless, it was possible to precession drill holes with nearly zero or even a negative taper angle onto 0.6 mm and 1 mm substrates, which was impossible to achieve employing the conventional laser drilling process. Also, a significant reduction of holes' taper angle was achieved on 2 mm substrates, where the aspect ratios were up to 20:1, compared with the conventional laser drilling.

In summary, the precession drilling process has demonstrated clear advantages in producing micro-holes with a higher dimensional and geometrical accuracy when optimised processing strategies were applied. Moreover, the precession machining setups can be developed further to avoid any beam clipping and consequent power dropping, and thus to use fully the attractive processing capabilities offered by this machining method.

Acknowledgements

The authors would like to acknowledge the support obtained through the UKRI Future Leaders Fellowship under grant number MR/V02180X/1 and the collaboration with LASEA SA, Belgium within the framework of the ESIF project “Smart Factory Hub” (SmartFub).

References

1. Pattanayak, S. and Panda, S., *Laser beam micro drilling–a review.* Lasers in Manufacturing and Materials Processing, 2018. **5**(4): p. 366-394.
2. Krüger, R.A., Schulz-Ruhtenberg, M., Rösener, B., Ostermann, O., Ostholt, R., and Ambrosius, N. *LIDE: high aspect ratio glass processing technology for the mass production of microfluidic devices for biomedical applications*. in *Microfluidics, BioMEMS, and Medical Microsystems XVII*. 2019. SPIE.
3. Wang, H.-J. and Yang, T., *A review on laser drilling and cutting of silicon.* Journal of the European Ceramic Society, 2021. **41**(10): p. 4997-5015.
4. Sharp, M., *Laser processing of medical devices.* Biophotonics for Medical Applications, 2015: p. 79-98.
5. Marimuthu, S., Antar, M., and Dunleavey, J., *Characteristics of micro-hole formation during fibre laser drilling of aerospace superalloy.* Precision Engineering, 2019. **55**: p. 339-348.
6. Gautam, G.D. and Pandey, A.K., *Pulsed Nd: YAG laser beam drilling: A review.* Optics & Laser Technology, 2018. **100**: p. 183-215.
7. Jia, X., Zhang, Y., Chen, Y., Wang, H., Zhu, G., and Zhu, X., *Combined pulsed laser drilling of metal by continuous wave laser and nanosecond pulse train.* The International Journal of Advanced Manufacturing Technology, 2019. **104**(1): p. 1269-1274.
8. Petkov, P., Dimov, S., Minev, R., and Pham, D.T., *Laser milling: pulse duration effects on surface integrity.* Proceedings of the Institution of Mechanical Engineers, Part B: Journal of Engineering Manufacture, 2008. **222**(1): p. 35-45.
9. Weck, A., Crawford, T.H.R., Wilkinson, D.S., Haugen, H.K., and Preston, J.S., *Laser drilling of high aspect ratio holes in copper with femtosecond, picosecond and nanosecond pulses.* Applied Physics A, 2008. **90**(3): p. 537-543.
10. Hamad, A.H., *Effects of Different Laser Pulse Regimes (Nanosecond, Picosecond and Femtosecond) on the Ablation of Materials for Production of Nanoparticles in Liquid Solution*, in *High Energy and Short Pulse Lasers*. 2016.
11. Doan, H.D., Naoki, I., and Kazuyoshi, F., *Laser processing by using fluidic laser beam shaper.* International Journal of Heat and Mass Transfer, 2013. **64**: p. 263-268.
12. Le, H., Penchev, P., Henrottin, A., Bruneel, D., Nasrollahi, V., Ramos-de-Campos, J.A., and Dimov, S., *Effects of Top-hat Laser Beam Processing and Scanning Strategies in Laser Micro-Structuring.* Micromachines, 2020. **11**(2): p. 221.
13. Nasrollahi, V., Penchev, P., Jwad, T., Dimov, S., Kim, K., and Im, C., *Drilling of micron-scale high aspect ratio holes with ultra-short pulsed lasers: Critical effects of focusing lenses and fluence on the resulting holes' morphology.* Optics and Lasers in Engineering, 2018. **110**: p. 315-322.

14. Bhattacharyya, B. and Doloi, B., *Chapter Four - Machining processes utilizing thermal energy*, in *Modern Machining Technology*, Bhattacharyya, B. and Doloi, B., Editors. 2020, Academic Press. p. 161-363.
15. Hasan, M., Zhao, J., and Jiang, Z., *A review of modern advancements in micro drilling techniques.* Journal of Manufacturing Processes, 2017. **29**: p. 343-375.
16. Kim, S.H., Balasubramani, T., Sohn, I.-B., Noh, Y.-C., Lee, J., Lee, J.B., and Jeong, S. *Precision microfabrication of AlN and Al 2 O 3 ceramics by femtosecond laser ablation*. in *Photon Processing in Microelectronics and Photonics VII*. 2008. International Society for Optics and Photonics.
17. Calabrese, L., Azzolini, M., Bassi, F., Gallus, E., Bocchi, S., Maccarini, G., Pellegrini, G., and Ravasio, C., *Micro-Milling Process of Metals: A Comparison between Femtosecond Laser and EDM Techniques.* Journal of Manufacturing and Materials Processing, 2021. **5**(4): p. 125.
18. Tangwarodomnukun, V. and Dumkum, C., *Experiment and analytical model of laser milling process in soluble oil.* The International Journal of Advanced Manufacturing Technology, 2018. **96**(1): p. 607-621.
19. Nasrollahi, V., Penchev, P., Batal, A., Le, H., Dimov, S., and Kim, K., *Laser drilling with a top-hat beam of micro-scale high aspect ratio holes in silicon nitride.* Journal of Materials Processing Technology, 2020: p. 116636.
20. Salama, A., Yan, Y., Li, L., Mativenga, P., Whitehead, D., and Sabli, A., *Understanding the self-limiting effect in picosecond laser single and multiple parallel pass drilling/machining of CFRP composite and mild steel.* Materials & Design, 2016. **107**: p. 461-469.
21. Martin, P.-E., Estival, S., Dijoux, M., Kupisiewicz, A., and Braunschweig, R., *Laser cutting and drilling with zero conicity.* Journal of Laser Applications, 2017. **29**(2).
22. LASEA. *LS-Precess*. 2021 [cited 2022 June 22]; Available from: https://www.lasea.eu/en/oem/ls-precess/.
23. Aerotech. *AGV5D Five-Axis Laser Micromachining Precession Scanner*. 2022 [cited 2022 June 22]; Available from: https://uk.aerotech.com/product/laser-scan-heads-en-uk/agv5d-five-axis-laser-micromachining-precession-scanner/.
24. Photonics, N. *Precession Elephant 2*. 2022 [cited 2022 June 22]; Available from: https://novantaphotonics.com/product/precession-elephant-2/.
25. Scanlab. *precSYS Micromachining System*. 2022 [cited 2022 June 22]; Available from: https://www.scanlab.de/en/products/advanced-scanning-solutions/precsys-micromachining-system.
26. Auerswald, J., Ruckli, A., Gschwilm, T., Weber, P., Diego-Vallejo, D., and Schlüter, H., *Taper Angle Correction in Cutting of Complex Micro-mechanical Contours with Ultra-Short Pulse Laser.* 2016.
27. See, T.L., Liu, Z., Liu, H., Li, L., Chippendale, J., Cheetham, S., and Dilworth, S., *Effect of geometry measurements on characteristics of femtosecond laser*

ablation of HR4 nickel alloy. Optics and Lasers in Engineering, 2015. **64**: p. 71-78.
28. Zhao, W., Liu, H., Shen, X., Wang, L., and Mei, X., *Percussion drilling hole in Cu, Al, Ti and Ni alloys using ultra-short pulsed laser ablation.* Materials, 2019. **13**(1): p. 31.
29. Semaltianos, N., Perrie, W., French, P., Sharp, M., Dearden, G., Logothetidis, S., and Watkins, K., *Femtosecond laser ablation characteristics of nickel-based superalloy C263.* Applied Physics A, 2009. **94**(4): p. 999-1009.
30. Le, H., Pradhani, C., Penchev, P., Nasrollahi, V., Karkantonis, T., Wang, Y., Dimov, S., and Ramos-de-Campos, J.A., *Laser precession machining of cross-shaped terahertz bandpass filters.* Optics and Lasers in Engineering, 2022. **149**.
31. Estival, S., Martin, P.-e., and Kupisiewicz, A., *Machining device*. 2019, US Patents.
32. Martin, P.-E., Estival, S., Dijoux, M., Laygue, P., Kupisiewicz, A., and Braunschweig, R. *Laser cutting and drilling with zero conicity*. in *Laser-based Micro-and Nanoprocessing XI*. 2017. International Society for Optics and Photonics.
33. Mastanaiah, P., Reddy, G.M., Prasad, K.S., and Murthy, C., *An investigation on microstructures and mechanical properties of explosive cladded C103 niobium alloy over C263 nimonic alloy.* Journal of Materials Processing Technology, 2014. **214**(11): p. 2316-2324.
34. Davies, S., Jeffs, S., Coleman, M., and Lancaster, R., *Effects of heat treatment on microstructure and creep properties of a laser powder bed fused nickel superalloy.* Materials & Design, 2018. **159**: p. 39-46.
35. Shastri, R.K. and Mohanty, C.P., *Sustainable electrical discharge machining of Nimonic C263 superalloy.* Arabian Journal for Science and Engineering, 2021. **46**(8): p. 7273-7293.
36. Xampeny, R., Grima, P., and Tort-Martorell, X., *Selecting significant effects in factorial designs: Lenth's method versus using negligible interactions.* Communications in Statistics-Simulation and Computation, 2018. **47**(5): p. 1343-1352.
37. Michalek, A., Batal, A., Qi, S., Penchev, P., Bruneel, D., See, T.L., and Dimov, S., *Modelling ultrafast laser structuring/texturing of freeform surfaces.* Applied Surface Science Advances, 2020. **2**.

CHAPTER 7

CONTRIBUTIONS, CONCLUSIONS AND FUTURE RESEARCH

This chapter summaries the key contributions to knowledge claimed in the conducted research together with main conclusions and the key findings. Also, future research directions are discussed in the chapter.

7.1. Contributions to knowledge

Different approaches/methods for altering the beam energy distribution, optimising the pulse train energy levels and temporal distributions, and realising complex relative movements between laser beam and workpiece were investigated to fulfil the overall aim and specific objectives of this PhD research. Specifically, the research presented in Chapters 3 to 6 reports advances in laser micro-machining technology to achieve both, quality and process efficiency improvements in producing components/products in different materials. The main objectives of the research were achieved and the contributions to knowledge claimed in this PhD research are as follow:

1. A nanosecond pulsed laser micro-machining setup with integrated refractive beam shaping device was investigated to fabricate micro-structures on silicon wafers with a top-hat beam intensity profile. The surface integrity, structuring quality and process efficiency attained by altering the beam profiles while varying machining conditions were analysed and compared with those achieved with Gaussian beam.
2. MHz burst mode processing was investigated as a tool for achieving material removal rates scalability in ultrashort laser machining of different materials. The advantages and limitations MHz burst mode were analysed over various machining conditions. In addition, a novel methodology was proposed to assess

the effects of heat accumulation, plasma shielding and material redeposition on processing efficiency.

3. A novel ultrashort laser manufacturing process, called precession laser machining, is implemented to address a key limitation of laser micro-machining/micro-drilling, i.e. the tapering effect at sidewall of fabricated micro-structures. The impact of this machining process on the taper angle was studied and successfully demonstrated on copper plates used as cross-shaped THz bandpass filters. The dimensional and geometrical accuracy of fabricated structures and the functional performance of the manufactured THz filters was investigated to validate this manufacturing route.
4. A further investigation of ultrashort laser precession machining was carried out to understand the underlying mechanism in details and the effects of key processing parameters in drilling micro-holes. The influence of three key parameters on dimensional and geometrical accuracy of machined micro-holes was investigated systematically through an empirical study on an aerospace material. The attained results provided an insight into the capabilities and limitations of this micro-drilling technology.

7.2. Conclusions

The existence of inherent shortcomings and the prospects for further improvements of laser micro-machining technology motivated this PhD research. The research led to advances of this technology in achieving both, quality and processing efficiency improvements in producing components/products in different materials. Therefore, it can be concluded that the aim together with the four main objectives of this PhD research are achieved and the respective research results to support this claim are

reported in Chapters 3 to 6. Three different technologies, i.e. refractive beam shaping, MHz burst mode processing and laser precession machining, were investigated systematically to improve the process efficiency and quality of machined micro-structures.

Firstly, the capabilities and limitations of top-hat beam processing when machining micro-structures onto silicon wafers were investigated and compared with those achieved with Gaussian beam processing. Different machining conditions were considered to assess the advantages and limitations of top-hat beam machining (**Chapter 3**). The main findings of this research are:

- The top-hat beam processing can reduce the tapering effect at sidewalls of the produced micro-structures by adjusting the machining strategies compared to that achieved with Gaussian beam. Especially, combining hatching and outlining passes in the machining strategy minimises the taper angles compared to hatching or reduction outlining passes, only.
- The improvements in geometrical accuracy are not in expense of process efficiency, especially the ablation rates achieved are nearly the same with top-hat and Gaussian beam processing on silicon wafers. In addition, the surface roughness of produced structures with the top-hat beam are better when hatching and a combination of hatching and outlining passes are included in the machining strategies.
- The machining of microstructures with a top-hat beam can be carried out with a higher pulse energy without reducing the structuring quality and surface integrity and thus the available average laser power can be utilised better.

Secondly, the scalability of ultrashort laser processing with the use of the MHz burst mode was clearly demonstrated in micro machining of metals. The side effects associated with the burst mode processing, such as heat accumulation, material redeposition and plasma shielding, were also systematically analysed and quantified (**Chapter 4**). The main findings of this research are:

- MHz burst mode processing has clear advantages in regard to processing efficiency in ultrashort laser processing of copper and stainless steel. Especially, the available laser power can be fully utilised while maintaining the pulse fluence close to the optimum level while increasing the beneficial heat accumulation effect.
- High processing efficiency is achieved at relatively high number of sub-pulses per burst compared to the published research so far. Specifically, the maximum specific removal rates (SRRs) were obtained at 15 to 20 and 20 to 50 sub-pulses per burst on copper and stainless steel, respectively, while the reported results so far referred to SRRs achieved with up to 10 sub-pulses. It is important to stress that the reported ablation efficiency improvements in the MHz burst mode machining can be attained only at specific machining conditions. SRRs achieved with the burst mode was higher than single pulse mode machining only when the overlap level between the bursts was less than 87%.
- There are similarities in the dependence of SRRs on the number of sub-pulses per burst at lower pulse durations, i.e. 500 fs and 1 ps, and higher durations, i.e. 5 and 10 ps, investigated in this research.

- A novel methodology is proposed to assess the heat accumulation effects on SRRs when small (from 1 to 3) and high (above 100) numbers of sub-pulses per burst are applied.
- The improvements in processing efficiency are not in expense of an inferior surface roughness of produced micro-structures. Especially, the burst mode machining achieved a similar surface roughness compared with the single pulse one of the same micro-structures.

Thirdly, the capabilities and limitations of precession laser machining were studied in detail to explain the underlying mechanism and the effects of different processing parameters on quality of fabricated micro-structures. The improvements in dimensional and geometrical accuracy achievable with this laser machining technology were demonstrated in specific industrial applications, i.e. the fabrication of THz devices and drilling micro-holes onto aerospace materials (**Chapter 5 and 6**). The main findings of these research are:

- Precession laser machining can significantly reduce and almost eliminates the tapering effect on sidewall of micro-structures by controlling the attacking angle of the laser beam to achieve an efficient ablation at the sidewalls. The taper angle can be reduced three to six times compared to the two-side machining method and such improvements will not be in expense of machining time in fabrication of THz mesh filter.
- There can be significant dimensional deviations of the produced “through” structures in X and Y directions if the effects of the precession beam quality, i.e. the beam ellipticity and its sensitivity to variations focal distance, are not compensated.

- The functional performance of fabricated THz bandpass filters was excellent with clear transmission poles and acceptable frequency deviations from simulation results. The insertion loss was less than 1 dB and thus satisfied the requirements.
- There can be some side effects, i.e. oxidation of both the structure top surface and also at its sidewalls, from the precession process in spite of the ultrashort laser processing. The formation of copper oxides can be attributed to some heat accumulation due to the accumulated fluence during the precession laser machining. This also contributed to some insertion loss of THz signals.
- All three key parameters, i.e. incident angle, FPB-FIB distance and scanning speed, have a significant impact on taper angle of micro-holes when drilling on Nickel alloy substrate. More specifically, an increase of incident angle and FPB-FIB distance led to a decrease of the taper angle in most of cases while an increase of scanning speed led to an increase of the taper angle. Effects of the scanning speed are the most significant among the three investigated parameters.
- Some clipping of the precession beam at the hole entrance can occur when machining high aspect-ratio holes. This can negatively affect the ablation efficiency with the increase of hole depths and result in an increase of the taper angle.
- The optimisation of precession laser machining can improve the machining accuracy significantly and holes with zero and negative taper angles can be achieved in drilling micro holes with higher aspect ratios. Especially, high aspect-ratio holes (20:1) was successfully produced onto 2 mm substrates.

- Precession laser processing can be applied in micro-machining/micro-drilling aerospace materials.

7.3. Future research

The opportunities for further development of the laser micro-machining process are wide ranging and this research is focused on only three of its enabling technologies. The research reported in this PhD thesis suggests some prospective research directions and they are outlined below:

- Top-hat beam and burst mode machining share some similarities in the approach employed to improving the processing efficiency, especially through the use of pulse fluence closer to the optimum levels compared to that achievable with the original Gaussian beam. Therefore, it can be possible to combine these two approaches and thus to achieve some synergistic improvements in laser micro processing. In short, a use of a top-hat beam in MHz burst mode machining could lead to further improvements in processing efficiency and quality of micro-structures.
- The empirical methodology proposed in Chapter 4 to analyse the effects of heat accumulation and plasma shielding in MHz burst mode processing was limited due to the available measurement setup. A higher resolution measurement instrument, e.g. atomic force microscopy (AFM), that allows to measure the ablation of a sub-pulse can help to investigate the influence of plasma shielding and incubation effect within a burst in burst mode processing.
- The results in Chapter 6 showed that the layer-based machining strategies have important role to play in improving the quality of the machined micro-structures.

Therefore, the effects of scanning strategies with varying numbers of layers should be investigated and optimised further. An optimisation scanning strategy can further improve the process efficiency and quality of produced micro-structures.

- The effects of considered key processing parameters in laser precession machining can be investigated further with more levels while the parameter ranges could be broadened. Also, other laser parameters such as frequency and pulse energy should be investigated, too, to understand better their effects in precession laser processing. In this way, the effects of a broader parameters' domain associated with this technology can be quantified, and the technology optimised further. The collected data can be used to develop AI-based predictive models for process optimisation.
- Precession laser machining was mainly employed to fabricate structures on planar surface in this research. However, this technology can be used in combination with multi-axis machining strategies to produce 3D micro-structures on 3D surfaces. This is completely feasible with the capabilities that the current control technologies can offer. This will further broaden the application areas of this technology in different industrial sectors.

_____ End of the thesis _____

Appendix

Appendix 1 – Design of experiment in Chapter 3

Three sets of experiments

Set 1 – Structuring with different processing strategies

Fixed parameters:

Parameter	Unit	Value
Power	W	22.5
Pulse energy	mJ	0.15
Pulse duration	ns	65
Frequency	kHz	150
Scanning speed	mm/s	1500
Number of layer	N/A	30
Pulse distance	µm	10
Hatch distance	µm	15

List of experiment:

Standard order	Beam profile	Strategy
1	Gaussian	a
2	Gaussian	b
3	Gaussian	c
4	Top-hat	a
5	Top-hat	b
6	Top-hat	c

Set 2 – Structuring with varying hatching and pulse distance

Fixed parameters:

Parameter	Unit	Value
Power	W	22.5
Pulse energy	mJ	0.15
Pulse duration	ns	65
Frequency	kHz	150
Number of layer	N/A	30
Strategy	N/A	a

List of experiment:

Standard order	Beam profile	Hatch distance [µm]	Pulse distance [µm]
1	Gaussian	5	5
2	Gaussian	5	6.33

3	Gaussian	5	7.67
4	Gaussian	5	9
5	Gaussian	5	10.33
6	Gaussian	5	11.67
7	Gaussian	5	13
8	Gaussian	5	14.33
9	Gaussian	10	5
10	Gaussian	10	6.33
11	Gaussian	10	7.67
12	Gaussian	10	9
13	Gaussian	10	10.33
14	Gaussian	10	11.67
15	Gaussian	10	13
16	Gaussian	10	14.33
17	Gaussian	15	5
18	Gaussian	15	6.33
19	Gaussian	15	7.67
20	Gaussian	15	9
21	Gaussian	15	10.33
22	Gaussian	15	11.67
23	Gaussian	15	13
24	Gaussian	15	14.33
25	Gaussian	20	5
26	Gaussian	20	6.33
27	Gaussian	20	7.67
28	Gaussian	20	9
29	Gaussian	20	10.33
30	Gaussian	20	11.67
31	Gaussian	20	13
32	Gaussian	20	14.33
33	Gaussian	25	5
34	Gaussian	25	6.33
35	Gaussian	25	7.67
36	Gaussian	25	9
37	Gaussian	25	10.33
38	Gaussian	25	11.67
39	Gaussian	25	13
40	Gaussian	25	14.33
41	Top-hat	5	5
42	Top-hat	5	6.33
43	Top-hat	5	7.67
44	Top-hat	5	9
45	Top-hat	5	10.33

46	Top-hat	5	11.67
47	Top-hat	5	13
48	Top-hat	5	14.33
49	Top-hat	10	5
50	Top-hat	10	6.33
51	Top-hat	10	7.67
52	Top-hat	10	9
53	Top-hat	10	10.33
54	Top-hat	10	11.67
55	Top-hat	10	13
56	Top-hat	10	14.33
57	Top-hat	15	5
58	Top-hat	15	6.33
59	Top-hat	15	7.67
60	Top-hat	15	9
61	Top-hat	15	10.33
62	Top-hat	15	11.67
63	Top-hat	15	13
64	Top-hat	15	14.33
65	Top-hat	20	5
66	Top-hat	20	6.33
67	Top-hat	20	7.67
68	Top-hat	20	9
69	Top-hat	20	10.33
70	Top-hat	20	11.67
71	Top-hat	20	13
72	Top-hat	20	14.33
73	Top-hat	25	5
74	Top-hat	25	6.33
75	Top-hat	25	7.67
76	Top-hat	25	9
77	Top-hat	25	10.33
78	Top-hat	25	11.67
79	Top-hat	25	13
80	Top-hat	25	14.33

Set 3 – Structuring with varying pulse energy

Fixed parameters:

Parameter	Unit	Value
Pulse duration	ns	65
Frequency	kHz	150
Scanning speed	mm/s	1500
Number of layer	N/A	30
Strategy	N/A	a
Pulse distance	µm	10
Hatch distance	µm	15

List of experiment:

Standard order	Beam profile	Pulse energy [mJ]
1	Gaussian	0.04
2	Gaussian	0.081
3	Gaussian	0.12
4	Gaussian	0.161
5	Gaussian	0.2
6	Gaussian	0.238
7	Gaussian	0.256
8	Top-hat	0.04
9	Top-hat	0.081
10	Top-hat	0.12
11	Top-hat	0.161
12	Top-hat	0.2
13	Top-hat	0.238
14	Top-hat	0.256

Appendix 2 – Design of experiment in Chapter 4

Set 1 – Influence of burst mode under different conditions

Fixed parameters

Parameter	Unit	Value
Power	W	10
Pulse energy	µJ	90
Pulse duration	fs	500
Frequency	kHz	100
Intra-burst frequency	MHz	40
Beam spot size	µm	30
Number of layer	N/A	10

List of experiment

Acronym and Unit:

SO: Standard Order [N/A] **NoS**: Number of Sub-pulse [N/A]

PD: Pulse Duration [picosecond] **SS**: Scanning Speed [mm/s]

SO	PD	NoS	SS
1	0.5	1	20
2	0.5	1	60
3	0.5	1	100
4	0.5	1	140
5	0.5	1	200
6	0.5	1	400
7	0.5	1	800
8	0.5	1	1200
9	0.5	1	1600
10	0.5	1	2000
11	0.5	2	20
12	0.5	2	60
13	0.5	2	100
14	0.5	2	140
15	0.5	2	200
16	0.5	2	400
17	0.5	2	800
18	0.5	2	1200
19	0.5	2	1600
20	0.5	2	2000
21	0.5	3	20
22	0.5	3	60

SO	PD	NoS	SS
23	0.5	3	100
24	0.5	3	140
25	0.5	3	200
26	0.5	3	400
27	0.5	3	800
28	0.5	3	1200
29	0.5	3	1600
30	0.5	3	2000
31	0.5	5	20
32	0.5	5	60
33	0.5	5	100
34	0.5	5	140
35	0.5	5	200
36	0.5	5	400
37	0.5	5	800
38	0.5	5	1200
39	0.5	5	1600
40	0.5	5	2000
41	0.5	10	20
42	0.5	10	60
43	0.5	10	100
44	0.5	10	140

SO	PD	NoS	SS
45	0.5	10	200
46	0.5	10	400
47	0.5	10	800
48	0.5	10	1200
49	0.5	10	1600
50	0.5	10	2000
51	0.5	15	20
52	0.5	15	60
53	0.5	15	100
54	0.5	15	140
55	0.5	15	200
56	0.5	15	400
57	0.5	15	800
58	0.5	15	1200
59	0.5	15	1600
60	0.5	15	2000
61	0.5	20	20
62	0.5	20	60
63	0.5	20	100
64	0.5	20	140
65	0.5	20	200
66	0.5	20	400

SO	PD	NoS	SS
67	0.5	20	800
68	0.5	20	1200
69	0.5	20	1600
70	0.5	20	2000
71	0.5	50	20
72	0.5	50	60
73	0.5	50	100
74	0.5	50	140
75	0.5	50	200
76	0.5	50	400
77	0.5	50	800
78	0.5	50	1200
79	0.5	50	1600
80	0.5	50	2000
81	0.5	100	20
82	0.5	100	60
83	0.5	100	100
84	0.5	100	140
85	0.5	100	200
86	0.5	100	400
87	0.5	100	800
88	0.5	100	1200
89	0.5	100	1600
90	0.5	100	2000
91	0.5	200	20
92	0.5	200	60
93	0.5	200	100
94	0.5	200	140
95	0.5	200	200
96	0.5	200	400
97	0.5	200	800
98	0.5	200	1200
99	0.5	200	1600
100	0.5	200	2000
101	0.5	400	20
102	0.5	400	60
103	0.5	400	100
104	0.5	400	140
105	0.5	400	200
106	0.5	400	400
107	0.5	400	800
108	0.5	400	1200
109	0.5	400	1600
110	0.5	400	2000
111	1	1	20
112	1	1	60
113	1	1	100
114	1	1	140
115	1	1	200
116	1	1	400
117	1	1	800
118	1	1	1200
119	1	1	1600
120	1	1	2000
121	1	2	20
122	1	2	60
123	1	2	100
124	1	2	140
125	1	2	200
126	1	2	400
127	1	2	800
128	1	2	1200
129	1	2	1600
130	1	2	2000
131	1	3	20
132	1	3	60
133	1	3	100
134	1	3	140
135	1	3	200
136	1	3	400
137	1	3	800
138	1	3	1200
139	1	3	1600
140	1	3	2000
141	1	5	20
142	1	5	60
143	1	5	100
144	1	5	140
145	1	5	200
146	1	5	400
147	1	5	800
148	1	5	1200
149	1	5	1600
150	1	5	2000
151	1	10	20
152	1	10	60
153	1	10	100
154	1	10	140
155	1	10	200
156	1	10	400
157	1	10	800
158	1	10	1200
159	1	10	1600
160	1	10	2000
161	1	15	20
162	1	15	60
163	1	15	100
164	1	15	140
165	1	15	200
166	1	15	400
167	1	15	800
168	1	15	1200
169	1	15	1600
170	1	15	2000
171	1	20	20
172	1	20	60
173	1	20	100
174	1	20	140
175	1	20	200
176	1	20	400
177	1	20	800
178	1	20	1200
179	1	20	1600
180	1	20	2000
181	1	50	20
182	1	50	60
183	1	50	100
184	1	50	140
185	1	50	200
186	1	50	400
187	1	50	800
188	1	50	1200
189	1	50	1600
190	1	50	2000
191	1	100	20
192	1	100	60

SO	PD	NoS	SS
193	1	100	100
194	1	100	140
195	1	100	200
196	1	100	400
197	1	100	800
198	1	100	1200
199	1	100	1600
200	1	100	2000
201	1	200	20
202	1	200	60
203	1	200	100
204	1	200	140
205	1	200	200
206	1	200	400
207	1	200	800
208	1	200	1200
209	1	200	1600
210	1	200	2000
211	1	400	20
212	1	400	60
213	1	400	100
214	1	400	140
215	1	400	200
216	1	400	400
217	1	400	800
218	1	400	1200
219	1	400	1600
220	1	400	2000
221	5	1	20
222	5	1	60
223	5	1	100
224	5	1	140
225	5	1	200
226	5	1	400
227	5	1	800
228	5	1	1200
229	5	1	1600
230	5	1	2000
231	5	2	20
232	5	2	60
233	5	2	100
234	5	2	140

SO	PD	NoS	SS
235	5	2	200
236	5	2	400
237	5	2	800
238	5	2	1200
239	5	2	1600
240	5	2	2000
241	5	3	20
242	5	3	60
243	5	3	100
244	5	3	140
245	5	3	200
246	5	3	400
247	5	3	800
248	5	3	1200
249	5	3	1600
250	5	3	2000
251	5	5	20
252	5	5	60
253	5	5	100
254	5	5	140
255	5	5	200
256	5	5	400
257	5	5	800
258	5	5	1200
259	5	5	1600
260	5	5	2000
261	5	10	20
262	5	10	60
263	5	10	100
264	5	10	140
265	5	10	200
266	5	10	400
267	5	10	800
268	5	10	1200
269	5	10	1600
270	5	10	2000
271	5	15	20
272	5	15	60
273	5	15	100
274	5	15	140
275	5	15	200
276	5	15	400

SO	PD	NoS	SS
277	5	15	800
278	5	15	1200
279	5	15	1600
280	5	15	2000
281	5	20	20
282	5	20	60
283	5	20	100
284	5	20	140
285	5	20	200
286	5	20	400
287	5	20	800
288	5	20	1200
289	5	20	1600
290	5	20	2000
291	5	50	20
292	5	50	60
293	5	50	100
294	5	50	140
295	5	50	200
296	5	50	400
297	5	50	800
298	5	50	1200
299	5	50	1600
300	5	50	2000
301	5	100	20
302	5	100	60
303	5	100	100
304	5	100	140
305	5	100	200
306	5	100	400
307	5	100	800
308	5	100	1200
309	5	100	1600
310	5	100	2000
311	5	200	20
312	5	200	60
313	5	200	100
314	5	200	140
315	5	200	200
316	5	200	400
317	5	200	800
318	5	200	1200

SO	PD	NoS	SS
319	5	200	1600
320	5	200	2000
321	5	400	20
322	5	400	60
323	5	400	100
324	5	400	140
325	5	400	200
326	5	400	400
327	5	400	800
328	5	400	1200
329	5	400	1600
330	5	400	2000
331	10	1	20
332	10	1	60
333	10	1	100
334	10	1	140
335	10	1	200
336	10	1	400
337	10	1	800
338	10	1	1200
339	10	1	1600
340	10	1	2000
341	10	2	20
342	10	2	60
343	10	2	100
344	10	2	140
345	10	2	200
346	10	2	400
347	10	2	800
348	10	2	1200
349	10	2	1600
350	10	2	2000
351	10	3	20
352	10	3	60
353	10	3	100
354	10	3	140
355	10	3	200
356	10	3	400
357	10	3	800
358	10	3	1200
359	10	3	1600
360	10	3	2000

SO	PD	NoS	SS
361	10	5	20
362	10	5	60
363	10	5	100
364	10	5	140
365	10	5	200
366	10	5	400
367	10	5	800
368	10	5	1200
369	10	5	1600
370	10	5	2000
371	10	10	20
372	10	10	60
373	10	10	100
374	10	10	140
375	10	10	200
376	10	10	400
377	10	10	800
378	10	10	1200
379	10	10	1600
380	10	10	2000
381	10	15	20
382	10	15	60
383	10	15	100
384	10	15	140
385	10	15	200
386	10	15	400
387	10	15	800
388	10	15	1200
389	10	15	1600
390	10	15	2000
391	10	20	20
392	10	20	60
393	10	20	100
394	10	20	140
395	10	20	200
396	10	20	400
397	10	20	800
398	10	20	1200
399	10	20	1600
400	10	20	2000
401	10	50	20
402	10	50	60

SO	PD	NoS	SS
403	10	50	100
404	10	50	140
405	10	50	200
406	10	50	400
407	10	50	800
408	10	50	1200
409	10	50	1600
410	10	50	2000
411	10	100	20
412	10	100	60
413	10	100	100
414	10	100	140
415	10	100	200
416	10	100	400
417	10	100	800
418	10	100	1200
419	10	100	1600
420	10	100	2000
421	10	200	20
422	10	200	60
423	10	200	100
424	10	200	140
425	10	200	200
426	10	200	400
427	10	200	800
428	10	200	1200
429	10	200	1600
430	10	200	2000
431	10	400	20
432	10	400	60
433	10	400	100
434	10	400	140
435	10	400	200
436	10	400	400
437	10	400	800
438	10	400	1200
439	10	400	1600
440	10	400	2000

Set 2 – Influence of burst mode to surface quality

Fixed parameters

Parameter	Unit	Value
Power	W	10
Pulse energy	µJ	90
Frequency	kHz	100
Intra-burst frequency	MHz	40
Beam spot size	µm	30

List of experiments

Experiment on Copper

SO	PD [fs]	NoS	SS [mm/s]	Number of layer
1	500	1	500	27
2	500	1	1000	27
3	500	1	1500	27
4	500	15	500	10
5	500	15	1000	10
6	500	15	1500	10
7	5000	1	500	27
8	5000	1	1000	27
9	5000	1	1500	27
10	5000	15	500	10
11	5000	15	1000	10
12	5000	15	1500	10

Experiment on Stainless Steel

SO	PD [fs]	NoS	SS [mm/s]	Number of layer
1	500	1	500	77
2	500	1	1000	77
3	500	1	1500	77
4	500	50	500	10
5	500	50	1000	10
6	500	50	1500	10
7	5000	1	500	77
8	5000	1	1000	77
9	5000	1	1500	77
10	5000	50	500	10
11	5000	50	1000	10
12	5000	50	1500	10